PROCEEDINGS
THIRD SYMPOSIUM ON
ELECTRON BEAM TECHNOLOGY

March 23-24, 1961
Boston, Mass.
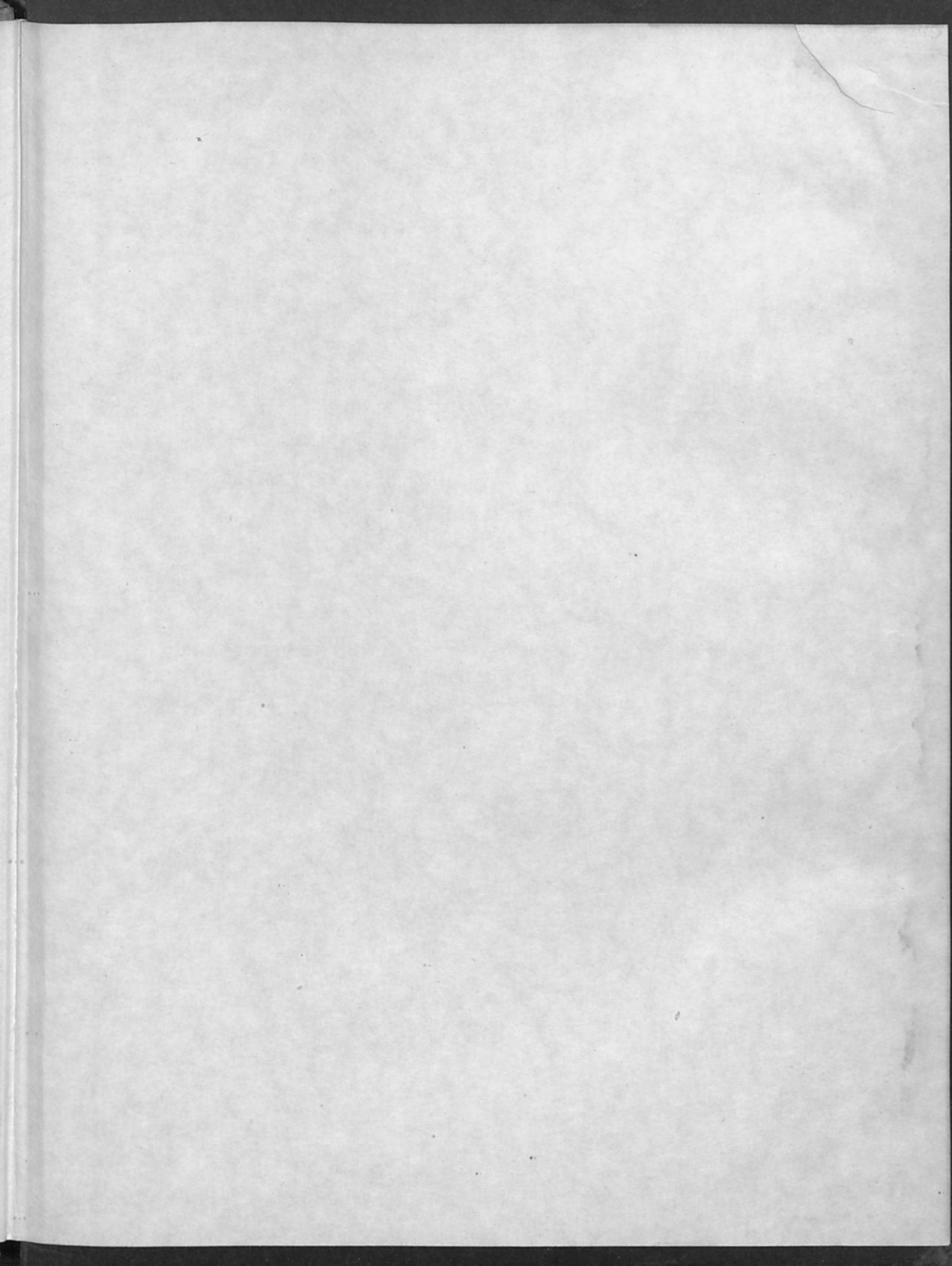## EDITOR - R. BAKISH

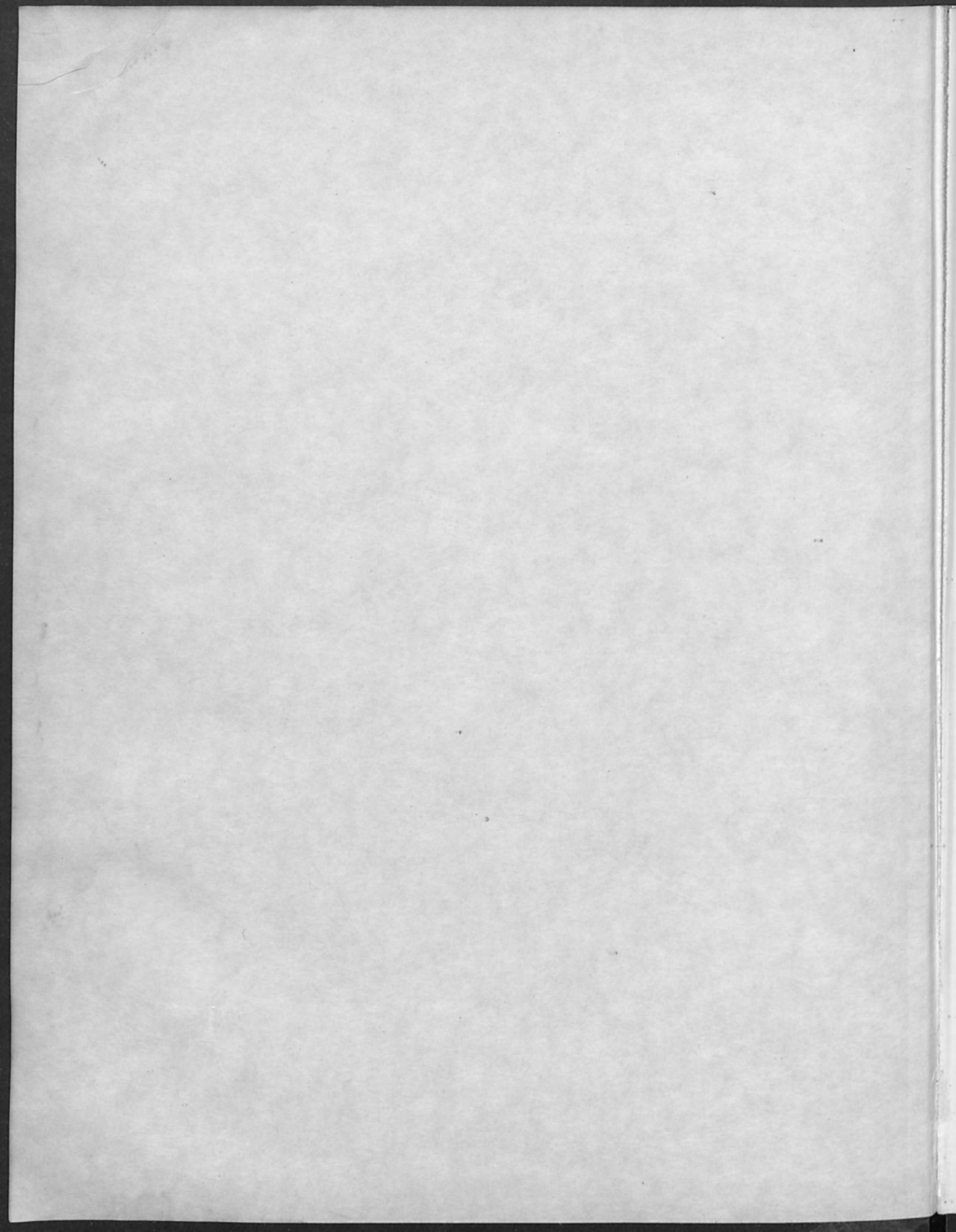## alloyd electronics corporation
CAMBRIDGE 42, MASSACHUSETTS

Proceedings of the Third
Symposium on Electron Beam Processes

March 23 and 24, 1961

Sheraton Plaza Hotel, Boston, Massachusetts

R. Bakish
Editor

Sponsored
By

ALLOYD ELECTRONICS CORPORATION
37 Cambridge Parkway
Cambridge 42, Massachusetts

ELECTRON BEAM SYMPOSIUM

TABLE OF CONTENTS

ELECTRON BEAM SYMPOSIUM

TABLE OF CONTENTS
(continued)

TABLE OF CONTENTS
(continued)

TABLE OF CONTENTS
(continued)

PREFACE

A great deal of progress has taken place since the appearance of the Proceedings of the First Alloyd Electron Beam Symposium. The pace in Electron Beam activities, however, has become so rapid that it is highly probable that the growth which has taken place in the last three years will be equaled or surpassed by the time we meet for our Fourth Symposium. Whereas in the past, scientists and engineers were learning of the existence and the potentials of electron beams, they are now aware of them. Consequently their efforts are directed to the perfection of existing and to the creation of new and more sophisticated electron beam systems, the tools for the breakthroughs of tomorrow.

We interpret the overwhelming response accorded our Third Symposium as a continuous endorsement of our judgment to organize and ability to conduct a meeting that scientists, engineers and their respective employers find interesting, worthwhile and profitable.

We feel that the Symposium has come of age and is presently as large as we will permit it to be. Attend-

1

ance of 350 people, in our opinion, is the maximum in
terms of a group which can be managed and which can
benefit from informal exchange of information. We sin-
cerely believe that as the technology grows the selected
group attending our Symposia will become the nucleus of
scientists and engineers working in the forefronts of
this technology. This group is comprised of men who
can come to listen, learn and question the reports of
recent progress in a suitable environment; men who wish
to discuss matters of interest at a high level of pro-
fessional competence, undisturbed by the pressures of
people promoting a miscellany of products.

In presenting the Proceedings to the public we
wish to present them as a product of a team effort of
researchers in this field of endeavor. Every corporation
or group which has lent support to this meeting by send-
ing a speaker should feel that it shares the achievements
of this Third Symposium in fostering the dissemination of
information and progress in the field of Electron Beam
technology. Much effort and many hours have gone into
the painstaking experimental and theoretical work which
produced the papers published here. To the individuals

who participated in this work and to those who came to present it to our audience we wish to say:
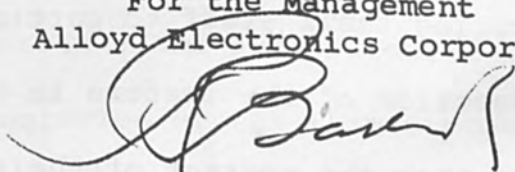
Gentlemen, these are your Proceedings. Thank you for making them what they are.

We wish to advise the speakers, participants, and readers of these Proceedings that we would be happy to receive their suggestions as to ways to better these Symposia in the future.

In conclusion, we wish to state that it is our sincere hope that this volume, the Proceedings of the Third Symposium, will bring to the many who could not attend our meeting, if not the spirit of it, its factual essence.

Last but not least let me thank my secretary Miss Marjorie Marte for her enthusiastic assistance, both in the course of organization of the Symposium and in the preparation of this manuscript.

For the Management
Alloyd Electronics Corporation

Robert Bakish, Vice President
Chairman of Alloyd's Symposia

INTRODUCTORY REMARKS

R. Bakish

Ladies and gentlemen, it gives me great pleasure to welcome you to the Third Electron Beam Symposium on behalf of the Alloyd Electronics Corporation.

As the Chairman of the Symposium Committee which organized this meeting, this opening address finds me with mixed feelings -- those of pleasure and gratitude on one side and that of apprehension on the other. Pleasure and gratitude prompted by the response given to our meeting and the confidence that you, representatives of three continents, five countries and one hundred and seventy companies have placed upon me by being present here today; apprehension in anticipation of your approval of the presentations and the organization of the meeting.

I do believe that the corporations, government agencies and educational institutions who have extended their hand in assistance and support of this Symposium by encouraging their staff to participate as speakers are a cross section of the leaders in this technology. I also believe that the content of their talks will indicate the

4

direction in which electron beam application technology
is progressing today.

It is with humbleness that I share this podium
with names as distinguished in their achievements as
Professor Möllenstedt of the University of Tübingen and
Dr. Steigerwald of Zeiss -- both of whom have crossed the
Atlantic to contribute to this Symposium. Unexpected
developments at the last minute prevented Dr. Stohr of
the French Atomic Energy Commission from being with us
today. However, his paper has arrived and will be read
by Mr. Solomon of Sciaky.

Many of our American contributors are no less
accomplished than our overseas guests in terms of their
achievements, and I sincerely hope that the newcomers in
this field of endeavor speaking at our sessions today
and tomorrow will become pacesetters in this dynamic new
technology.

But let me say a few words about the program of
this Symposium and the reasons for the choice of subjects.

The Physics of Electron Beams are scheduled to
be discussed because in the solution of the future problems

which we hope to solve, the understanding and command of the physics of electron beams will permit us to master the unknowns in these undertakings and resolve the challenges which they present.

We are discussing Electron Beam Welding because it is rapidly establishing its place as one of the processes for joining today's sophisticated materials. At the panel discussion on Electron Beam Welding at the Second Electron Beam Symposium held in 1960 in this very room, distinguished opinions presented the virtues and shortcomings of electron beam welding in general, and the high and low voltage systems in particular. The participants of that meeting had relatively little factual information on which to base their comments. It is my hope that the data which will be presented in our welding session today will transfer what were thoughts, opinions and speculations a year ago into an array of facts and figures.

The third session, on The Less Known Applications of Electron Beams was planned with the thought of bringing to your attention some lesser known electron beam applications and their great merit. These applications

could be useful to you and solve problems in your sphere of activities if you knew of them. This knowledge might germinate in your thoughts newer and more unusual applications with even greater promise for tomorrow.

The topic of the last session, namely Electron Beams in Microelectronics, was selected because of the great actuality of this subject and because of my belief and that of my company, that from now on microminiaturization and thin film component technology will depend on electron beams as one of its most important tools for research, for automated production, and for progress in general.

The two papers on ion beams given in the first and last sessions respectively, were scheduled on the program because we think that ion beams too will play an important role in electronics component technology in which some of you present here are involved. But so much for the contents of the program.

As I know that you are eagerly waiting to hear what our speakers have to say I will conclude my remarks by wishing you a profitable and enjoyable stay at our Symposium.

SOME ELEMENTARY CONSIDERATIONS IN THE DESIGN
OF ELECTRON BEAMS FOR WELDING AND HEATING

By

L. D. Smullin
Professor
Department of Electrical Engineering
Massachusetts Institute of Technology
Cambridge, Massachusetts

ABSTRACT

A review of the underlying principles in the
design of electron beams as heat sources is presented.
Beam voltage, cathode, gun design, spot size limitations
and focusing are discussed in some detail.

SOME ELEMENTARY CONSIDERATIONS IN THE DESIGN
OF ELECTRON BEAMS FOR WELDING AND HEATING

INTRODUCTION

The use of electron beams for welding, melting,
and evaporating on an industrial scale is a relatively
new development. It is a little hard, in retrospect, to
understand why this is such a recent development. The
electron beam is in competition with several other methods
of heating: induction heating, radiant heating by hot
filaments, resistance heating, and arc melting. Each of
the above methods of heating has its own peculiar advan-
tages; but the electron beam has certain properties that
put it entirely outside the range of competitive heating
systems. The most important advantage, by far, is its
ability to concentrate the power input to the work into
a very small spot. Power densities of megawatts per square
inch are relatively easy to achieve with accelerating volt-
ages of 10 to 20 kv, and power densities approaching 10^9
watts/sq. inch have been achieved at 100 kv. This power
may be applied selectively to any part of the exposed work
surface, no matter how complicated its shape. Either metals

or non-conductors may be heated. The most refractory

materials can be melted or evaporated, since no electrode

need be in contact with the heated spot, and because

the power is absorbed in the work from the kinetic energy

of the incident electron beam rather than from the thermal

radiation from another hot body.

In principle, the design of electron guns

for electron beam heating is very simple. The main elements

of an electron beam system are shown in Figure 1. They

are:

1. The electron gun

2. An auxiliary focusing lens

The electron gun is, basically, a triode. The beam is

accelerated from the cathode, and passes through the anode

aperture. The cathode electrode is usually operated at

nearly cathode potential, and the bias voltage between

it and the cathode is used as a focus control. The auxiliary

lens may be either magnetic or electrostatic; however, it

is not usually convenient to provide the variable high

voltage needed for electrostatic focusing, and magnetic

lenses are most commonly used. Certain parameters must

be established by the user: beam power, beam diameter
at the work, and distance from the gun to the work.
These parameters will be determined by metallurgical con-
siderations, the size of the work and of the vacuum
chamber, etc. The designer of the gun is now free to
choose some of the gun parameters. It should be noted,
in passing, that the thermodynamics of electron beam heat-
ing or welding has received practically no serious atten-
tion. Thus, there is today no theoretical basis for deter-
mining the optimum power density in a beam required to
make a weld in a given thickness of metal of specified
characteristics.

Beam Voltage

One of the first parameters to choose is the
accelerating voltage. Since the beam current is inversely
proportional to the voltage for a given power, and since
minimum spot size varies inversely with the voltage, one
would like to operate at the highest practical voltage.
The main factors that limit the practical voltage level
are: voltage breakdown, x-ray generation, and cost of
power supplies. Below about 50 kv one can use air

insulation without serious worries about breakdown. At
voltages of 10^5 or so, oil insulation becomes desirable,
if the apparatus is not to become too bulky. As the
voltage gets about 20,000 or so, the cost for a given
power begins to increase rather sharply with voltage
level. Finally, the x-ray hazard increases very rapidly
as the voltage goes beyond 50-60,000. With proper shield-
ing, of course, one can work at almost any voltage level.
However, the necessity for having easy and rapid access
to the vacuum chamber, and of being able to observe the
work through a window, make high voltage x-ray shielding
uneconomical for almost any applications except those
requiring the very smallest spot diameters. For welding
applications, many designers seem to have settled in
the range 10 to 20 kv. Although quite satisfactory per-
formance has been achieved at these voltages; from the
gun designers' point of view, it might be desirable to
push the operating level up to about 40 kv, if still
better focusing is to be achieved.

Cathode

Before discussing the details of gun design,
it is necessary to choose the cathode emitting materials.
In modern beam-type microwave tubes (such as the klystron
or traveling wave tube) the most commonly used emitters
are the barium-oxide-coated nickel cathode, and the
porous tungsten cathode impregnated with barium aluminate.
In carefully processed and evacuated tubes, these cathodes
may be operated at current densities of 1/2 to 2 amps/cm^2
for thousands of hours. However, the presence of such gases
as O_2, H_2O, and CO, or the vapors of metals like Zn or Cd,
or such heavy organic vapors as vacuum-pump oil can
poison these cathodes; that is, the available current
density may be reduced by orders of magnitude. In some
cases the poisoning may be overcome by allowing the re-
sponsible substance to re-evaporate from the cathode;
but in many cases it is irreversible, and the cathode must
be replaced. This high susceptibility to poisoning is a
concomitant of the fact that these cathodes operate at
rather low temperatures, 800 to 1100°C. Their great ad-
vantage lies in the fact that they can be indirectly heated

13

by radiation from a tungsten filament, and the emitting surface can be a unipotential surface. Under the comparatively poor vacuum conditions that are common in welding applications, it is not likely that either of these cathode types will be practical.

The lanthanum hexaboride (La B_6) [1] cathode operates at a some what higher temperature, 1400-1500°C. It is comparatively inert as far as susceptibility to poisoning is concerned, but there is little practical experience with it at present. Since it can be indirectly heated by a tungsten filament of relatively low power, the further study of this material may be of importance for electron beam welders.

At still higher operating temperatures, one can use thoriated tungsten, molybdenum, tantalum, and tungsten. Thoriated tungsten is very easily poisoned, and is probably not very interesting for our applications. The refractory, pure metals all operate in the range above 2000°C. They are capable of emission densities of 1 to 2 amps/cm^2; but it is not possible to heat them by radiation from another hot filament. They must be heated either directly by the passage of current through them, or by electron bombardment from another filament in back of the emitting surface. The
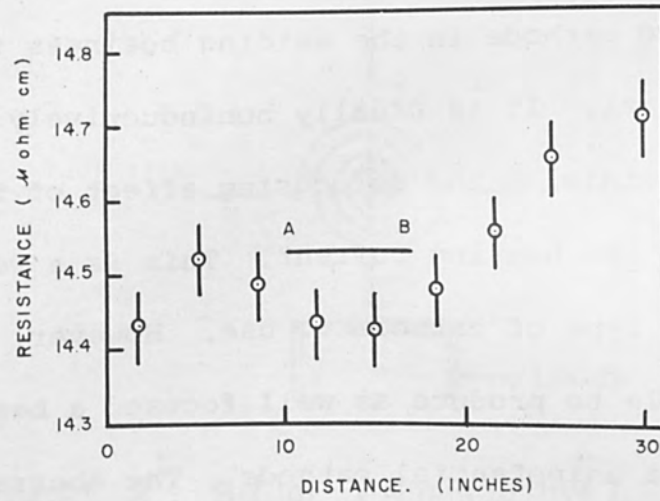
FIGURE I. Resistivity of zone refined niobium (20°C)
(zone movement in direction AB)
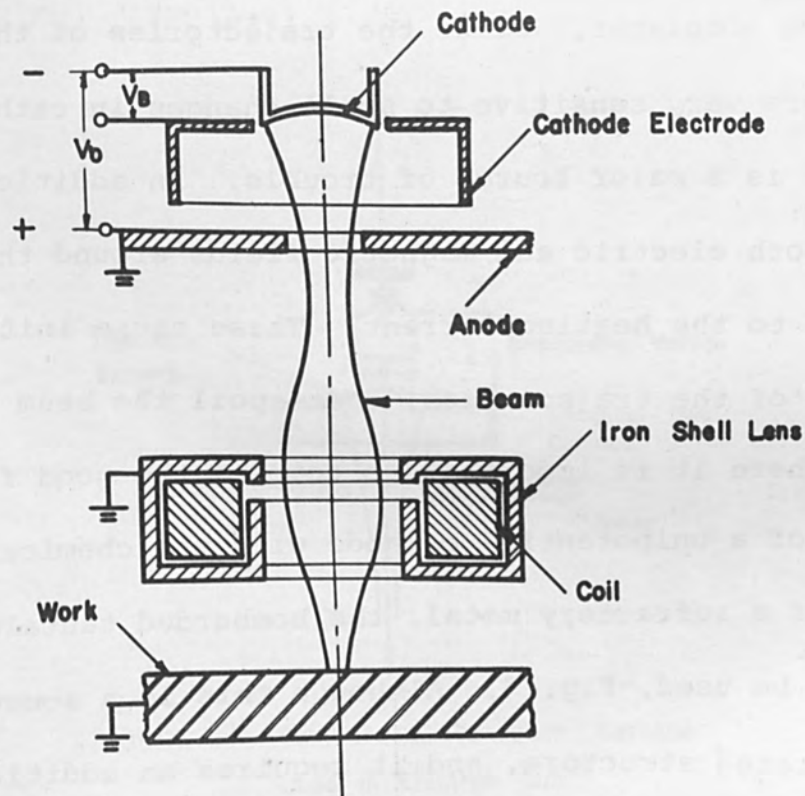
FIGURE I. Typical Electron Beam System
For Welding.

15

most commonly used cathode in the welding business is a
flat tungsten spiral. It is usually noninductively wound,
Fig. 2, so as to minimize the defocusing effect of the
magnetic field of the heating current. This is a very
simple, and cheap type of cathode to use. However, it is
inherently not able to produce as well focused a beam as
that produced by a unipotential cathode. The aberrations
in focusing are traceable to the following characteristics
of the filamentary cathode. At the high operating temper-
atures, it is not possible to keep the cathode from sagging
and becoming nonplanar. Since the trajectories of the
electrons are very sensitive to small changes in cathode
shape, this is a major source of trouble. In addition,
there are both electric and magnetic fields around the
cathode due to the heating current. These cause initial
deflections of the trajectories, that spoil the beam focusing.

Where it is important to combine the good focusing
properties of a unipotential cathode with the chemical
stability of a refractory metal, the bombarded tantalum
cathode can be used, Fig. 3. Although this is a somewhat
more complicated structure, and it requires an additional
bombarding power supply floating at the cathode potential
(10 to 30 kv) it has certain advantages. First since the
cathode geometry is well defined, good focusing can be

— Leads
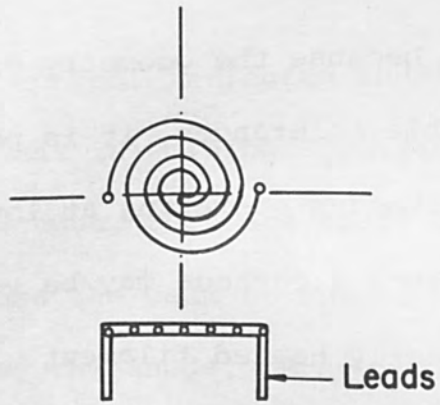
FIGURE 2. Bifilar (Noninductive) Directly
Heated Filament

Thin Wire
Supports

Bombarding Voltage

Tantalum Disc
Cathode

Anode

Beam
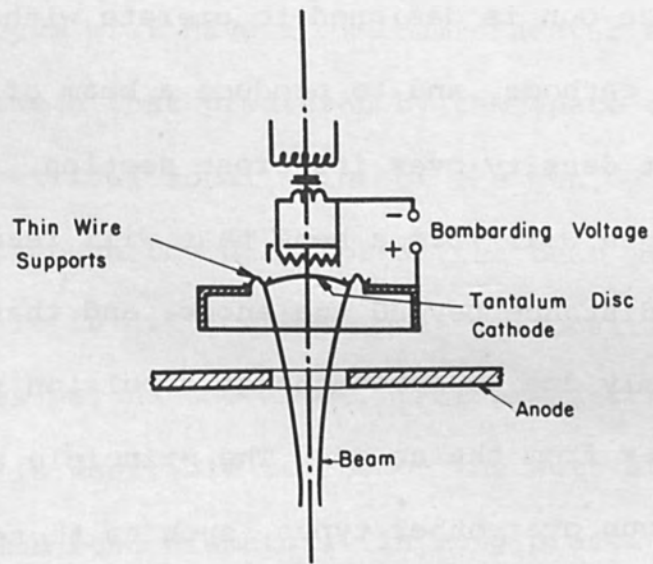
FIGURE 3. Bombarded Tantalum Cathode
Used in Electron Gun.

achieved. Second, because the geometry of the system can be held to reasonable tolerances, it is possible to use relatively large cathodes operating at low current densities. Thus, the life of such a cathode may be very much longer than that of a directly heated filament.

Gun Design

As indicated in Fig. 1, the gun is required to form an electron beam, and pass it through a hole in the anode into the field-free region beyond. One of the most satisfactory and straightforward methods of designing efficient guns of this general type is due to Pierce.[2] The so-called Pierce Gun is designed to operate with a space-charge-limited cathode, and to produce a beam of essentially uniform current density over its cross section. If properly designed, the gun will form a beam that will reach a minimum diameter some distance beyond the anode, and that will then diverge uniformly due to space-charge repulsion forces as it moves farther from the anode. The principle advantage of the Pierce gun over other types, such as those used in cathode ray tubes or electron microscopes, is its efficiency. More than 99.9% of the emitted cathode current can be focused through the anode aperture, in a reasonably well designed Pierce gun.

The beam contour indicated in Fig. 1 is probably and unrealizable ideal in welding applications. If the beam were in a perfect vacuum, then the space charge fields of the electrons would cause the beam to spread apart as it drifted in the region beyond the anode. Practically, however, the beam will produce ions at a rate proportional to the ambient pressure in the chamber. The positive ions will help to neutralize the space charge fields of the beam. As a result, the beam contour beyond the anode may not be predicted with any great accuracy, unless the current is so small that space charge forces are unimportant in the first place. In any event, the beam will have a minimum diameter at some axial position between that predicted by the space charge theory, and the geometrical focal point of the gun.

Although the diameter at the beam minimum may be very small, it is difficult to push its position more than 2 or 3 inches beyond the anode. For greatest thermal effectiveness, it is desirable to locate the work at the position of the minimum beam diameter. In many practical systems it is inconvenient to place the gun so close to the work, and it is desirable to focus the beam at a point 10 to 12 inches away. This must be done by the use of auxiliary lenses, Fig. 4. [2][3][4] There does not seem to be any pressing theoretical advantage on the side of either the electric or

19

magnetic lenses. It is possible to make lenses of comparable focal length of either type. There are a number of practical problems that must be considered in making a choice. The magnetic lens must dissipate the I^2R power of the current flowing through its windings. In addition it is heated by radiation from the hot spot on the work, only a few inches below it. Therefore, it may be necessary to water cool the lens in systems likely to be operated for extended periods of time. The electric lens dissipates no power, and since it can be made of high melting point metals, it needs no cooling. On the other hand, unless they are carefully shielded, the insulators may get coated with evaporated metal from the work. More important, however, is the fact that the required focusing voltage may be a sizable fraction of the total accelerating voltage. Thus, a variable voltage source for 10 to 20 kv and a capacity of about 1/10 of the beam current is needed. In addition, however, if the material being welded or heated is liable to give off bursts of gas, this may cause a breakdown in the electric lens. On balance, none of the problems associated with the two lens types is of over-riding importance, except the last; and for this reason magnetic lenses tend to be favored somewhat.

Although permanent magnet lenses have found some use in cathode ray tubes and electron microscopes, they have

not yet appeared in electron beam welders. This may be due partly to the relative inconvenience of having to vary the focal length of the lens by moving a magnetic shunt, from outside the vacuum. In addition, where the magnet may be exposed for long periods to intense heat from the work, it may have to be water cooled to prevent demagnetization due to overheating.

Limitations on Spot Size

There are many factors that can introduce aberrations into the focusing action of an electron gun, and therefore increase the minimum beam diameter. Mechanical errors in construction and stray electric and magnetic fields are the worst offenders. However, these sources of error can be eliminated, at least in principle. If one had an "ideal" gun, the minimum diameter of the beam beyond the anode would be determined by two basic phenomena. One is the mutual electrostatic repulsion between the electrons of the beam, the other is the random velocity with which the electrons are emitted from the cathode.

In designing an electron gun, it is common to assume that the electrons are emitted from the cathode with no initial energy. From a real cathode, they are emitted with a random kinetic energy whose magnitude is proportional to the absolute cathode temperature T_c. Since the initial velocity is random

21

both in magnitude and direction, the trajectory of an electron emitted from a certain spot on the cathode will deviate from that of the ideal, zero temperature case. This problem has been studied in detail by Danielson, Rosenfeld, and Saloom[5], and extensive numerical data are presented in the reference. It is difficult to summarize the results in any quantitative way except to make the following general comments. The minimum beam diameter (one that includes 95% of the current) will generally be about twice the size computed on the basis of a "cold" cathode. The minimum beam diameter is related to the cathode diameter. The latter is determined by the required beam current, and the current density capability of the emitter used as a cathode. Thus, if a practical cathode material could be found that would operate reliably at 10 amps/cm^2 instead, say, of 1 amps/cm^2, its linear dimensions could be reduced by about 3, and so could the diameter of the spot.

Another point of importance is the relation between compression ratio =(cathode area)/(min. beam area) and the position of the minimum beyond the anode. This is best illustrated by Fig. 5 in which the minimum beam diameter and its distance from the anode (both normalized to the cathode radius r_c) are plotted for a gun operating at perveance $I/V^{3/2} = 10^{-7}$ (at 20 kv the current is .280 amp, and the power is 5.6 kw).
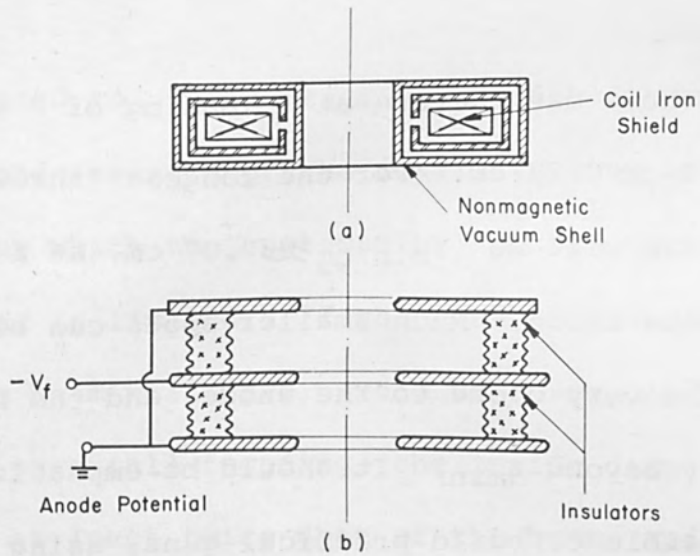
FIGURE 4. a) Hermetically Sealed Magnetic Lens.
b) Unipotential (Einzel) Lens.
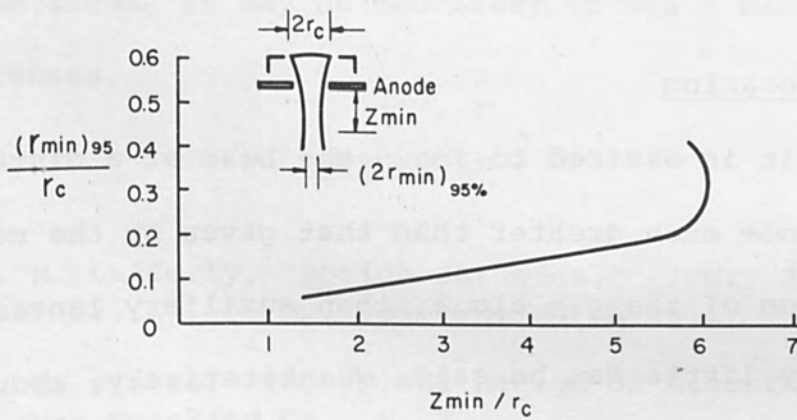
FIGURE 5. Relation Between Minimum Beam Diameter
And its Location for a Perveance 10^{-7} Gun
Having a 2000°k Unipotential Cathode.

Thus if the cathode can operate at a loading of 2 amps/cm^2 its radius is $r_c \approx 0.25$ cm. For the longest "throw" the minimum spot size will be $(r_{min})_{95} \approx .07$ cm, at a point 1.5 cm beyond the anode. Much smaller spots can be produced but they will be very close to the anode, and the beam will diverge rapidly beyond z_{min}. It should be emphasized here that it is possible to build practical guns, using uni-potential cathodes, whose performance comes very close to these calculations. However, this is possible only if mechanical tolerances are very closely controlled, and guns using filamentary cathodes will produce much more diffuse beams.

Refocusing

If it is desired to focus the beam at a distance beyond the anode much greater than that given by the natural focusing action of the gun alone, then auxiliary lenses must be used. Very little can be said, quantitatively, about the lens design. The quality of the "image" is directly related to that of the object. Usually the lens is adjusted to produce an image on the work of the first beam minimum. If there is a big velocity spread in the first minimum, the image will not be well focused due to "chromatic" aberrations in the lens. Similarly, since the presence of positive ions may drastically modify the beam trajectory beyond the first minimum,

24

one is forced to use empirical means for determining the position and strength of the auxiliary lens or lenses. The distance by which the spot can be "pushed forward" by a single lens is limited. If the lens is placed far from the anode, the beam will have spread to a very large diameter. For good (paraxial) focusing, the inside diameter of the lens should be at least twice that of the beam, and thus inconveniently large lenses may be required. (Because we are interested in overall efficiency, we cannot intercept the outer portions of the beam by a mask or iris as one commonly does in visible optics.) If the beam is to be projected some distance beyond the gun anode, it may be necessary to use a cascade of two or more lenses.

REFERENCES

1. J. M. Lafferty, "Boride Cathodes," Jour. Appl. Phys., Vol. 22, No. 3, pp. 299-309, March 1951.

2. J. R. Pierce, "Theory and Design of Electron Beams," D. Van Nostrand Co., N. Y.

3. O. Klemperer, "Electron Optics," (book) Cambridge University Press, 1953.

4. K. Spangenberg, "Vacuum Tubes," (book) McGraw-Hill Co., N. Y.

5. W.E. Danielson, J. L. Rosenfeld, and J. A. Saloom, "A Detailed Analysis of Beam Formation with Electron Guns of the Pierce Type," Bell System Tech. Jour., Vol. 35, No. 2, March 1956.

ELECTRON GUN DESIGN AND CATHODE LIMITATIONS

By

John R. Morley
Senior Project Engineer
High Voltage Engineering Corporation
Burlington, Massachusetts

ABSTRACT

With the wide interest, both in industry and
research, in electron beam equipment, the production and
focusing of electron beams has assumed some importance.
In the present paper, the parameters affecting cathode
operation and life under various conditions will be out-
lined and practical data presented.

Some of the fundamental properties of electron
gun design and electron beam handling and measurement to-
gether with practical data from both telefocus and gradient
focusing systems will be given.

ELECTRON GUN DESIGN AND CATHODE LIMITATIONS

Introduction

Most users of electron beam equipment will agree that the desirable cathode is one which requires the minimum amount of attention for the maximum length of time. From the design viewpoint, a small easily constructed high current density cathode having a minimum power input is likewise the ideal.

In practice, it is not possible simultaneously to translate all these factors into the ideal cathode, and hence cathode limitations exist.

Before considering the design of electron guns, let us first consider the cathodes which may be used in such structures since these in turn may modify the design.

Of the many questions asked about cathodes, the most frequent and also the most difficult to answer with any degree of certainty are: "Does it work?" "How long will it last?" "How much emission current is available?"

This paper attempts to answer these leading questions in some degree.

Cathode Limitations

Let us begin by examining the conditions under which the cathode must operate within beam welding or melting equipment or under any adverse conditions not encountered in conventional outgassed or sealed off structures.

In typical electron beam equipment, the operating pressure at the cathode will be in the range of 10^{-3} to 10^{-5} mm Hg. depending upon the work being done. The outgassing rate of the material being welded or melted, the use or otherwise of differential pumping, the speed of the vacuum pump and the geometry of the system all affect the working vacuum. The condition in

beam melters is more severe than in the case of welders, due to the larger amounts of gas released from the work. The composition of the residual gases will also vary according to the work being carried out, but in most cases, we may reasonably expect to find oxygen, nitrogen, and water vapor and perhaps carbon dioxide as well.

When the beam current is thermally controlled, the temperature of the cathode must increase as the current increases. If the cathode is operated in the space charged limited condition - that is, the beam current is controlled by a negatively biased electrode in front of the cathode which allows only a fraction of the saturated emission current to flow - then the cathode temperature should remain constant. In fact, electron collision with gas molecules produces positive ions which return to the cathode and raise its temperature, though little or no increase in beam current will be seen. Furthermore, this increase of cathode temperature will not be constant, but will vary with the beam current, the gas pressure, and the particular operating voltage of the electron gun.

These two conditions - the vacuum level and the temperature variation of the cathode, set the first limitations on the selection of a suitable cathode material, and it will be seen later that this eliminates many otherwise excellent cathodes.

A great variety of cathodes are available, ranging from the complex dispenser cathode to the hot tungsten filament. The characteristics of these cathodes vary from high current density, low temperature, as in the case of the dispenser cathodes, to the low current density, high temperature for the refractory metals; but more important than this is the vacuum level at which they will have to function. The dispenser cathode dispenses barium

metal through the pores of a tungsten plug and relies upon an excess of barium atoms at the surface for its emission properties. At the operating temperature the reaction between barium and oxygen is very rapid, and if the oxygen content of the residual gas with the system is in excess of the amount required to convert all the barium into barium oxide, only a very small fraction of the emission current will be available.

Figure 1 shows the effect of this oxidation for a 20% porous cathode. At the point where the emission current falls to a low value, the removal of barium atoms by oxidation from the cathode surface just exceeds the rate of their arrival at the surface. Table I reviews a variety of cathodes and shows the vacuum level at which they will just operate.

This table shows the severe restriction upon the choice of cathode which the vacuum level imposes, and, without resorting to methods of improving the vacuum, the choice is restricted to the refractory metals, or to these metals with suitable coatings applied to them.

Refractory Metal Cathodes

Since we have eliminated the cathodes which will not function at all at these pressure levels, let us now examine the properties and limitations of the refractory metal group.

For the refractory metal cathodes, the saturated emission current available may be calculated for practical cases from the Richardson equation, as modified by Dushman.* This is shown in fig. 2. This equation allows the calculation of the surface area required for a filament to provide the necessary emission current at a given temperature. The stage has now been reached

---

* $I_s = AT^2 E^{\frac{-e\phi}{kT}}$

TABLE I

CATHODE PROPERTIES

Cathode	Emission Amps/cm^2	Operating Temp. $^{\circ}$C	Work Function eV	Upper Pressure Limit For Operation, mm Hg.
Tungsten	0.6	2200	4.55	$\sim 10^{-4}$
Tantalum	0.5	2000	4.1	$\sim 10^{-5}$
Rhenium	0.2	2200	4.8	$\sim 10^{-4}$
Tungsten-Thoria	1-3	1750	2.6	$\sim 5 \times 10^{-6}$
Oxide-Coated	0.5	830	1.2	$\sim 10^{-6}$
Dispenser	0.5-10	960-1130	1.5-2.0	$\sim 5 \times 10^{-6}$

TABLE 2

RELATIVE LIFE DATA FOR REFRACTORY METALS AND COATED FILAMENTS

Material	Relative Life
.030 Ta	100
.030 Ta + NbC	130
.015W + NbC	370
.015W	425
.015W + ZrC	426
.020W + ThO$_2$	490
.020W + NbC	665
.020W	685

(at 1.35×10^{-4} mm Hg. and 100 ma. emission.)

30

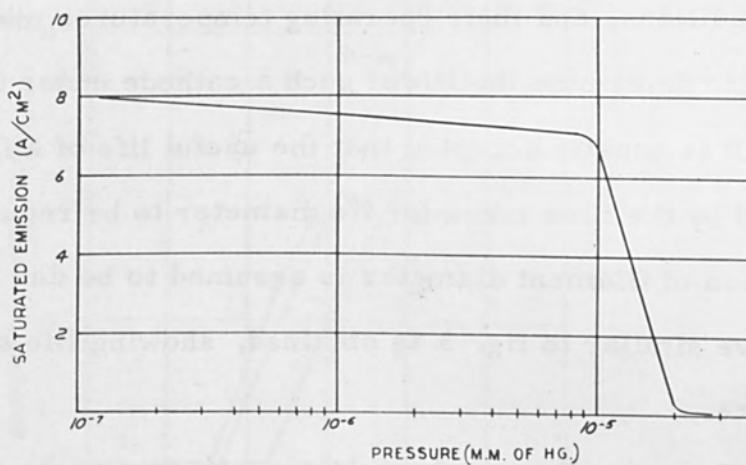# SATURATED EMISSION FOR A 20% POROUS CATHODE

FIG. 1

SATURATED CURRENT vs TEMPERATURE
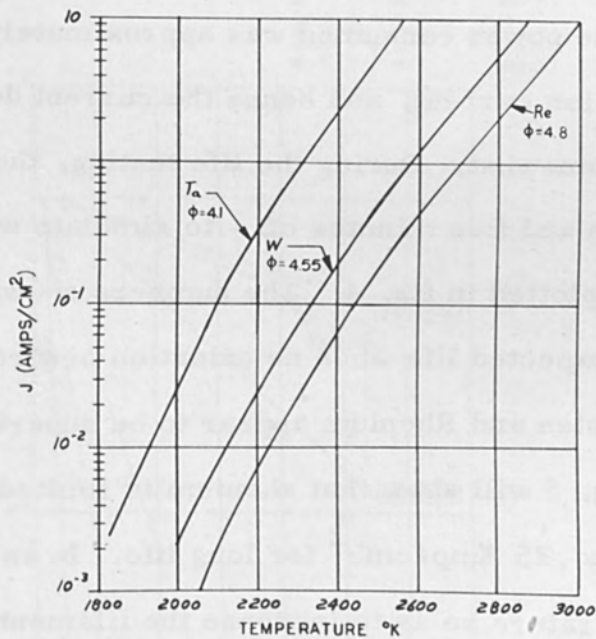# FOR VARIOUS WORK FUNCTIONS

FIG. 2

where a few materials have been found suitable for operation in these poor vacuum conditions, and their operating temperatures may be calculated. It remains to determine the life of such a cathode under these conditions.

It is usually accepted that the useful life of a filament is determined by the time taken for its diameter to be reduced by 10%. If the reduction of filament diameter is assumed to be due to evaporation only, then a curve similar to fig. 3 is obtained, showing life as a function of temperature.

However, these values do not take into account the considerable amount of refractory metal which will be removed by oxidation. In practice at the vacuum levels found in electron beam equipments, oxidation is the dominant factor in reducing the filament diameter and hence of cathode life. An experiment was made on some refractory metal filaments at various vacuum levels to obtain life data. The diameter of the materials selected was such that the power consumed was approximately the same for a given saturated emission current, and hence the current densities for each filament vary somewhat. During the life testing, the filaments were cycled - ten minutes on and five minutes off - to simulate working conditions. These data are plotted in fig. 4. The numbers shown at the end of each curve give the expected life when no oxidation occurs.

Tungsten and Rhenium appear to be superior to tantalum, but inspection of fig. 5 will show that rhenium is limited to an emission current of approximately .25 Amp/cm.^{2} for long life. In an attempt to lower the operating temperature so as to increase the filament life, refractory metal filaments were cataphoretically coated with low work function compounds such as columbium carbide. Table 2 shows the results of such a test, but it may be seen that no improvement in life was obtained.

EVAPORATION RATE FOR METALS

FIG. 3
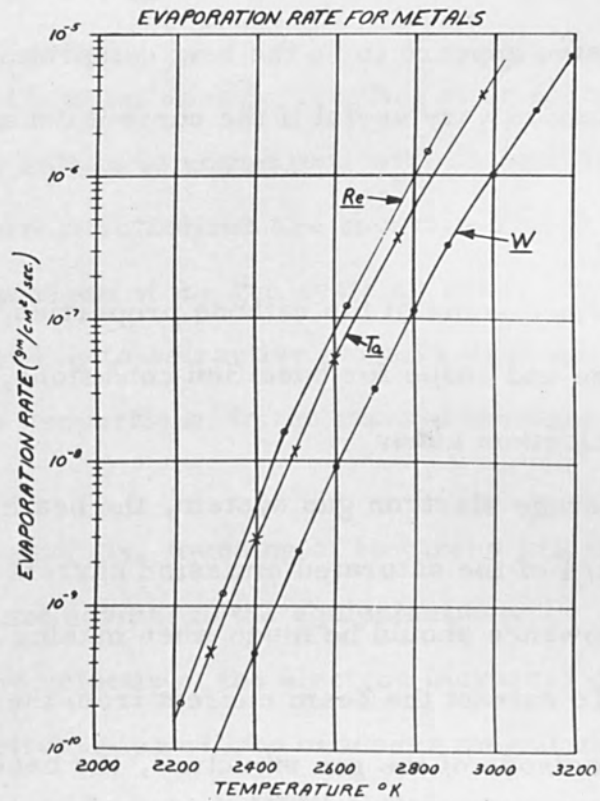
LIFE OF REFRACTORY METAL FILAMENTS

1).030 DIA. TA. 10 MA. EMISSION (.167 A/CM²)
2) "   "   100 "   "   (1.67 ")
3).020 " W 10 "   "   (.1 ")
4) "   "   100 "   "   (1 ")
5).025 " RE 10 "   "   (.139 ")
6) "   "   100 "   "   (1.39 ")
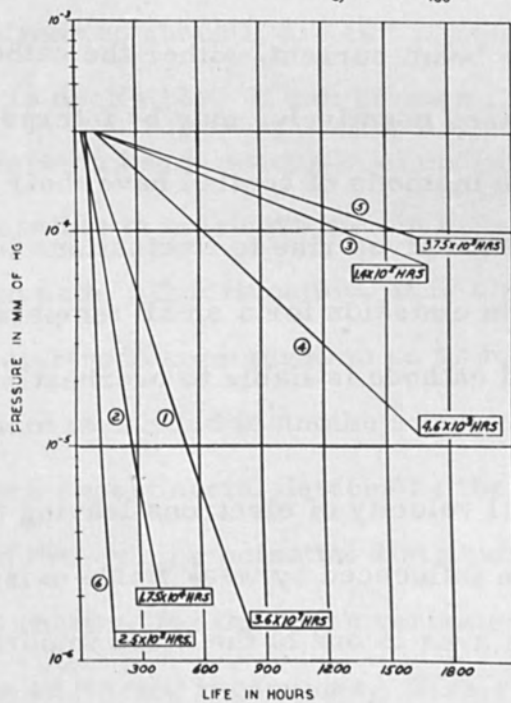
FIG. 4

Thus tungsten appears to be the best compromise for poor vacuum operation, and rhenium is very useful if the current density requirements are modest.

Electron Gun Design

Having defined some of the cathode properties, it is now possible to calculate their size and shape for specified conditions, and to consider their application to electron guns.

For an average electron gun system, the beam current is approximately 1/3 to 1/4 of the saturated emission current available from the cathode, and due allowance should be made when making life calculations for the filaments. To extract the beam current from the cathode through the first accelerating electrode of the gun structure, the necessary space charge limiting voltage may be calculated from the distance, $V \propto z^{4/3}$. This potential, or more accurately, the minimum electrical gradient in front of the cathode, must be maintained to allow the full beam current to be extracted.

To control the beam current, either the cathode may be thermally controlled, or a grid biased negatively, may be interposed between the cathode and anode. Both methods of control have their attendant disadvantages. The thermal method gives rise to fluctuations in the beam current due to the large change in emission for a small temperature variation, while the space charge limited cathode is liable to overheating and to a subsequently shorter life.

As the thermal velocity of electrons leaving the cathode is very low, they may readily be influenced by weak fields existing near the cathode and for this reason, this area is one of the more important regions of an electron gun.

34

For a qualitative understanding of an electron-optical system it is sometimes helpful to compare it with an equivalent light optical system. [1] Comparative refractive indices are shown in Fig. 6.

Comparison of the two systems shows that the quantity in electron optics corresponding to refractive index in light optics is electron velocity, which in turn is proportional to the ratio of the square roots of the initial and final potentials.

Consequently, focusing of electrons will take place if the path of the electron is not normal to the equipotentials.

As the velocity of the electron increases due to acceleration, the effective refractive index will be of lesser magnitude, and the focusing effect at the higher energies will be less for a given potential difference.

An electron leaving a cathode surface @ $2000^{\circ}C$ has an energy of about .2 eV. If this electron is accelerated through 100 volts, the refractive index is about 20. If a further 100 volt acceleration takes place, the refractive index drops to about 1.4. At 5 kilovolts, the change due to a further 100 volts is negligible. It can be seen, therefore, that the maximum effect upon the electron beam occurs in close proximity to the cathode.

It is possible to calculate the equipotential requirements to produce a given beam path. Unfortunately, it is almost impossible to relate this to an actual electrode configuration so as to produce the required beam. Usually the problem is tackled in another way, the equipotentials being determined by such experimental devices as the electrolytic trough, and the rays being traced through the potential distribution. Even this is only an approximation to reality, for the other variables, such as space charge, require elaborate additional techniques. This system then examines only one

LIFE OF RHENIUM vs EMISSION

(.025 DIA, 1.4 x 10⁻⁴ MM Hg)

FIG. 5

COMPARISON OF OPTICAL SYSTEMS

Light Optical	Electron Optical

$n_1 \sin i = n_2 \sin r$

$\mu = \dfrac{\sin i}{\sin r} = \dfrac{n_2}{n_1}$

μ (typical) = 1 to 2

$v_1 \sin i = v_2 \sin r$

$\mu = \dfrac{\sin i}{\sin r} = \dfrac{v_2}{v_1} = \dfrac{\sqrt{2V_2 \frac{e}{m}}}{\sqrt{2V_1 \frac{e}{m}}} = \dfrac{\sqrt{V_2}}{\sqrt{V_1}}$

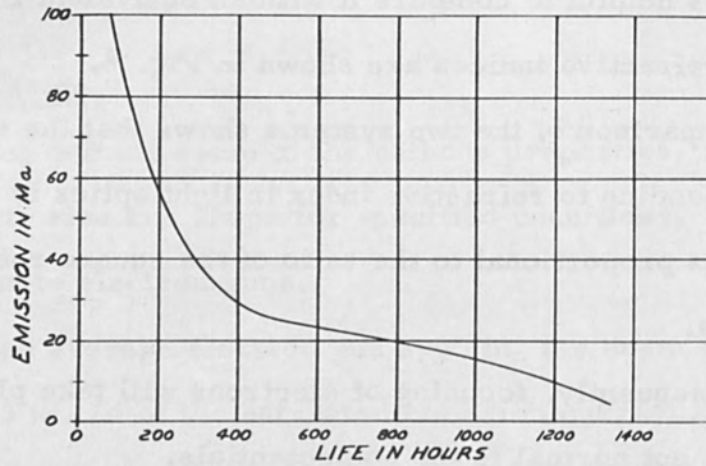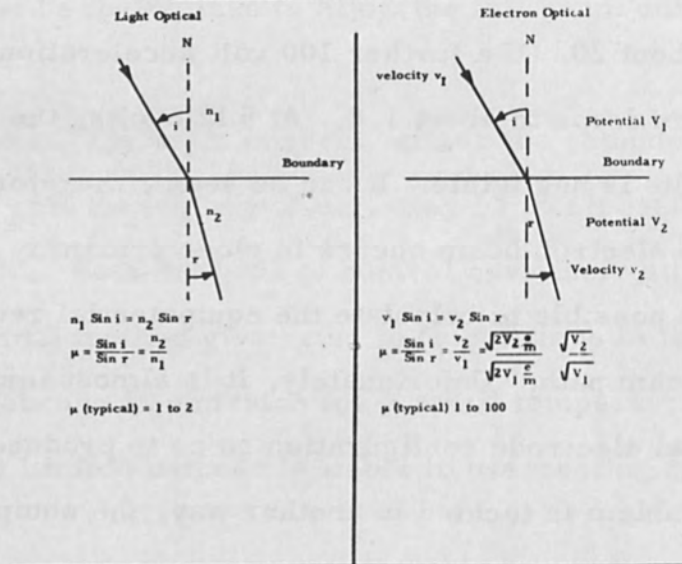μ (typical) 1 to 100

Figure 6

particular geometry at one time, perhaps with various potentials applied to the electrodes, and allows computation of the beam. Since a variety of electrode shapes produce similar beams, one might just as well construct one or two basic types of electron guns, measure the actual beam properties, and modify these according to the results found.

The general handling of electron beams therefore becomes important, and closer inspection of some gun types will help to clarify the situation.

In the telefocus system,[2] fig. 7, the fundamental reason for the long focus effect is that the equipotential lines are concave towards the cathode due to the hollow shape and negative bias of the Wehnelt[3] electrode. Consequently, electrons starting from the cathode are given a radial outward velocity and the beam begins to diverge. Between the Wehnelt[3] electrode and the anode the equipotentials first become flat and then convex towards the cathode. The beam therefore is given radial inward velocity, but of lesser magnitude due to the higher energy of the electrons. Consequently, the beam converges quite slowly and has a long focal length. The focal length is adjustable by changing the bias. More bias increases the focal length, by increasing the curvature of the equipotentials in the cathode region, thereby starting the beam with more divergence. This also has the effect of reducing the beam current. A further disadvantage of the long focal length system is that the repulsive space charge forces enlarge the beam over a longer length than the equivalent short focus system, and consequently this type of gun is limited in spot size by the beam current. With increase of beam current the abberations produced in the low gradient cathode area also increase and the quality of the beam deteriorates, even when auxiliary magnetic focusing is used.

WEHNELT ELECTRODE

ANODE
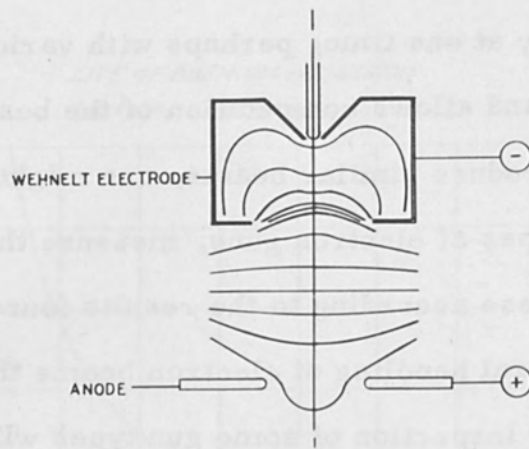
TELEFOCUS SYSTEM

FIG. 7

MINIMUM BEAM DIAMETER AS A FUNCTION OF BEAM CURRENT

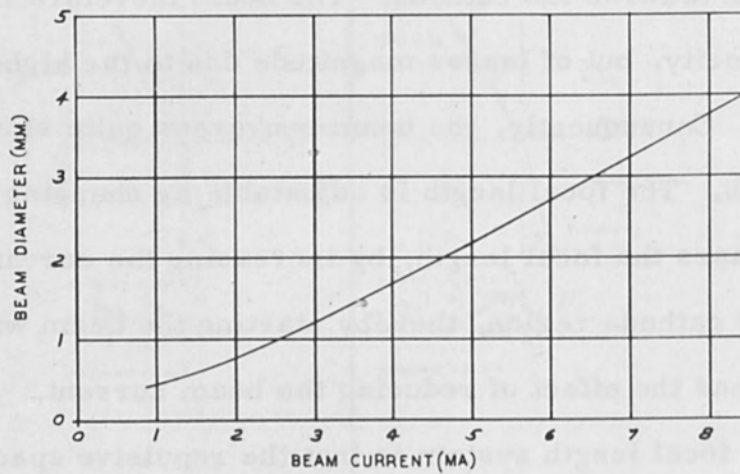
FIG. 8

Spot sizes down to approx. .010" at a few μa are obtained, with power densities of a few $KW/cm.^2$. Figure 8 shows the minimum beam diameter as a function of current at 25 kilovolts and with magnetic focusing.

To overcome these shortcomings, a second gun was built for operation within the range of 25-100 KV at several milliamperes and is shown in Fig. 9.

In this system a triode gun provides the initial acceleration to approximately 10 KV, the further increase of energy being provided by the gradient system.

It can easily be seen that the major effect on the beam shaping occurs within the triode structure where the refractive index is about 250. Since, with further acceleration of the beam from 10 to 100 kilovolts through the gradient lens system, the refractive index is approximately 1/80th of that of the triode, the final beam energy may be varied over a wide range with only a small effect upon its size.

The final spot size is a function of the ratio of the anode voltage to the first acceleration tube voltage, and this is shown in Fig. 10.

It will be noticed that a small ratio produces a smaller spot size, but continual reduction of V_1 will also reduce the beam current available. However, the larger beam produced by a high extraction voltage can be focused to a smaller diameter by an electromagnetic lens, positioned at the base of the accelerating tube.

As an alternate to this, high beam currents may be obtained by reducing the cathode/anode spacing, thus maintaining the gradient at low V_1 permitting more beam current to flow. A compromise must be made at this point between the operating voltage range, the $\dfrac{V_1}{V_2}$ ratio, and according to the beam current for which the gun is to be used.
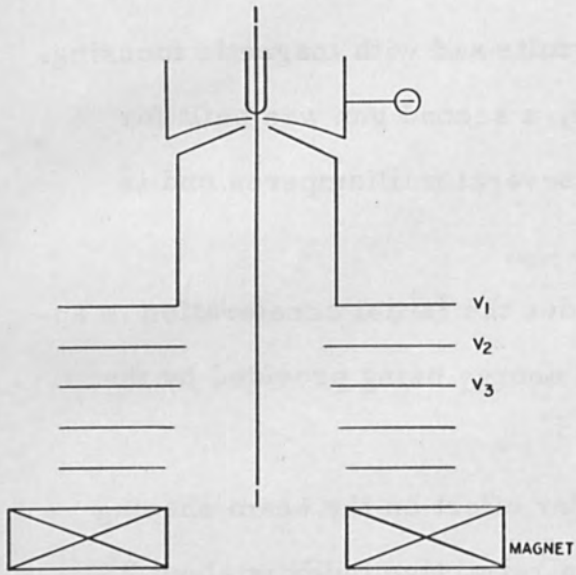
GRADIENT SYSTEM

FIG. 9

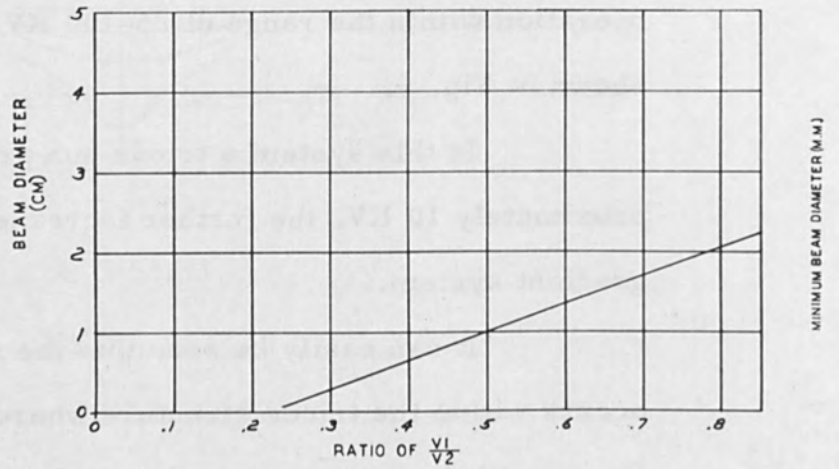THE EFFECT OF $\frac{V1}{V2}$ ON BEAM DIAMETER

FIG.10

POWER DENSITY & MINIMUM BEAM DIAMETER

	BEAM DIAMETER FOR 100 VOLT BIAS
1)	" " " 100 VOLT BIAS
2)	" " " 270 " "
3)	POWER DENSITY " 100 " "
4)	" " " 270 " "

FIG 11

40
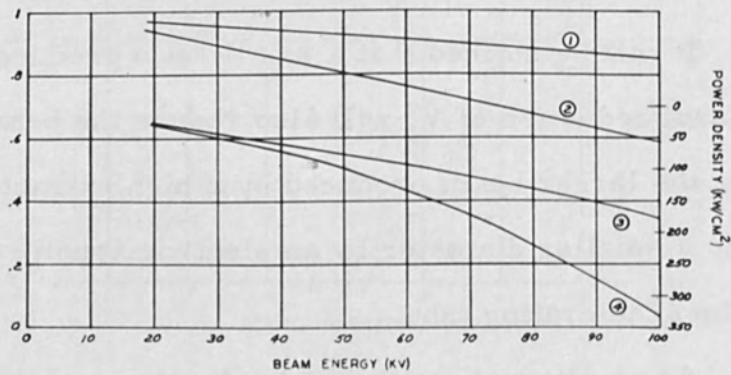
In this particular electron gun, approximately 10 ma. of current were required at voltages from 20 KV to 100 KV. Figure 11 shows the beam diameters obtained 35 cms. from the base of the magnet for two different bias values. By adjustment of V_1 the beam current was maintained at 10 ma. over the entire beam energy range. The final focusing was done with the electromagnet.

The power density curves for the beam are also shown in fig. 11 and are computed from the total beam current. At 100 KV the maximum power density is 330 KW/cm^2 or 2.13 MW/in^2, but because the current distribution within the beam is gaussian, the power density will be considerably higher at the center of the beam than the figures given.

REFERENCES

1. Jacob L., An Introduction to Electron Optics
   J. Wiley & Sons N.Y. 1951, p.7

2. Steigerwald, K. H. Optik 5 469 1949

3. Wehnelt A. & Jentsch F. Ann Phys., Lpz 28, 541 1909

GENERAL REFERENCES

1. Moss H. Electron Gun of the Cathode Ray Tube Part I
   Jnl. Brit. I. R. E. Dec. 1945 and Engineering Methods in the
   Design of the Cathode Ray Tube.

2. Klemperer O. Electron Optics Second Edition
   University Press, Cambridge, Eng. 1953.

3. Spangenberg K. R. Vacuum Tubes Second Edition
   McGraw-Hill, N.Y. 1948.

SOME ASPECTS OF ELECTRON GUN DESIGN FOR WELDING

By

M. H. Hablanian
Chief Development Engineer
NRC Equipment Corporation
Newton, Massachusetts

ABSTRACT

Design of electron sources for metallurgical work
presents problems not usually encountered in more convention-
al applications. This paper discusses design considerations
for pure metal electron emitters of Pierce type and their
comparison to simpler filament emitting systems.

Performance of an electron gun (few kw at 20 kv)
using an indirectly heated replaceable concave tantalum
cathode are described.

SOME ASPECTS OF ELECTRON GUN DESIGN FOR WELDING

INTRODUCTION

In the process of electron beam welding two distinct modes of fusion zone geometry may be obtained. One may be called a shallow mode with a bead formation similar to arc welding, the other a deep mode where depth to width ratios exceed approximately 2:1. As shown in Fig. 1 a transition region is also possible.

All three fusion zone types can be obtained at the same power and speed by selecting current and voltage combinations or simply by changing the degree of focusing of the electron beam.

The deep penetration of the beam into the material is difficult to explain without postulating formation of a cavity under the beam permitting "depth heating". Actually such cavities can be easily observed under certain conditions, for example when welding materials with sufficiently low melting points (such as magnesium) so that the glare from the molten pool does not obstruct the vision.

Suggestion has been made that the formation of the cavity was due to the vaporization of the material [1] and that higher voltages were primarily responsible due to higher electron velocities obtained [2].
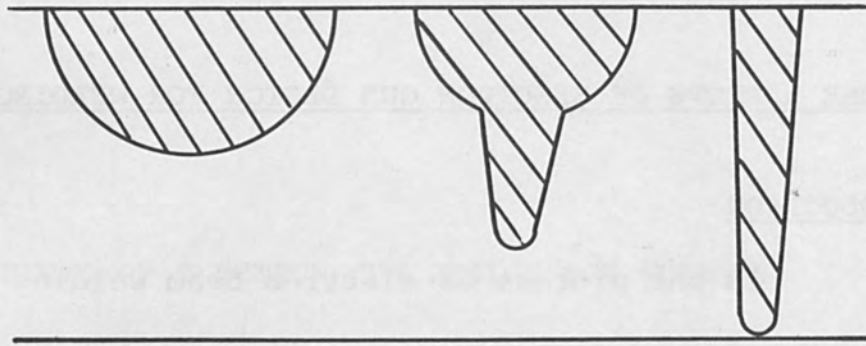
Figure 1. Typical electron beam weld cross sections
obtained at the same power and speed.
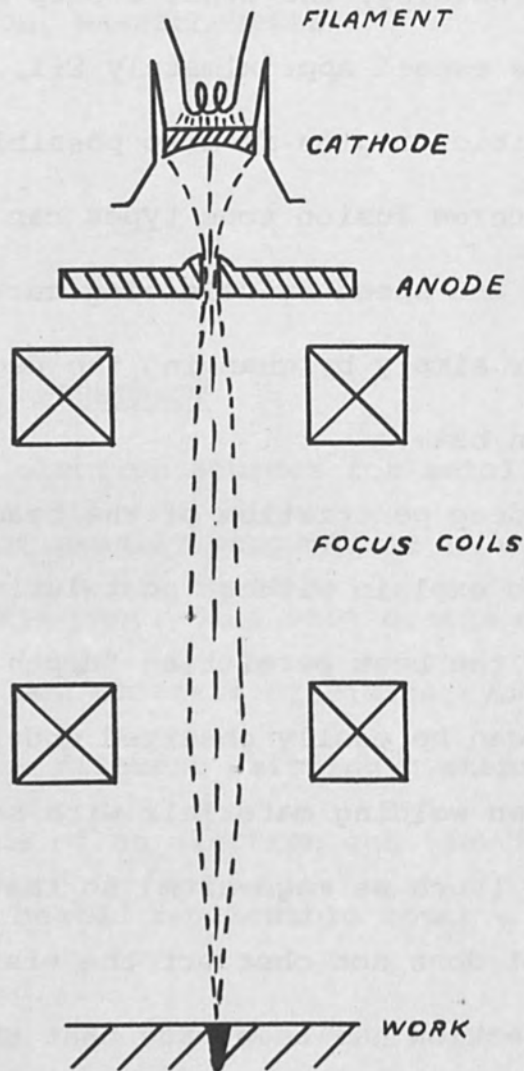
Figure 2. Schematic diagram of the experimental
Pierce type gun.

Actually it should be possible using extremely high power densities to vaporize a hole with little melting of the surrounding material. However it is questionable whether such operation is practical for the welding application since excessive evaporation can cause serious weld porosity.

The possibility of obtaining sufficiently high power densities for deep welding at relatively low voltages (20 kv) has been mentioned by E. Franco-Ferreira during the discussion of electron beam welding a year ago [2].

THE EFFECT OF BEAM PRESSURE

The exact description of the electron beam welding process when deep welds are obtained may be not simple. However, as shown below the pressure of the beam can have a very significant effect. Dr. E. B. Bas (Swiss Federal Institute of Technology in Zurich) was apparently first to note that there may be a considerable force involved due to the impact of electrons on the workpiece during welding and that the pressure of the beam is actually greater for lower accelerating voltages if the power density is the same [3]. The reason is simple - the pressure is proportional to the change of momentum of electrons which

is linear with velocity and linear with mass. However the velocity is only proportional to the square root of the accelerating voltage so that with lower voltage and same power density the effect of higher current (larger number of electrons) dominates the effect of decreased velocity. The relativistic mass increase at velocities considered here is not high enough to upset this advantage.

The pressure produced by the beam when it is stopped by the workpiece can be expressed as

$$p = n\,m\,v$$

where $\underline{n}$ is the number of electrons striking the target per unit time and per unit area, $\underline{m}$ is the mass of an electron (9.1×10^{-28} gr), $\underline{v}$ the velocity of the electrons in the beam and $\underline{mv}$ is the momentum change of a single electron assuming the final velocity to be zero.

Following substitutions can be made for $\underline{n}$ and $\underline{v}$:

$$n = \frac{a}{e}\ \frac{w/V}{e} \quad \text{and} \quad v = \sqrt{\frac{2e\ V}{m}}$$

where $\underline{a}$ is the current density in the focused spot, $\underline{e}$ is the electron charge (1.6×10^{-12} ergs per volt), $\underline{w}$ is the power density and V the accelerating voltage.

The expression for pressure can now be rewritten as

$$p = a\ \sqrt{\frac{2mV}{e}}\ =\ w\ \sqrt{\frac{2m}{eV}}$$

As an example, using $w = 15$ kw/mm^2 and $V = 20$ kv, $p = 4$ gr/cm^2 approximately; with $w = 50$ kw/mm^2 and $V = 100$ kv, $p = 5$ gr/cm^2.

As will be shown below the assumed power densities are not unrealistic and they can be twice as high in the center of the beam where the density is usually higher.

It can be easily ascertained that the calculated pressure is sufficient to depress the surface of a molten metal by noticing for example that the hydrostatic pressure of a half inch high liquid steel column is approximately 10 gm/cm^2. The effect can also be demonstrated by directing a small jet of air on the surface of liquid mercury although the analogy is not exact. For example a glass nozzle with an orifice of about 0.010" calibrated by adjusting the inlet air pressure (about 5 psig) to give a force of 0.1 gr will produce a conical depression more than 1/4" deep and about 1/16" diameter when held above a pool of mercury. The pressure in this case is again in the order of 10 gr/cm^2.

The above, incidentally, may explain the difficulty to obtain a correlation between the power used for welding and the properties of the workpiece. As far as the beam characteristics are concerned, not only power and speed of welding are significant but also the degree of focusing of the beam or the power density and its distribution.

As far as material properties are concerned, not only the thermal conductivity, the melting point and the volume specific heat (pc) are important, but also the density itself and the surface tension. In addition the latter properties show considerable variation with temperature.

ELECTRON GUN DESIGN FOR WELDING

The assumption of the same power density in preceding section is of course unjustified since it is well known that it is easier to produce higher density at higher beam voltages. For lower voltage and consequently higher current larger electron emitting surface is required to obtain reasonable cathode life so that a well defined hairpin filament cannot be used. There are many other filament shapes possible but none are completely satisfactory for various reasons. Suffice it to say that it is very difficult to obtain a complete axial symmetry of electron emission from a wire wound filament cathode to produce a well defined uniform small beam spot.

Electron guns having axial symmetry and using a plane or concave surface cathodes are commonly called Pierce[4] type guns. There is reason to believe that very significant improvements in performance can be obtained by

using Pierce type guns at 15 to 25 kv to produce sufficient power densities for deep penetration welds.

The complete theory of designing such guns cannot be attempted here. Dr. R.E. Thun presented excellent papers on the subject at the symposium last year [5] and elsewhere [6]. Unfortunately his chosen cathode form (a wire filament) almost eliminated the advantages of curved electrodes and he reported a decrease of beam density at higher power, overheating of the anode and relatively high spot diameter. Following the practical design procedures from the last chapters of the book by Pierce [4] and Dr. Thun's papers mentioned above it should be possible to design an electron gun to produce a beam of few kilowatt power at 20 kv and focus it into a spot of about 1/64" diameter. It should be pointed out that those figures are by almost an order of magnitude below the calculated theoretical limitations.

EXPERIMENTAL RESULTS

A Pierce type gun as outlined above having a concave machined tantalum emitting surface has been built and its performance evaluated. The schematic drawing of the gun is shown in Fig. 2. The diameter of the cathode and its radius of curvature are approximately

1/4" and the anode aperture diameter about 0.1". The
overall dimensions are 2" dia. and 2.5" long exclusive
of the focus coils.

The tantalum cathode is heated by electron
bombardment from an auxiliary beam originating from a
tungsten filament placed behind the main cathode. Both
the filament and the tantalum button are replaceable. The
cathode heating power is obtained from an auxiliary power
supply (1200 v, 300 ma) and it is between 100 and 150 watt
during operation. Two electromagnetic lenses are used
to focus the beam. The experimental set up is such that
it is more convenient to place the focus coils inside the
vacuum chamber so that it is impossible to adjust their
position in operation. Despite this difficulty the beam
spot size is small enough to pass between two 1/2" high
steel plates placed 1/64" apart without heating either
piece.

The gun has been operated at voltages up to
25 kv (2.5% ripple) and currents up to 200 ma (limit of the
power supply) and its performance has been very close to
design expectations. Definite improvement in beam uniform-
ity and the size and reproducibility of its focal spot
have been observed compared to guns with filament cathodes.

Fig. 3 shows an example of a deep weld produced
with the new gun at 20 kv, 150 ma and 10 ipm on stainless
steel. The difference between the two photomicrographs is
due to light and heavy etching. To eliminate the additional
variable of part fit up the beam was traversed across a
solid plate instead of joining two plates together. No
chilling or clamping devices were used. Taking the greatest
width at the top surface the depth to width ratio of the
molten zone is 4:1, considering the average or mean width
the ratio is close to 8:1. The thickness of the plate
is 1/2".

Fig. 4 shows a similar weld done at 20 kv, 100
ma and 10 ipm. The material is again 1/2" thick stainless
steel.

Fig. 5 demonstrates that the phenomenon of deep
penetration occurs even at 10 kv. At the right is a butt
weld of 1/4" thick zircaloy and the left a weld through
the same thickness of stainless steel. Both welds were
made at only 10,000 volts, 100 ma and 10 ipm welding speed.
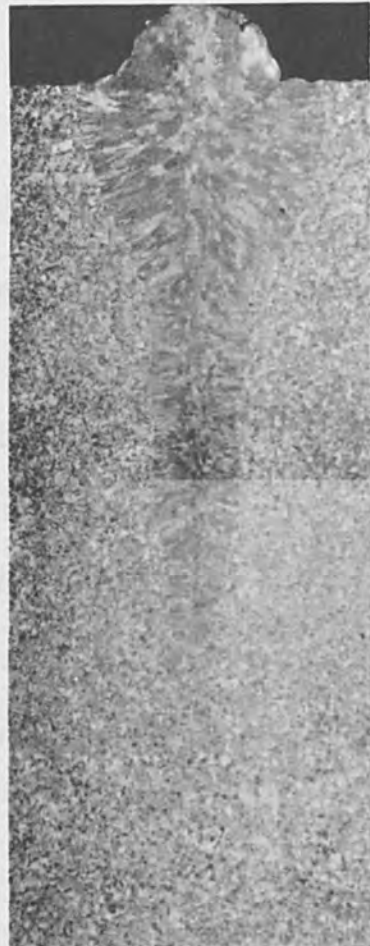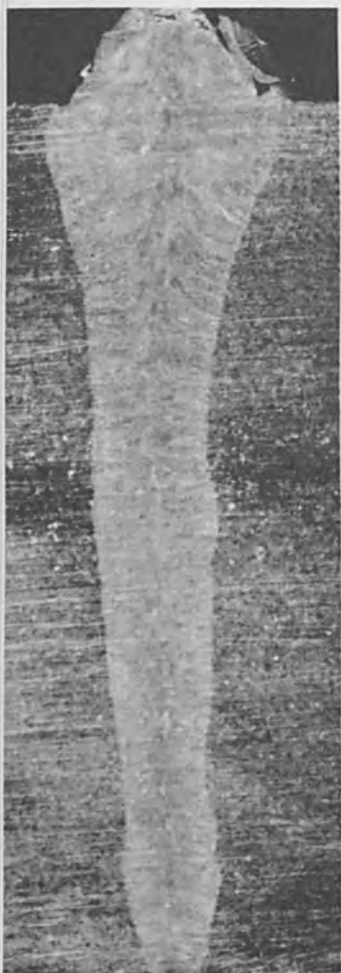
Figure 3. Photograph of weld cross section. Left-light etch, right-heavy etch. Material – stainless steel. Depth of weld 1/2". Conditions: 20,000 volts, 150 ma (3kw), 10 in/min.

Figure 4. Cross sectin of weld made at 20 kv, 100 ma, 10 in/min. Material: 1/2" thick stainless steel as seen on right portion of photograph.
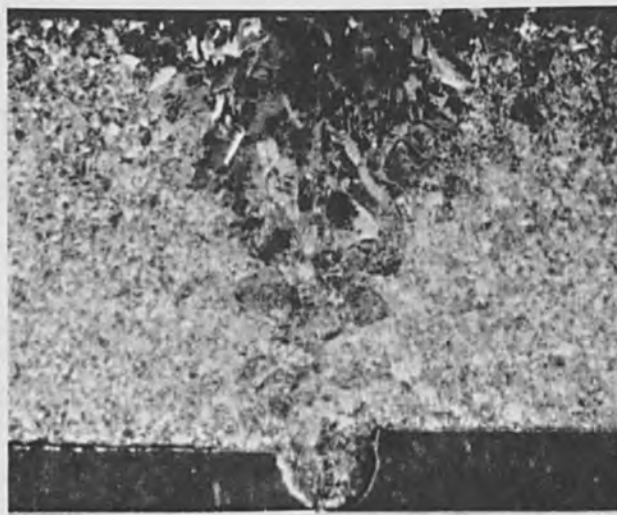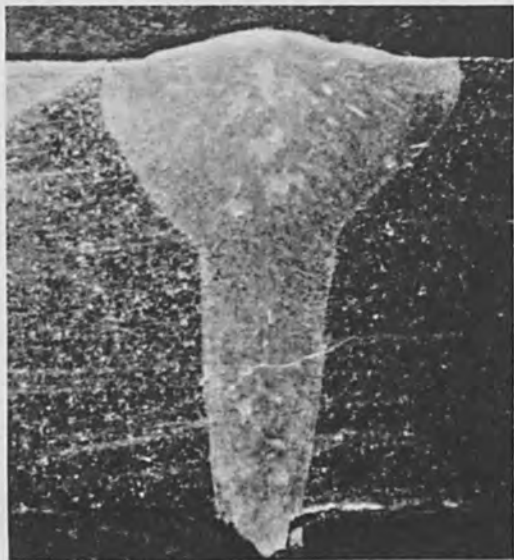
Figure 5. Cross sections of butt welds made at 10,000 volts, 100 ma and 10 in/min. Left: 1/4" thick stainless steel. Right: 1/4" thick zircaloy.

REFERENCES

1. Burton, G. and Frankhouser, W. L.,
   Welding J., 38 4015 (1959).

2. Second symposium on electron beam processes,
   Alloyd Corp. 1960. Discussion on welding. p. 131.

3. Bas, E.B. and Cremosnik, G., Vakuum-Technik, 7,
   p. 181-188. (1959)

4. Pierce, J.R., Theory and Design of Electron Beams,
   Van Nostrand, New York, 1954.

5. Thun, R.E., Second Symposium on electron beam
   processes, Alloyd Corp. 1960. p. 70.

6. Thun, R.E. and Ramsey, J.B., Vacuum Symposium
   Transactions 1959 p. 192 Pergamon, New York.

DISCUSSION

H. Schwarz
Hamilton Standard Division
United Aircraft Corporation

Mr. Hablanian points out that the electron pressure
is inversely proportional to the square root of the voltage,
if the power concentration is kept constant. This is mathe-
matically correct. But it seems to me that the speaker did
not consider the physics of electron beams which show that
it is impossible to maintain the power concentration $\frac{i\,U}{A}$
constant for all combinations of currents i,
voltages U, and workpiece areas A struck by the electrons
that fulfill his requirement.

The relations which exist between i, U, and A shown in the following make Mr. Hablanian's requirement of constant power concentration unrealistic for any electron beam equipment, no matter how well its electron optics has been designed. The power concentration, D, contains three variables, beam current i, voltage U, and the workpiece area A which is struck by a steady electron beam. In any electron beam these three variables are not independent from each other. The diameter of the beam spot is a function of the beam current i and U as for example given in the well-known Langmuir equation[1]:

$$i = c_o \cdot U \cdot d^{8/3} \tag{1}$$

where   i = beam current

         c_o = a number that depends only on the electron optics and the characteristics of the electron source

         U = accelerating voltage for the electron beam

         d = diameter of area A

It is, therefore, not possible to choose arbitrarily any combination of i, U, and A which would fulfill the speaker's requirement, namely

$$D = \frac{i\,U}{A} = \text{constant} \tag{2}$$

unless i and U are chosen such that they fulfill at the same time the following requirements:

$$i \cdot U^7 = \text{constant} \tag{3}$$

which can easily be derived by combining equations (1) and (2).

---

1.   see f. expl. V. K. Zworykin, Morton, Ramberg, Hillier, Vance, Electron Optics and the Electron Microscope, John Wiley and Sons, Inc. New York 1945, page 750, formula A 12.

Taking data published on different electron beam machines, we find for example that in a machine # 1 (see table) at a current i = 0.01 amp and a voltage **U** = 100,000 volts and an area $A = \frac{\pi d^2}{4}$ (d = 10 mil = 2.54×10^{-4} meters)^2,

the electron pressure is 3.2 mmHg, and in a machine #2 (see table) at a current of i = 0.3 amp, U = 15,000 volts, and d = 1.8×10^{-3} meters^3, the electron pressure calculates to 0.74 mmHg.

Assuming that in an imaginary machine # 3 (see table) one could obtain at 15,000 volt the same power concentration, then in order to fulfill the other necessary requirement (3) the current i should reach a value of 6,000 amps in a circular area of 3 inches diameter which are obviously impossible figures for any electron gun. But even then we would have gained only an increase of electron pressure by a factor of $\sqrt{\frac{10^5}{1.5 \times 10^{-4}}}$ = 2.6, which would mean a pressure of 8.3 mmHg; however, this pressure is as impossible to reach as this is the case for the current of 6,000 amp.

Because of fundamental technical limitations of electron sources and electron optics, the electron pressure decreases with decreasing voltage.

I do not want to discuss here whether such small pressures would have at all an influence on the deep penetration of electron beam welding.

---

2. see G. Burton and R. L. Matchett, American Machinist, February 23, 1959.

3. W. J. Green, R. R. Banks and R. M. Niedzielski, Welding Journal 1960, pages 791-796.

	U $[volts]$	D $[Watt/m^2]$	P $[mmHg]$	i $[amp]$	d $[mil]$
Machine #1 (reference 2)	100,000	20 x 10^9	3.2	0.01	10
Machine #2 (reference 3)	15,000	2.6 x 10^9	0.72	0.3	71
Machine #3	15,000	20 x 10^9	8.3	6000	3000

Machine # 3 represents a hypothetical machime that fulfills
Mr. Hablanian's requirement, viz. having the same power
density as for example Machine # 1 but working at 15,000
volts. The last two columns show how unrealistic such a
machine is.

AUTHOR'S REPLY

M. H. Hablanian
NRC Equipment Corporation

The main point of the discussion seems to be
that it is possible to produce higher power densities at
higher beam voltages. This was never disputed in my paper.

The so-called requirement of constant power con-
centration allegedly postulated in my paper was never implied.
In fact to avoid exactly such a misunderstanding on page 6
(first sentence in section entitled Electron Gun Design for
Welding) the statement was made that "it is well known that
it is easier to produce higher density at higher beam volt-
ages."

Nowhere was it mentioned as implied by H. Schwarz
that it is possible to choose any arbitrary combinations of
current and voltage to keep the power density constant.

In fact specific references always were made to approx. 20,000 volts (see page 3 line 8 from bottom, page 5 line 9 from top, page 7 line 8 from top, page 8 top line).

In view of the above the first part of the discussion whether correct or incorrect is actually irrelevant.

The requirement for approximately the same welding performance in the practical range considered here is not the same power density but the same beam pressure at the same total power. For example if the voltage is decreased by a factor of 6.7 in going from machine # 1 to machine # 2 then the power density could be reduced by 2.58 ($= \sqrt{6.7}$) which would require a 1 KW beam into a spot of 16 mil diameter instead of 10 mil as in machine # 1, i.e. the area can be 2.58 times larger provided the power is sufficient to reach the melting point of the workpiece. (As mentioned in the paper extremely high power densities may not always be beneficial for the welding application).

It should be noted that the example of machine # 2 is chosen rather arbitrarily by H. Schwarz and does not nearly represent the best possible results obtainable at 15,000 volt aside of being 4.5 times higher in power compared to machine # 1. For better correspondence the 2nd example should have been 15 KV, 66.7 ma beam (1 KW) into a spot of 1/64" dia. or better still a 25 KV, 40 ma beam.

Concerning the imaginary machine # 3 it should be noted that the value of C_0 need not be the same for the two guns in question.

The author regrets that he is drawn into the discussion of relative merits of high and low voltage guns. This was certainly not the intent of the paper. Rather the intent was to dispute the widely published claims that it is impossible to produce deep welds at voltages below approximately 80 KV and in this respect at least the photomicrographs speak for themselves.

57

HOLLOW ELECTRON BEAMS

By
Lawrence A. Harris
Physicist
General Electric Research Laboratory
Schenectady, New York

ABSTRACT

There are a number of possible methods of uniformly

focusing dense hollow cylindrical electron beams. Each

method requires a particular relationship between magnetic

field in the beam and that at the cathode. Of particular

interest is the electrostatically focused hollow beam and

the corresponding arrangement of magnetic field in the cathode

vicinity. Of a number of possible devices for launching such

beams, two have been the subject of investigation. Toroidal

guns are modifications of Pierce guns for hollow beams. Vari-

able perveance guns, in which the beam is radially deflected

in a drift space, offer the advantage of high perveance but

require high accelerating voltages and are sensitive to

scattering at the gun.

HOLLOW ELECTRON BEAMS

Introduction

The motivation for the work summarized in this paper came primarily from the needs of microwave tubes. For this reason no direct applications to the industrial uses of electron beams are discussed, but possibly the account of some of the techniques used may suggest their use in the industrial field. A complete discussion of all significant work on hollow beams would be too much for this brief account; attention is therefore confined to a summary of the work of the author.

A description of some methods of passing dense hollow beams of electrons through longitudinally uniform structures occupies the first part of this account.[1] Among the requirements of these methods are particular conditions at the entrance plane which determine the kind of beam to be injected into this structure. These conditions lead to a consideration of some methods of producing or generating such beams and bringing them up to the injection plane. In particular we shall discuss the toroidal electron gun[2] and a variable-perveance triode gun which, through the use of severe deflections, gains several novel features.[3]

The Focusing of Hollow Beams

We consider first the problem of passing a dense hollow beam of electrons with constant radius down a cylindrical drift space composed of one or two coaxial conducting cylinders. This situation is depicted in Fig. 1. It is a relatively simple arrangement in which we require that each electron maintain a constant radius and that all electrons have a common axial velocity. The entire region shown in Fig. 1 may be placed in a uniform axial magnetic field.

The maintenance of the equilibrium described above requires that each electron have a stable radius at which it experiences no net radial force. If an electron departs from its stable or equilibrium path the forces acting on the electron must tend to return it to that radius.

In a beam of given current, axial velocity, and dimensions, the one force over which we have no control is the space-charge spreading force due to the mutual repulsion of electrons. Indeed it is this force which necessitates the focusing schemes with which we are concerned. The other radial forces at our disposal are an applied electric force, due to a potential difference between the coaxial drift tubes, a magnetic force due to possible circumferential motion in the axial magnetic field, and a centrifugal force due to this same motion.

When these forces are balanced to provide a stable focusing condition each electron rides in its own effective potential trough so far as radial motion is concerned. If the balance is maintained while the component forces are increased, the sides of the troughs become steeper. The beam is rendered less sensitive to perturbation and the focusing is said to be stiffer.

In the calculation of these focusing conditions, the conservation of the total angular momentum plays an important role. The angular momentum p_θ of an electron with charge e, mass m, angular velocity $\dot{\theta}$ at radius r in a magnetic field of vector magnetic potential A_θ is given by $p_\theta = mr^2\dot{\theta} + eA_\theta r$. In our axially symmetric system this conservation law takes a form, known as Busch's theorem,[4] which states that

$$\dot{\theta} = \frac{e}{m} \frac{(\psi_c - \psi)}{2\pi r^2}$$

60

where $\dot\theta$, r and the flux linkages ψ and ψ_c are defined in Fig. 2. The flux ψ is that linking a circle concentric with axis and through the electron's position, while ψ_c is the flux linking a similar circle through the point on the cathode from which that same electron started its flight.

One effect of Busch's theorem is to simplify the calculation by specifying the angular velocity, and therefore the magnetic and centrifugal forces, as functions of position only. More importantly, it deals with the relationships between flux in the beam and at the cathode without regard to the details between these places. This circumstance enables us to specify various possible locations of the cathode with respect to the magnetic field. These, in turn, determine the different types of focusing in which all electrons in the beam can travel on their own equilibrium radii.

The best known focusing scheme is applied to solid cylindrical beams and is commonly known as Brillouin focusing.[5,6] In this arrangement the cathode is placed completely outside the magnetic field so that $\psi_c = 0$. The beam crosses magnetic field lines as it enters the field and in doing so acquires an angular velocity. In ideal Brillouin focusing the angular velocity is the same for all electrons so the beam rotates as a unit. The charge density, hence the current density, is independent of radius. The outward radial forces are the space charge and centrifugal forces which are just balanced throughout the beam by the inward magnetic force.

The first special case of hollow-beam focusing is derived from Brillouin flow. An inner core of the solid beam is removed and its effect on the remaining electrons is replaced by a suitable negative charge on an inner conductor. The hollow electron shell that remains rotates rigidly as before and the charge and current density are independent of radius. The arrangement of gun and drift tubes is shown in Fig. 3. The only difference between this and the solid beam case is that the outward radial electric force, which is really unchanged in magnitude, must now be ascribed to both space charge and applied fields.[7]

When we allow ψ_c to take on non-zero values we find that we cannot keep an entire beam of finite thickness in equilibrium unless ψ_c is the same for all electrons. The cathode must be so arranged that no magnetic flux penetrates the emitting surface, thus it must lie along magnetic field lines as in a magnetron, or be placed inside a magnetic shield with a pole piece threading the cathode, as indicated in Fig. 4.

With this arrangement the angular velocity is not uniform so cylindrical shells in the beam shear over each other. The charge density ρ is given by

$$\rho = \frac{e}{m}\,\frac{\varepsilon}{2}\left(\frac{\psi_c^2}{\pi^2 r^4} + B^2\right)$$

where ε is the permittivity of space and B is the magnetic flux density in the beam. From this it is apparent that the uniform magnetic field in the beam is associated with the constant term and the term in r^{-4} is associated with the cathode flux.
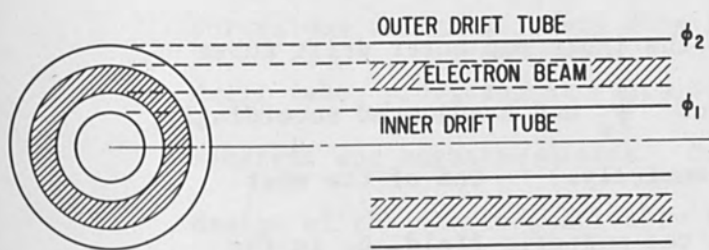
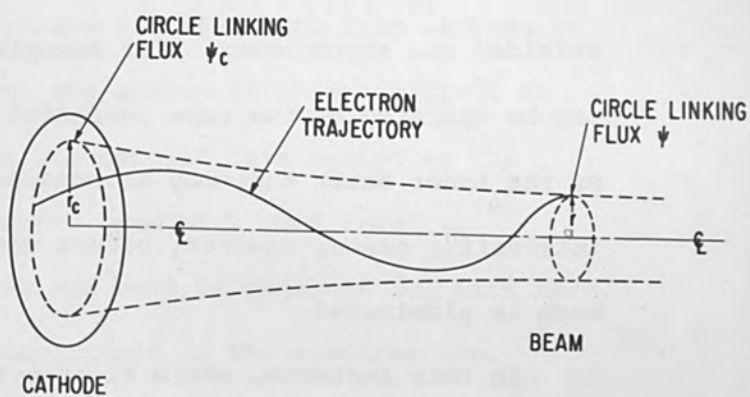FIGURE 1   A HOLLOW BEAM OF ELECTRONS BETWEEN COAXIAL DRIFT TUBES

FIGURE 2   DEFINITION OF THE FLUX LINKAGE APPEARING IN BUSCH'S THEOREM
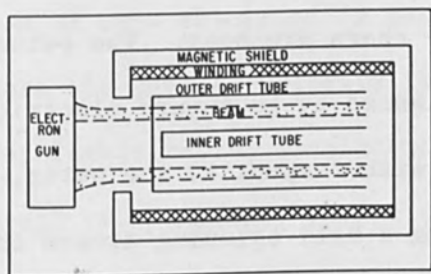

FIGURE 3   ARRANGEMENT FOR BRILLOUIN FOCUSING
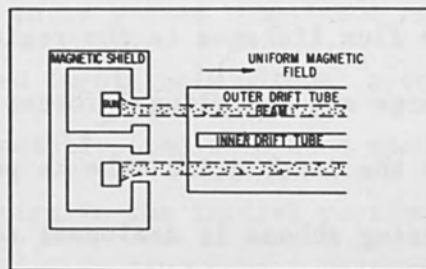OF A HOLLOW BEAM

FIGURE 4   SHIELDED ELECTRON GUN ARRANGEMENT
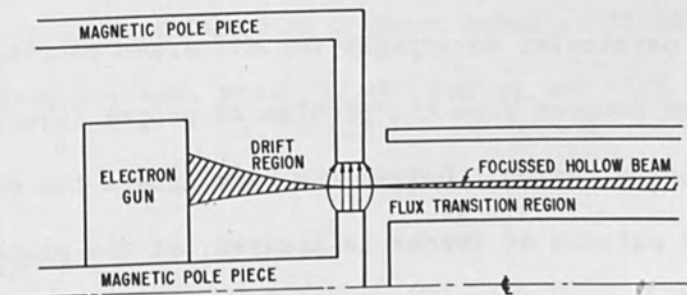FOR FOCUSING WHEN THE CATHODE FLUX
LINKAGE IS NOT ZERO

FIGURE 5   IDEALIZED HOLLOW-BEAM INJECTION SYSTEM SHOWING THE SEPARATE REGIONS

63

A number of special cases arise in connection with this general shielded gun arrangement. For example, the inner and outer drift tubes may be operated at the same potential and ψ_c and B adjusted accordingly, or the inner drift tube may be removed entirely.[8] One of the most interesting cases, however, occurs when the magnetic field, B, in the beam is eliminated.[1]

In this instance, where electrostatic focusing of the hollow beam is achieved, the cathode flux is retained. The charge density varies as r^{-4} and the beam shears circumferentially. Its angular velocity is acquired where electrons cross flux lines in going from a region where there are flux linkages to the region where there are none. The outward space-charge and centrifugal forces are balanced by an inward electric force, so the inner drift tube is positive with respect to the outer. This focusing scheme is analogous to keeping a ball spinning around the sides of a bowl in a gravitational field, or to refer to an example more in the news, keeping a satellite in orbit.

The advantages of focussing without a magnetic field are considerable but need no elaboration here. Each of the special focusing conditions has its own particular advantages for different possible requirements. All of them however pose the problem of proper injection of the beam into the focusing region. Unless the beam enters the region, in which the required balance of forces is assured, at the proper radius, with the proper charge and velocity distributions, it will be subject to oscillations about the equilibrium which may be excessive.

Proper injection conditions can be achieved in some cases by scrupulous design of every detail of the electron path from cathode to drift tube, providing at every point the appropriate combinations of electric and magnetic fields. Cook has applied this method to the design of the electrostatically focused beam with good results.[9] The design is difficult and complex and must be repeated for each case. Moreover it does not provide for convergence in the electron gun.

These difficulties are ignored in an approximate design procedure which divides the whole system into a number of distinct regions. Figure 5 shows these regions for the electrostatically focused case. A beam of zero thickness is assumed to enter a thin transition region where the angular velocity is imparted impulsively without producing appreciable radial displacement. Hopefully, the thin beam readjusts itself to the proper charge distribution in the initial portion of the focus region. While this approach is obviously incorrect it may meet the practical requirement of establishing an acceptable beam.

In what follows we consider only the part of the system up to the injection plane. Magnetic fields are thus excluded from consideration. The object now is to produce at a given cross-sectional plane a hollow beam with given current, velocity and radius and with vanishing thickness.

Toroidal Guns

One approach to generating hollow beams is through the use of toroidal electron guns.[2] These guns are an obvious extension of the more conventional Pierce guns.[10] A cylindrical Pierce gun, designed

to produce a sheet beam becomes a toroidal gun, if it is bent into a
circle so the sheet beam becomes a hollow cylindrical one. A half
cross-section of such a gun is shown in Fig. 6.

To design a toroidal gun; i.e., to arrive at suitable shapes for
the focusing rings and anodes, it is necessary to solve Poisson's
equation in the space occupied by the beam. An approximate method has
been used, in which a local cylindrical coordinate system centered at
the cross-sectional center of convergence is employed. Poisson's equa-
tion in this cylindrical system is modified in one term to account for
the curving of the gun around the main axis of symmetry.

Just as in the normal Pierce gun design, the solution to Poisson's
equation provides the necessary potential profile along the beam edges.
Appropriate shaping of the gun electrodes in a model in the electrolytic
tank provides this profile at each beam edge. Electron paths leaving
the gun are determined by a lens formula applicable to an annular
slit, [11,12] and by a theory of the space-charge spreading of hollow
beams. [13]

Experiments with these guns indicate that the theories mentioned
above are only partially satisfactory. Toroidal guns can be designed
with a given perveance and, if the anode opening is closed, the electron
paths are acceptably close to the design paths. With the anode slit opened,
however, so the beam can leave the gun, the paths differ seriously from
what they were designed to be. Figure 7 illustrates a typical example
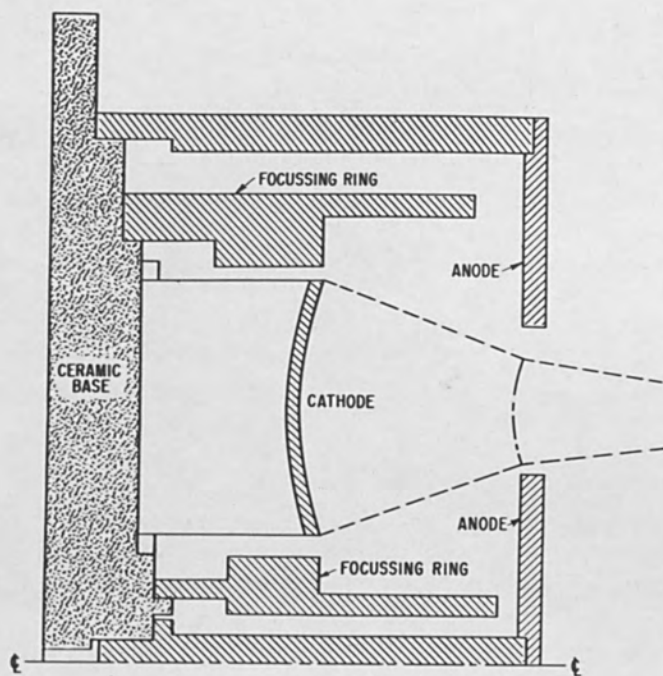of this discrepancy.

FIGURE 6   HALF CROSS SECTION OF AN EXPERIMENTAL TOROIDAL GUN
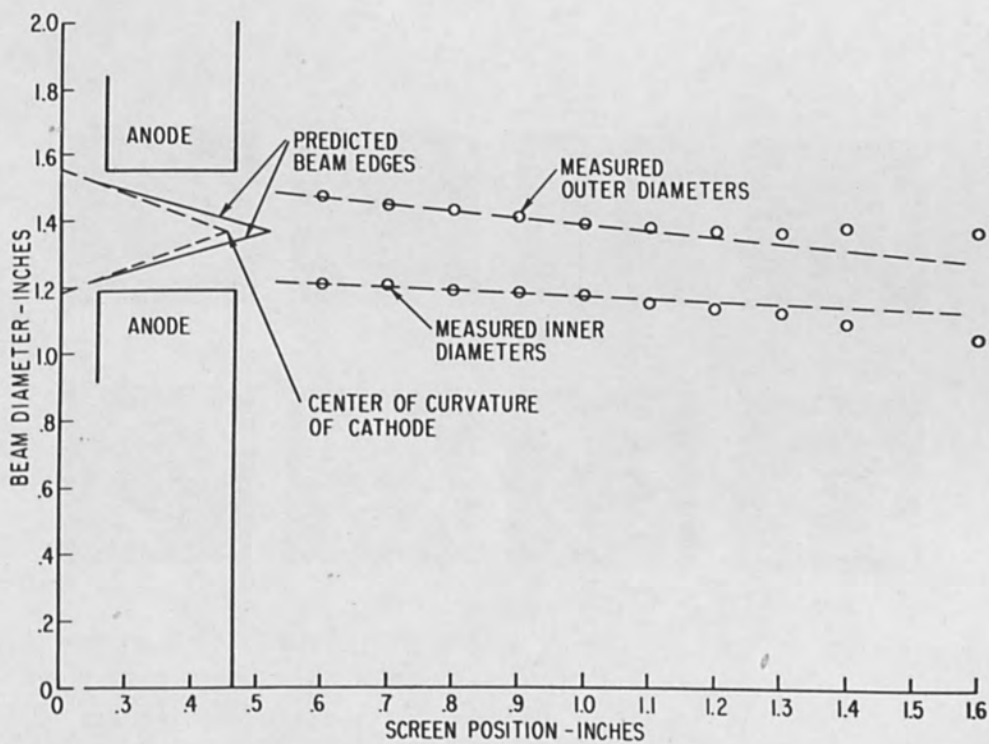

FIGURE 7   BEAM PROFILE OBSERVED FROM A TOROIDAL GUN, ILLUSTRATING THE
DISCREPANCY IN ELECTRON PATHS

The most serious error is excess strength -- by factors of 2
to 4 -- of the diverging anode lens. The inner edge is deflected more
strongly than the outer edge so that, in addition to excess divergence,
the beam suffers a net inward deflection. Even so, quite respectable
hollow beams can be produced, if the perveance is not too high, as
Fig. 8 shows.

These discrepancies in the electron-optical part of the theory
have not yet been explained quantitatively, but the qualitative reasons
for them seem fairly clear. The excess divergence is a cumulative
or "thick-lens" effect due to the extensive fringing field in the gun
from the anode slit. The net inward deflection is associated with the
increase in field strength of these lens fields toward the main axis of
symmetry.

SCREEN POSITION
.60 IN.   .80 IN.   1.00 IN.   1.20 IN.

1.40 IN.   1.80 IN.   2.00 IN.   2.20 IN.
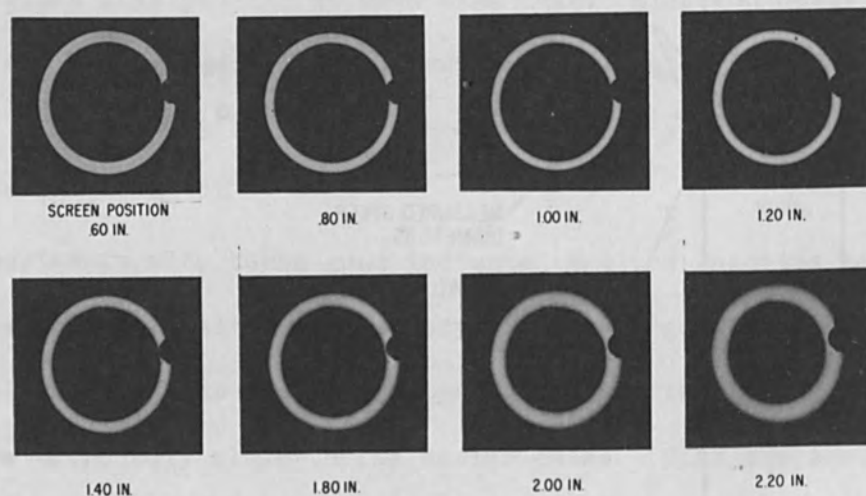
Figure 8   Traces of a beam from a toroidal gun
           observed at various distances from
           the gun. Average diameter is about
           1.3 inches.

68

Our present inability to predict the paths quantitatively is a real and serious limitation, but is hardly a fundamental one. Even when these lens effects are completely calculable, however, the use of these guns will be limited. The demonstrated strength of the anode lens demands a large angle of convergence, hence a large cathode. If the emission capabilities of the cathode are to be used effectively, large beam currents should be employed. On the other hand, the fringing of the field requires a narrow aperture or wide cathode-to-anode spacing. Only at high voltages are these requirements of low perveance and high current compatible. It is here that toroidal guns are most likely to find their application.

Triode Gun and Deflection Systems

Another method of producing a thin, high-density hollow beam at a given cross section is provided by the triode gun and deflection system we now consider.[3] A particularly attractive feature of this arrangement is its variable perveance; i.e., its current can be controlled without affecting the beam voltage or the electron paths very seriously.

In guns like the Pierce gun, or the toroidal gun just discussed, space charge plays an important part in determining electron paths and the electrode shapes. Consequently any changes in beam current are bound to have a serious effect on beam focusing. In the system now under discussion all electric fields due to voltages on the electrodes are very much greater than the fields due to space charge, so beam focusing is insensitive to changes in beam current.

The heart of this system is a coaxial drift region in which a hollow beam is strongly deflected in the radial direction. How this deflection reduces space charge is illustrated in Fig. 9 where the spreading of the deflected beam is seen to be much less than that of the undeflected one. [13]

Figure 10 shows how this deflection is used to inject a thin hollow beam into a transition region. To produce such a path a large potential difference is required between the inner and outer drift tubes. The kinetic energy of the beam at the outer drift tube, which is also the gun anode is much greater than it is at the waist where only the axial velocity remains. In other words the electron gun perveance is lower than the beam perveance at the waist.

The effect of this low gun perveance is illustrated in Fig. 11 which shows the proportions of a Pierce gun for such a beam. These impractical dimensions may be made more reasonable by converting the gun to a triode with a negative grid. The grid provides a convenient means for controlling current without varying other voltages. Shortening the grid-to-anode space increases the field strength there and obscures any space-charge effects.

Figure 12 shows the construction of an experimental triode gun designed on this basis. The electrodes near the grid and the anode electrodes are shaped to guide the beam through the anode slit at the required angle to the axis.
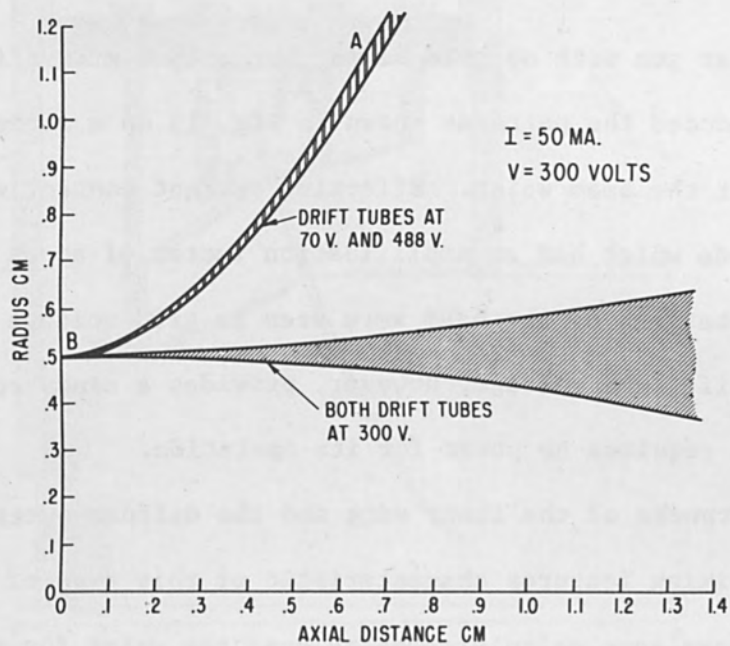
FIGURE 9 THE SPREAD OF A HOLLOW ELECTRON BEAM IN STRONG AND WEAK RADIAL
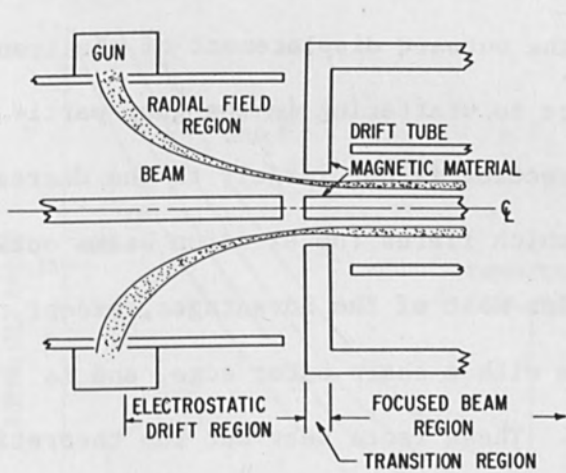ELECTRIC FIELDS

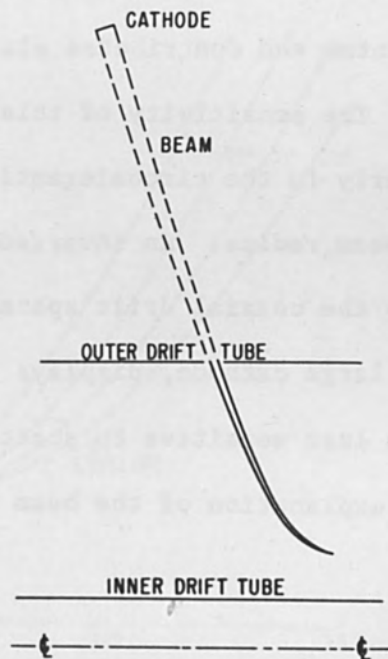FIGURE 10 DEFLECTION INJECTION SYSTEM FOR HOLLOW BEAMS

FIGURE 11 IMPRACTICAL PROPORTIONS OF A DIODE GUN
FOR INJECTING A HOLLOW BEAM INTO A
COAXIAL DEFLECTION REGION

A similar gun with no grid wires, but only a grid slit to control current, produced the patterns shown in Fig. 13 on a screen placed slightly past the beam waist. Effective current control was achieved by this triode which had an amplification factor of about 22. Only minor perturbations of the beam were seen as grid voltage was varied. The inner drift tube voltage, however, provides a handy control of beam diameter and requires no power for its operation.

The sharpness of the inner edge and the diffuse outer edge of the beam are striking features characteristic of this type of system. Figure 14 shows some calculated paths near the waist for electrons moving in a radial plane and differing only in their initial angles. The inner envelope defines a limit beyond which electrons cannot pass, hence the sharp inner edge. Any circumferential velocity detracts from radial momentum and contributes also to the outward displacement of electrons.

The sensitivity of this device to scattering in the gun, particularly in the circumferential direction is due largely to the decrease in beam radius. An inverted gun which flares the electron beams outward into the coaxial drift space retains most of the advantages, except the large cathode, displays a beam with a sharp outer edge, and is much less sensitive to scattering. These facts bear out the theoretical explanation of the beam characteristics.
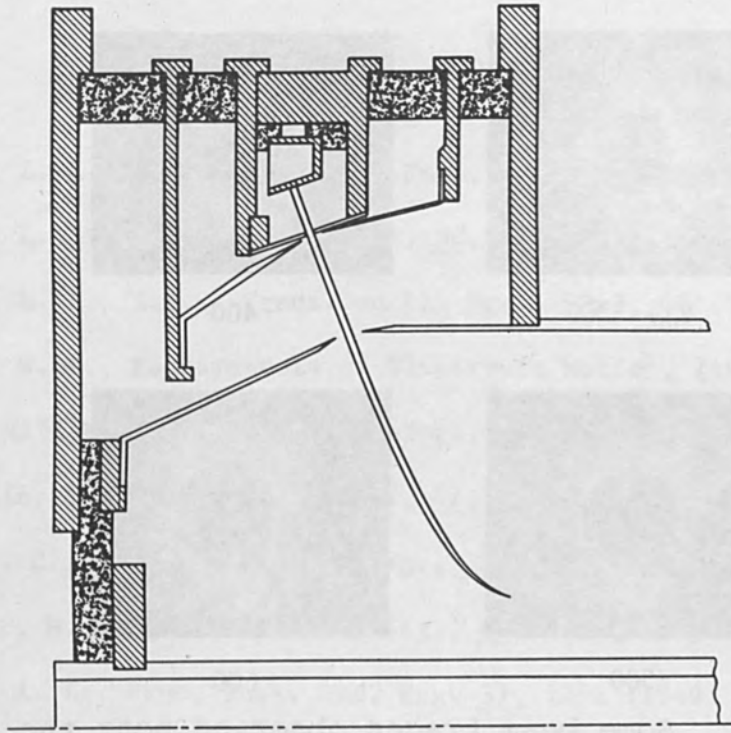
FIGURE 12 HALF CROSS SECTION OF AN EXPERIMENTAL TRIODE DEFLECTION SYSTEM
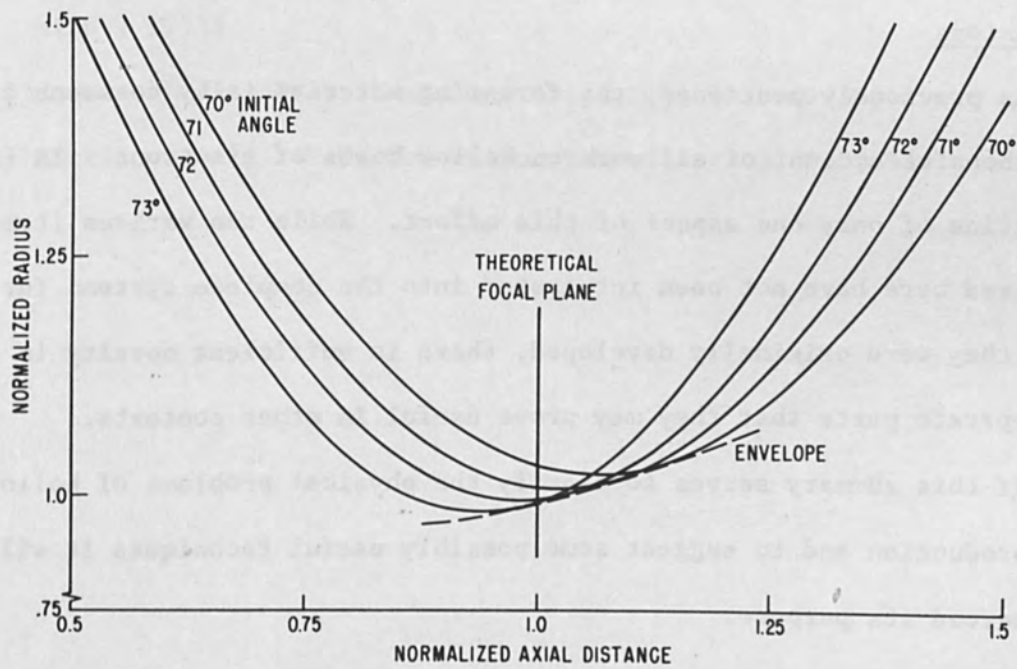
FIGURE 14   CALCULATED TRAJECTORIES NEAR THE WAIST FOR SEVERAL
INITIAL ANGLES IN THE RADIAL PLANE ILLUSTRATING THE
FORMATION OF THE INNER ENVELOPE

73
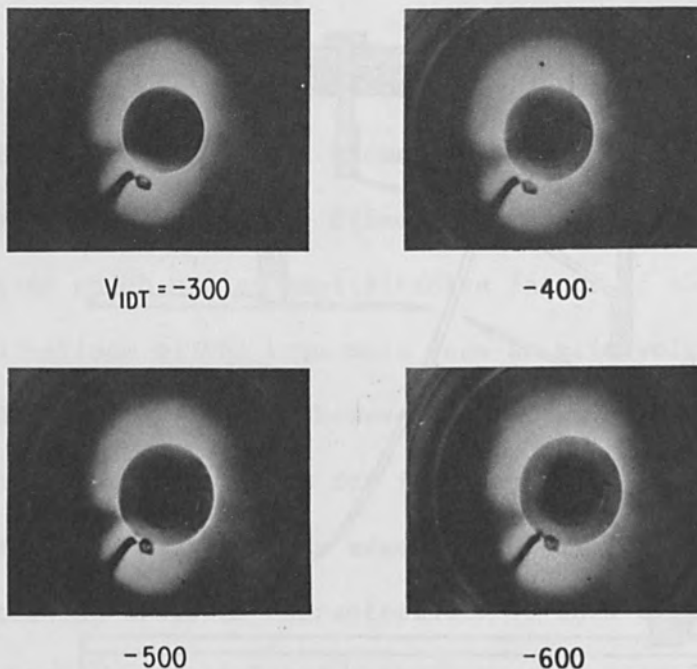
Figure 13   Some beam traces observed near the
waist of the beam from a triode gun.
Note diameter control achieved by
variation of the inner drift tube
voltage.

Conclusions

As previously mentioned, the foregoing material is by no means a

comprehensive account of all work on hollow beams of electrons. It is

an outline of only one aspect of this effort. While the various items

discussed here have not been integrated into the complete systems for

which they were originally developed, there is sufficient novelty in

the separate parts that they may prove useful in other contexts.

If this summary serves to clarify the physical problems of hollow

beam production and to suggest some possibly useful techniques it will

have served its purpose.

References

(1) Harris, L. A., Proc. Inst. Rad. Eng., $\underline{40}$, 700 (1952)

(2) Harris, L. A., Jour. Appl. Phys., $\underline{30}$, 826 (1959)

(3) Harris, L. A., I.R.E. Trans. on El. Dev., $\underline{ED-7}$, 46 (1960)

(4) Harman, W. W., Fundamentals of Electronic Motion, (1953),
     McGraw-Hill Book Co., Inc., New York, p. 111

(5) Brillouin, L., Phys. Rev. Ser. 2, $\underline{67}$, 260 (1945)

(6) Wang, C. C., Proc. Inst. Rad. Eng., $\underline{38}$, 135 (1950)

(7) Lally, P. M., Proc. Inst. Rad. Eng., $\underline{49}$, 514 (1961)

(8) Samuel, A. L., Proc. Inst. Rad. Eng. $\underline{37}$, 1252 (1949)

(9) Cook, E. J., I.R.E. Trans. on El. Dev. (to be published)

(10) Pierce, J. R., Jour. App. Phys., $\underline{11}$, 548 (1940)

(11) Glewwe, C. W., M.S. Thesis (University of Minnesota, Minneapolis,
     Minn., 1955)

(12) Harris, L. A., Proc. Inst. Rad. Eng., $\underline{46}$, 1655 (1958)

(13) Harris, L. A., I.R.E. Convention Record, pt. 3, 11 (1956)

USE OF DIGITAL COMPUTERS IN ELECTRON BEAM CALCULATIONS

By

John W. Lotus
Staff Member
Research Division
Raytheon Company
Waltham, Massachusetts

and

Richard C. Gunther
Mathematician
Missile and Space Division
Raytheon Company
Waltham, Massachusetts

ABSTRACT

Relaxation techniques are considered as a means of computing potentials in electron beam problems. Numerical methods of integrating the equations of motion are also considered. It is shown that the effects of space charge and magnetic fields can be included. Two examples are given to show the utility of the method.

USE OF DIGITAL COMPUTERS IN ELECTRON BEAM CALCULATIONS

Introduction

An IBM 704 computer has been used to investigate electron beam devices. The procedure has the distinct advantage that linearization of the equations of motion is not necessary. Also, space charge can be included. Problems normally considered intractable mathematically can be solved by the computer. The machine is efficient with respect to time and money. Only useful data in its final form is obtained from the machine. The rest is stored internally. In ten minutes, an IBM 704 computer can compute the potential and several trajectories in an electron gun. A complete problem can be stored in a deck of cards so that no equipment is ever "tied up." Potentials, geometries, and other parameters of a problem can be quickly and easily altered by changing a few cards of the program deck. Because changes are made in the program deck and not in the computer itself, no special equipment is necessary for a particular problem. When not in use for beam problems, the computer is free for other uses.

A digital computer performs only four arithmetic operations: addition, subtraction, multiplication, and division. All other operations such as exponentiation, integration, and differentiation are reduced by numerical analysis to the four arithmetic operations. Differential equations are approximated by finite difference quotients; transcendental functions, by truncated infinite series of difference quotients, etc. The accuracy of the approximation is determined in every computation by the size of the interval

between points and the number of points included in the computation. Great accuracy is obtainable by taking minute intervals and many points.

GENERAL DISCUSSION

There are two approaches in the design and study of electron beams. One is to try a number of geometries and potential distributions, and to select the one giving the best beam. The other is to decide beforehand the properties wanted in an electron beam and then calculate a focussing scheme to achieve it. One is empirical; the other, analytical.

It turns out, however, that focussing schemes arrived at analytically are not always practical; nevertheless, they remain as guideposts in design. Practical considerations normally dictate the ultimate design. These include manufacturing costs, ease of fabrication and reliability. For this reason, it is often necessary to compute trajectories in a gun based on a design from an analytic procedure.

It is apparent that present-day electron guns often involve the solution of high density beams where it is necessary to take space charge into account.

Electron beam studies involve two basic problems when viewed for digital computer solution: the solution of the potential in the region through which the electrons pass, and the solution of the equations of motion of electrons moving in that region. These problems are considered separately except when the space charge produced by the trajectories is large enough to influence the potential distribution. In such a case an initial potential is estimated. Trajectories are computed in it. A charge distribution is computed from the trajectories, and a new potential is derived from this charge distribution. The process is continued until "self-consistency" is achieved.

A typical potential problem is the solution of an elliptic partial differential equation as a boundary value problem. Poisson's equation, Eq.(1), will serve to illustrate the techniques used with the digital computer:

$$\nabla^2 V(x,y) = \frac{-\rho(x,y)}{\epsilon}$$ (1)

For this equation, specification of the potential and/or the field on the boundaries, and the charge in the interaction space, completely determines the potential in the interaction space. To be solved on a digital computer, Eq. (1) must be approximated by a finite difference equation[1] Eq. (2) is such an approximation:

$$\nabla^2 V(x_1, y_j) = \nabla^2 V_{i,j} \sim \frac{V_{i,j-1} - 2V_{i,j} + V_{i,j+1}}{(\Delta y)^2}$$

$$+ \quad \frac{V_{i-1,j} - 2V_{i,j} + V_{i+1,j}}{(\Delta x)^2} = \frac{-\rho_{i,j}}{\epsilon}$$ (2)

$$x_i = i\Delta x \; ; \; y_j = j\Delta y$$

A network of points is placed over the interaction space within which the potential is to be calculated. The potential is calculated at grid points. It can be interpolated as accurately as desired between grid points. By making the grid spacing small enough and arranging the points to suit the particular geometry, very high accuracy may be attained. Figure 1 shows two geometries with suitable grids superimposed. Figure 1a shows a regular boundary which fits the net points. Figure 1b illustrates how an irregular boundary may be fitted approximately.

The digital computer uses a technique of "relaxation" to evaluate Eq. (2). The potential at the boundary grid points is determined by the boundary conditions of the differential equation. Values for the potential at each interior grid point are assumed. A "residual," $R_{i,j}$ as defined by Eq. (3) is associated with each interior grid point:
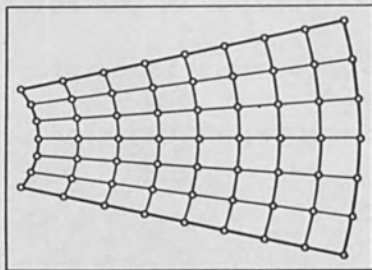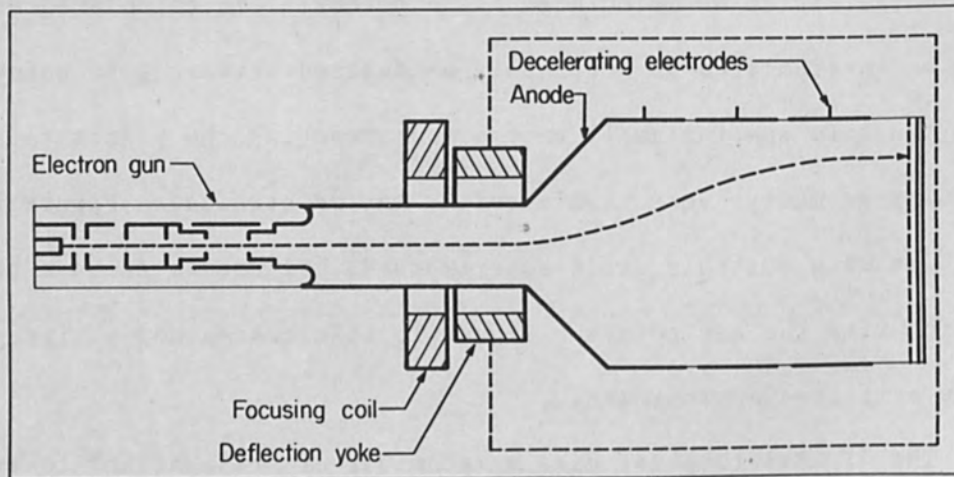
A POLAR COORDINATE GRID FOR
A REGULAR GEOMETRY
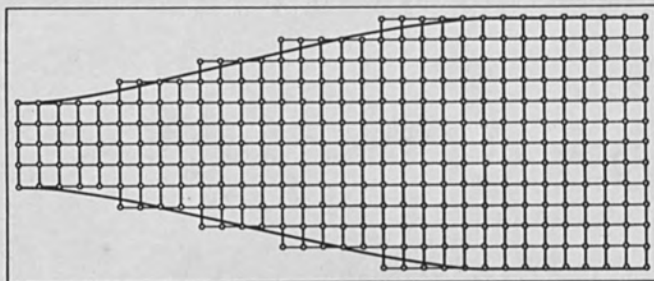
FIGURE la

A CARTISIAN COORDINATE GRID FOR AN IRREGULAR GEOMETRY

FIGURE lb

SCHEMATIC OF STORAGE TUBE

FIGURE 2

$$R_{i,j} = -\frac{\rho_{i,j}}{\epsilon} - \frac{V_{i,j-1} - 2V_{i,j} + V_{i,j+1}}{(\Delta y)^2} - \frac{V_{i-1,j} - 2V_{i,j} + V_{i+1,j}}{(\Delta x)^2} \quad . \tag{3}$$

The residual is the amount by which the potential varies from the correct value at each point. Inspection of Eq. (3) reveals that $R_{i,j}$ is zero when Eq. (2) is satisfied. For each interior grid point the residual is computed and added to the corresponding potential.[2] The potential is then systematically modified again and again in this same manner until the largest residual is a small enough fraction of its associated potential to provide the desired accuracy. The potential obtained through relaxation is in digital form (an array of numbers representing the potential).

Once the potential is known, the paths of electrons in it can be computed. The very simple Eq. (4) will suffice to illustrate the techniques used:

$$\ddot{x} = e/m \left(- \frac{\partial V}{\partial x} \right)$$

$$\ddot{y} = e/m \left(- \frac{\partial V}{\partial y} \right) \tag{4}$$

To evaluate Eq. (4), the gradient of the potential must be found in the x and y directions. This is done by fitting partially differentiated interpolating polynomials to the potential grid. As with all difference equations, the accuracy of approximation is determined by the grid spacing and the number of points of the grid included in the quotient. The simplest polynomial which will satisfy Eq. (4) is what is known as a four-point bi-variate Lagrange polynomial.[3] The derivatives of this polynomial are given by Eq. (5):

$$\frac{\partial V}{\partial x} \sim \frac{1}{\Delta x \Delta y} ((y - y_{j+1})(V_{i,j} - V_{i+1,j}) - (y-y_j)(V_{i,j+1} - V_{i+1,j+1}))$$

(5)

$$\frac{\partial V}{\partial y} \sim \frac{1}{\Delta x \Delta y} ((x - x_{i+1})(V_{i,j} - V_{i,j+1}) - (x-x_i)(V_{i+1,j} - V_{i+1,j+1})) \; .$$

Eqs. (5) are evaluated and substituted into Eqs. (4), Eqs. (4) are integrated to yield $\dot{x}$ and $\dot{y}$, and $\dot{x}$ and $\dot{y}$ are integrated to yield x and y.

The integration is performed by approximate methods similar to the familiar Simpson's Rule.[4],[5] All such methods compute an initial value of the integrand at time $t + \Delta t$ from the information known at time t and compute a final value by correcting the first value one or more times.

For simple trajectories, a fixed integration interval, Δt, produces results optimum with respect to speed and accuracy. For sharply twisting trajectories, a variable interval which automatically becomes small for small curvature, large for large curvature, is used. This is accomplished by comparing the final, or corrected, value of the integrand with the initial, or predicted, value. If the difference is greater than the allowable error, the interval is decreased and the test is made again. If the difference is an order of magnitude less than the allowable error, the interval is increased. Otherwise, the same interval is maintained.

As each point of a trajectory is computed, its coordinates are stored for future display. The finished curve may be in tabular form, displayed on a cathode ray tube or plotted graphically. Several trajectories may be summed to form a beam. Additional data such as energies and incident angles are readily computed and displayed.

Problems not involving space charge or where space-charge effects are negligible, can be solved quickly and accurately. Such problems involve analyzing low-density beams with regard to deflection and focussing. Deflection defocussing, deflection linearity, crossover size, chromatic aberration and the like may be considered.[6],[7]

Space charge is important in the region of crossover. Here, the charge can be computed from the trajectories themselves and stored at the proper net points in the region of crossover. The potential distribution can be recalculated with the space charge included and trajectories recomputed.

To investigate guns producing dense beams, space charge must be taken into account. One can start with a known solution taken from the analytic form which resembles the design under consideration. The rather complex problem of matching the beam in the transition region between the gun and any other associated structure, such as an rf slow wave structure, can also be investigated.

EXAMPLES

Computation of Potential for a Collimating Electron Lens System

The electron storage tube uses a collimating lens system. In our study we considered only the collimating region. A schematic of the tube is shown in Fig. 2. The region surrounded by the dotted line is the one under investigation. This region extends from the center of deflection to the storage element. The geometry may be thought of as two right circular cylinders joined by a truncated right circular cone. The electrodes are located on the outer surface and are axially symmetric. The potential variation between electrodes on the boundary is assumed to be linear. Space charge is neglected.

In cylindrical coordinates, Laplace's equation is:

$$\frac{\partial^2 V}{\partial r^2} + \frac{1}{r}\frac{\partial V}{\partial r} + \frac{1}{r^2}\frac{\partial^2 V}{\partial \Theta^2} + \frac{\partial^2 V}{\partial z^2} = 0 \qquad , \qquad (6)$$

in our case

$$\frac{\partial^2 V}{\partial \Theta^2} \equiv 0 \qquad . \qquad (7)$$

Then, we have

$$\frac{\partial^2 V}{\partial r^2} + \frac{1}{r}\frac{\partial V}{\partial r} + \frac{\partial^2 V}{\partial z^2} = 0 \qquad . \qquad (8)$$

This is the equation to solve subject to the potentials on the boundary. To do this digitally, it is rewritten as a finite difference equation. It now takes the form

$$\frac{V_{n+1,m} - 2V_{n,m} + V_{n-1,m}}{(\Delta r)^2} + \frac{V_{n+1,m} - V_{n-1,m}}{2r_n(\Delta r)} + \frac{V_{n,m+1} - 2V_{n,m} + V_{n,m-1}}{(\Delta z)^2} = 0 \; .$$

$$(9)$$

In this form, the index n locates the point in r, and the index m locates the point in z. Therefore, instead of being a function of r and z; $V\,(r,z)$, V is a function of n and m; $V\,(n,m)$. Δr is the distance between points in the r direction. Δz is the distance between points in the z direction. To make the computation simpler Δr is made equal to Δz. Because all potentials are known on the boundary, the equation can be solved by relaxation and the potential at all interior points found. Figure 3 shows the bounded region considered with the calculated equipotential lines indicated. Also

84

shown are some net points to indicate the size of the net. The trajectory

shown was computed by integrating the equations of motion by the Runga Kutta

method. To determine the accuracy of the computation, the trajectory was

computed backward and forward. There was no error in the radial direction

to the third decimal place; the angle of incidence differed by $0.05°$. The

computational procedure for solving the potential requires three minutes,

the trajectory, about fifteen seconds. About three days of programming and

an hour of computer time was required to set up, check out and compute the

potential and trajectory.

Computation of Trajectories in a Pierce Gun with a Space Varying Axial Magnetic Field

In this example the potential in the region is known exactly. The ef-

fect of space charge was included. The data for the potential was taken from

Spangenberg[8] and applied to a praticular kylstron gun in which we were in-

terested. The interesting thing about this problem is that the equations of

motion are three dimensional because we are considering the effect of the

magnetic field.

The equations of motion are:

$$\ddot{r} - r\dot{\Theta} = e/m \ [- \frac{\partial V}{\partial r} + r\dot{\Theta}H_z]$$

$$1/r \ d/dt \ (r^2\dot{\Theta}) = e/m \ [\dot{z}H_r - \dot{r}H_z] \tag{10}$$

$$\ddot{z} = e/m \ [-\partial V/\partial z - r\dot{\Theta}H_r]$$

The values of H, the magnetic field, were given as numerical values obtained

from measurements along the axis of the gun. The radial variation was deter-

mined from these by approximation in a Taylor series.

The equations are :

$$H_r = - \frac{dH(z)}{dz} \frac{r}{2} + \frac{d^3H(z)}{dz^3} \frac{r^3}{4x2^2}$$

(11)

$$H_z = H(z) - \frac{dH(z)}{dz} \frac{r^2}{2^2} + \frac{d^3H(z)}{dz^3} \frac{r^4}{2^2x4^2}$$

In the computation it was found that the third order terms are negligible.

Figure 4 shows the gun region and trajectories calculated with zero magnetic field.

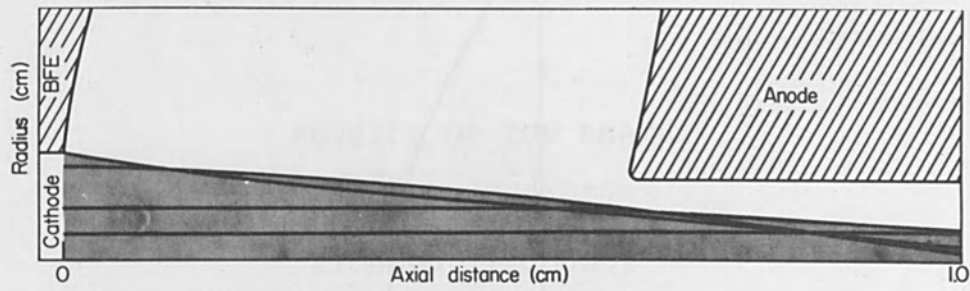Figure 5 shows the same trajectories calculated with an applied magnetic field.

Figure 6 shows the axial variation of the magnetic field in the region of interest.

Figure 7 shows the angular variation of a trajectory to indicate the rotational behavior introduced by the applied magnetic field.
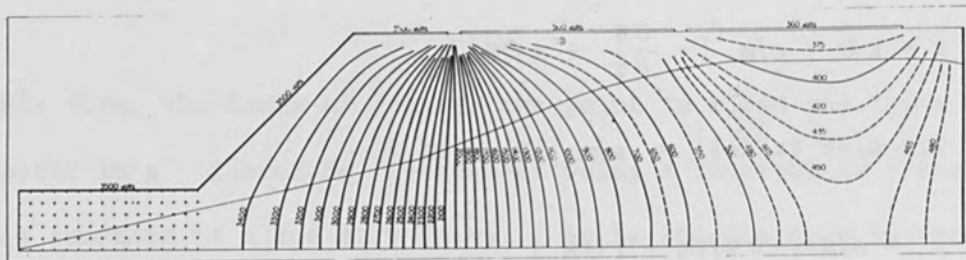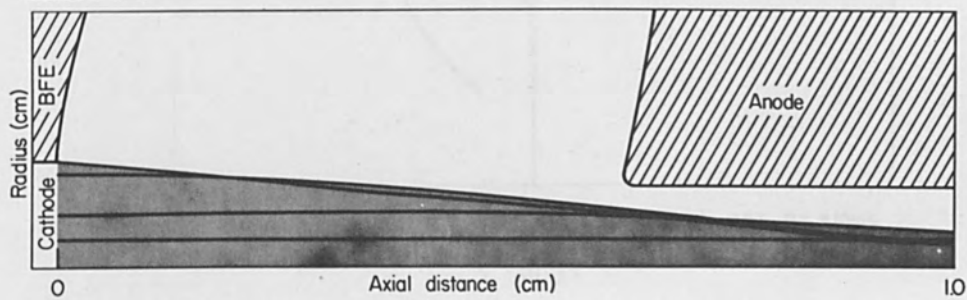

POTENTIAL SOLUTION AND TRAJECTORY FOR COLLIMATING LENS
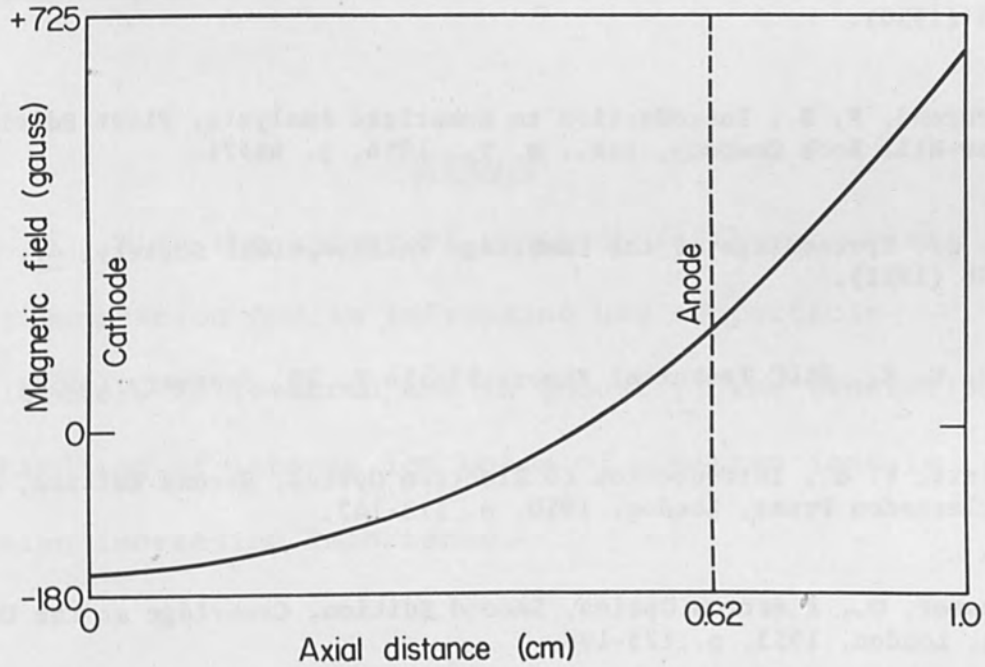
FIGURE 3
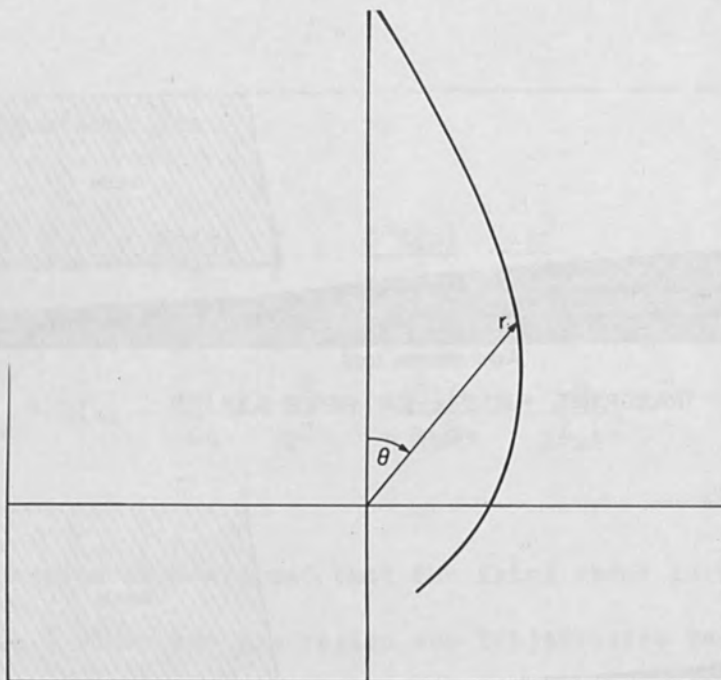
TRAJECTORIES FOR SPHERICAL PIERCE GUN

FIGURE 4

TRAJECTORIES FOR SPHERICAL PIERCE GUN WITH NON UNIFORM MAGNETIC FIELD

FIGURE 5

VARIATION OF MAGNETIC FIELD ALONG THE AXIS

FIGURE 6

ANGULAR VARIATION OF TRAJECTORY WITH APPLIED MAGNETIC FIELD

FIGURE 7

References

1

Hildebrand, F. B., Methods of Applied Mathematics, First Edition, Prentice-Hall, Inc., N. Y., 1952, p. 292-345.

2

Frankel, S. P., Mathematical Tables and Other Aids to Computation, $\underline{4}$, 65-75 (1950).

3

Hildebrand, F. B., Introduction to Numerical Analysis, First Edition, McGraw-Hill Book Company, Inc., N. Y., 1956, p. 64-71.

4

Gill, S., Proceedings of the Cambridge Philosophical Society, $\underline{47}$, Pt. 1, 96-108 (1951).

5

Milne, W. E., WADC Technical Report 57-556 $\underline{I}$, $\underline{28}$, February (1958).

6

Cosslett, V. E., Introduction to Electron Optics, Second Edition, Oxford at the Clarendon Press, London, 1950, p. 113-147.

7

Klemperer, O., Electron Optics, Second Edition, Cambridge at the University Press, London, 1953, p. 173-198.

8

Spangenberg, K. R., Vacuum Tubes, First Edition, McGraw-Hill Book Company, Inc., N. Y., 1948, p. 454-464.

PHYSICS OF ION BEAMS

By

Richard J. Connor
Senior Project Manager
High Voltage Engineering Corporation
Burlington, Massachusetts

ABSTRACT

With the advent of research in thermonuclear

power generation and in increasing use of particle

accelerators in research and in industry, the generation

and handling of intense ion beams of positive ions is

assuming increasing importance.

The emphasis of modern technology on nuclear physics and the advent of research in thermonuclear power generation coupled with an increasing use of particle accelerators in both industry and the laboratory has led to a considerable effort in the generation and handling of intense beams of positive ions. In the past decade, ion sources have become available that are capable of producing currents in the region of 100 ma. and there are some reports of currents in the 1 ampere region.[1] The problem has shifted to the proper control of the beam and if one talks of well controlled beams, the intensity drops to the order of 30 ma. The space charge forces are largely responsible for the difficulty encountered in dealing with beams of this magnitude.

It would be futile to describe the many types of sources that may be found in the literature and it would seem that each experimenter has developed his own source that fills his particular need. Perhaps the best compilation and summary of the literature available is that of Von Ardenne[2]. In general, a problem exists in the generation of positive ions that is not present in the case of electron emission and this is the handling of the large amounts of gas or vapor that is present. Usually, the ions are formed by creating a plasma in a closed region and extracting by means of a negative probe the ions desired. The material efficiency of this process is low and usually is about 10% for the great majority of sources; thus, if one desires a 10 ma. beam at 10% efficiency, the corresponding gas flow that must be handled is 2.10^{-2} atmos. cc/s and requires a pumping capacity of 1500 1/s at a pressure of 10^{-5} mm of Hg. The requirements are somewhat less stringent in the case of molecular gases.

Of the many schemes used in the porduction of positive ions, the following types are chiefly used and other reported sources are variations of these few.

Capillary Arc Source

In this source a low pressure arc is passed through a small diameter (2 mm) canal and the ions are extracted through a small hole in the canal perpendicular to the discharge. Material efficiency is approximately 5% and the maximum currents reported are 5 ma. The source operates at 5.10^{-2} mm. with an arc of 100 volts at between 0.1 and 5A. In general, the source is difficult to operate, shortlived and gives ion beams of high molecular ion percentage.

Penning Discharge Source

In this source electrons are confined to spiral motion about an axis defined by a magnetic field of approximately 1000 gauss. They are reflected at both ends of the field by cold cathodes and the plasma is formed and confined to this central region. Ions are extracted through a small aperture (1-2 mm) in one of the cathodes. Electrons may be injected into the plasma region by secondary emission or by emission from an incandescent filament.

The material efficiency of this source is reasonably high and may approach 40%. Extracted currents are tens of milliamperes for arc currents of 3-5A at 150 volts.

RF Ion Sources

RF Ion Sources are characterized by generation of the plasma by a high frequency electrode-less discharge in a ceramic or glass envelope. The power is fed to the plasma either inductively or capacitively. In the first case the frequency used is about 20 mc/s, in the second, about 100 mc/s.

In general, an axial magnetic field is used to further concentrate the plasma. The beam is extracted either through a canal or an aperture. Beam currents are usually less than 10 milliamperes. The interesting feature of this source is the great atomic purity of the beam and the fact that in general less than 100 watts of power are required for its operation. Efficiency is of the order of 10%.

It should be noted that in all of the above mentioned sources, attempts are usually made to concentrate the plasmas by magnetic fields in the Penning and RF sources, by forcing the discharge through a small canal in the capillary arc. Since the plasma density depends directly on the electron density, the trapping of many energetic electrons in a small volume will produce an intense plasma. Such a source has been described by Von Ardenne[2]. In this source electrons from a heated filament (See Fig. 1) are injected at approximately 30 ev toward a canal and in this region form a plasma. The resulting arc is constricted by the small diameter of the canal. Between the exit of this canal and the anode of the source is a non homogeneous magnetic field of approximately 2000 gauss that more tightly confines the electron paths and hence the plasma. This thread of plasma, approximately 1/4 mm dia., extends through a small hole in the anode and is a source of ions of great brilliance.

In fact, the current density obtainable from such a source is between 10 and 100 A/cm^2. Neutral gas atoms or molecules passing through such a dense plasma have a high probability of being ionized and the efficiency in this source approaches 100%; measurements confirm this within an experimental error of 5%. Figure 2 is a photograph of a source of this type.
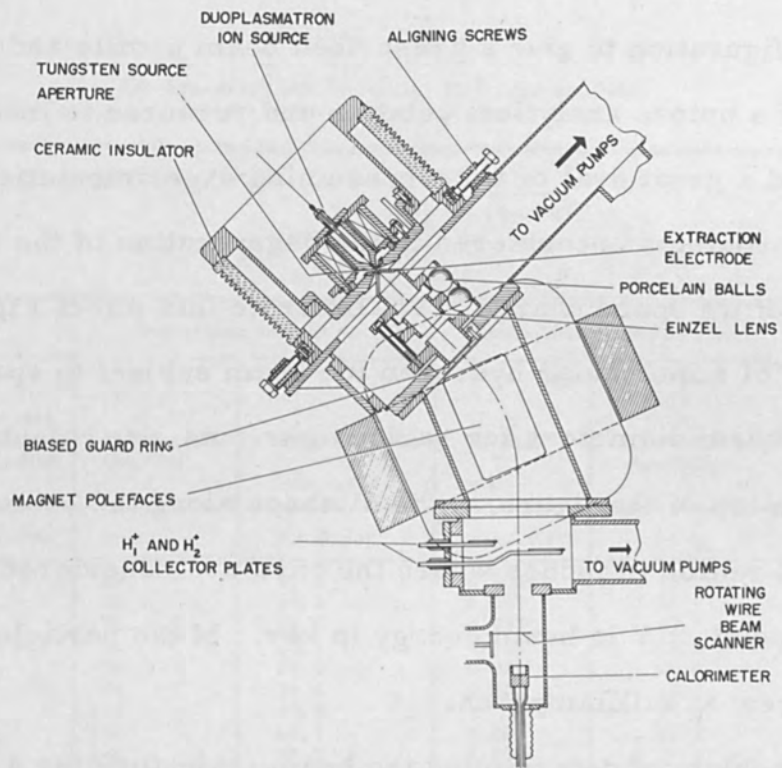
DUOPLASMATRON
ION SOURCE

ALIGNING SCREWS

TUNGSTEN SOURCE
APERTURE

CERAMIC INSULATOR

TO VACUUM PUMPS

EXTRACTION
ELECTRODE

PORCELAIN BALLS

EINZEL LENS

BIASED GUARD RING

MAGNET POLEFACES

H_1^+ AND H_2^+
COLLECTOR PLATES

TO VACUUM PUMPS

ROTATING
WIRE
BEAM
SCANNER

CALORIMETER

FIGURE 1   DUOPLASMATRON SOURCE, LENS AND ANALYZING SYSTEM
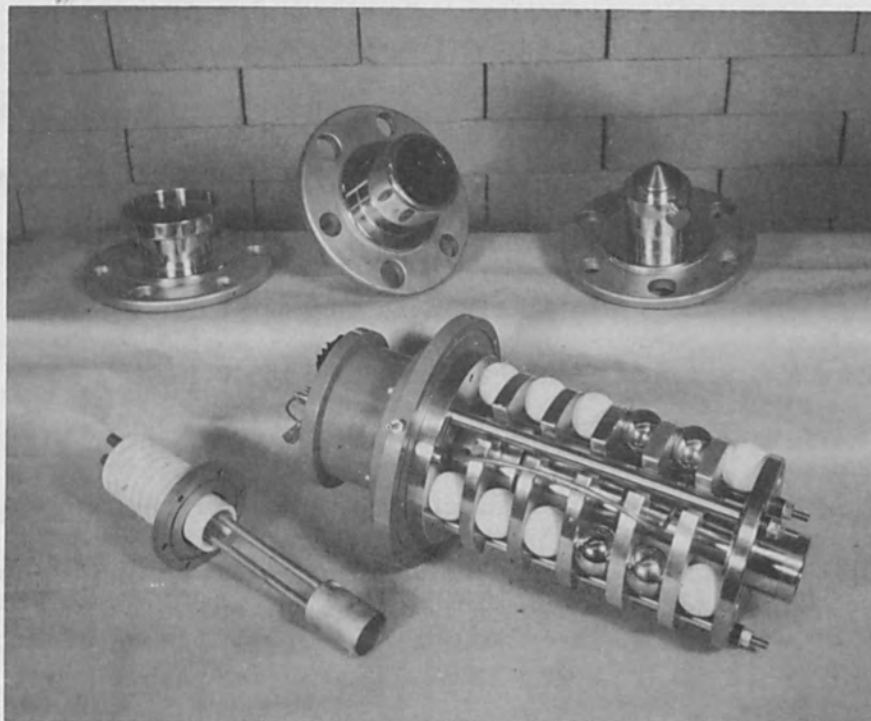

FIGURE 2   VON ARDENNE TYPE SOURCE

93

Using such a source as an example, the problems encountered in handling the ion beam must now be discussed. The problem of the proper electrode configuration to give a prescribed beam profile and trajectory is not capable of a unique analytical solution and recourse is made to analogue techniques and a great deal of time-consuming experimentation. Paramount of the problems encountered is the degeneration of the ion beam under the influence of its space charge. To illustrate this effect Figure 3 shows the expansion of a molecular hydrogen ion beam subject to space charge forces. The beam diameters for various currents are calculated using the relation at the top of the figure. x is distance along the beam axis in inches, r_0 its initial radius in inches where the rays are considered parallel, r its radius at point x; V is beam energy in kev.; M the particle mass number and I the current in milliamperes.

The problem of determining the beam trajectory for a given geometry can be calculated and figure 4 shows the result of such a calculation. The method used is to determine the field equipotentials by a relaxation technique and then to use this field in the trajectory equations. This last required use of an IBM 704 computer. Space charge is not included in the trajectory results shown here. The figure is used to illustrate the focusing geometry typically employed. The arrangement shown is a 2 inch diameter Einzel lens in which the beam enters with an initial energy of 40 Kev. is decelerated to 7 Kev., and then reaccelerated to 40 Kev.

The influence of space charge is strikingly shown in Figure 5 where the beam diameter is shown as a function of beam current for a given geometry. The results shown are actual data points for beam current and diameter at 26 inches from the source. The apparatus on which this data

The Expansion of a Molecular Hydrogen Ion Beam
Subject to Space-Charge Forces

$$x/r_o = \frac{9.844}{M^{1/4}} \frac{V^{3/4}}{I^{1/2}} \int^{\sqrt{\ln r/r_o}} \epsilon^{t^2} dt$$

	Extraction voltage 40 KV		Einzel lens diameter 2 inch	
Initial Beam Radius	Extracted Current	Magnification r/r_o at	Radius r at	Current within 1 inch Diameter Aperture
Inches	m. a.	x = 4. 63"	x = 4. 63"	m. a.
0. 025	10	10. 6	0. 265	10
	20	16. 3	0. 407	20
	30	21. 0	0. 525	27. 2
	40	26. 1	0. 652	23. 6
	50	29. 5	0. 739	23. 0
	60	33. 4	0. 835	21. 6
	100	44. 7	1. 12	20. 0
	120	49. 4	1. 23	19. 7
	150	55. 7	1. 39	19. 4

FIGURE 3

TRAJECTORIES AND EQUIPOTENTIALS
THROUGH AN EINZEL LENS

V=40KV   V=7KV   V=40KV

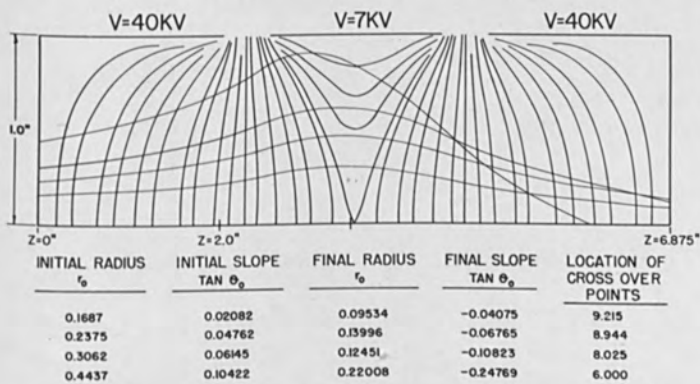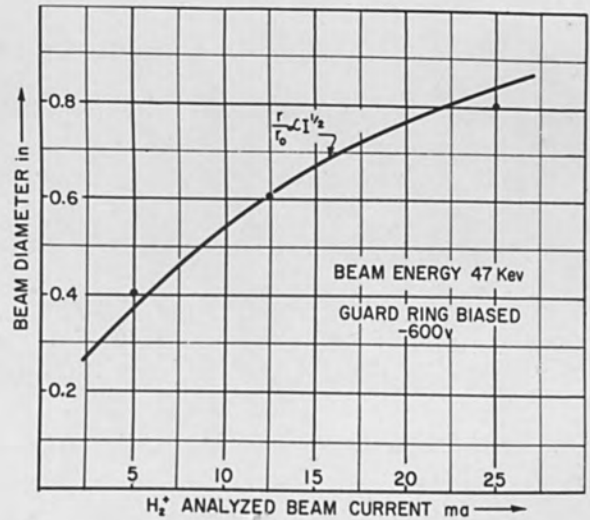| INITIAL RADIUS r_o	INITIAL SLOPE TAN θ_0	FINAL RADIUS r_o	FINAL SLOPE TAN θ_0	LOCATION OF CROSS OVER POINTS
0.1687	0.02082	0.09534	−0.04075	9.215
0.2375	0.04762	0.13996	−0.06765	8.944
0.3062	0.06145	0.12451	−0.10823	8.025
0.4437	0.10422	0.22008	−0.24769	6.000

FIGURE 4

FIGURE 5   BEAM DIAMETER DEPENDENCE ON BEAM CURRENT FOR A FIXED GEOMETRY

was taken is that shown in line drawing on the first slide. Focusing was accomplished with an Einzel lens similar to that in the previous slide. Figure 6 is a photograph of the apparatus.

The remaining slides show other characteristics of this particular device. They are all rather typical of such equipments.

Figure 7 shows the variation in beam analysis with source pressure for operation with hydrogen. Generally the H_2^+ component decreases with increasing pressure while the H_3^+ increases. H_1^+, the proton fraction increases somewhat also but relatively slowly. This apparatus was designed for production of an H_2^+ beam and the beam current and diameter information given in the other figures are for H_2^+ beam with the source operated at low pressures where about 80% of the beam was this component. A 45 degree analyzing magnet deflected other masses out of the beam measuring system.

Figure 8 shows the result of increasing the current output at the source. Plotted along the abscissa are values for the total high voltage current supplied to the source head.. This is not true ion output but is more or less proportional to ion current and can be used as its measure. As the source output is increased, the analyzed H_2^+ beam increases linearly at first, then levels off, and finally actually drops. This occurs when the beam diameter in the lens has increased because of space charge to a value larger than the "effective" lens diameter. Results for both 20 and 40 kilovolts are shown; the higher voltage results, of course, are better. Comparison of these results with the computed values for space charge blowup of a 40 Kev beam shown in Figure 3 indicate that this 2 inch lens has an
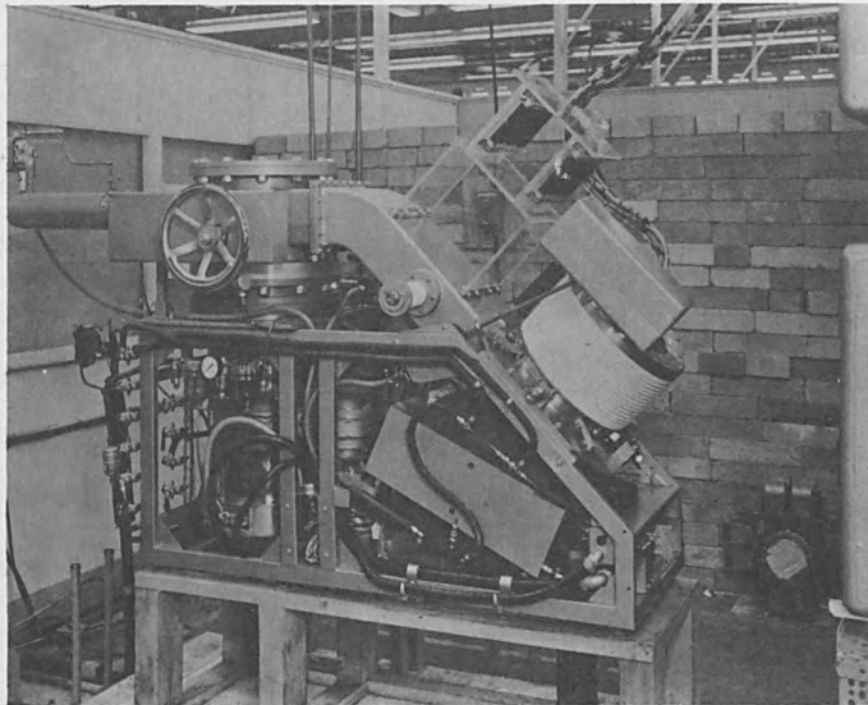
FIGURE 6   EXPERIMENTAL SYSTEM USED FOR OBTAINING THE DATA DISCUSSED
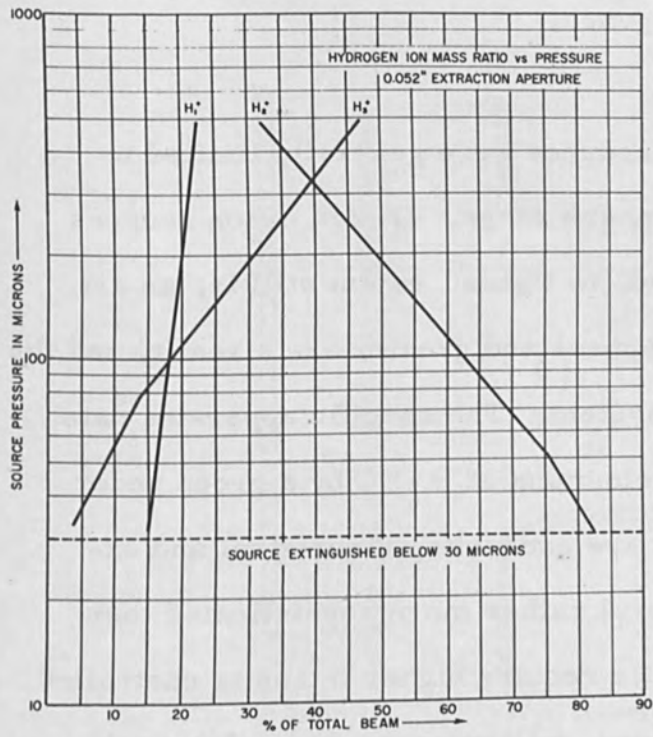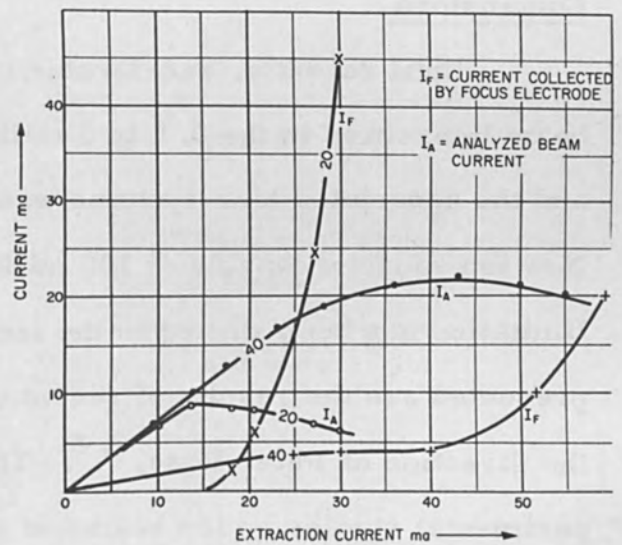

FIGURE 7

FIGURE 8

"effective" diameter of slightly greater than 1 inch.

Figure 9 shows the maximum analyzed beams obtainable vs extraction potential. The data agree fairly well with expected $I = V^{3/2}$.

Figure 10 shows the effect of changing the position of the center of the lens relative to the source output aperture. Maximum analyzed beam current and diameter for a fixed energy are both plotted against position. For lens positions close to the source, the source output could be raised to higher values before filling the "effective" lens diameter; but the system magnification was, of course, increased accordingly with corresponding increase in beam diameter.

Figure 11 is a schematic diagram of a beam scanner. A thin wire mounted on a rotating disc within the vacuum chamber is swept through the beam and the pickup signal displayed on an oscilloscope. This produces a beam profile. Comparison of the two signals generated in a single rotation permits an estimate of beam divergence.

Conclusions

Until recently, accelerator ion sources were generally limited to beam intensities in the 0.1 to 1 milliampere range. Design of ion sources and the associated lens systems was, and, to a great extent still is, an art. Now ion sources capable of 100 milliamperes and greater are a reality and the limitation has been shifted to the lens system. The specific apparatus data presented are the results of recent development at HVEC by a group under the direction of Peter Rose,[3,4] They are conducting theoretical and experimental studies on ion beams at a level rather more sophisticated than has been necessary to us in the past. We require higher intensity controlled ion beams chiefly for tandem accelerators, millimicrosecond pulse work, and for special injectors. Ion rocket devices are also of interest.
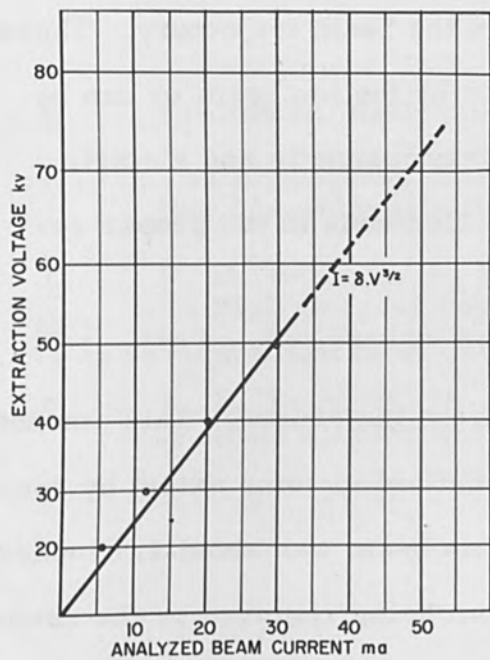
FIGURE 9

EXTRACTION VOLTAGE DEPENDENCE ON ANALYZED BEAM CURRENT
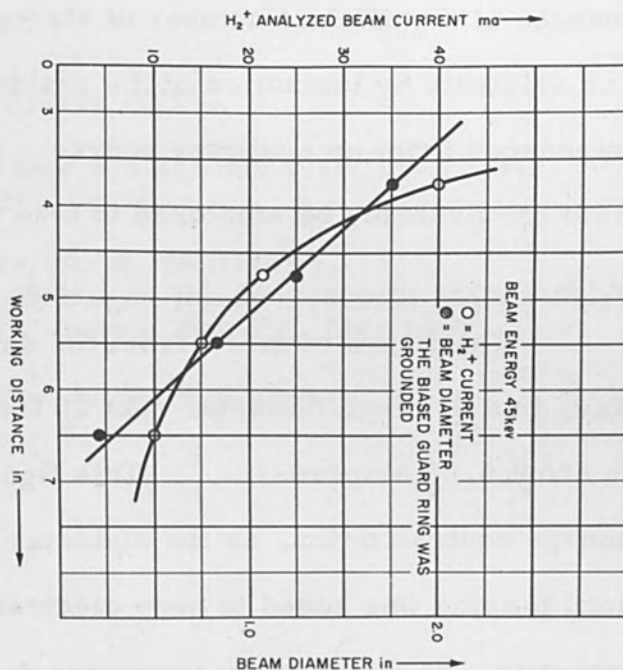
$I = 8.V^{3/2}$

FIGURE 10   EFFECT OF VARIATION OF THE POSITION OF THE CENTER OF THE LENS RELATIVE TO SOURCE OUTPUT APERTURE
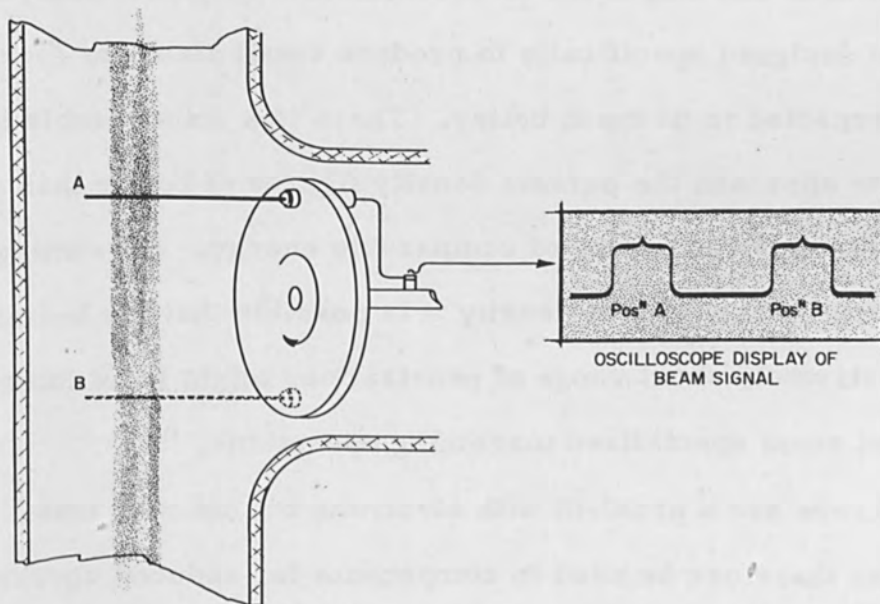

FIGURE 11   SCHEMATIC DIAGRAM OF A BEAM SCANNER

Considerable gains can be expected from improved optics but the main limitation is space charge. Neutralization by electrons seems a practical approach to space charge compensation. This involves maintenance of a sufficient number of electrons in the beam trajectory. These can originate by ionization of the residual gas by the ion beam or can be introduced from an auxiliary source. Auxiliary magnetic and electric field can probably be employed to trap these electrons in the proper region.

The figure of merit from the data given is 25 milliamperes at 47 Kev. in a 0.8 inch diameter spot 26 inches from the source. This amounts to about 0.05 amperes/in.^{2}. This figure benefited to some extent by space charge neutralization, as the diameter for this beam was about 1.1 inches until biasing was added to keep electrons from being removed by the source potential. The particular apparatus described, however, was designed to produce a nearly parallel beam; and it also incorporated sufficient distance between source and output end to accommodate magnetic analysis. An equipment designed specifically to produce small diameter focused spots could be expected to do much better. There is a considerable improvement required to approach the current density figures of better than 10 amps/in^2 reported for electron beams of comparable energy. Presuming sufficient improvement in the current density it is possible that ion beams, because of their extremely short range of penetration, might be of interest for cutting and some specialized machining operations.

X-rays are a problem with electrons but not with ions. Increased voltage can therefore be used to compensate for reduced current density. I've added these last comments presuming that the possible use of ion beams in this field lies behind the inclusion of this subject in the Symposium.

REFERENCES

1.   Frolich H. Nukleonik 1 183-188 (1959).

2.   Von Ardenne M. Tabellen Der Electronenphysik Ionephysik
        Und Ubermikroskopie 1956 Berlin.

3.   P. H. Rose, R. P. Bastide, A. B. Wittkower,
        "A High Current Positive Hydrogen Ion Source with Mass Analysis",
        to be published in Rev. Sci. Instr. Vol. 32, May 1961.

4.   P. H. Rose, R. P. Bastide, A. B. Wittkower
        (Private Communication).

ELECTRON BEAM WELDING IN FRANCE

By

J. A. Stohr
Head of Technology Division
French Atomic Energy Commission
Saclay, France

ABSTRACT

Discussion of the scope of electron beam

welding in France and its application to welding metals

and alloys in the nuclear power field. A number of

experimental systems used in the Saclay group are dis-

cussed.

ELECTRON BEAM WELDING IN FRANCE

The studies on electron beam welding started in the French Atomic Energy Commission, at Saclay, in 1954. Figure 1 shows the first apparatus we used; it was simply composed of a glass vessel, a small vacuum pumping unit, and electron gun of x-ray tube type, and a motor clock for moving the piece to be welded. Our main goal was to weld fuel elements, in order to obtain:

1. no gas filling in the gap between the fuel and the can, in the case of mechanical canned fuel elements, that means fuel elements in which the can is applied by hydrostatic or thermopneumatic machines.

   For such fuel elements, welding under vacuum permits a close tolerance between fuel and can and avoids surface contamination of the fuel, thus improving the heat transfer from the fuel to the can.

2. improved depth penetration of the weld and lessened amount of heating of the fuel element during the welding process.

The first application of electron beam welding was done on EL.3 reactor fuel elements. This fuel element is composed of an uranium-molybdenum alloy tube 30 cm long, 30 mm in diameter, 3 mm thick, canned with aluminum. An uranium-molybdenum pellet is welded at each end of the uranium tube, the U-Mo tube is placed in the aluminum can. This assembly is put in the welding machine, in which:

a)   the end aluminum cap is put in welding position.
b)   the welding is made.

After welding, the can is applied by thermopneumatic

machine.   Figure 2 shows the parts and the assembly of EL.3

fuel element.

A comparison between two sets of EL.3 fuel elements,

one welded by automatic argon arc process and the other one

welded by automatic electron beam process, showed:

1.   a 30% leak on the set welded by argon arc process,
     no leak on the set welded by electron beam process.
     All the sets were tested by helium mass spectrometer
     leak detector;

2.   low temperature increase on the part of the fuel
     element in the very close neighbourhood of the
     welded part, that was not the case with argon arc
     welded fuel element;

3.   a depth of penetration increased about 3 times with
     electron beam welding as compared to argon arc;

4.   after decaning, the EL.3 fuel elements welded by
     electron beam showed no trace of oxidation, the
     uranium-molybdenum surface was perfectly clean;
     the same fuel element welded by argon arc showed an
     uranium oxidized surface, due to air contamination;

The results obtained led to using electron beam

welding for the fabrication of all the next sets of EL.3

fuel elements.   Figure 3 shows the machine built by the

French Society SCIAKY and used for fabrication in the plant

of Society C.E.R.C.A., near Paris.   This machine is composed

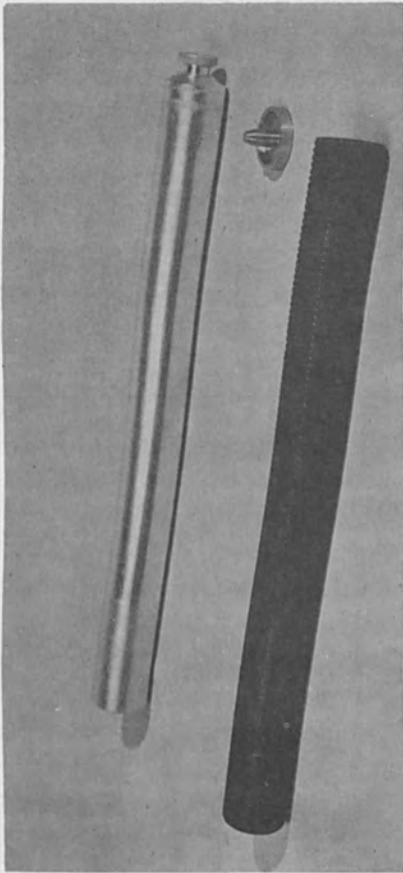of a working vessel with 3 large lead glass windows, so as

FIGURE 2. EL.3 FUEL ELEMENT: a) PARTS
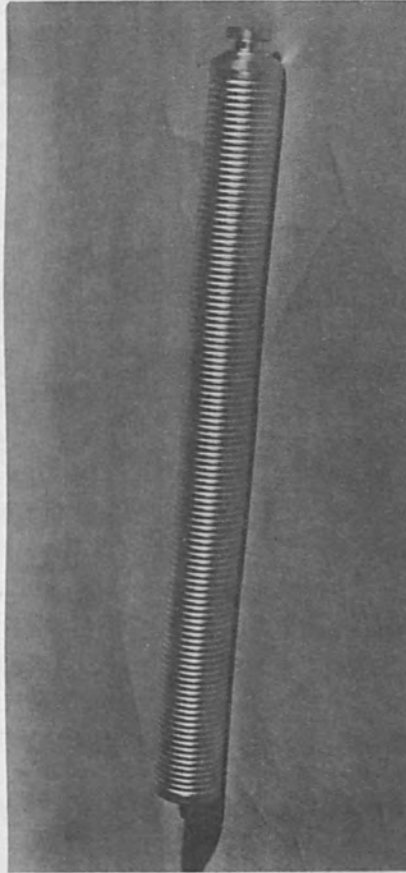U-Mo TUBE WITH END PELLETS WELDED,
Al CAN AND END Al CAP.

FIGURE 2. EL.3 FUEL ELEMENT: b) ASSEMBLY
AFTER END CAP WELDING, THE CAN IS FORCED
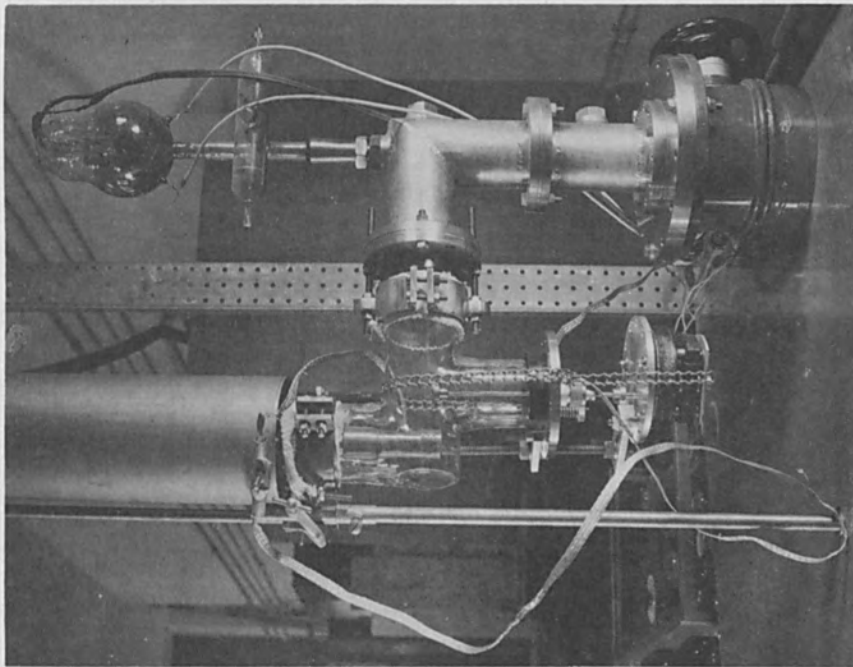INTO GROVES BY PRESSURE (THERMOPNEUMATIC MACHINE)

FIGURE 1. FIRST ELECTRON BEAM WELDING UNIT.

to get an easy view of the work, a vacuum pumping system, a 20 kV .1 A generator, and a relatively simple electron gun. A rotating support allows the welding of 14 fuel elements without breaking the vacuum.

The fabrication of five sets by electron beam and two sets by argon arc welds showed that if electron beam welding is in itself more expensive than argon arc, its use for EL.3 fuel elements fabrication lowers the total cost, mainly by avoiding leak defect, and improving the performance of the fuel element; the temperature drop between fuel and can is in this case very important, the thermal flux is as high as 220 W/cm^2. Since our first experiment and the first application of electron beam welding to EL.3 fuel element fabrication we have conducted extensive studies and developed new applications continuing these, mainly in the field of fuel elements.

The studies may be divided into 5 parts:

1. welding of various materials; aluminum and its alloys, beryllium, zirconium and its alloys, stainless steel, refractory metals like 80Ni-20Cr alloys, uranium and its alloys, niobium;

2. design of electron guns, in the range of 20 to 120 kV from 1 to 5 kW power, in close cooperation with Mr. Sommeria of the Society PRECIS, in France;

3. relation of specific power with depth of penetration and welding speed;

4. improvement of depth penetration by chopping the current in order to obtain a greater speed and a smaller thermal affected zone;

5. design of apparatus able to solve our specific problems in close connection with the Society SCIAKY in France.

We succeeded in welding the various metals used in the field of Atomic Energy, for example some UO_2 fuel elements canned with beryllium are tested in ORR reactor at Oak Ridge and have worked without failure since September 1960. Figure 4 shows the components and the assembly of this fuel element. Good results were obtained on UO_2 fuel elements canned zirconium, special alloys and stainless steel. In the stainless steel, we succeeded to weld end cap and tube each of .07 mm thickness.

The question of electron gun, of voltage supply and of focus size, is a little more complicated. Some data are not available, due to the fact that they were obtained for special purposes.

It is possible to say that we succeeded in welding a thickness of about 15 mm on two pieces of aluminum, edge to edge, at a speed of about 30 cm/min and with a melted zone of 1.5 mm width. The complete penetration was obtained in one pass. The same result was obtained on a stainless steel piece of about 1 cm thickness. We used in each case

FIGURE 3.   EL.3 FUEL ELEMENT FABRICATION
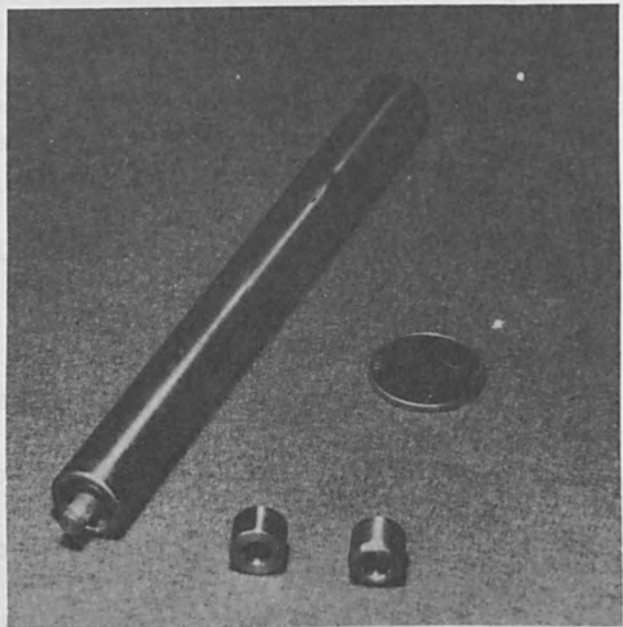(SCIAKY MACHINE, AT C.E.R.C.A. PLANT)

FIGURE 4. UO_2 FUEL ELEMENT (BERYLLIUM CAN), HELIUM TEST SHOWS
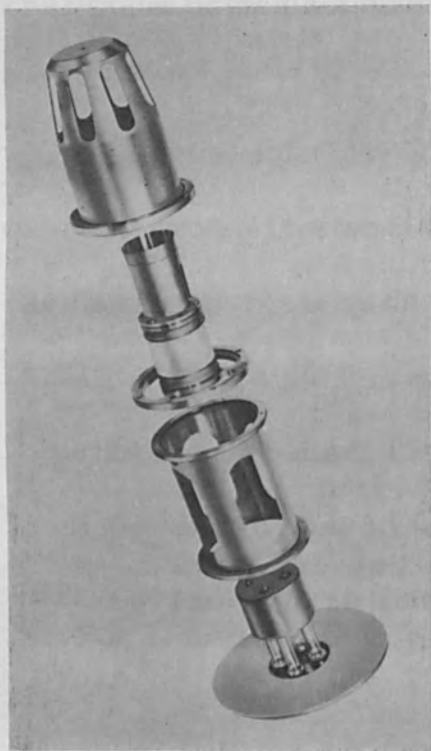95% WELDS TIGHT. (WITH PECHINEY BERYLLIUM TUBE) **

FIGURE 5.

a) EXPLODED VIEW OF THE 5 KW ELECTRON GUN.

FIGURE 6.
5 KW ELECTRON GUN ASSEMBLY.
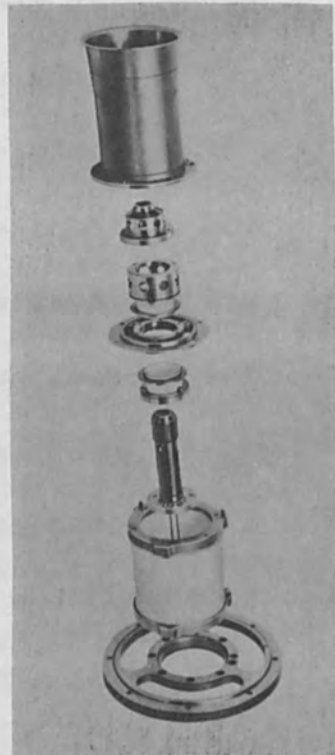(SOCIÉTÉ PRECIS, PARIS).

FIGURE 5.

b) 5 KW ELECTRON GUN.   PARTS OF THE CATHODE.

a 20 kV, 3 phase full wave rectifier. The intensity of the electron beam was about .2 A; the size of the focus was about .8 mm in diameter.

If we consider the results obtained on thinner pieces of the same materials, we think it will be possible to improve the welding speed on such pieces, by chopping the current. We did not try it on very thick pieces because our power supply was insufficient at the time for such thickness and our apparatus giving chopping frequencies was not suitable for a speed higher than 30 cm/min. We feel that in order to obtain perfect and continuous welded lines it is necessary to have perfect overlapping. We hope to succeed in this task with our new guns and with another chopping system. Figure 5 shows the exploded view of our new electron gun. Figure 6 shows the assembly. This gun, of the Pierce type, gives a power of 5 kW at an accelerating voltage of 60 kV. All the insulation parts are in ceramics, so it is possible to heat the assembly at a temperature of 700°C if necessary. The focus size is .8 mm at a distance of 7 cm.

Mr. Sommeria, of the Society PRECIS, developed two other guns of 40 kW and 100 kW power. Such a power is unnecessary for welding purposes, but their design led

to some modifications on the initial design of the welding gun.

For a study system, we built a special unit (figure 7) on which it is possible to replace any part by another one of a special design. The electron gun is supported by a mechanism allowing it to have any desired position on any point of the plan, so it is possible to weld along a complicated welding line, by means of a manual of automatic device. (figure 8). Such an apparatus is very versatile; so it is possible to try on it a new electron gun as well as welding a tube as long as five meters.

Since EL.3 fuel elements fabrication, many other applications have been achieved. We can examine two of these applications, in which the use of electron beam welding lowers the total fabrication cost and improves the quality of the fuel element. The first application concerns the fabrication of the well known plate fuel elements, zircaloy 2 canned, alloy U-Zr as a fuel.

This type of fuel elements are obtained by co-rolling the fuel and the can in an iron shell. Still to obtain a perfect bounding, it is necessary to use a vacuum inside the shell, or inside the can fuel assembly, or in both of them. The designs generally used are rather
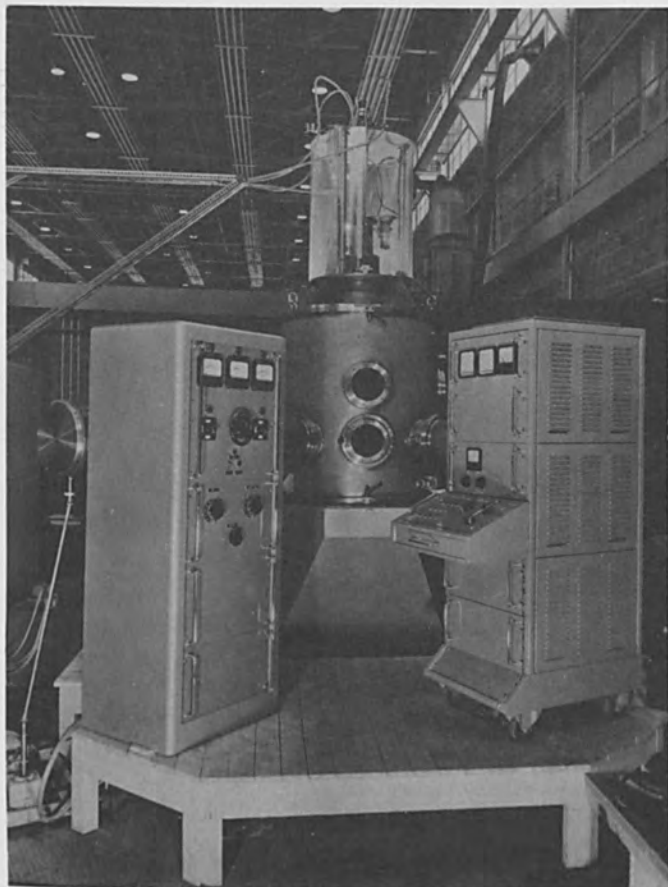
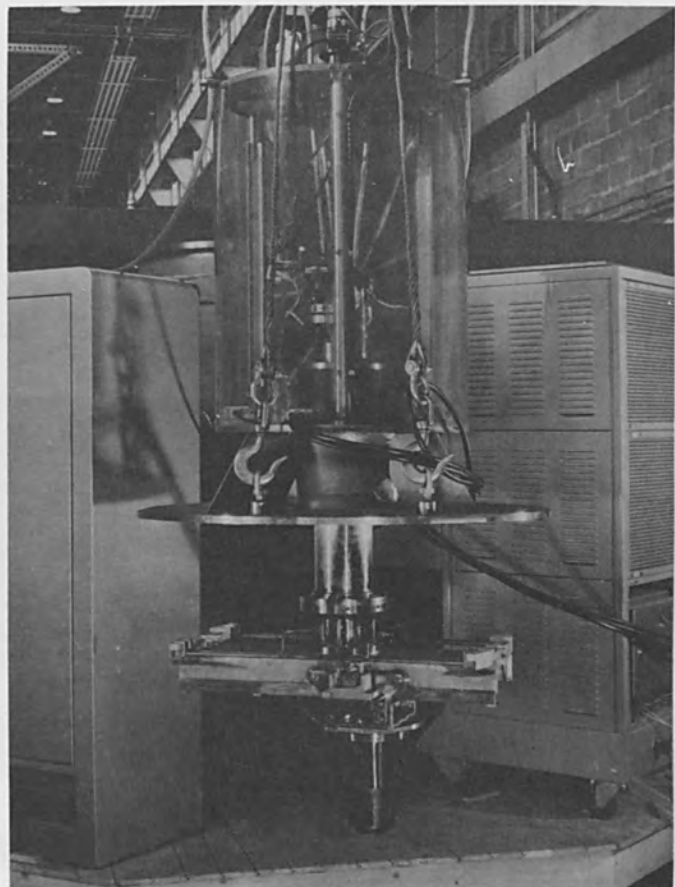FIGURE 7. LABORATORY VERSATILE APPARATUS (SACLAY)

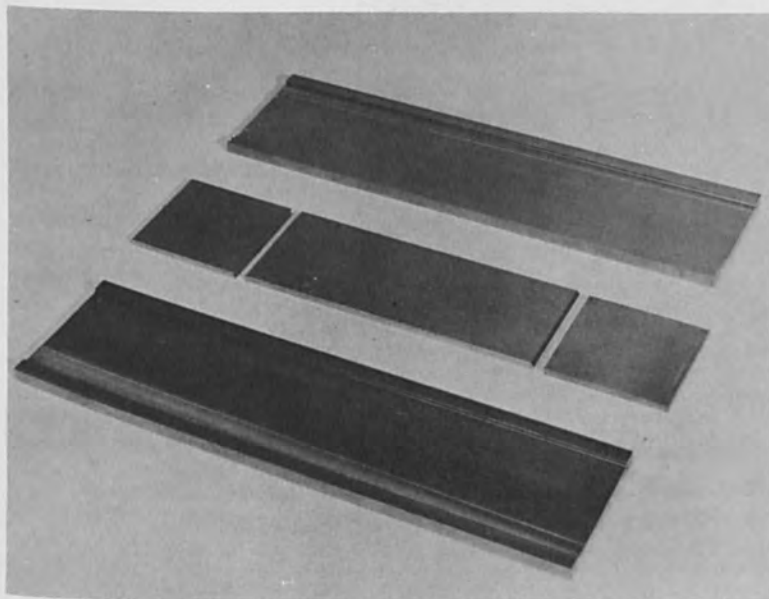FIGURE 8. SPECIAL DESIGN FOR MOVING ELECTRON GUN.

FIGURE 9. PARTS OF PLATE FUEL ELEMENT BEFORE WELDING AND ROLLING.
FUEL AND ZIRCALOY CAPS IN THE CENTER. HALF PARTS OF
CAN ON EACH SIDE. HALF PART OF CAN IS OBTAINED BY
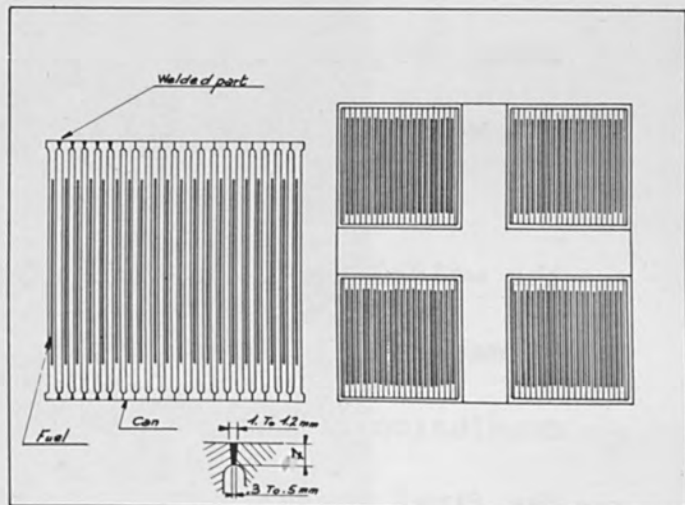EXTRUSION (INCLUDING THE THICK PART OF THE SIDE).

FIGURE 10. TWENTY PLATE FUEL ELEMENT BUNDLE.

complicated. We used a more simple one, in which the can
is composed of two parts obtained by extrusion and slightly
machined (figure 9). The fuel is put between these two
plates and the assembly so obtained is welded by electron
beam. The usual process is then used for the preparation
of the assembly to be co-rolled. This scheme is more
simple than the first one used, in fact by means of electron
beam we obtained in the same operation a vacuum inside the
fuel-can assembly and the welding of it. All the tests,
whether mechanical, ultrasonic or metallographic, showed
a perfect bond.

The plates thus obtained are welded on each other
to form a bundle of 20 plates (figure 10). It is necessary
to get with a depth of penetration of about 7 mm without
injuring the fuel. This can only be achieved by electron
beam. Figure 11 shows the machine on which fuel elements
are welded. The plates have a length of about 120 cm.

The corrosion tests showed that the behavior of
the welded zone, in the as welded condition without chemical
or mechanical cleaning, was perfectly satisfactory. The
conclusion of these tests led to use electron beam for
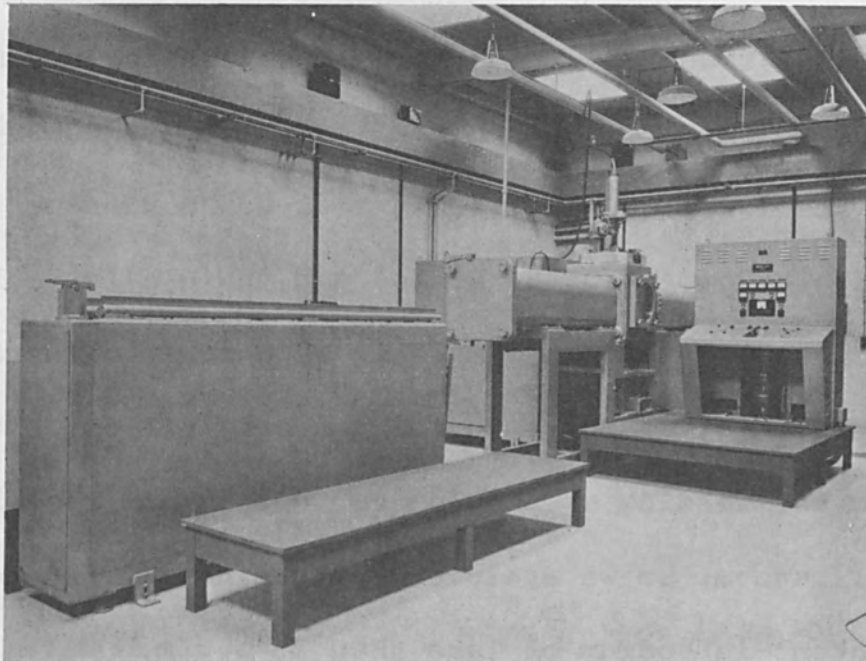the final assembly obtained by welding 4 bundles in a
zircaloy case.

FIGURE 11.   MACHINE USED FOR WELDING FUEL PLATES BUNDLE.
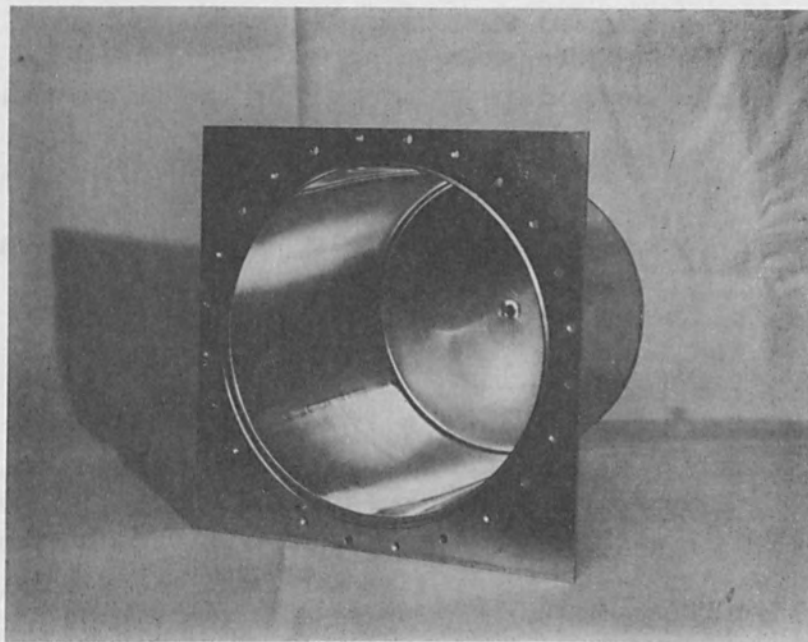(BUILT BY SCIAKY, USED IN C.E.A. PLANT)

FIGURE 12.   ZIRCONIUM TANK OF PROSERPINE HOMOGENEOUS REACTOR.

The second application concerns the fabrication of the blanket fertile fuel elements of our fast neutron, sodium cooled, reactor. The fuel element is an hexagonal bundle of seven needles. Each needle is composed of a stainless steel can in which is introduced an uranium alloy rod. The gap between the rod and the can is filled with sodium. We developed a machine in which the introduction of uranium alloy rod into the can, the filling of sodium and the welding of the end cap of the can are all done under vacuum; so we avoid any contamination and get oxygen content in sodium of less than 15 p.p.m.

Of course, we use other welding methods for fuel elements fabrication; for example, we use argon arc welding for uranium fuels canned with magnesium-zirconium alloy; the choice of the method is a matter of metal cost and performance.

We always use electron beam welding when one or many of the following parameters are necessary:

> working under vacuum,
> sealing under vacuum,
> getting a significant depth of penetration,
> avoiding to heat in excess the pieces to be welded,
> welding with a very accurate position of the welded line.

We use electron beam welding also for purposes other than welding of fuel elements, for example the welding

of the zircaloy tank of our homogeneous plutonium power

reactor (figure 12). In that case, the soundness and the

safety of the welded parts were the only significant

considerations with cost being of no importance.

There are probably a lot of applications of

electron beam welding in fields other than Atomic Energy.

I hope other speakers will be kind enough to give us some

information on these applications. We are especially

interested in the field of refractory metals like molybdenum,

tantalum, etc...

ELECTRON BEAM WELDING AT HIGH VOLTAGES
(100,000 - 150,000 volts)

By
H. H. Hoffman
Senior Engineer
Nuclear Fuel Research Laboratory
Olin Mathieson Chemical Corporation
New Haven, Connecticut

ABSTRACT

Data on electron beam welding with a high
voltage system are presented. Materials processed
were zircaloy, inconel, stainless steels, aluminum,
1100 and 2024 aluminum alloys, columbium and tungsten.

ELECTRON BEAM WELDING AT HIGH VOLTAGES

(100,000 - 150,000 VOLTS)

A. Introduction

In the several years since the commercial introduction of electron beam welding in this country, interest has continued to grow in the application of the process. Reports from earlier papers[1,2,3,4,5,6] and the titles of some of today's presentations indicate considerable experimental work has been underway in various laboratories to develop techniques and parameters for welding the reactive, refractory, and other difficult to weld materials. It is in the joining of these metals and alloys that the unique characteristics of the electron beam welding process appear most useful.

In the area of machine design both the low and high voltage type machines have received continued development. Electron gun design has settled on the self-accelerated type which has been found to eliminate the many problems encountered when using work-accelerated units. At Olin Mathieson Chemical Corporation, work has been under way for over two years with a 2 KW - 150 KV electron beam welding machine designed and constructed by Carl Zeiss, Incorporated of Germany. This unit is probably the most versatile and sophisticated design electron beam machine on the market today. Voltage is continuously variable up to 150 KV at currents from zero to 20 milliamperes. From the self-accelerated gun, its electron optics and magnetic lens system can produce an electron beam focussed to less than 0.010-inch diameter. As will be shown later, this beam is capable of penetrating and fusing virtually all materials up to at least one-half-inch thickness. Before reviewing the techniques employed to

join the various metals and alloys with this machine and the metallographic results, it will be of interest to briefly explain its operation and potential capabilities.

B. Operation and Basic Parameters

Fig. 1 shows a photograph of the machine and associated equipment as installed in the Nuclear Fuel Research Laboratory of Olin Mathieson Chemical Corporation in New Haven, Connecticut. All possible precautions were taken on its installation to prevent accidents involving either high voltage shock or x-radiation which is produced during operation. The chassis of the unit was grounded by four separate leads to preclude even minor shock hazard. In addition, the floor of the laboratory was covered with both rubber matting and 3/8-inch thick polyethylene to prevent accidental grounding of operating personnel during use or maintenance of the unit. While the gun column and vacuum chamber of the machine were lined with 5 mm thick lead sheet the unit was completely checked with sensitive radiation monitoring instruments after installation. In addition, the unit is regularly rechecked to assure the shielding materials have not been dislocated in operation. All operating personnel must wear radiation film badges which are changed weekly to assure rapid detection of potential radiation exposure. To date no x-radiation exposure has been found and the high voltage shock hazard is completely under control. In brief, with the precautions used, the operation is very safe.

Fig. 2 is a schematic diagram of the electron gun column and vacuum chamber. The electron gun is located at the top of the column. The filament cathode in the gun is available in two designs, a simple hair pin shape or a multiturn

118
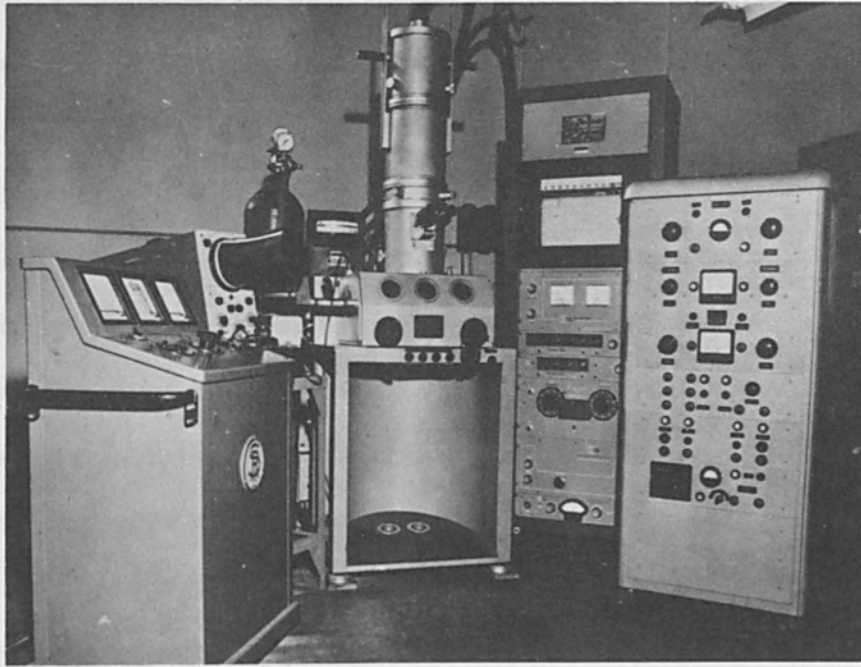
Fig. 1. Photograph of the 2 KW – 150 KV Capacity Zeiss Electron Beam Welding Machine and Associated Equipment
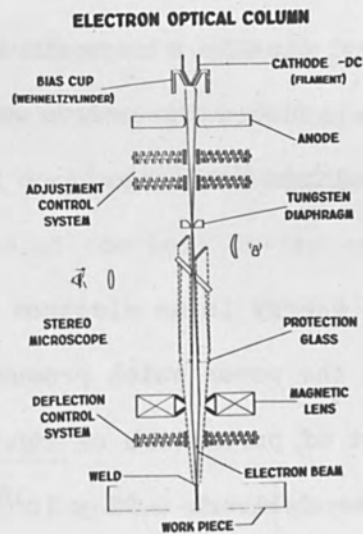
Fig. 2. Schematic Diagram of Electron Gun Column and Work Chamber of Electron Beam Welding Unit.

119

coil unit. The greater available surface area of the coil filament permits it to emit a larger number of electrons and therefore produce greater energy at equivalent parameters.

In operation, a separate circuit heats the filament to incandescence and initiates thermionic emission of electrons. The machine operator can control the filament current and thus its electron output. Surrounding the cathode and also cathodically charged is a shaped cup which serves to electrostatically focus the electrons emitted by the filament. A potential of up to 150 kilovolts can be obtained between the cathode and the ring anode. On emission from the cathode the electrons speed toward the anode. Electrostatically focussed by the cathode cup to form a concentrated beam, the electrons pass through the ring anode on their way to impinge on the work piece. A cluster of electromagnetic coils placed just below the anode serves to properly align the beam. Next, a heavy tungsten diaphragm eliminates stray electrons and finally a magnetic lens produces the finely focussed electron beam which produces the unique weld configuration characteristic of the high voltage machines.

An analysis of the potential energy in an electron beam as detailed in the Appendix readily reveals the power which produces such feats of penetration. At an arbitrary set of parameters of 150 kilovolts and 10 milliamperes the electron beam delivers 6.28×10^{16} electrons per second. At this voltage the electron velocity is more than 135,000 miles per second and their relativistic mass is approximately 1.5 times[7] the rest mass. On impact with the work piece 349 calories are released as heat energy. At a beam focal diameter of 0.100-inch this energy is capable

of heating a 1/4-inch thick tungsten at 16,950°C per second. A beam diameter of 0.010-inch such as is normally obtained with the Zeiss machine can theoretically yield a one-hundred fold increase in the rate of heating. While conduction, vaporization of material and radiation losses reduce the actual efficiency of energy transmittal the indicated power is sufficiently large to explain the unprecedented weld penetration to weld width ratio obtained with this machine. As will be subsequently shown, the location of the beam focal point also affects the degree of weld penetration.

The mode of operation of the electron beam in producing a weld seam has aroused considerable interest. The experiments of Burton and Frankhauser[8] at Bettis Atomic Power Laboratory and work at Olin indicate the electron beam drills a conical cavity into the surface of the work piece. Our earlier calculations suggest there is more than sufficient heat energy to vaporize the material within this cavity. The metal surrounding this cavity is fused and deposited at the rear as the beam traverses the seam. The rapid cooling and solidification of the narrow molten weld pool in the wake of the beam cavity causes it to retain its shape as deposited.

C. Welding at High Voltages

Naturally, any process capable of the penetration capability indicated by electron beam welding has considerable promise in applications where its unique weld characteristics and basic advantages outweigh the normal economic considerations. At Olin, we have been interested primarily in obtaining full penetration of thick butt joints in the reactive materials

121

and have thus been operating the machine in or near the 100,000 - 150,000 voltage range. In such applications the inherent vacuum of the process and the characteristic narrow fusion zone become significant advantages. One of the materials that has been explored in the Olin development program is Zircaloy-2, which is a zirconium base alloy containing small amounts of tin, iron, and chromium. As is well known, Zircaloy-2 is highly reactive at fabrication temperatures and can dissolve both oxygen and nitrogen with deleterious effects on its mechanical, physical, and corrosion properties. Particular precautions must be taken in welding this alloy to prevent its reaction with the atmosphere. Great success has been obtained through the use of large dry boxes which are initially pumped out to remove the internal air and back filled with an inert gas such as argon or helium[9,10]. While this procedure produces sound welds which have been proved to maintain the necessary mechanical and corrosion properties, the process is time consuming, expensive, and is dependent on the maintenance of gas purity. Further, the fusion of Zircaloy-2, with its 1800°C melting point, by the tungsten arc process requires the use of relatively high power input with a wide fusion zone in relation to the depth of penetration.

In contrast, electron beam welding provides an inherent dynamic operating vacuum of 10^{-4} millimeters Hg which is an ideally pure atmosphere,[2,5,6,11] for joining Zircaloy-2. It should be noted here that great care must be taken to assure a leak tight chamber. The pumping system capacity normally provided for in vacuum chambers are capable of producing excellent vacuum readings despite minute leaks. Under the dynamic conditions of electron beam welding such leaks can introduce sufficient gas contaminants to seriously affect the properties of Zircaloy-2.

Fig. 3 shows a cross-section of a single pass fusion weld in 0.440-inch thick Zircaloy-2 produced using 150,000 volts, 9 milliamperes and a speed of 15-inches per minute. This weld was produced with the electron beam focussed at the surface of the sample. A more spectacular depth to width configuration can be obtained by focussing the electron beam lower in the specimen. Fig. 4 shows a weld in the same thickness of material and at the same basic parameters as Fig. 3 except that the beam was focussed at the center of the specimen. Note the sharp transition between fusion zone and base metal. Fig. 5 shows the grain structure of this weld. The fine grain size evident is typical of the structure obtained on electron beam welding. The large columnar grain structure normally associated with tungsten arc welding is not found in electron beam welding.

Knowledge of the operating conditions of the process suggests that the properties of electron beam welded Zircaloy should be at least equal to those of tungsten arc welded samples. The weld is, in effect, vacuum melted while the narrowness of the fusion zone causes rapid cooling to promote relatively fine grain size thus assuring retention of corrosion properties and good strength and ductility. A series of butt welds were produced in 0.125-inch thick Zircaloy-2 plates and specimens machined for tensile and corrosion testing. Tensile samples as shown in Fig. 6 were tested at room temperature, 300°F, 450°F, and 600°F in both the as-welded and annealed condition. The results in Table I show properties equivalent to or better than the base metal. Ductility of the welds was equal to or better than the base metal which is in basic agreement with data reported by Burton and Frankhauser[8]. Table II shows a compilation of corrosion test results on the coupons pictured in Fig. 7. Again, the

Fig. 4

Macrograph of Electron Beam Fusion Pass in
0.440-Inch Thick Zircaloy-2 at 150,000 Volts,
9.0 Milliamperes and 15-Inches Per Minute
Travel Speed. Weld Parameters were Basically
the Same as Used in the Weld Shown in Fig. 3
but Electron Beam was Focussed at Specimen
Center.

Etchant: 45% HNO_3 Magnification: 7X
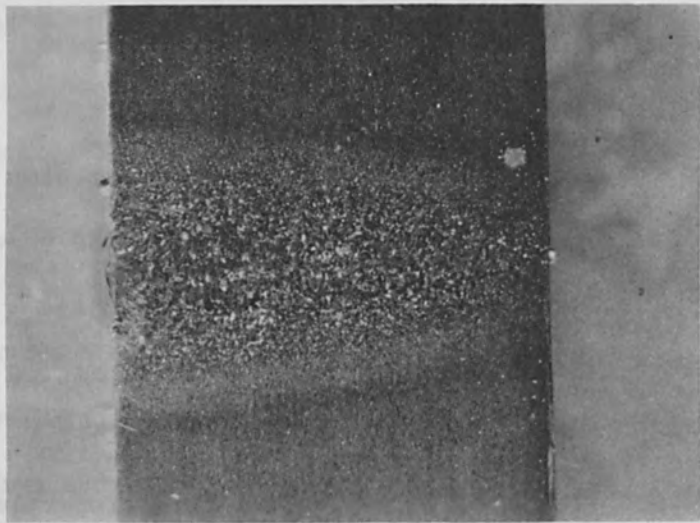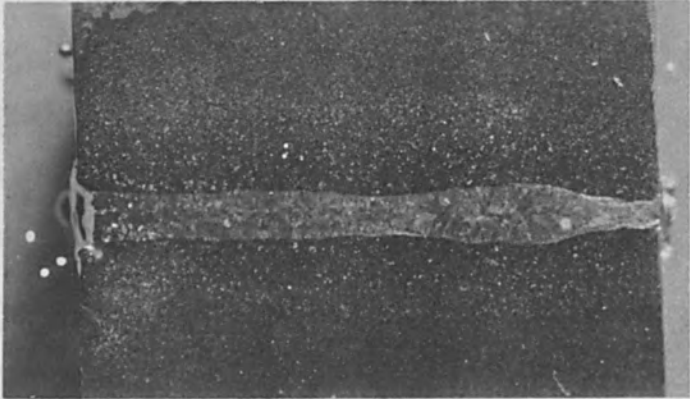   10% HF
          45% H_2O

Fig. 3.

Cross-sectional View of Electron Beam
Fusion Pass in 0.440-Inch Thick Zircaloy-2.
Note Presence of Heat Affected Zone Adjacent
to Fusion Zone. Electron Beam was Focussed
at Specimen Surface.

Etchant: 45% HNO_3 Magnification: 7X
          10% HF
          45% H_2O
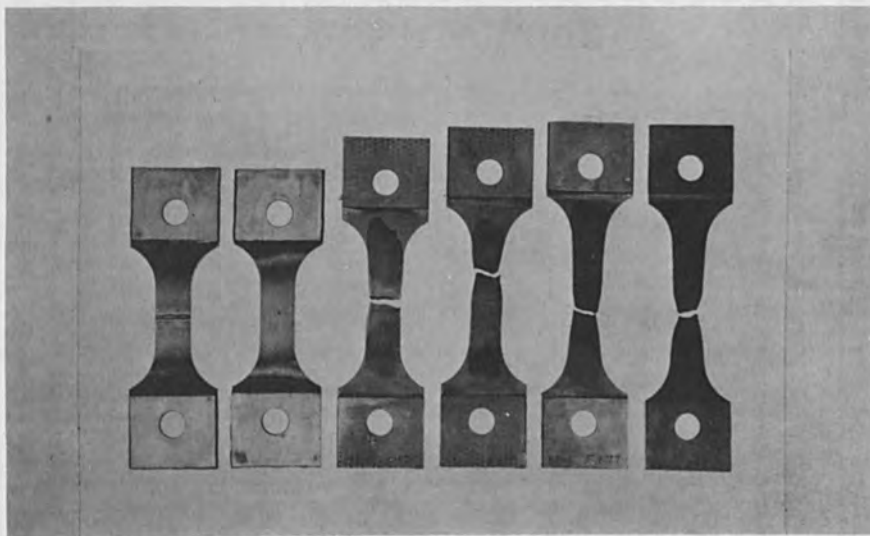
Fig. 5 Microstructure at Center of Weld in Fig. 4
Showing Widmanstatten Pattern of Quenched β
Phase Produced on Rapid Cooling from the
Molten Condition in Welding.

Etchant: 45% HNO$_3$ Magnification: 200X
            10% HF
            45% H$_2$O

Fig. 6. Electron Beam Weld Tensile Test Samples. Pictured in Order
are Specimens As Welded (Far Left), As Machined, Tested As
Welded at Room Temperature, Tested As Welded and Annealed
at Room Temperature, 300°F and 600°F.

TABLE I

TENSILE PROPERTIES OF ELECTRON BEAM WELDED 0.125-INCH THICK ZIRCALOY-2 AT R.T., 300°F, 450°F and 600°F. REFERENCE MATERIAL TEST REQUIREMENTS PER SPECIFICATIONS MIL-Z-19859-1957 AND MIL-Z-19859A-1959 "WROUGHT ZIRCALOY PRODUCTS"

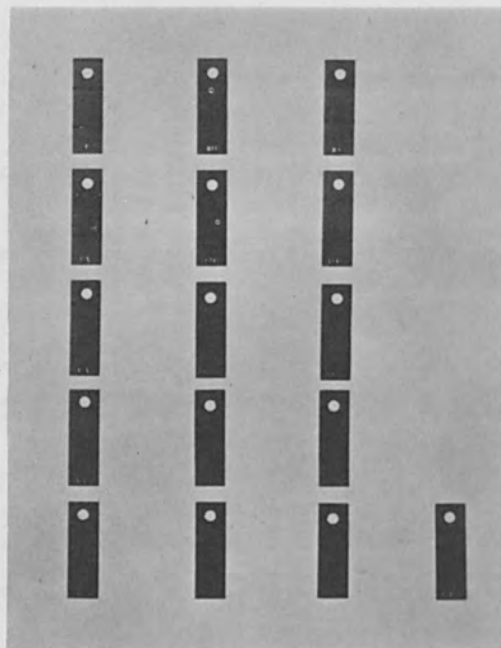| Spec. No.	Condition of Test Specimen	Test Temp., °F	Yield Str., PSI	Ultimate Tensile Str., PSI	Elong., %	Fracture Location
	MIL-Z-19859-1957 Spec. (Min. Transverse)					
ST-1	Standard Specimen – Not Welded	R. T.	51,000	57,000	15.0	Base Metal
ST-2	" "	R. T.	66,700	76,400	26.0	"
RW-1	As-Welded – No Heat Treatment	R. T.	70,200	80,000	25.0	Notch in Weld
RW-2	" " " "	R. T.	68,400	85,600	9.0	"
*RW-3	" " " "	R. T.	68,800	86,000	11.0	Weld
*RW-4	" " " "	R. T.	55,200	69,600	20.0	Notch in Weld
RW-5	Not Machined	R. T.	53,700	69,700	10.0	Edge of Weld
RW-6	"	R. T.	53,500	76,300	15.3	Base Metal
RA-1	Welded and Annealed @ 600°C	R. T.	52,700	78,100	23.0	Base Metal
RA-2	" 600°C	R. T.	57,000	81,900	23.0	"
RA-3	" 500°C	R. T.	59,600	81,000	25.0	"
RA-4	" 500°C	R. T.	51,800	77,800	23.0	"
RA-5	" 500°C	R. T.	51,750	78,000	24.0	"
RA-6	" 500°C	R. T.	46,750	76,600	22.0	"
3A-1	" 600°C	300	39,400	57,000	38.0	Weld Metal
3A-2	" 600°C	300	41,600	59,300	38.0	"
3A-3	" 500°C	300	37,000	53,600	29.5	"
3A-4	" 500°C	300	33,100	53,000	32.5	"
3A-5	" 500°C	300	41,800	59,200	29.0	"
4A-1	" 500°C	450	36,200	48,200	29.0	Base Metal
4A-2	" 500°C	450	37,900	49,400	28.0	"
4A-3	" 500°C	450	35,900	47,900	28.0	"
4A-4	" 500°C	450	37,000	48,900	28.0	"
	MIL-Z-19859A-1959 Spec. (Min. Transverse)					
6A-1	Welded and Annealed @ 600°C	600	18,400	29,000	35.0	Weld
6A-2	" 600°C	600	28,500	39,000	39.0	Base Metal
6A-3	" 500°C	600	29,000	39,700	39.0	"
6A-4	" 500°C	600	32,200	41,600	29.0	"
6A-5	" 500°C	600	29,900	39,400	30.5	"
6A-6	" 500°C	600	31,450	40,900	31.5	"

*Fracture more crystalline than other specimens. Weld parameters for these specimens were 130 KV and 18-inches/minute carriage speed compared to 150 KV and 24-inches/minute for all other specimens.

TABLE II

CORROSION PROPERTIES OF ELECTRON BEAM WELDED 0.125-INCH THICK ZIRCALOY-2 IN GRADE "A" WATER AT 680°F AND 2705 PSI. REFERENCE SPECIFICATIONS MIL-Z-19859-1957 AND MIL-Z-19859A-1959 "WROUGHT ZIRCALOY PRODUCTS"

Spec. Designation	Test Duration	Weight Gain	Surface Appearance
Coupon No. 1A	14 Days	16.7	OK
" 2A	"	17.3	"
" 3A	"	16.0	"
" 4A	"	18.5	"
" 5A	"	16.0	"
" 1B	"	18.4	"
" 2B	"	19.0	"
" 3B	"	17.7	"
" 4B	"	16.9	"
" 5B	"	17.7	"
" 1C	"	17.5	"
" 2C	"	18.2	"
" 3C	"	18.6	"
" 4C	"	16.2	"
" 5C	"	18.4	"
" 5D	"	15.9	"

Fig. 7. Electron Beam Welded Corrosion Test Coupons Following 14-Day
Immersion in Grade "A" Water at 2705 Psi and 680°F. Standard
Base Metal Specimens are Shown Lined Across Bottom of Photograph.
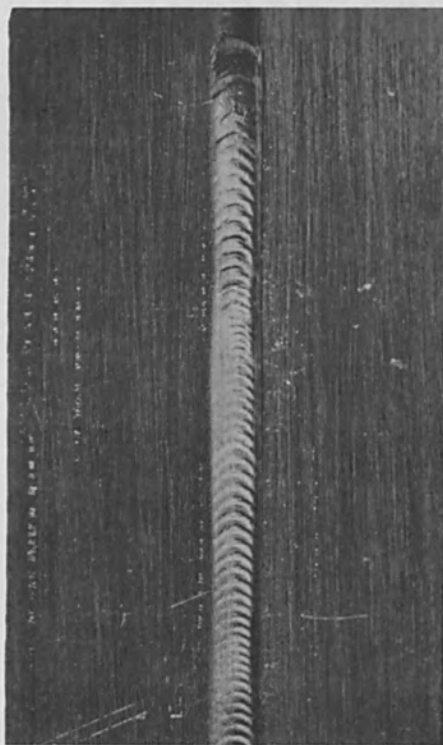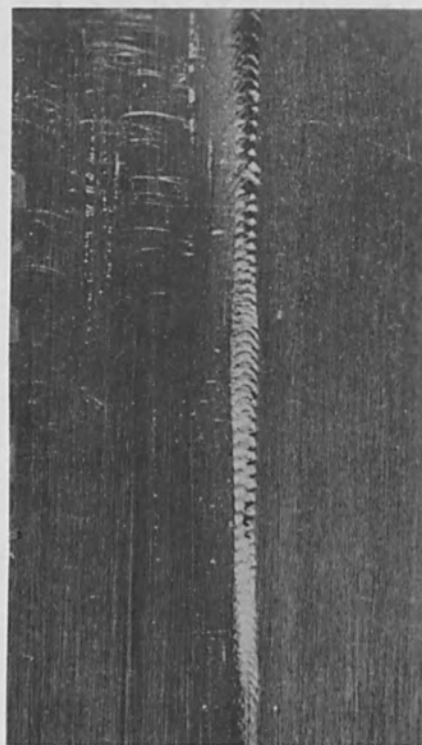
Weld Surface   Weld Root

Fig. 8   Weld Surface and Weld Root of Electron Beam
Weld in 0.012-Inch Thick Zircaloy-2 at 7X
Magnification. Joint was Made at 38,000 Volts,
2.0 Milliamperes, 28-Inches per Minute Travel
Speed.

results indicate corrosion resistance at least equal to the base metal. These data definitely show proof that electron beam welded Zircaloy-2 retains the required properties and that equally satisfactory results should be obtained with other reactive and refractory materials.

As was noted earlier, the Zeiss machine provides continuously variable voltage control. Indication of the versatility thus obtained is shown in Fig. 8 which denotes the weld surface and weld root of a seam weld in 0.012-inch thick Zircaloy-2. The weld parameters employed were 38,000 volts, 2.0 milliamperes, 28-inches per minute carriage speed and using 1.00 mm beam oscillation. Beam oscillation across the faying edges of the joint during welding diffuses the beam and compensates for minor fitup deviations which might normally produce overpenetration.

The most spectacular fusion zone configurations in electron beam welding are encountered with stainless steel and nickel base alloys. The moderate melting points and low thermal conductivity of these alloys combine to produce weld penetration to width ratios of up to 25:1. Fig. 9 shows the cross-section of a joint in 1/4-inch thick Inconel welded at 130,000 volts, 9.5 milliamperes and 24-inches per minute. Note the approximately 15:1 weld penetration to fusion zone width ratio. A weld in 1/2-inch thick stainless steel made at 150,000 volts, 9.5 milliamperes and 15-inches per minute travel speed is pictured in Fig. 10. The indicated weld penetration to weld width ratio here is even greater.

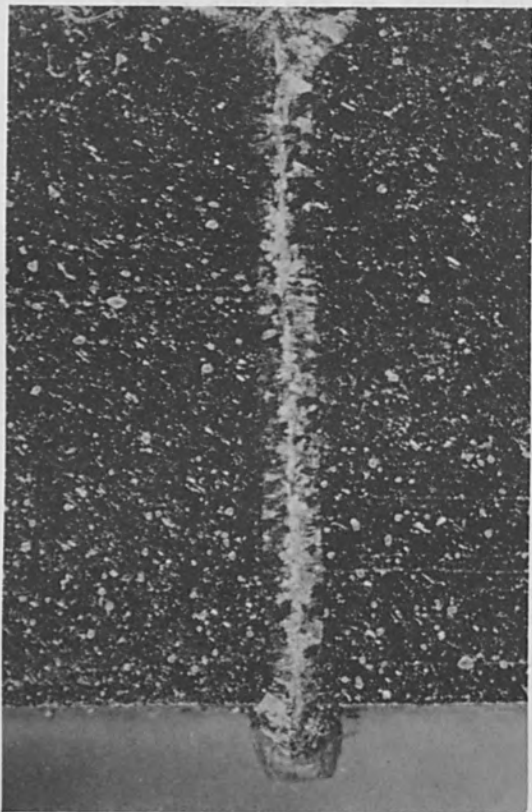One very important aspect of joining these materials is the absence of a

Fig. 9

Cross-Section of Electron Beam Welded 1/4-Inch
Thick Inconel Plate at 130,000 Volts, 9.5
Milliamperes and 24-Inches Per Minute Carriage
Speed.

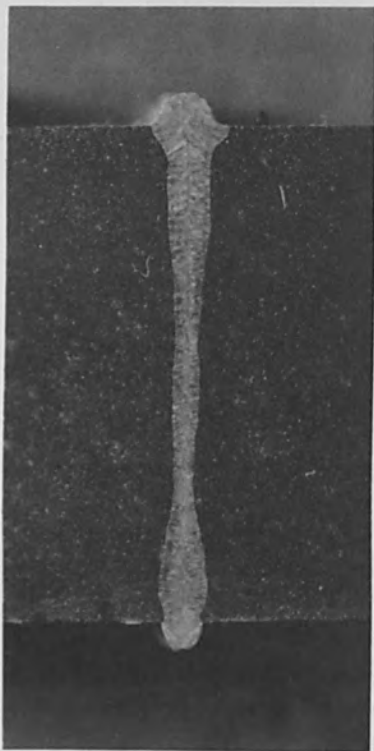Etchant: Aqua Regia   Magnification: 7X

Fig. 10

Cross-Section of Electron Beam Weld in 1/2-Inch
Thick Stainless Steel Made at 150,000 Volts,
9.5 Milliamperes, and 15-Inches per Minute
Carriage Speed.

Etchant: 10% Oxalic Electrolytic – Magnification: 7X

heat affected zone. Note the abrupt transition from weld to base metal revealed by the photomicrograph of the stainless steel weld in Fig. 11. The loss of corrosion resistance associated with sensitization of these alloys in the heat affected zone when using the tungsten arc process is thus eliminated by electron beam welding. It can be expected that electron beam welding will also improve the mechanical properties of these joints and, in particular, weld ductility. Further, the very rapid cooling rate should materially minimize the incidence of hot short cracking often encountered in joining these alloys.

Another possible application of the electron beam welding process is in the joining of aluminum and its alloys. The high conductivity of aluminum can be expected to diffuse the energy input to a greater extent but its relatively low melting point facilitates fusion. Fig. 12 shows the cross-section of a direct fusion pass in 1-1/8-inch thick aluminum made at 150,000 volts, 12 milliamperes, and approximately 5-inches per minute carriage speed. The electron beam was focussed 9/16-inch below the specimen surface. The photograph in Fig. 13 denotes a butt weld joint in 1/2-inch thick 2024 aluminum alloy made at 150,000 volts, 9.5 milli- amperes, and 10-inches per minute speed. This particular alloy is a high strength, precipitation hardening material containing 4.5% copper, 1.5% magnesium, and 0.6% manganese which is extremely hot short on welding. Our experiments show a single pass fusion butt weld can readily be made in this material by electron beam welding. A second weld pass, however, invariably produces cracking. Figs. 14 and 15 show the base metal and fusion zone structures respectively. Note the continuous grain boundary precipitate in the weld. The cracking found
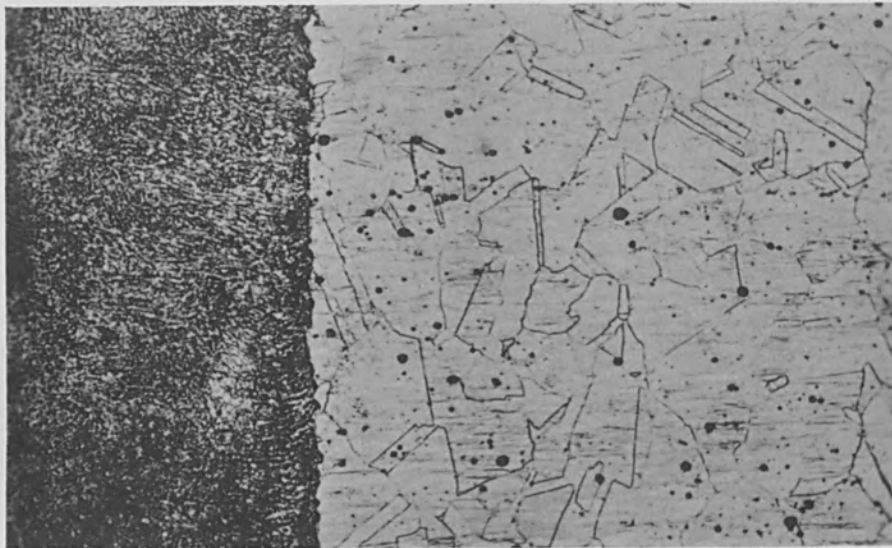
Fig. 11 Microstructure of Fusion Zone to Base
Metal Transition in Weld Shown in
Fig. 10. Note the Total Absence of a
Heat Affected Zone.

Etchant: 10% Oxalic Electrolytic

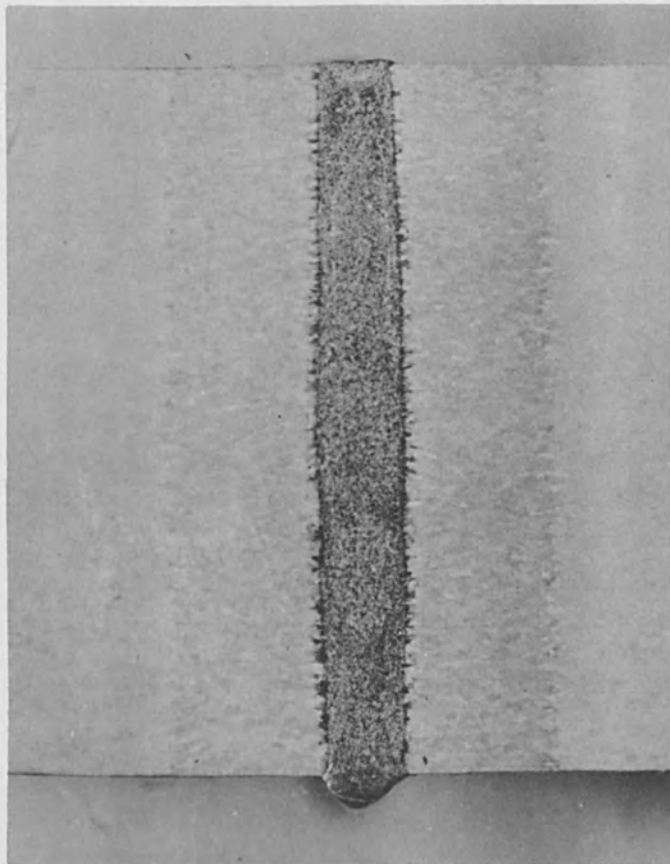Magnification: 200X
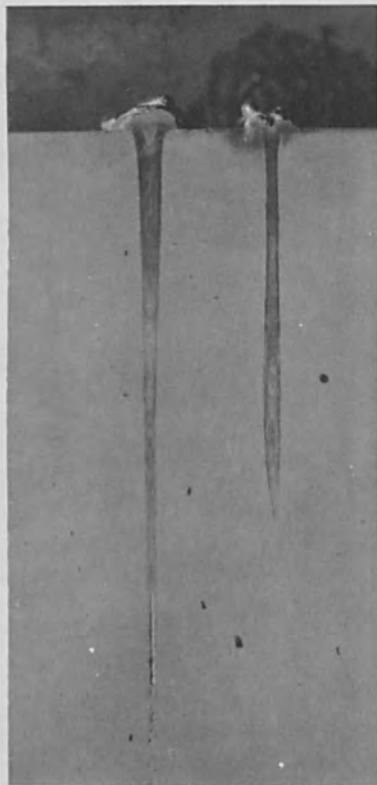
Fig. 12

Direct Fusion Pass in 1-1/8-Inch Thick
1100 Aluminum Alloy to Show Penetration
Potential of the Electron Beam. Electron
Beam was Focussed Near the Center of
Specimen.

Etchant: 0.5% HF Solution Magnification: 7X
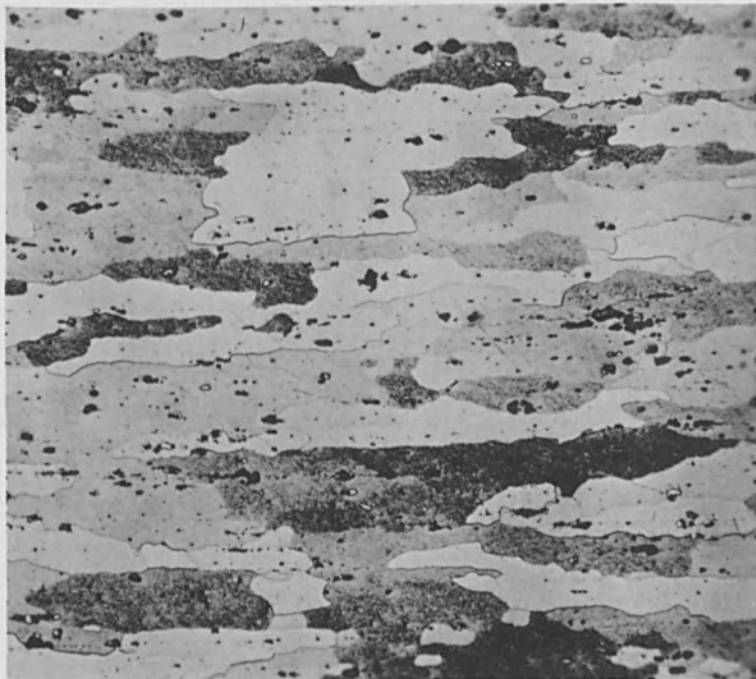
Fig. 13

Butt Weld Joint in 1/2-Inch Thick 2024
Aluminum With Electron Beam Focussed at
Center of Sample. Note the Wide Heat
Affected Zone Resulting from the High
Conductivity of Aluminum.

Etchant: Modified Keller's Reagent

Magnification: 7X

Fig. 14
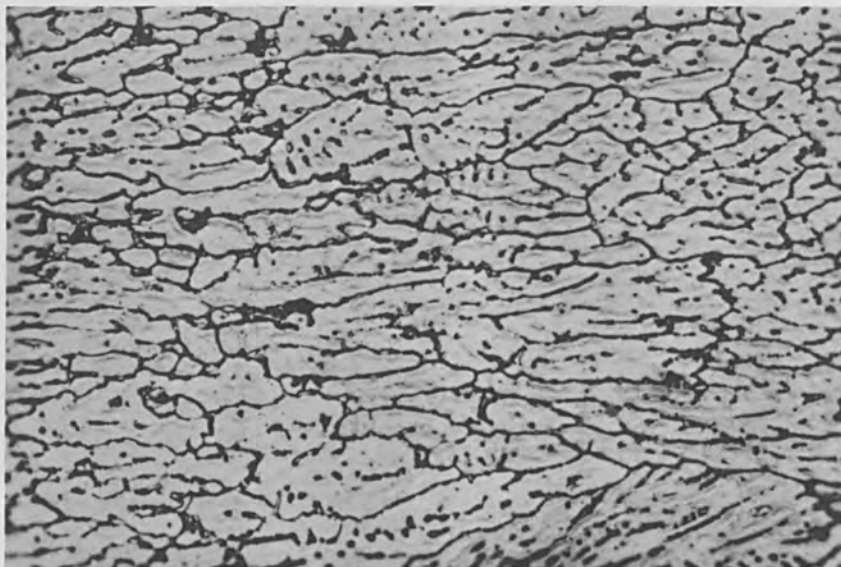
Base Metal Microstructure of 1/2-Inch
Thick 2024 Aluminum Alloy Plate.

Etchant: Modified Keller's Reagent

Magnification: 200X

Fig. 15   Fusion Zone Microstructure of Weld in
           1/2-Inch Thick 2024 Aluminum.   Note
           the Continuous Precipitate Network at
           the Grain Boundaries of the Weld Structure.

           Etchant: Modified Keller's Reagent

           Magnification: 200X
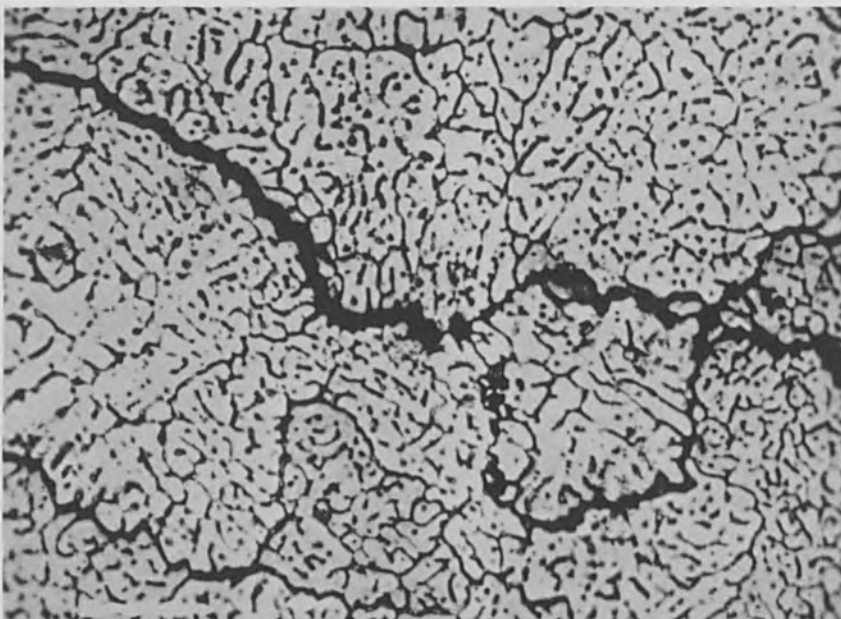
Fig. 16   Photomicrograph of Hot Short Cracking in
           2024 Aluminum Alloy after Welding Second
           Pass.   Note Cracks Follow Grain Boundary
           Precipitate Formed on Welding First Pass.

           Etchant: Modified Keller's Reagent

           Magnification: 200X

Fig. 17.

Weld Cross-Section of Joint in 1/16-Inch Thick 1100 Aluminum Alloy Produced at 50,000 Volts, 8.0 Milliamperes, and 26-Inches Per Minute.
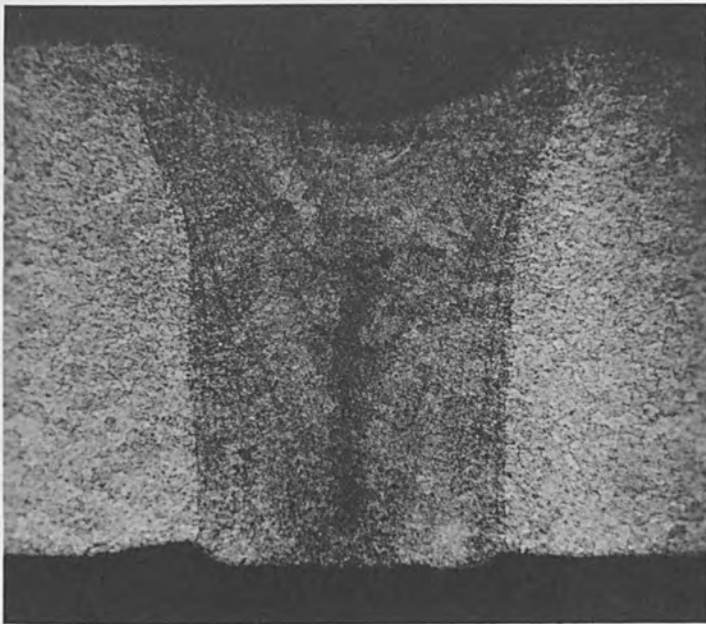
Etchant: Modified Keller's Reagent

Magnification: 50X

Weld Surface   Weld Root
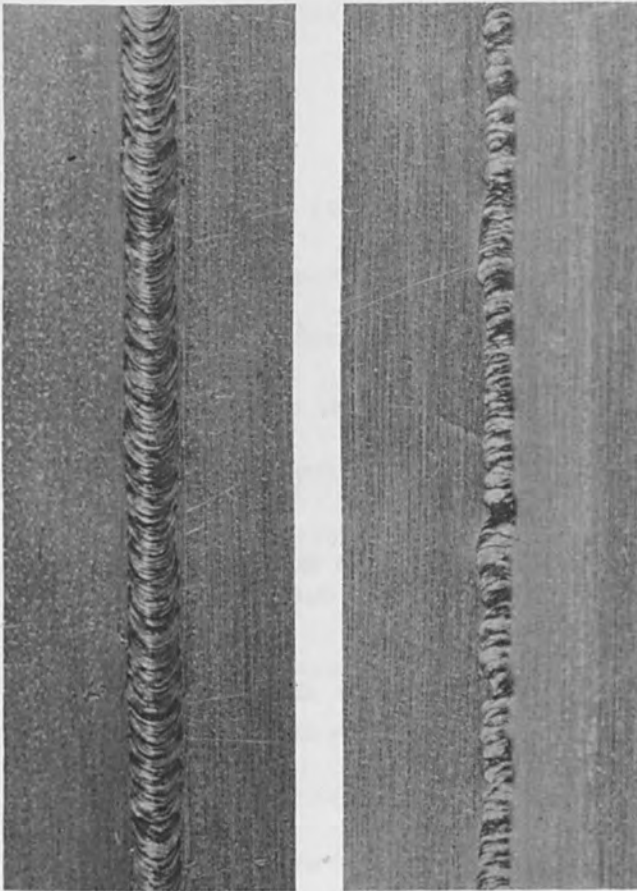
Fig. 18.

Photographs of Weld Surface and Weld Root in 0.023-Inch Thick 1100 Aluminum Alloy Note Smooth Contour of Root of Weld at the Right.

Magnification: 7X
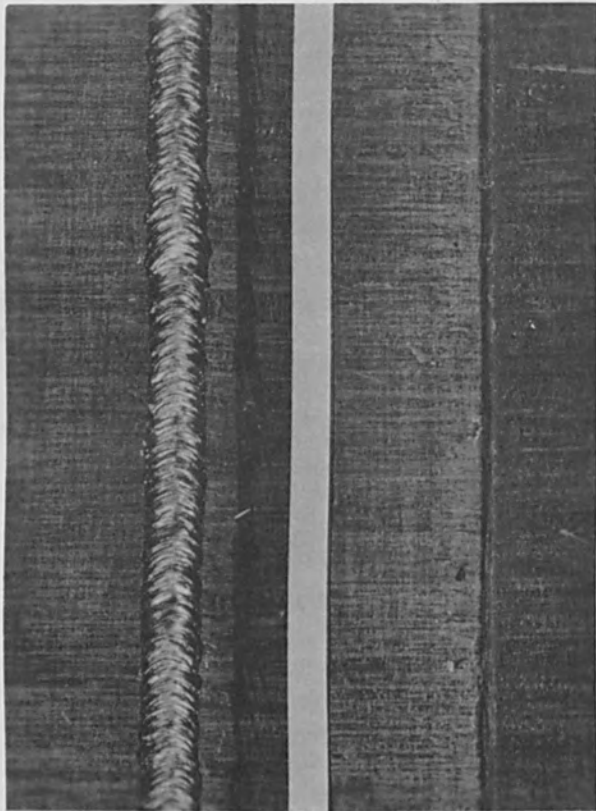
Weld Surface   **Weld Root**

Fig. 19

Weld Surface and Weld Root Appearance of
an Electron Beam Weld in 0.062-Inch Thick
Columbium at 7X Magnification.
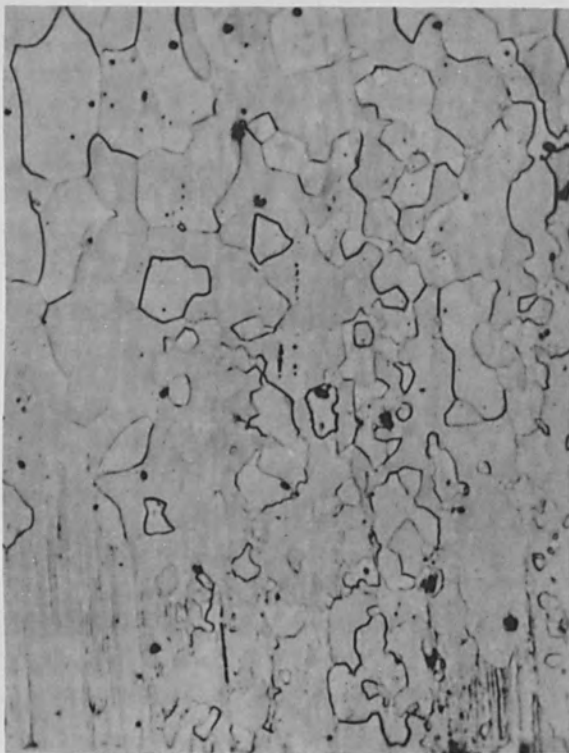
Fig. 20

Microstructure of Base Metal to Fusion Zone
Transition of Weld in 0.062-Inch Thick
Columbium.

Etchant: 30 cc Lactic Acid   Magnification: 200X
          10 cc HNO_3
          10 cc HF

136

the relatively fine weld grain size in the fusion zone. Contrasting the penetration possible in welds in heavier thickness of tungsten are the photographs of the weld and root surfaces of a seam weld in 0.010-inch thick tungsten sheet shown in Fig. 23. This weld, made at 50 KV, 6.5 milliamperes and 28-inches per minute travel speed again demonstrates the flexibility of the high voltage electron beam welder and that voltage is the primary weld parameter for producing deep penetration. Note that variations in current have relatively little effect in the weld penetration obtained in 0.060-inch thick or 0.010-inch thick tungsten butt welds. Penetration was obtained by raising voltage from 50 KV to 130 KV to fully fuse the heavier cross-section.

SUMMARY

In summation, it can be stated that electron beam welding has proved itself to be a highly versatile process. At the high voltages its ability to penetrate material thicknesses up to at least 1/2-inch thick has been demonstrated. At the same time, reduction of weld parameters, particularly voltages, permits successful joining of members as thin as 0.010-inch in cross-section.

The dynamic vacuum inherent in the process provides an ideal atmosphere for welding those materials susceptible to contamination by impurity gases such as oxygen and nitrogen. Zircaloy-2 can be welded with assurance of retaining the necessary corrosion properties and mechanical properties at least equal to the base metal. Application of the process to similarly reactive materials such as titanium, columbium, tantalum, etc. should produce equally gratifying results.

Fig. 21 Cross-Section of Electron Beam Weld in
0.060-Inch Thick Tungsten Plate Made at
130,000 Volts, 6.0 Milliamperes, and 15-
Inches per Minute.
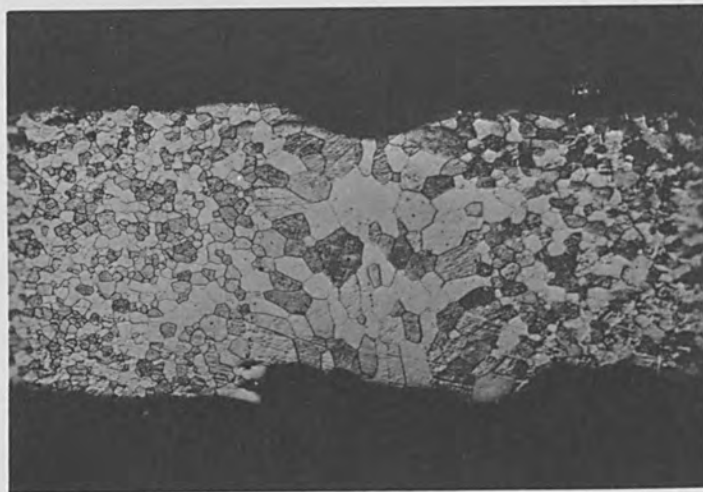
Etchant: Murakami's Reagent

Magnification: 25X
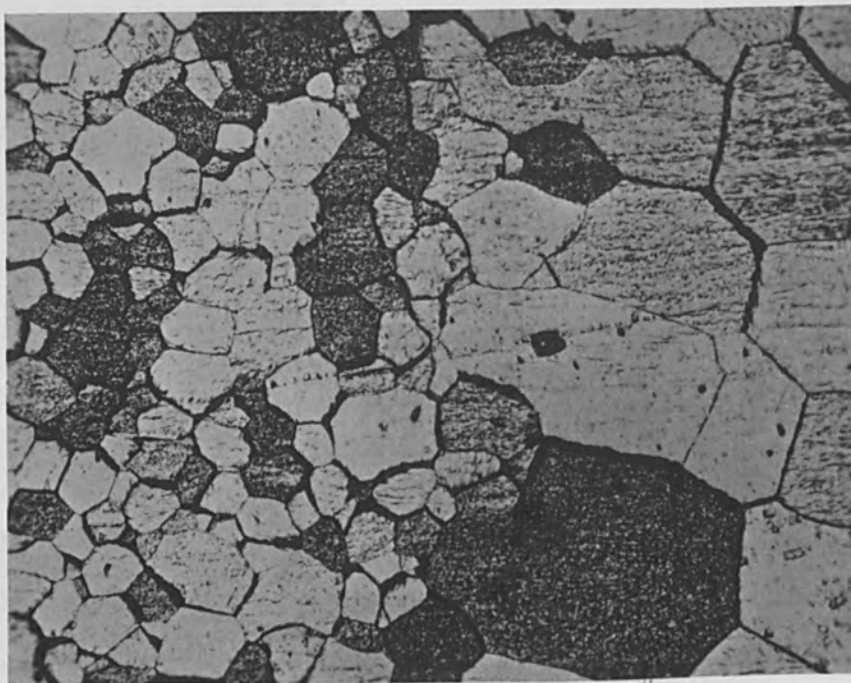
Fig. 22 Microstructure of Base Metal to Fusion
Zone Transition in Electron Beam Weld in
0.060-Inch Thick Tungsten Plate Showing
Relative Grain Size.

Etchant: Murakami's Reagent

Magnification: 200X
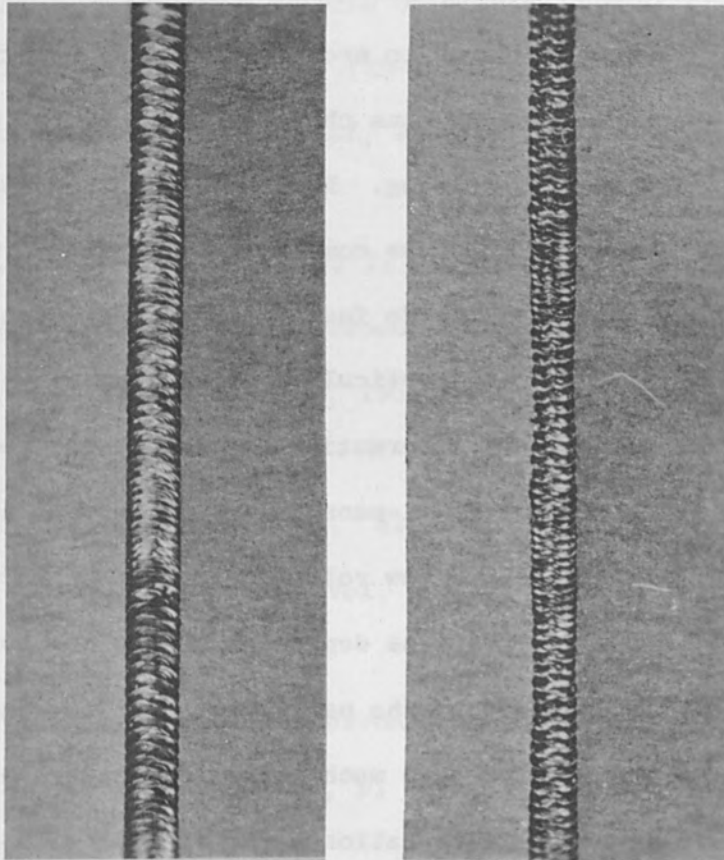
Weld Surface   Weld Root

Fig. 23 Weld Surface and Weld Root Appearance of
         Electron Beam Weld in 0.010-Inch Thick
         Tungsten Sheet at 7X Magnification.
         Oscillation of the Electron Beam Has Pro-
         duced the Smooth Weld Root Appearance
         Evident at the Right of the photograph.

The high voltage electron beam welding machines provide several basic improvements over standard welding techniques. The great concentration of energy possible with these electron beam welding units drastically reduces the power input required to produce necessary penetration. At the same time the narrow fusion zone characteristic of the process minimizes weld shrinkage in joining. Both heat input and weld shrinkage are significant factors which cause component distortion. The tungsten arc welding process produces a wide fusion zone in relation to the depth of penetration obtained with a particular combination of weld parameters. On solidification significant deformation can occur, particularly in heavy sections which require multi-pass welds and in very thin sections which possess little rigidity. Low voltage electron beams provide improved fusion zone configurations depending on the degree of focalization of the electron beam achieved by the particular design. The electron optical design of the high voltage machines is capable of producing weld penetration to fusion zone width ratios of up to 25:1 with a proportionate reduction in weld shrinkage. In joining of certain critical components in the aircraft and missile fields electron beam welding may prove to be the only possible technique for fabrication of such parts.

Finally, the virtually unlimited power and energy of the electron beam will be vital in the joining of the refractory metals and alloys which by virtue of their high melting points and other physical characteristics defy joining by other techniques. Certainly, electron beam welding has not realized its full potential and other applications of the process will be found as its capabilities are further explored.

REFERENCES

1. Stohr, J. A. "Electronic Welding of Metals." Fuel Elements Conference, Paris, November 18-23, 1957. TID-7546, Book 1, pp. 9 to 17, United States Atomic Energy Commission, Washington, D. C.

2. Wyman, W. L. and Steinkamp, W. I. "Electron Beam Welding - Development of Process." Hanford Atomic Products Operations, General Electric, Richland, Washington, April 8, 1958, HW-55667.

3. Burton, G. and Matchett, R. L. "Electrons Shot From Guns Make High-Purity Welds." American Machinist, Vol. 103, No.4, February 23, 1959.

4. Wyman. W. L. "High Vacuum Electron Beam Fusion Welding." Welding Journal, Vol. 37, No. 2, February 1958, p. 49-s.

5. Hoffman, H. H., "Vacuum Joining By Electron Beam Welding." Third Annual Vacuum Metallurgy Conference, New York University, June 1960.

6. Kalish, H. S. "Electron Beam Welding - An Evaluation." Fourth Annual New England Welding Conference, October 21, 1959.

7. Kaplan, Irving "Nuclear Physics." First Edition, Addison-Wesley, Reading Massachusetts.

8. Burton, G. Jr. and Frankhouser, Wm. L. "Electron Beam Welding." Welding Journal, Vol. 38, No. 10, October 1959, pp. 401-s to 409-s.

9. Stone, C. C., Noland, R. A., McCusig, F. P., Walker, D. K., "Borax IV Reactor - Manufacture of Fuel and Blanket Elements", ANL Report No.5721, Argonne National Laboratory, March 1958.

10. Mills, L. E., "Zircaloy Welding Techniques, Etc.", Welding Journal, Vol.40, No.2, February 1961, pp 141-151.

11. Stohr, J. A. and Briola, J. "Vacuum Welding of Metals." Welding and Metal Fabrication, October 1958, pp 366 to 370.

12. Steinkamp, W. I. and Wyman, W. L. "Electron Beam Welding - A New Development for Industry," Welding Engineer, April 1959.

13. Stohr, J A. "Vacuum Welding by Electron Beam." Nuclear Power, June 1958. pp. 272 to 274.

14. "Electron Beam Welding Process Operates in a Vacuum." The Iron Age, March 26, 1959, p. 156.

15. "New Heat for Electron Beam Processing." Chemical Week, March 7, 1959.

16. Merriam, J. C. "The New Welding Process" M/DE Manual No.166, Materials in Design Engineering, January 1960.

APPENDIX

A. Calculation of heat output from an electron beam:

Assume Weld Parameters:

<div align="center">

150,000 volts
0.010 amperes

</div>

1 Electron Volt = 1.6×10^{-12} ergs.

1 Erg = 2.39×10^{-8} calories.

1 Electron Volt = $1.6 \times 10^{-12} \times 2.39 \times 10^{-8} = 3.7 \times 10^{-20}$ calories.

At 150,000 volts, each electron carries:

$3.7 \times 10^{-20} \times 1.5 \times 10^5 = 5.56 \times 10^{-15}$ calories.

1 ampere = 6.28×10^{18} electrons per second.

0.010 ampere = 6.28×10^{16} electrons per second.

Beam energy = $6.28 \times 10^{16} \times 5.56 \times 10^{-15} = 349$ calories per second.

An electron beam at 150,000 volts and 0.010 amperes current delivers 349 calories per second of energy at the work.

B. Calculation of theoretical temperature rise:

Assume:

<div align="center">

1/4-inch thick tungsten

Beam focussed to 0.100-inch diameter

</div>

$$\frac{Q}{MC} = T$$

Where Q = Heat input in calories

M = Mass of metal in grams

C = Specific heat in calories per gram per °C

T = Temperature rise in °C

Specific Heat of Tungsten = 0.033

Volume of metal involved = $\pi (0.05)^2$ x 0.250 = 0.00197 in.^{3}

Weight of Tungsten   =   0.00197 x 0.697 x 454 = 0.624 gms

Tungsten = $\dfrac{349}{0.624 \times 0.033}$ = 16,950°C Temperature Rise Per Second

ELECTRON BEAM WELDING CHARACTERISTICS OF
SEVERAL MATERIALS

By

John W. Meier
Development Engineer
Hamilton Standard Division
United Aircraft Corporation
Windsor Locks, Connecticut

ABSTRACT

Compilation and discussion of electron beam
welding data and evaluation of physical properties of
electron beam weldment in 302 stainless, 4340, 17-7 PH
stainless, 6Al-4V Titanium and 61S Al are presented.
Tensile and fatigue properties of weldments and information
on the depth of penetration as function of thermal con-
ductivity for these alloys are also discussed.

ELECTRON BEAM WELDING CHARACTERISTICS OF SEVERAL MATERIALS

INTRODUCTION

Electron beam welding is a new technology. Accordingly, relatively little technical data is available concerning the effects of operating parameters such as accelerating voltage, beam current, welding speed, etc. on the electron beam welding characteristics of various materials. Required information also is lacking on the physical and mechanical properties of weldments so produced. This paper presents preliminary data of this nature obtained at Hamilton Standard Division of United Aircraft Corporation as part of an extensive long-range electron beam welding program.

PROCEDURES

The equipment used in carrying out this investigation is a standard high energy-density Zeiss electron beam welder. This machine is rated at 2KW with normal accelerating voltages between 80-150KV and a beam cross sectional diameter of about 0.010 inch at the workpiece. Welding speeds up to 30 inches per minute are available. A vacuum of about 5×10^{-5} mmHg is maintained during welding. Although various filament configurations are available, a simple hairpin filament was used during this investigation.

Simulated welds in a solid block of material were used in most cases to investigate the effects of operating parameters. Simple butt welds were used for all weldment tests. All welds were made with a single pass and no filler materials were employed.

EFFECT OF OPERATING PARAMETERS

The effects of accelerating voltage, beam current, and welding speed have been investigated for several materials. Representative data are presented for Type 302 stainless and AISI 4340 steels. It should be noted, however, that similar trends have been observed in all materials studied to date.

Figure 1 shows the effect of current and voltage on penetration in Type 302 austenitic stainless steel welded at constant speed. It readily can be seen that penetration increases with both current and voltage. Figure 2 shows that penetration is approximately proportional to the product of current and voltage, or power. Assuming that the spot size remains essentially constant, this means that penetration is a function of energy density at the workpiece.

Figure 3 shows the effect of welding speed on the depth of penetration in AISI 4340 steel. As might be expected, penetration increases with decreasing welding speed.

EFFECT OF MATERIAL PHYSICAL PROPERTIES

Intelligent application of the electron beam welding process is dependent, in part, on an understanding of the effects of material physical properties on the resulting welding characteristics. For example, a correlation between physical properties and welding charac-teristics would be useful in predicting the weldability of new or untested materials. Therefore, a comprehensive program is under way to correlate weld-zone characteristics such as depth of penetration and
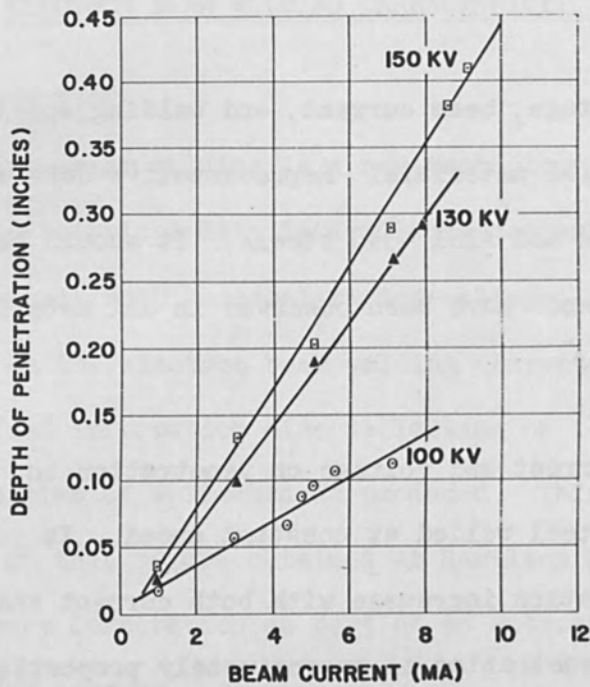
Figure 1
Depth of Penetration Vs
Beam Current
Type 302 Stainless Steel
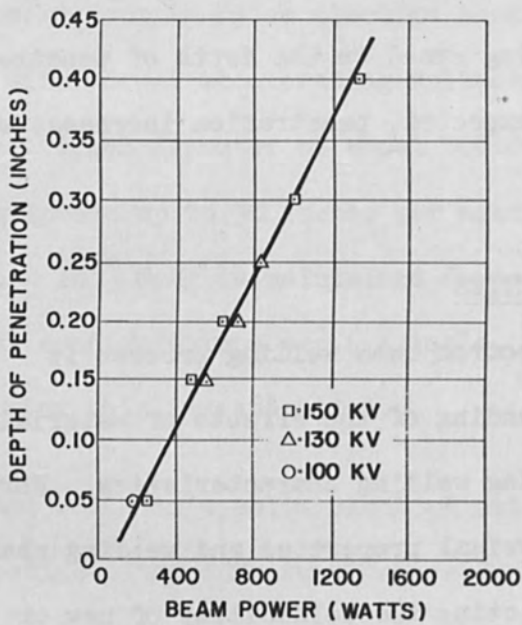Welding Speed: 27 inches
per minute

Figure 2
Depth of Penetration Vs
Beam Power
Type 302 Stainless Steel
Welding Speed: 27 inches
per minute

148

depth-to-width ratio with physical properties such as thermal conductivity, specific heat, melting point, and density.

Preliminary results of the program indicate a strong dependence of weld-zone properties on thermal conductivity. As might be expected, weld penetration generally increases with decreasing thermal conductivity. This is shown in Figure 4 which is an empirical plot of penetration versus thermal conductivity, the latter plotted on a logarithmic scale. However, other data clearly indicates that thermal conductivity is not the only controlling factor. For example, at identical machine settings, the penetration in AISI 4340 low alloy steel is roughly double that observed in pure columbium; yet the thermal conductivities of the two materials are almost equal. Clearly the relationship of material physical properties to weld-zone characteristics is very important and, therefore, worthy of continued detailed study.

WELDMENT EVALUATION

The metallurgical, mechanical, and chemical properties of electron beam welds in several materials have been investigated. The following summarizes the results obtained.

A.   Annealed Type 302 Austenitic Stainless Steel

Extremely deep narrow welds can be produced in this material as shown in Figure 5. Depth-to-average width ratios greater than 20-1 are quite readily attained. This photo is interesting in that it shows a "pinch" effect which could be the
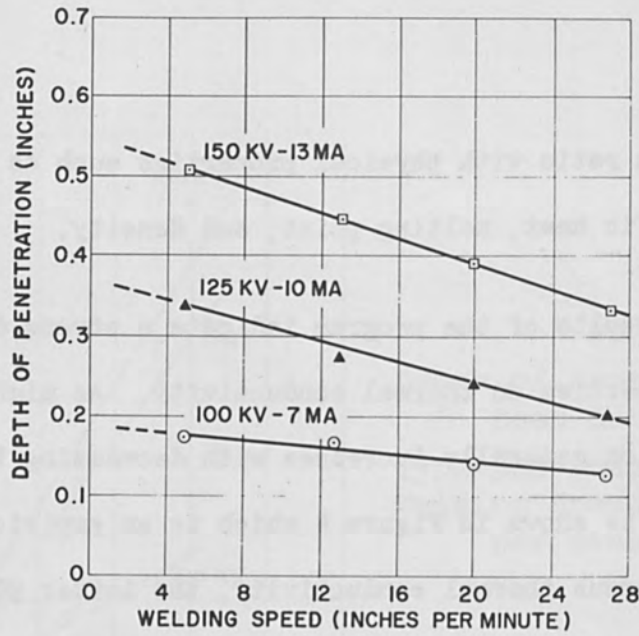
Figure 3
Depth of Penetration Vs Welding Speed
AISI 4340 Low Alloy Steel

Figure 4
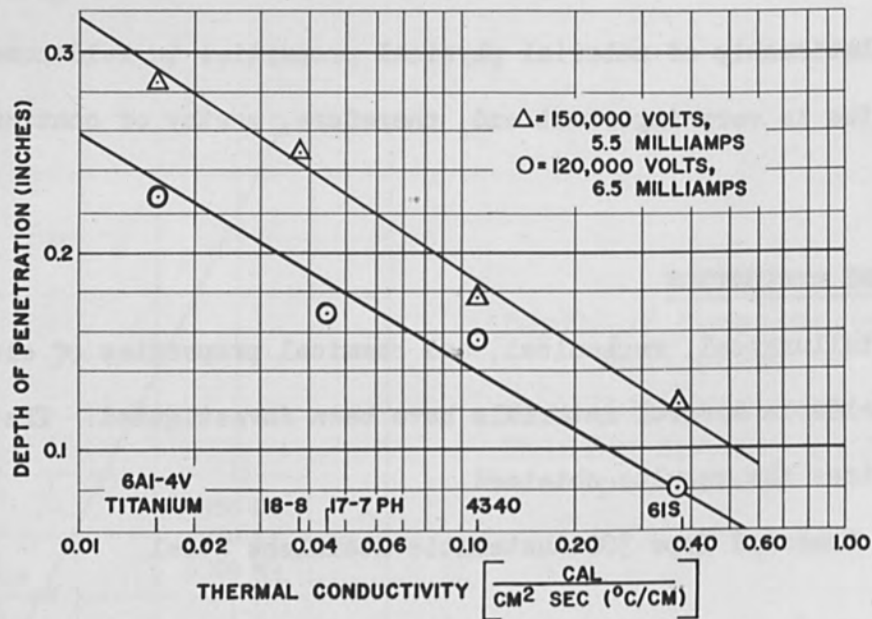Depth of Penetration Vs Thermal Conductivity
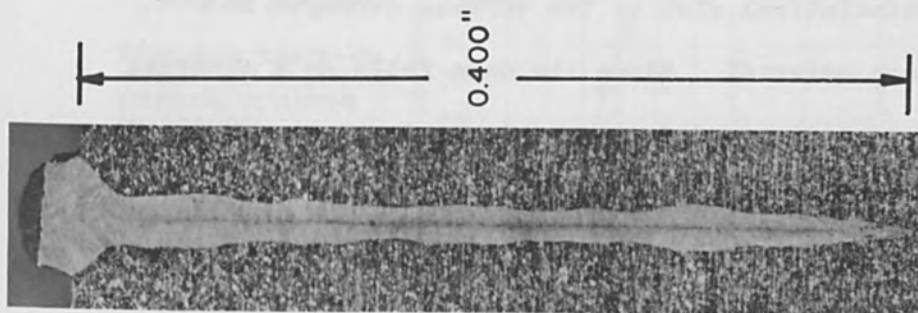Welding Speed: 27 Inches Per Minute

150

1.00"

Figure 6
Electron Beam Welds
Type 302 Stainless Steel

0.400"

Figure 5
Electron Beam Weld
Type 302 Stainless Steel
Welding Speed: 27 inches per minute

result of refocusing of the electron beam by low density
vapor which is formed during the welding operation. This
effect, together with reflection of electrons from the
edge of the vaporized zone, may explain the extremely deep
weld penetrations that can be realized at high energy
densities. Figure 6 shows two deep narrow simulated welds
which have penetrated one inch of stainless steel. From
Figure 7, which is a photomicrograph of the weld transition
zone, it can be seen that the fusion zone is extremely fine
grained and that a very sharp transition region exists.
The recrystallization observed in the unfused material is
the result of cold work which occurred during shearing of
the material.

Tensile tests were conducted on butt welded material in the
as-welded condition with no surface preparation after welding.
Figure 8 is a statistical plot of the tensile strength of
welded 0.062 inch material. Since the data falls on a straight
line, a normal distribution of strength is indicated. Also,
since the line is very steep, the standard deviation or spread
in strength is small. The △'s represent fractures in the
weld; ○'s fractures in the base metal. The random distri-
bution of △'s and○'s, all on the straight line, show con-
clusively that the weldments and the base metal have the same
strength. The solid ▲'s and ● 's are of further signifi-
cance. These specimens were subjected, subsequent to welding,

152

BASE METAL　RECRYSTALLIZED ZONE　WELD ZONE

0.005
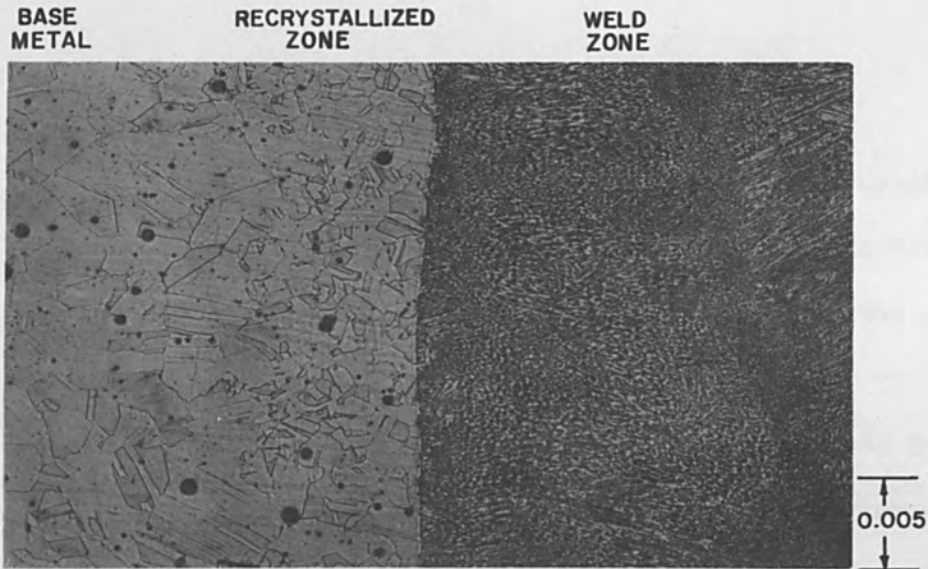
Figure 7
Electron Beam Weld-Zone Boundary
Type 302 Stainless Steel

FRACTURE IN BASE METAL
○ AS-WELDED
● STRAUSS EXPOSED
FRACTURE IN WELD
△ AS-WELDED
▲ STRAUSS EXPOSED

TOTAL DATA POINTS-40
AVERAGE ($\bar{X}$)=92,500 PSI
STANDARD DEVIATION
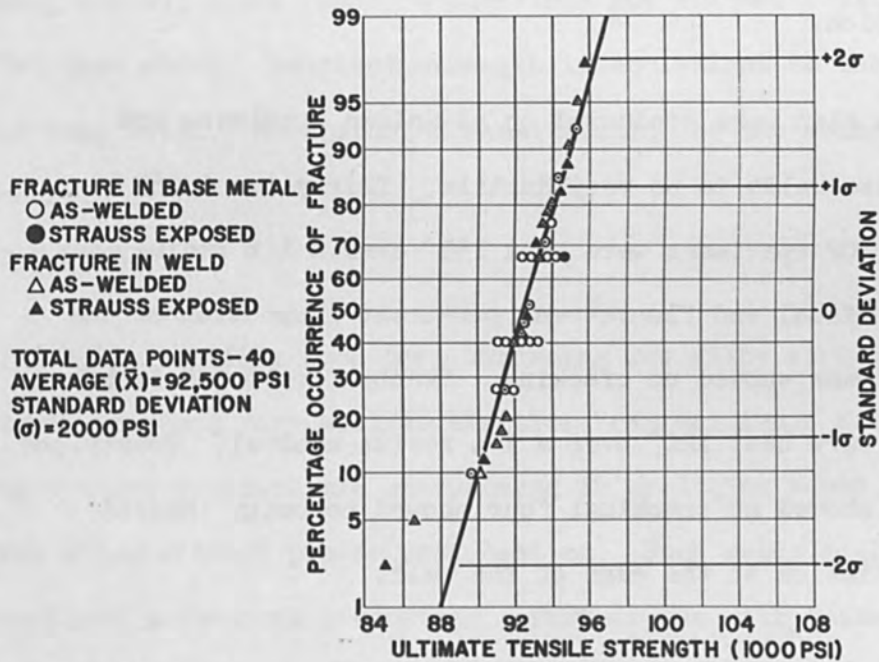(σ)=2000 PSI

Figure 8
Ultimate Tensile Strength
Electron Beam Butt-Welded Type 302 Stainless
Steel (0.062 inch annealed sheet)

153

to the Strauss test -- a corrosion test to determine if
austenitic stainless steel has been sensitized and thus has
lost its corrosion resistance. Since the strength was not
affected by the corrosive environment as shown by the distri-
bution of these solid points, it is obvious that no sensiti-
zation occurred. Similar results were obtained with 0.275
inch material. No attempts were made to chill any of these
specimens during welding. The extremely small fusion zone
and the high speed possible with electron beam welding
undoubtedly permitted the material to pass through the
critical temperature range at a rate sufficient to prevent
sensitization.

Bend tests also were conducted on as-welded specimens and
showed these welds to be very ductile. Thirty-two 0.062
inch Type 302 specimens were bent 155° over a 1 t radius
mandrel. Visual and fluorescent penetrant inspection of the
bent specimens showed no cracking. Twenty-five 0.275 inch
specimens were bent 120° over a 1 t radius mandrel. Twenty-one
specimens showed no cracking; four showed porosity induced
crack initiation at the edge of the weld.

Welds were found to be sound. Visual and fluorescent penetrant
inspection of weldments failed to reveal any cracking. Radio-
graphic inspection showed welds in general to be free of voids
except for a few of the 0.275 inch specimens which showed some

154

porosity. This porosity was traced to unsatisfactory edge preparation which appears to be important for thicker materials.

As is to be expected with annealed austenitic material, hardness of the weld zone was the same as that of the base material.

Comparative spectrographic analysis showed the fusion zone and the base material to have identical chemical compositions.

To summarize, electron beam techniques can be used to produce deep, narrow, sound welds in annealed Type 302 austenitic stainless steel. Weldment strength is equivalent to that of the base metal. No corrosion sensitization of the material occurs.

B. AISI 4340 Steel

AISI 4340, a widely used deep hardening low alloy structural steel, responds very well to electron beam welding. No significant problems are encountered in producing sound, crack free welds without pre-or post heating. Such welds displayed excellent mechanical properties. Further, as with austenitic stainless steel, deep narrow welds can be produced as shown in Figure 9 with depth-to-average width ratios of 12 to 1 very common.
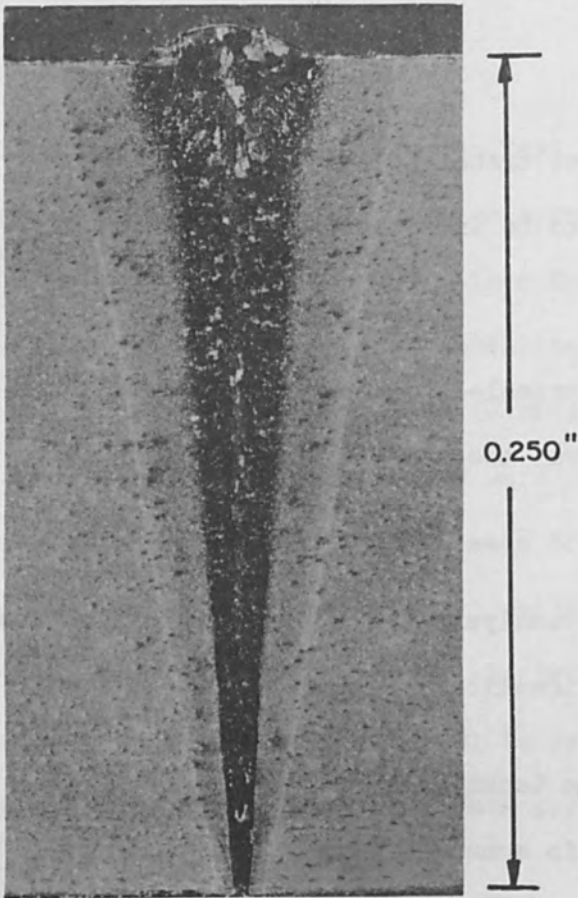
Figure 9
Electron Beam Weld
AISI 4340 Low Alloy Steel

0.250"

○ FRACTURE IN
   WELD
▲ FRACTURE IN
   BASE METAL

TOTAL DATA POINTS −23
AVERAGE ($\bar{x}$) = 144,500 PSI
STANDARD DEVIATION
   (σ) = 4500 PSI

Figure 10
Ultimate Tensile Strength
Electron Beam Butt-Welded AISI 4340 (0.250 inch
annealed plate, heat treated to R_c 26-32 after
welding)

Tensile and fatigue tests were conducted on 4340 welded both before and after heat treatment. Figure 10 is a statistical plot of the tensile strength of 1/4 inch thick butt weldments made in the annealed condition and heat treated to R_c 26-32 after welding. The data shows a normal distribution with weldment strength equal to that of the base material. Figure 11 is a similar plot for weldments heat treated to R_c 47-50 after welding. Again, normal distribution and base metal strength were obtained.

Tensile tests also were conducted on welds made in heat treated 4340. The results were quite remarkable in that, once again, base-metal strength was maintained in the weld zone. Figure 12 is a statistical plot of tensile strength for 0.062 inch material welded at a hardness of R_c 26-32 and stress relieved at 1050°F after welding. Figure 13 is a similar plot for material welded at R_c 40-44 and stress relieved at 650°F after welding. It should be noted that the few specimens which failed at the weld zone exhibited base-metal strength. Undoubtedly the small fusion zone and high welding speed associated with high-voltage electron beam welded limited the heat-affected zone to a point where no reduction in strength occurred. Welding of high-strength steels after heat treatment without strength reduction is of great practical significance. Thus the above results are extremely important.

TOTAL DATA POINTS – 25
AVERAGE ($\bar{X}$) = 246,000 PSI
STANDARD DEVIATION
(σ) = 3500 PSI

▲ – FRACTURE
IN WELD

O – FRACTURE
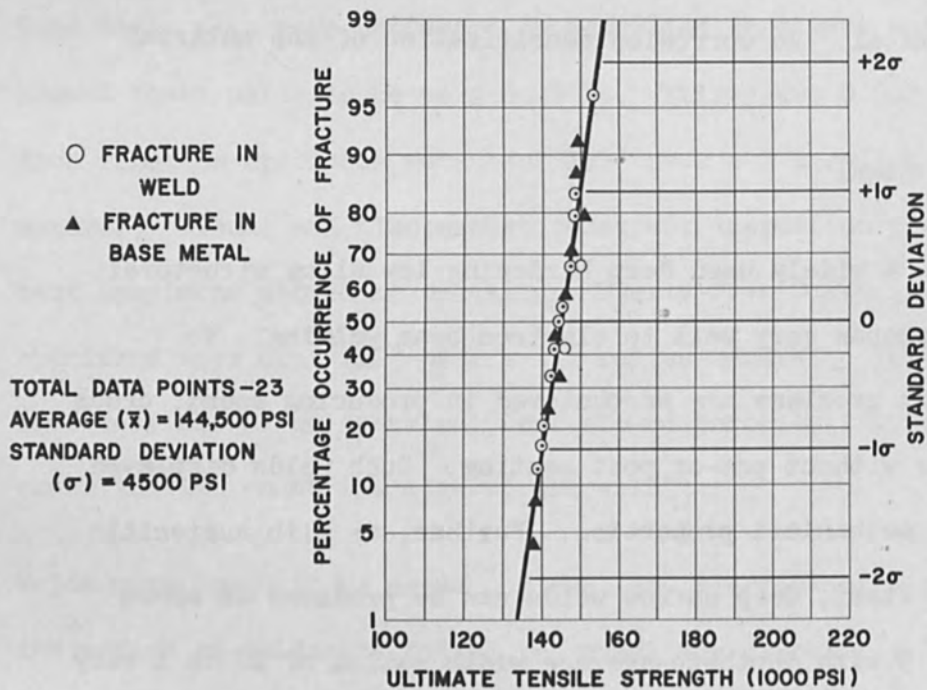IN BASE
METAL

Figure 11
Ultimate Tensile Strength
Electron Beam Butt-Welded AISI 4340 (0.250 inch
annealed plate, heat treated to R_c 47–50 after
welding)

▲ = FRACTURE
IN WELD

O = FRACTURE
IN BASE METAL

TOTAL DATA POINTS – 33
AVERAGE ($\bar{X}$) = 138,200 PSI
STANDARD DEVIATION
(σ) = 3600 PSI

Figure 12
Ultimate Tensile Strength
Electron Beam Butt-Welded AISI 4340 (0.062 inch
R_c 26–32 sheet, stress relieved after welding)

158

TOTAL DATA POINTS-36
AVERAGE ($\bar{X}$)=196,500 PSI
STANDARD DEVIATION
(σ)= 7000 PSI

▲FRACTURE IN WELD
○FRACTURE IN BASE METAL
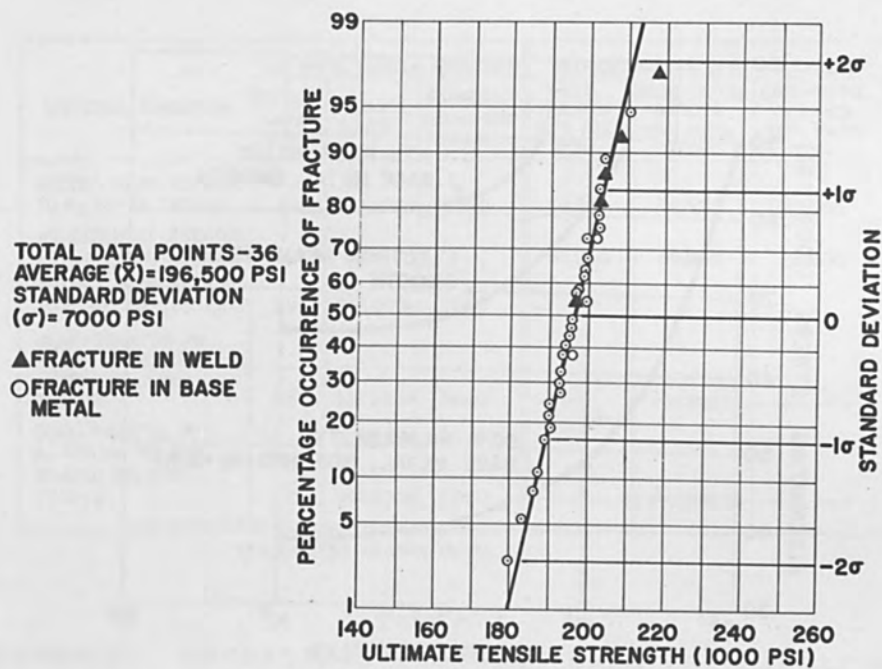
Figure 13
Ultimate Tensile Strength
Electron Beam Butt- Welded AISI 4340 (0.062 inch
R_C 40-44 sheet, stress relieved after welding)
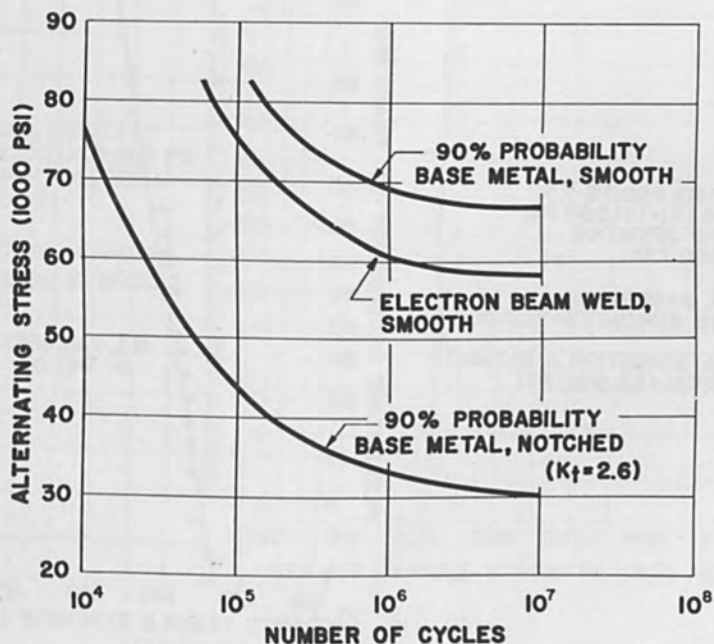
Figure 14
Specimen Fatigue Results
Electron Beam Butt-Welded AISI 4340 (Heat treated
to R_C 26-32 after welding)

159
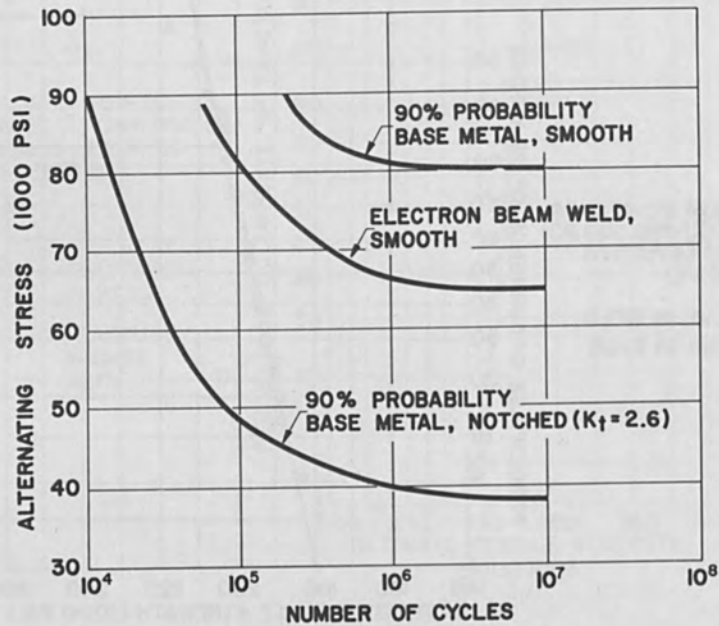
Figure 15
Specimen Fatigue Results
Electron Beam Butt-Welded AISI 4340 (Heat
treated to R_C 40-44 after welding)
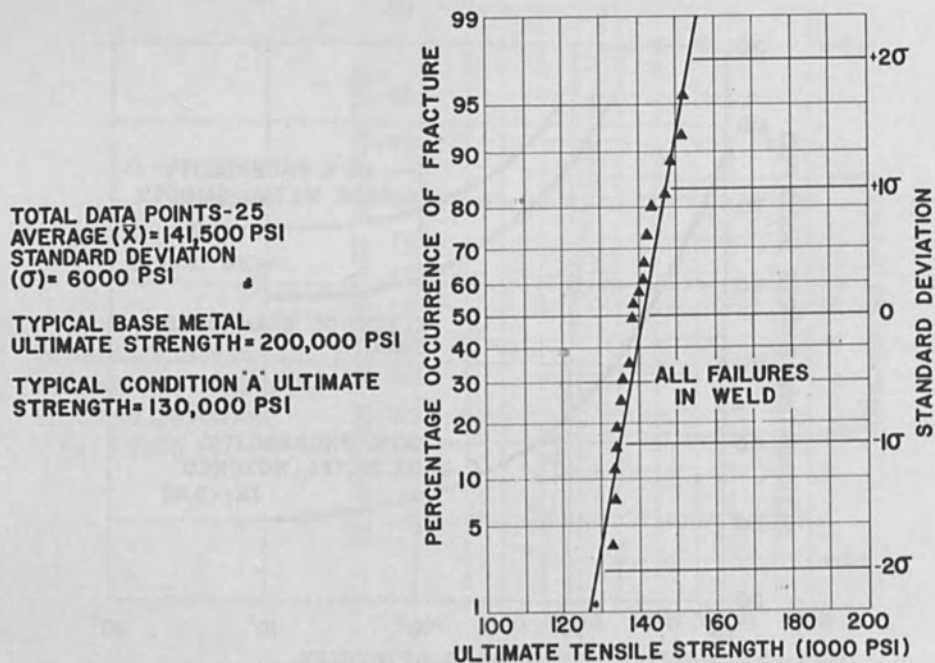
Figure 16
Ultimate Tensile Strength
Electron Beam Butt-Welded 17-7PH Stainless Steel
(0.062 inch TH1050 sheet, tested as welded)

160

MATERIAL CONDITION	ULTIMATE TENSILE STRENGTH			FATIGUE STRENGTH AT 10^7 CYCLES		
	TOTAL DATA POINTS	AVERAGE ($\bar{x}$) PSI	STANDARD DEVIATION (σ) PSI	WELD SMOOTH 90% PROB. (PSI)	BASE–METAL SMOOTH 90% PROB. (PSI)	BASE–METAL NOTCHED 90% PROB. (PSI)
WELDED, HEAT–TREATED TO R_c 26-32, TESTED	23	144,500*	4500	58,000	66,000	30,000
WELDED, HEAT–TREATED TO R_c 40-44, TESTED	—	—	—	65,000	80,000	38,500
WELDED, HEAT–TREATED TO R_c 47-50, TESTED	25	246,000*	3800	—	—	—
HEAT–TREATED TO R_c 26-32, WELDED, STRESS RELIEVED, TESTED	33	138,200*	3600	←———— IN PROGRESS ————→		
HEAT–TREATED TO R_c 40-44, WELDED, STRESS RELIEVED, TESTED	36	196,500*	7000	←———— IN PROGRESS ————→		

*EQUIVALENT TO BASE METAL

Table I
Summary: Mechanical Property Data for Electron
Beam Welded AISI 4340 Low Alloy Steel

TOTAL DATA POINTS-10
AVERAGE ($\bar{X}$)=205,500 PSI
STANDARD DEVIATION
(σ)=1500 PSI

▲ FRACTURE IN WELD
○ FRACTURE IN BASE METAL

Figure 17
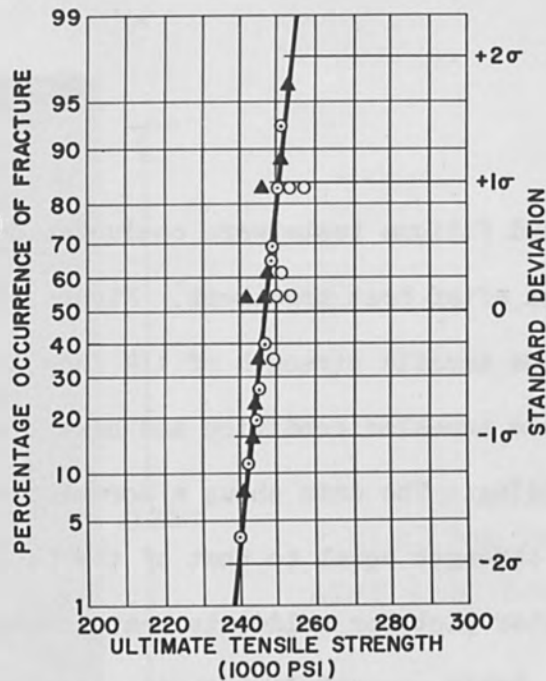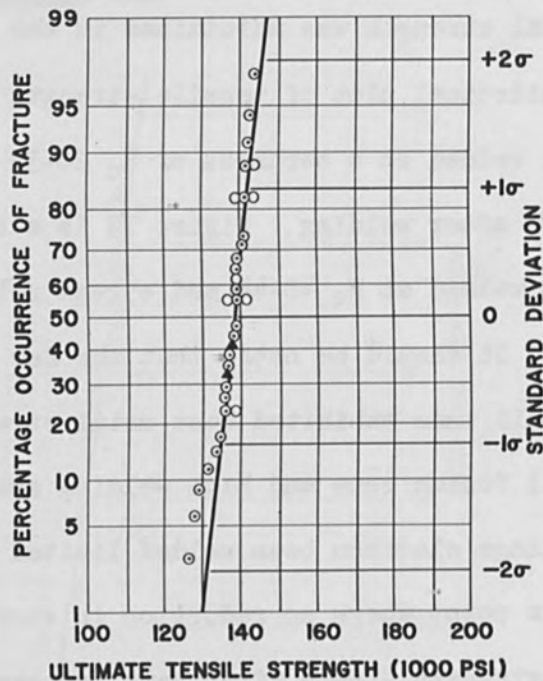Ultimate Tensile Strength
Electron Beam Butt–Welded 17-7PH Stainless Steel
(0.062 inch annealed sheet, heat treated to TH1050
after welding)

161

Results of the fatigue testing of 4340 weldments also are outstanding. Simple beam type specimens were used. These specimens were machined on all sides prior to testing in order to minimize surface effects.

Figure 14 shows the endurance properties of weldments produced in annealed material and heat treated to R_c 26-32 after welding. As can be seen, the endurance properties of the weldment approach those of the smooth base material, and they are significantly better than the endurance properties of the base material containing a standard notch. Figure 15 presents similar data for material heat treated to R_c 40-44 after welding. Again, fatigue strength of the weldments approaches that of the smooth base material.

Fatigue testing of 4340 welded in the heat treated condition is underway, but significant results are not yet available.

Table I summarizes the tensile and fatigue data obtained on AISI 4340. For comparison, base-metal properties also are included.

C.   Other Materials

Initial welding experiments with 17-7PH age hardenable stainless
steel, 6 Al-4V titanium, and 61S aluminum were quite promising.
Limited tensile data were obtained for these preliminary welds
which indicate that with refined welding techniques, outstanding
mechanical properties can be realized.

Figure 16 is a statistical plot of tensile data obtained for
0.062 inch 17-7PH sheet electron beam welded in the hardened
condition (TH1050). As expected, fractures occurred in the
weldment at strengths slightly above those for annealed
material. Figure 17 presents data obtained for 17-7PH welded
in Condition A (annealed) and subsequently solution treated
and aged. In this case, base metal strength was obtained in
the weldment. Figure 18 shows the tensile strength obtained with
material welded in the solution treated condition and aged to the
TH1050 condition after welding. Weldment strengths were only
slightly below the base-metal properties

The 6 Al-4V titanium exhibited excellent electron beam weld-
ability. Figure 19 is a plot of tensile strength for this
material welded in the annealed condition, the condition in
which this material normally is used. Here again, base-metal
strength properties were retained in the weld.

Based on preliminary work, 61S aluminum alloy exhibited good
weldability in the T4 condition although some porosity was

TOTAL DATA POINTS-8
AVERAGE ($\bar{X}$)=183,000 PSI
STANDARD DEVIATION
(σ)=7500 PSI

TYPICAL BASE-METAL
ULTIMATE STRENGTH=
200,000 PSI

ALL FAILURES
IN WELD

PERCENTAGE OCCURRENCE OF FRACTURE
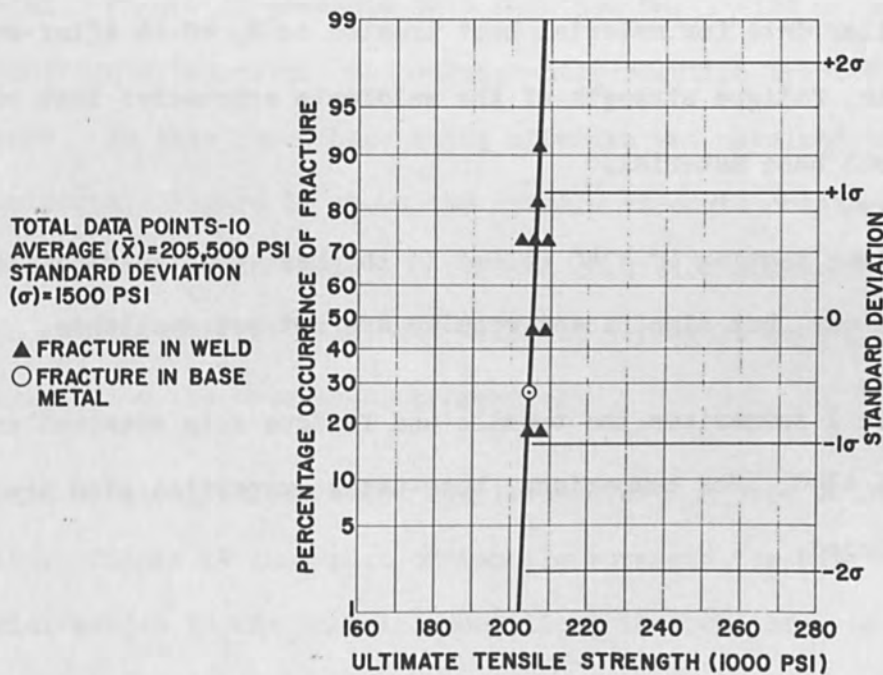
STANDARD DEVIATION

ULTIMATE TENSILE STRENGTH (1000 PSI)
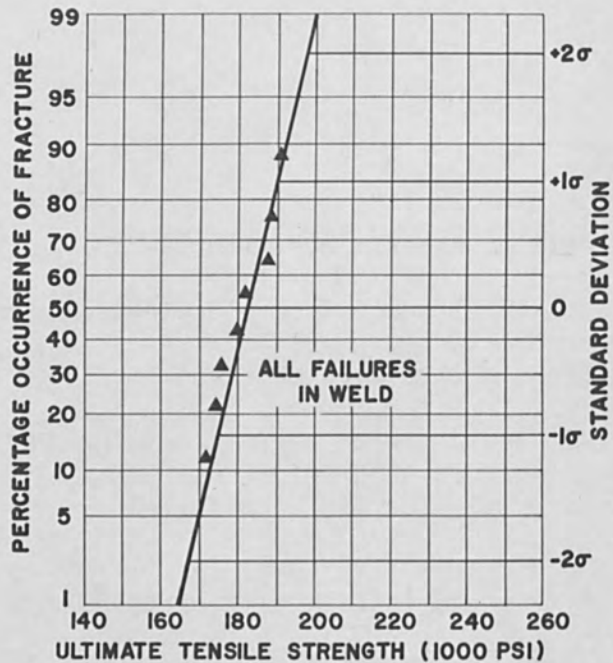
Figure 18
Ultimate Tensile Strength
Electron Beam Butt-Welded 17-7PH Stainless Steel
(0.062 inch solution treated shee, aged to TH1050
after welding)

TOTAL DATA POINTS-12
AVERAGE ($\bar{X}$)=137,500 PSI
STANDARD DEVIATION
(σ)=2500 PSI

▲FRACTURE IN WELD

○FRACTURE IN BASE
METAL

PERCENTAGE OCCURRENCE OF FRACTURE

STANDARD DEVIATION

ULTIMATE TENSILE STRENGTH(1000 PSI)

Figure 19
Ultimate Tensile Strength
Electron Beam Butt-Welded 6Al-4V Titanium
(0.050 inch annealed sheet, tested as welded)

164

encountered. Figure 20 is a plot of tensile strength of weldments of this material which were aged to the T6 condition after welding. As can be seen, approximately 85% of expected base metal strength was obtained. It is anticipated that refined welding techniques will reduce porosity and thus improve weld strength characteristics.

CONCLUSIONS

All of the alloys investigated responded very well to electron beam welding techniques. Extremely narrow but very deep fusion zones were obtained with a relatively high-speed single-pass weld resulting in very little distortion of the workpiece. Mechanical and chemical properties of the resulting weldments were outstanding, especially those in heat treated material. Based on these results it can be expected that many useful industrial applications will be found for the electron beam welding process.

FUTURE WORK

A comprehensive study of the properties of electron beam welded AISI 4340 continues including detailed metallographic studies, refined ductility measurements within the weldment, and residual stress studies. Comprehensive programs also are underway with H-11 steel, 17-7PH steel, various titanium and aluminum alloys, and tungsten and molybdenum, the latter two materials under Air Force sponsorship. It is hoped that the data obtained in these investigations will be useful to industry in applying electron beam techniques.
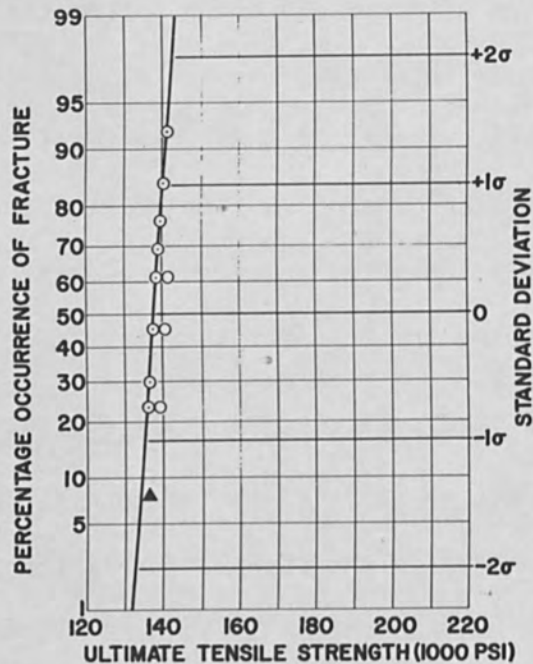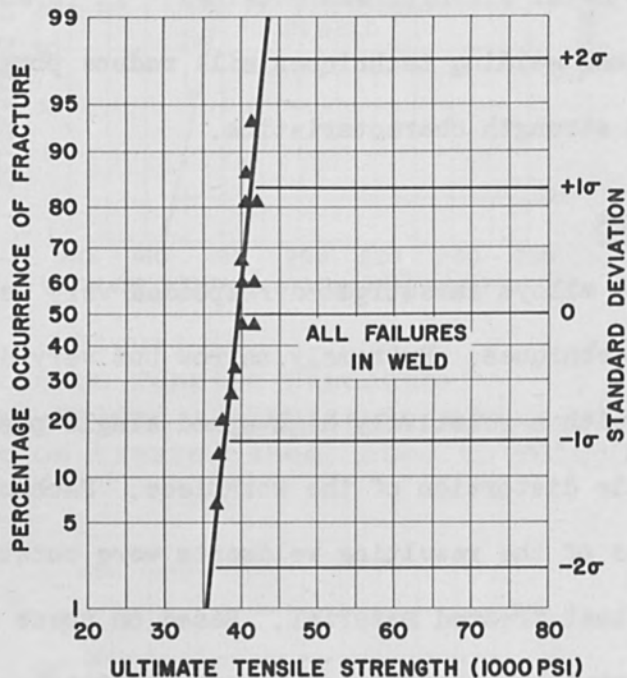
Figure 20
Ultimate Tensile Strength
Electron Beam Butt-Welded 6061 Aluminum
(0.062 inch -T4 sheet, aged to -T6 after welding)

ACKNOWLEDGMENT

ELECTRON BEAM WELDING OF BERYLLIUM

By

W. T. Hess
Project Supervisor
Alloyd Corporation

H. J. Lander
Senior Project Engineer
Alloyd Electronics Corporation

S. S. White
Supervisor Materials Joining
Alloyd Electronics Corporation
Cambridge, Massachusetts

ABSTRACT

An electron beam system for welding beryllium
and the results obtained with it are discussed. Emphasis
in the studies was placed on obtaining welds with shallow
penetration and in attempting to obtain welds with strengths
equivalent to the parent metal.

167

ELECTRON BEAM WELDING OF BERYLLIUM

I   INTRODUCTION

Beryllium, fourth lightest element known to man, with its very high strength to weight ratio, high stiffness, and low specific gravity, has become one of the most important materials under consideration for the fabrication of missile, satallite, and aircraft components or other light weight, high performance structures including ordnance and naval applications. Due, in large measure to the high free energy of oxide formation, extensive use of this metal has been limited by production techniques and means of fabricating end items from stock thus produced. The development of joining techniques for beryllium has not led to reliable procedures, and despite extensive work in this area, welding and/ or brazing of this material is still in its infancy. Previous work has included braze welding, conventional welding, pressure welding and soft soldering.[1]

Braze welding has involved either the conventional inert gas shielded tungsten arc welding process or the consumable electrode inert arc welding process.[2] In either case, a filler metal substantially lower in melting point than the base metal has been used. Braze welds have been made; however, porosity, weld bead cracking, and the formation of intermetallic compounds in both the fusion and heat affected zones have limited the use of this technique.[3]

Considerable effort has been devoted to fusion welding beryllium using the atomic hydrogen, carbon arc, TIG and MIG processes. Serious contamination problems have been encountered which involve minute metallic transfer from the electrode to the work for those techniques dependent upon essentially non-consumable electrodes. Presumably

such difficulties may be overcome, as they have been for titanium welding
by the TIG process, or for steel welding utilizing the atomic hydrogen
process. However, a prime obstacle to successful joining by these
techniques is the great affinity of beryllium for oxygen and nitrogen.
Also, oxidation of the beryllium has been so serious that base metal wetting
is inconsistent, causing the formation of stress risers at the junction of
the meniscus of the weld and the oxidized base plate. Such notches
inevitably propagate as cracks along the heat affected zone and weld metal
interface.

Submerged arc welding has yielded similar results since solid
fluxes, in general, are more dense than the metal itself.[4] Thus these
fluxes become entrapped within the molten zone. Fluxes such as chlorine
and freon might be more satisfactory since they are compatible with
beryllium but they are highly corrosive to almost all hot electrodes.

Pressure welding of beryllium has also been investigated. When
pieces of beryllium are held in contact under pressure at elevated
temperature below the melting point, they can be joined through a
combination of plastic flow, recrystallization and grain coalescence
across the interface. Such welds are best made in vacuum or in an
atmosphere of pure argon. Prime requisites for such joining are flat,
clean surfaces, and resultant joint tensile strengths approach those of
the base material. However, the structure generally exhibits excessive
grain growth, poor ductility,[1] and unlike fusion welded structures, are
limited to the formation of specific shapes.

Thus, it would appear that a successful method of joining
beryllium would involve a technique not requiring filler metal of different

composition and utilizing an atmosphere which would be relatively non-reactive to beryllium. Consequently, a program to evaluate the feasibility of electron beam welding of beryllium was conducted. The program was conducted in two phases. The first phase comprised a general study of weldability characteristics to determine overall welding parameters. The second phase involved utilizing such data to make specimens suitable for transverse tensile testing. Specifically, the program was designed to produce fusion zones of 0.020" depth to allow sheet stock of this thickness to be welded in one pass, be free of microcracks, and possess helium leak tightness.

II   PARAMETERS STUDY; PROCEDURE

All welding for Phase I was conducted in an Alloyd Electronics Corporation E-Beam welder, utilizing a welding chamber fabricated from steel with a 12 inch inside diameter and a 12 inch inside height (see Figure 1). One and one-eighth inch diameter, 1/8" wall cylinders approximately 1" long were used since they were ideally suited for such a study due to specimen and jigging simplicity. The chamber was modified to weld cylindrical parts by rotating them under the gun with a variable speed motor drive. The chamber was equipped with a sight port allowing full viewing of the welding operation. The pumping system consisted of a roughing pump for initial evacuation and diffusion pump with fore pump, allowing a vacuum of 10^{-6} mm of mercury to be attained 10-15 minutes after pump down initiation. All welding was carried out with a work accelerated gun, since weld lengths were short and it was felt that violent outgassing probability would thereby be small. The maximum rated output of the unit was twenty thousand volts at 300 milliamperes. Linear
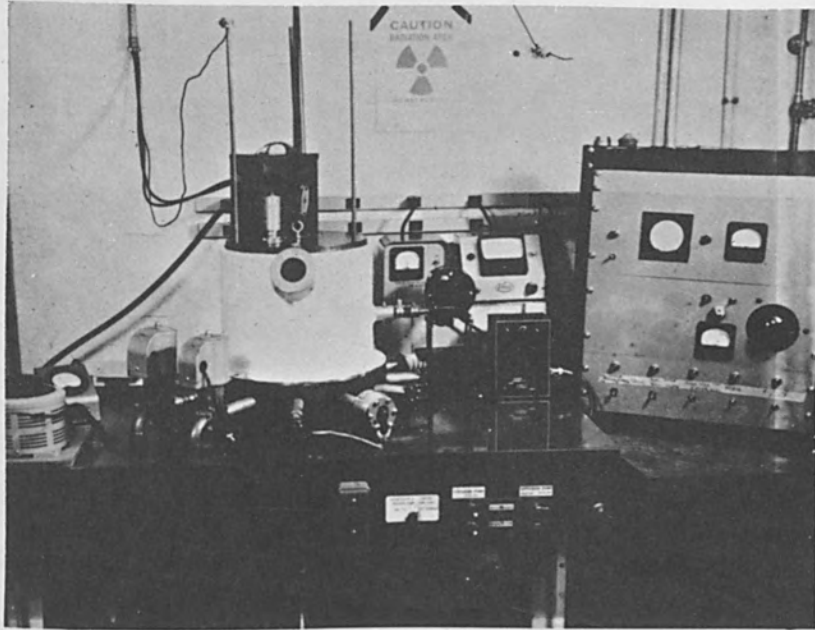
Figure 1
Alloyd's Circular Symmetry Beryllium Components   E-Beam Welder
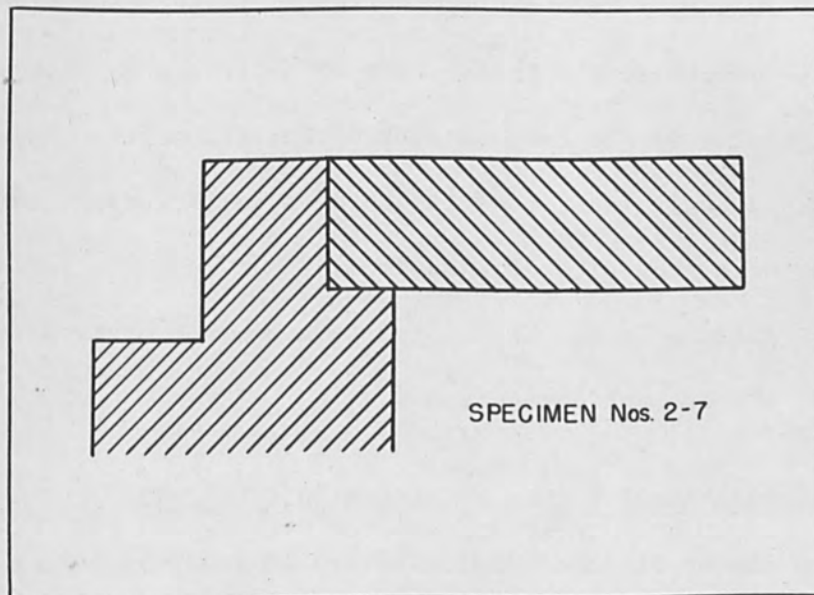

SPECIMEN Nos. 2-7

Figure 2
Simulated Housing Joint Geometry Specimens Nos. 2 thru 7

circumferential travel rates of 64 inches per minute were attainable, although not found to be necessary in the present work. Chamber operating pressure varied from 10^{-4} for Runs 1 and 2 (Samples 1 and 2) to 10^{-5} for subsequent Runs 3 through 7 (Samples 3-7).

Specimen 1, typical of the cylinder-end cap welds used in this series, was identical in geometry to all specimens used in this investigation (see Figure 2) with the exception that Specimen 1 involved a joint alteration consisting of a one degree relieved edge face (see Figure 3). It was intended that this relief lessen the chance of weld cracking. However, because of the tight initial fitup it was found impractical to evacuate this small area; thus subsequent specimens were not altered.

A complete record was kept of all power settings and vacuum changes. Periodic sampling of various portions of the pumping system were conducted to assure safe minimum operating levels consistant with the maximum allowable dosage intake rate of beryllium as prescribed by the Board of Health of the Commonwealth of Massachusetts. Even during vigorous physical cleaning of the chamber walls, dosage rates were found to be far below the allowable maximum.

After welding, the cylinders were leak checked, sectioned, polished, etched, and photographed.

III   PARAMETERS STUDY; METALLOGRAPHIC RESULTS

Almost all specimens utilized in studying parameters were welded at approximately 12,000 volts, 0.025 amperes, with various spot sizes, and at various chamber pressures.

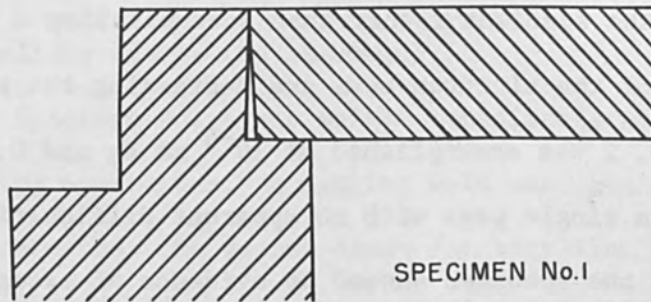Specimen No. 1 was the only sample welded at as high a voltage

172

SPECIMEN No.1

Figure 3
Simulated Housing Joint Geometry Specimen No. 1

Figure 4
Specimen No. 2 Cross Section of Weld Zone Etched at 100X

as 16,000 volts. It was also subjected to a small spot size of 0.006 inches in diameter and to a moderate pressure of 10^{-4} mm Hg. In this case, excessive power imput combined with very small spot size resulted in machining a groove in the specimen rather than accomplishing a weld.

By widening of the electron beam and decreasing the power input, welding on Specimen No. 2 was accomplished at 10^{-4} mm Hg and 0.1115" diameter spot size in a single pass with no apparent difficulties. The external appearance of the specimen showed no evidence of excessive over-heating or weld cracking, with a crazed surface oxide appearing on the weld bead.

The specimen was then helium leak checked, found to be tight, and sectioned. Figure 4 illustrates an etched cross section of the weld. Weld penetration was as required, with a weld surface width of approximately 0.112 inches. Figure 4 illustrates that the as-welded structure appears to be very similar to that of the base material, although somewhat more free from inclusions. There was no evidence of root cracking or beryllium vaporization.

At this time, the vacuum system was improved to allow for more efficient gun operation at lower pressures.

During welding of Specimen No. 3, which took place at 6×10^{-5} mm Hg and 0.126" spot size, there was definite outgassing from the melt indicating that a porous weld would result. This was evidenced by many surface cavities. Root cracking resulted from a combination of porosity within the weld zone and excessive gas pressure straining the joint. Both problems probably originated from a cavity left by an improper fit between cap and cylinder. Because the cap and cylinder were preassembled with a press fit, this space could not be evacuated despite the fact that the

specimen was under vacuum for 24 hours prior to welding. There was also slight evidence of metal volatilization as indicated by a recession in the weld zone. Volatilization was substantiated by beryllium deposition on glass slides within the chamber.

Specimen No. 4 was welded immediately after No. 3 using the same welding conditions. A similar weld was obtained. It was evident from the weld that the vacuum range for beryllium welding is critical. Although gas evolution was prevelant during initiation of the welding cycle, vaporization became apparent when the vacuum approached 6×10^{-5} mm of mercury, at which pressure the joint was performed.

Prior to welding the next specimen, a vacuum study was made using a specimen section as a target. In this case, there was no joint and no cavity within which to entrap gas. Glass sides were placed within the chamber on which beryllium, if vaporized, would be plated. The chamber was evacuated to 4×10^{-4} mm Hg. and the target bombarded until a molten pool was produced. The pressure immediately began to decrease. At 6×10^{-5} mm Hg., vaporization began to take place and at 10^{-5} mm Hg. the rate had increased considerably. At this point, the high vacuum value was closed, stopping all mechanical and diffusion pumping from the chamber. It was found possible to maintain 10^{-5} mm Hg. by adjusting the electron beam density, demonstrating the affinity of beryllium for gas within the chamber. Throughout this test, although vaporization took place, there was no evidence of any gas evolution from within the molten pool. Thus, although some beryllium stock may be high in gas content resulting in porosity, one prime source of porosity was found to be joint design,

Prior to welding Specimen No. 5, an attempt was made to produce a welding atmosphere of 2×10^{-4} mm Hg. by building a manually controlled leak into the vacuum system. It was felt that this would minimize vaporization and decrease any outgassing which might occur from the fusion zone. However, welding progressed with a spot diameter of 0.086" and at a pressure of 7×10^{-5} mm Hg. where vaporization was just perceptible. Upon completion of welding, the vacuum returned to 10^{-4} mm Hg., pointing to the need for automatic vacuum range control for beryllium electron beam welding. A heavy oxide layer on the surface, caused by an unsuccessful prewelding attempt to remove a thin vapor deposited beryllium film, tended to act as an insulator. Weld penetration was considerably less than in Run Nos. 2, 3, and 4. Specimen No. 5 was not leak tight due to root cracking produced by insufficient weld size for the stresses developed within the weldment.

Figure No. 5 shows a cross section of Specimen 6 (Run 6). This specimen, welded with an 0.134" diameter spot size and at 4×10^{-5} mm Hg. was argon quenched. This caused the fusion zone to cool prior to extensive recrystallization and thus delineates its boundary and the almost non-existance of heat-affected zone. Although there was no weldcracking, the specimen leaked through pinholes which resulted from occasional gas eruptions. As can be seen in the area of the weld zone, there is evidence of metal evaporation, substantiated by metal deposition upon glass slides within the chamber. Attempts to repair weld the leaks resulted in further violent evolution of gas, presumably because the cavities were air filled since the specimen was exposed to atmospheric pressure prior to the repair welding attempt.
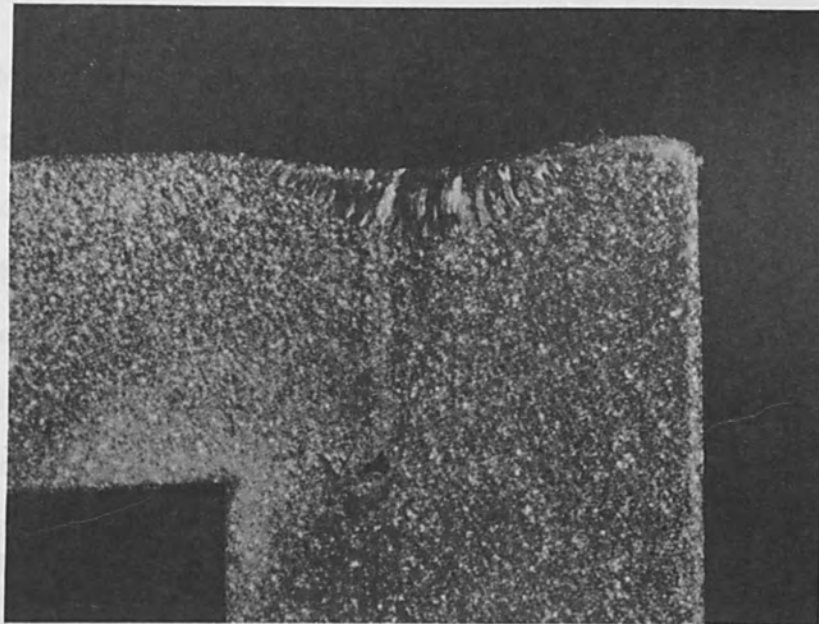
Figure 5
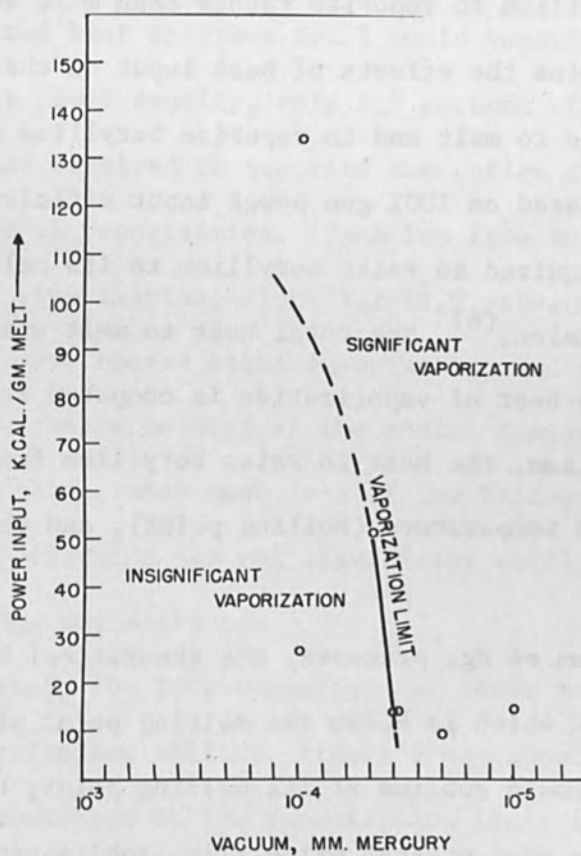Specimen No. 6 Cross Section of Weld Etched at 14X

Figure 6
Power Input, K.Cal/GM Melt vs Vacuum, mm Mercury

Again, as in the case of Specimen No. 6, Specimen 7, welded with a 0.161" spot size and at 10^{-5} mm Hg., showed metal volatilization. The gas entrapping fit-up cavity caused, in this case, perhaps more violent evolution of gas than was the case in Run No. 6. Attempts to repair weld this cylinder after the initial weld was exposed to air were also' futile and the specimen was sectioned for metallograph study.

IV   PARAMETERS STUDY; SUMMARY

From the foregoing, it is obvious that there is a definite optimum vacuum range within which volatilization of beryllium is insignificant. There is also some suggestion that power input influences the ability of beryllium to vaporize rather than melt and weld.

To determine the effects of heat input on the welds, calculations of the heat required to melt and to vaporize beryllium were made. These calculations were based on 100% gun power input efficiency and on the known heat input required to raise beryllium to its melting point[5] plus its know heat of fusion.[6] The total heat to melt was so calculated at 1100 cal/gram. The heat of vaporization is computed from the sum of the heat to melt beryllium, the heat to raise beryllium from the molten state to the vaporization temperature (boiling point), and the heat of vaporization.

At 10^{-4} mm of Hg. pressure, the theoretical boiling point of beryllium is 1440°K which is below the melting point of 1550°K. In other words, beryllium should sublime at its melting point; however due to the impedance of an ever present oxide film, sublimation is reduced. Therefore, the heat to vaporize has been assumed to be the heat to melt plus the heat of vaporization of 4450 calories/gram. If a pressure of

178

10^{-5} mm Hg. were used less heat would be required for vaporization.

Based on these calculations and the total volume of melted metal, as determined metallographically, power required to either entirely melt or entirely evaporate the fusion zone was determined. In each run, the heat required to melt the fusion zone was less than the total heat input. This is obviously true since a certain percentage of the heat in all welding processes goes into heating the base plate. When comparing percentages of heat input required for vaporization or fusion, little vaporization would be expected in Runs 3, 4, 6 and 7 and very little in Run 2, since very many calories would be necessary to vaporize the large fusion zones resulting from the large spot sizes used. However, it would be expected that Specimen No. 1 would vaporize since under such conditions of high power density, only 3.3 percent of the total available power was required to vaporize the entire fusion zone. Run 2 showed no evidence of vaporization. Each run from Nos. 3-7 showed a varying degree of vaporization, since 7.2-47.2 percent of total power input would have caused total vaporization and only 2.1-11.7 percent total power caused melting of the entire fusion zone. Thus, both melting and evaporating, with much less of the latter was seen. In each case, however, vaporization was not significant until a vacuum range of below 10^{-4} mm of Hg. was attained.

To ascertain the interdependence of power input and chamber pressure upon vaporization ability, Figure 6 was constructed. Runs 3, 4, and 5 which were conducted at the Vaporization Limit are seen to define the separation of conditions causing or preventing evaporation under the particular conditions of end quenching used. Figure 7 defines, according to Runs 2 and 5, the Thermal Cracking Limit, or the power input
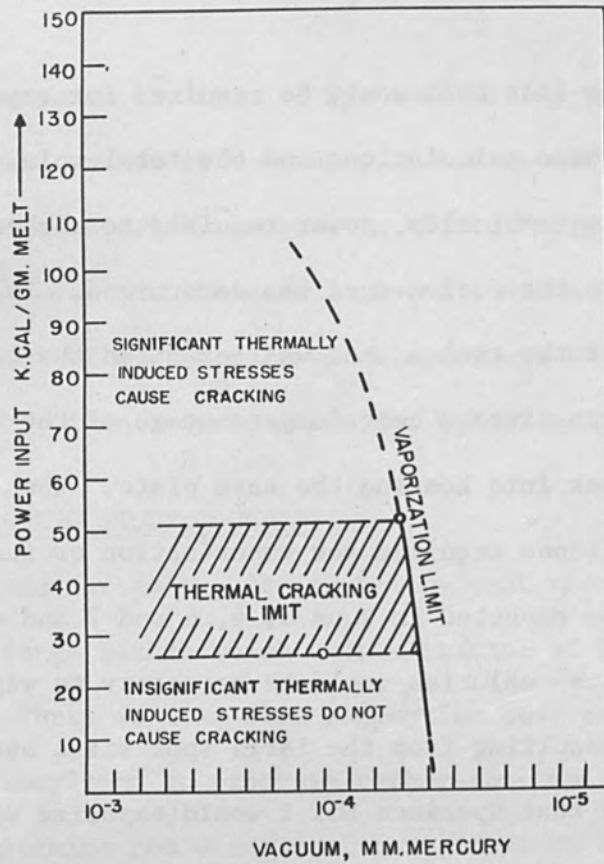
Figure 7

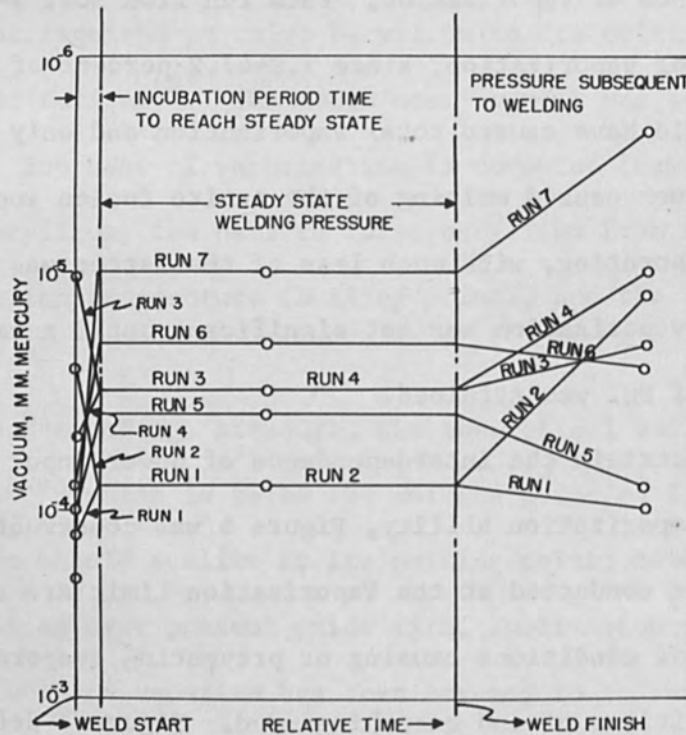Power Input, K.Cal/GM Melt vs Vacuum, mm. Mercury

Figure 8

Vacuum, MM. Mercury vs Relative Time

above which significant thermal stresses are introduced to cause cracking, and below which such stresses become too small to cause cracking. The intersection of the Thermal Cracking Limit and Vaporization Limit curves defines the area of beryllium weldability (lower left hand region of Figure 7) for this particular specimen and quench block size.

Chamber pressure was often quite different during a run as compared to the pressure just prior or subsequent to welding. For ease of reference, these pressures are plotted in Figure 8. Change in slope may be due to the affinity of beryllium for oxygen and nitrogen which was present within the welding chamber, to leakage, or to oxygen or nitrogen entrapped within the beryllium stock itself. Although the last point was not conclusively proved, one lot of pressed and sintered beryllium seemed more weldable than another. The vacuum plateaus in Figure 8 are shown to be a function of spot size (Figure 9). This is to be expected since evaporation rate is a function of the area heated to a sufficient temperature for volatilization. Because of the rapid stirring of the weld puddle, the entire molten volume is constantly exposed to the melt surface. Hence, the vacuum plateaus are also a function of the molten volume (see Figure 10). The similiarity between these two functions suggests that molten area and volume are interdependent, as shown in Figure 11, for the particular specimen configuration and gun type used during this phase of the work.

V   PARAMETERS STUDY; CONCLUSIONS

1. Leak-proof beryllium welds can be made by the electron
    beam process.

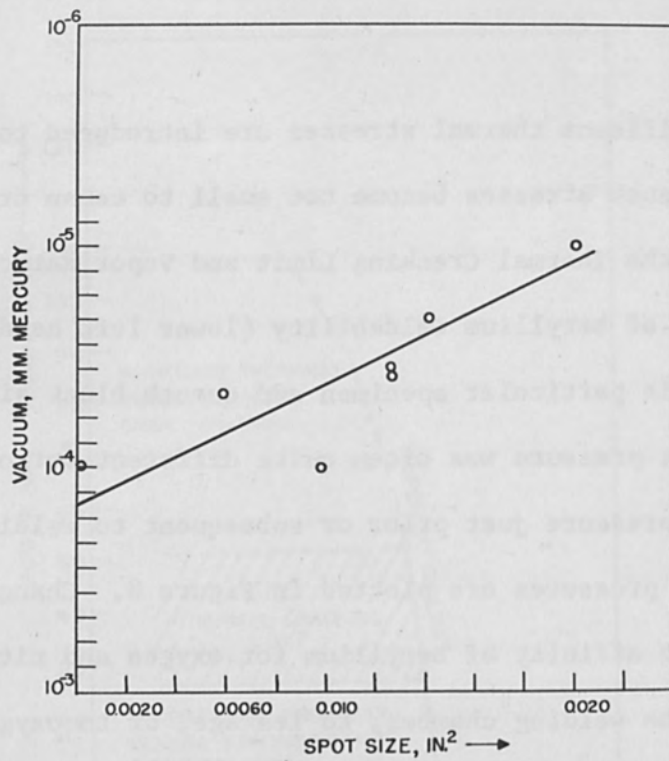2. Vaporization, outgassing, and thermally induced stress
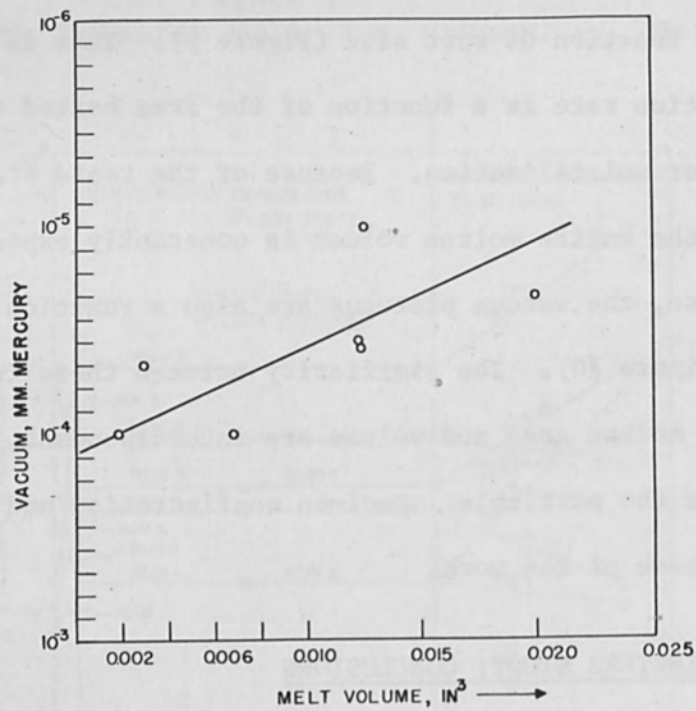
Figure 9

Vacuum, mm. Mercury vs Spot Size, In.^{2}

Figure 10

Vacuum, mm. Mercury vs Melt Volume, In.^{3}

182

cracking are prime causes of weldment failures.

3. Vaporization and thermal cracking limits for power input and operating vacuum may be defined for a particular specimen and quench block geometry.

4. Repair welding of cracks or voids is not feasible for specimens exposed to air prior to repair welding attempts.

5. Chamber pressure during welding is a function of molten spot size and volume.

6. Welding apparatus may be designed such that molten spot size and volume are interdependent.

7. The beryllium oxide insulating surface must be kept at a minimum thickness in order to obtain reproducible penetration.

8. Adequate joint design is essential. The parts must fit tightly with no cavities within the joint which might outgas during welding.

VI   WELDMENT TENSILE TESTING; PROCEDURE

A preliminary evaluation of the 0.020 inch thick rolled beryllium sheet indicated that although this sheet had a decided direction of rolling, the microstructure was fine grained indicating recrystallization produced by heat treatment after final rolling. The longitudinal direction of rolling was elected for axial loading of both welded and unwelded tensile samples.

Prior to welding several equipment changes were made. A traversing table was installed in the chamber driven by a reversible D.C. motor, capable of linear travel speeds up to 60 inches per minute with the specific gearing chosen. In order to make welds under optimum vacuum
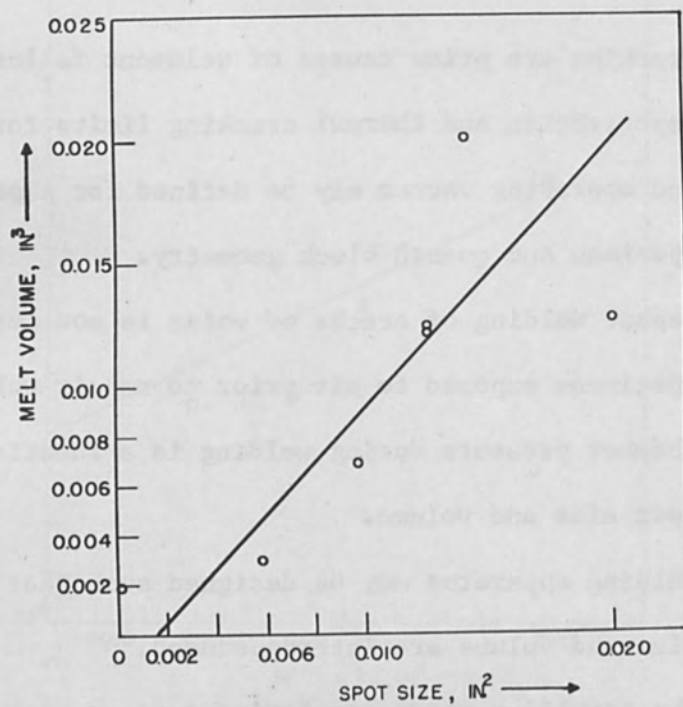
Figure 11

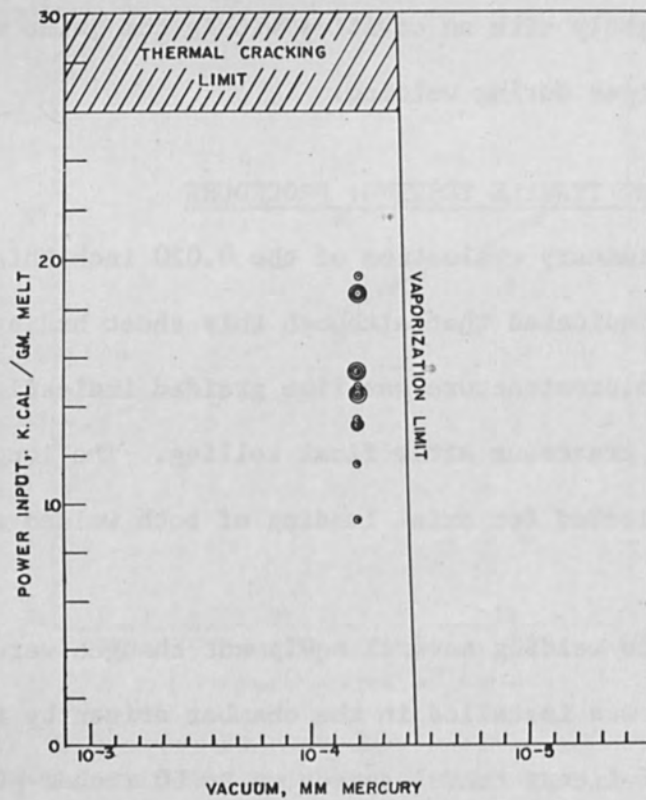Melt Volume, In.^{3} vs Spot Size, In.^{2}

Figure 12

Power Input, K.Cal/GM Melt vs Vacuum, mm. Mercury

conditions, a vacuum control circuit and automatically controlled leak were incorporated into the vacuum system.

Specimen preparation included grinding the edges to be welded in order to provide proper fitup. The specimens were held in place with moderate restraint to prevent parting during initial welding. No backup bar was provided and insulated tie-down bars were used to allow a large molten pool to form (i.e. low cal/gm of melt) and thus avoid thermal cracking. The welding variables were thus selected on the basis of preliminary results which indicated a parameter eliminating thermal cracking. All welding was performed at a vacuum of 8×10^{-5} mm, using a power input of 9000 volts and 20 milliampers. The specimens were preheated to approximately $500^{\circ}F$ prior to welding by making several passes over the joint with a defocused beam to aid in providing a larger molten volume, reduce surface gas, and reduce cracking outside the fusion zone. All melting was performed in a single pass with no post heat applied. Figure 12 shows that successful welding conditions were within the range delineated by the earlier cylindrical specimens.

Tensile specimens were machined according to ASTM specifications for flat sheet specimens. The average base metal longitudinal tensile specimen ultimate strength was 55,250 psi. Of 16 weldment tensile specimens, 7 broke in the base metal and 9 in the weld metal. Some of the specimens from each group fell in a range approaching the unwelded base metal tensile strength. The other group fell considerably below in the range of 15,000 psi (see Figure 13). Fractures in this group definately originated from notches along the edge of the specimen and possibly thermal cracks in the base metal, resulting from excessive restraint during welding. Of most importance is the fact that weldment
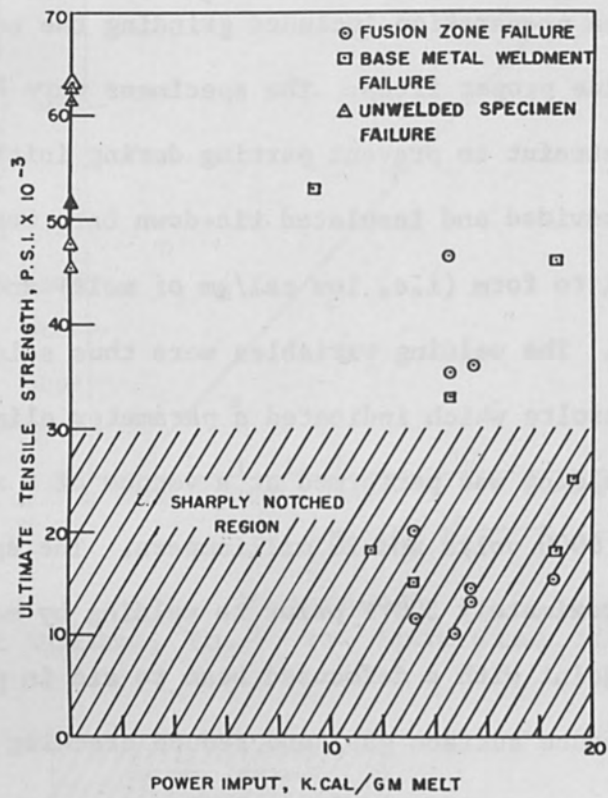
Figure 13

Ultimate Tensile Strength, P.S.I. vs Power
Input, K.Cal/GM Melt

tensile strengths can approach those of the unwelded base metal and that weldment fractures may occur in fusion or base metal zones. Due to the notch sensitivity of this material it would be advisable to electro-polish all further specimens.

Metallographic examination of welds indicated grain growth in the weld zone with no micro-cracking in the weld or heat affected zones. However, there was definate evidence of layered cracking in the middle of the sheet running in planes parallel to the surface of the sheet. This cracking appeared to have taken place during rolling and was typical of that resulting from excessive reduction between stress relief anneals.

Thus, it is shown that with proper heat input and operating pressure conditions, leak tight beryllium weldments having equivalent tensile strengths in the fusion, heat-affected, and base plate zones could be accomplished through electron beam welding.

In the future, emphasis will be placed on specimen preparation to eliminate or reduce the effect of notches. Further emphasis will be placed on the effect of surface oxide during welding, since there is evidence that this oxide plays an important role in the control of heat input and metallic vaporization during welding of beryllium.

VII   ACKNOWLEDGMENT

VIII   <u>REFERENCES</u>

1. Keil, R. W., Hauks, G. S., and Taub, J. M., "Brazing and
    Soldering of Beryllium", Welding Journal, 39, 406, 1960.

2. Monroe, R. E., Marthin, D. C., and Voldrich, C. B., "Welding
    and Brazing of Beryllium to Itself and to other Metals", BMI-
    836, 28 May 53.

3. Brundige, E. L., Kirby, R. S., Hawks, G. S., and Taub, J. M.,
    "Welding of Beryllium", Welding Journal, 38, October 59.

4. Martin, D. C., "Joining of Beryllium", The Metal Beryllium,
    ASM 283-1955.

5. Kelley, K. K., Bureau of Mines Bulletin 477, 1948.

6. Lillie, D. W., "Properties of Beryllium", The Metal
    Beryllium ASM 304-1955.

188

ELECTRON BEAM WELDING
OF
ROCKET CASING MATERIALS

By

H. J. Lander
Senior Project Engineer
Alloyd Electronics Corporation

W. T. Hess
Project Supervisor
Alloyd Corporation

S. S. White
Supervisor Materials Joining
Alloyd Electronics Corporation
Cambridge, Massachusetts

ABSTRACT

Electron beam welds of three different widths

were made in each of five titanium alloys with a 20,000

volt gun. These welds were evaluated by tensile and impact

testing and chemical and metallographic examination. The

mechanical properties were comparable with base metal

properties and independent of weld width. No substitution

element composition changes were found.

ELECTRON BEAM WELDING OF ROCKET CASING MATERIALS

INTRODUCTION

Titanium, with its very high strength-to-weight ratio, has often been considered as a structural material for high performance vehicles, and for other structures requiring high strength and stiffness in which the need for weight savings is paramount. The production of this material has met with serious difficulties owing to the high reactivity of titanium with almost all other materials at elevated temperatures.

Production techniques have, however, been improved sufficiently so that titanium sheet and bar stock in a variety of alloyed compositions are available at one quarter the market price of ten years ago. Although this means that titanium is still considerably more expensive than steel, its prime competitor, titanium is available in amounts desired. Thus, one of the last major obstacles to the more frequent utilization of this metal is the difficulty in joining it, where again, its high reactivity becomes a problem.

Most arc fusion welding studies to date have produced weldments with substantially less impact resistance and ductility than unwelded base metal.[1] In many cases, weldment strengths have been erratic, showing either increases or decreases in strength as compared to unwelded material. Generally, the production of such brittle and unreliable joints has been felt to be related to oxygen and nitrogen contamination during tunsten-arc or metal-inert-arc welding. Since perhaps 80 to 90% of all structural joining is best accomplished by fusion welding, a study was undertaken to determine the effects of welding several titanium alloys in vacuum.

Vacuum welding, better known as electron beam welding has,

190

during the last several years, been publicized as an optimum way to realize maximum joint efficiencies with minimum contamination for even the most reactive metals. Historically, equipment to accomplish such joining has fallen into two somewhat arbitrary divisions. High voltage welding utilizes equipment of the 75,000 to 150,000 volt range, while more common low voltage welding utilizes equipment of the 15,000 to 30,000 voltage range.

The ability of high voltage equipment to make very narrow deep fusion zones, in comparison to those normally obtained from low voltage electron beam equipment, suggests very different weldment properties. The reduced extent of the heat-affected-zone occurring in very narrow welds, and the ability to control gas content closely with changes in weld width, suggested that a variety of fusion zone widths be used on several titanium alloys. In this way, not only would the advantages of electron beam welding these materials be realized, but the characteristics of specific joint configurations would be determined.

The five Department of Defense Titanium sheet rolling alloys; i.e., the 6Al-4V alloy, the 4Al-3MO-1V alloy, the 2 1/2 Al-16V alloy, the 5Al-2 1/2 Sn alloy, and the all beta alloy (B120VCA) were used since these materials are of the highest interest in sheet form to missile and airframe fabricators at the present time.[2]

EQUIPMENT

A diagram of the equipment used for the subject program is shown in Figure 1. The equipment consists of a square chamber specifically designed for the welding of flat tensile and impact specimens in square butt weld configuration. The chamber was evacuated by mechanical and

diffusion pumping and was capable of obtaining the operating pressure range of 10^{-4} to 10^{-5} microns pressure within 10 to 20 minutes from the beginning of the pump-down cycle.

The massive copper chill bars and back-up plate were used not only to restrict the width of heat-affected-zone, but to confine and help control the fusion zone geometry.

Using a self-accelerated gun having a power density of 1,000 KW/in^2, it was possible to accurately control weld widths such that joints of 0.050 inches to 0.300 inches in 1/8 inch material could be made in a single pass using a power supply rated at 22,000 volts and at 300 m.a. maximum output. The particular gun used for this work was developed to produce fusion zone geometries reproducing those obtainable with standard high voltage E.B., low voltage E.B., and tungsten-arc sources. A high degree of reproducibility and ruggedness was obtained in the gun, with both electrostatic and electromagnetic principles used in focusing. Spot size could be controlled from 0.005 inches to 0.035 inches in diameter, depending on total power input.

To minimize friction, the carriage assembly rode on a three-point suspension utilizing linear ball bearings. A conventional electronic speed control driving a variable speed D.C. motor was used. In conjunction with the specific gearing chosen, welding speeds varying from 0 to 240 inches per minute could be reproducibly obtained.

All welding operations were monitored with film badges mounted on the outside of the pyrex viewing window for x-ray emission. During these experiments, no x-ray count significantly higher than that of background was observed.

192

EXPERIMENTAL PROCEDURES

The five titanium alloys used in this study were cut to specimen size for subsequent manufacturing into weldment tensile and impact specimens. All edges to be joined were Blanchard ground to ensure proper joint fit-up. Square butt joints were found to be adequate for single pass full penetration with all alloys used. Subsequent to grinding, specimens were carefully cleaned in ethyl alcohol dried at room temperature, and welded.

On welds of more than four inches in length, it was found necessary to electron beam tack both joint ends prior to welding in order to eliminate any occurrence of root opening. With chill bars accurately placed at specific distances from the centerline of the joint, any misalignment of the electron beam from the centerline could be corrected before initiation of the welding operation by minor adjustments in the horizontal position of the entire carriage assembly.

All joining was accomplished utilizing 14,000 volts, 250 m.a., and 8 to 10 inches per minute travel rate, depending on exact specimen thickness, which varied from 0.084 to 0.125 inches among the several sheets (one for each alloy) used. Gun efficiency was found to be approximately 50 per cent, allowing joints to be accomplished at an average of 10,000 to 15,000 Joules/In. energy input.

With these relatively low energy inputs, as compared to those common in arc welding,[3] distortion was held to a minimum and hold-down plates were used primarily to prevent spreading of the molten pool beneath the copper chill bars, thus inadvertently increasing weld width. With this tooling, upsetting of the fusion zone took place. It was found that minor adjustments of the travel rate could virtually eliminate
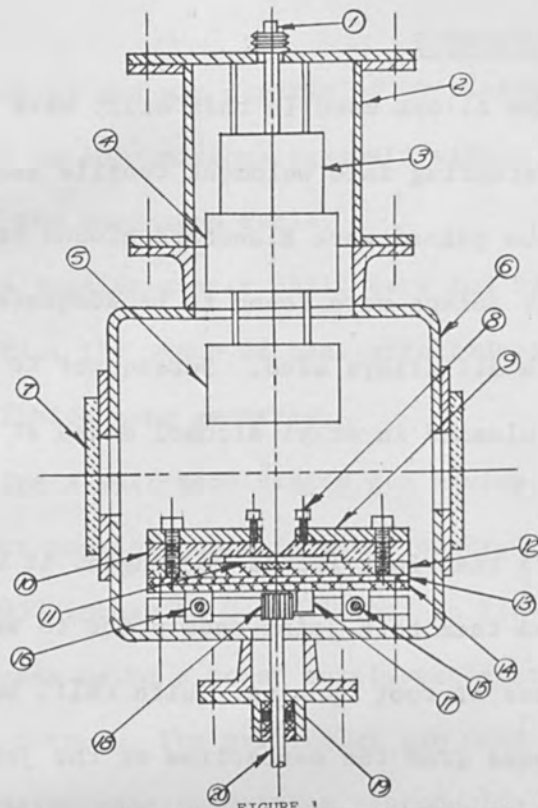
FIGURE 1   DIAGRAM OF SPECIMEN WELDING SYSTEM

1. Power Feed Through Assembly, 2. E. B. Gun Chamber, 3. E. B. Gun Filament,
4. E. B. Gun Electrostatic Focusing Section, 5. E. B. Gun Electromagnetic
Focusing Section, 6. Welding Chamber, 7. Pyrex View Port, 8. Hold Down Screw,
9. Hold Down Plate, 10. Chill Plate, 11. Specimen, 12. Back Up Plate With
Insert, 13. Transverse Table, 14. Longitudinal Table, 15. Table Support Rod,
16. Linear Ball Bushing, 17. Rack, 18. Pinion, 19. Rotary Ball Bearing Seal,
20. Drive Shaft

FIGURE 2

Cross - Section of 5Al-2 1/2 Sn Alloy Weldment, Fusion Zone Width: 0.090
Inches, Voltage: 14,000, Amperage: 250 m.a., Speed: 9 i.p.m.

194

undercutting, hence eliminating the need for filler material of similar composition. A cross-section of a typical weld produc ed by these techniques is shown in Figure 2.

Subsequent to welding, specimens representing all fusion zone widths and alloys used were radiographed. Figure 3 shows two different weld widths in one of the alloys used. It may be seen that porosity is a function of weld width. Although substantially straight-sided fusion zones were obtained, the term "weld-width," refers to the width of the molten and resolidified zone on the topside of the weldment.

Three transverse tensile specimens of each weld width and alloy were machined to standard A.S.T.M. flat tensile specifications. These 8 to 9 inch long bars having a 2 inch reduced gage section of 1/2 inch width were then subjected to the photogriding process. This technique originally developed at the Watertown Arsenal Laboratories,[4] allows a grid of accurate dimensions to be directly photographed onto the specimens. In this way, the real incremental strains existing in the differing metallurgical portions of the weldments could be and were determined, rather than average strain values for weld and base metal obtained when measuring strains over standard gage lengths. Using conventional techniques, the total elongation existing in two inches of weldment including fusion and heat-affected regions totaling only 1/2 to 3/4 inch in width could completely mask either a high degree of ductility or a serious loss of ductility in the narrow confines of these latter areas. In the current study, a grid of 0.001 inch lines accurately placed in square array 0.049 inches on a side was used. Incremental strain measurements were made at 20 magnifications utilizing a microscope having a movable micrometer base.
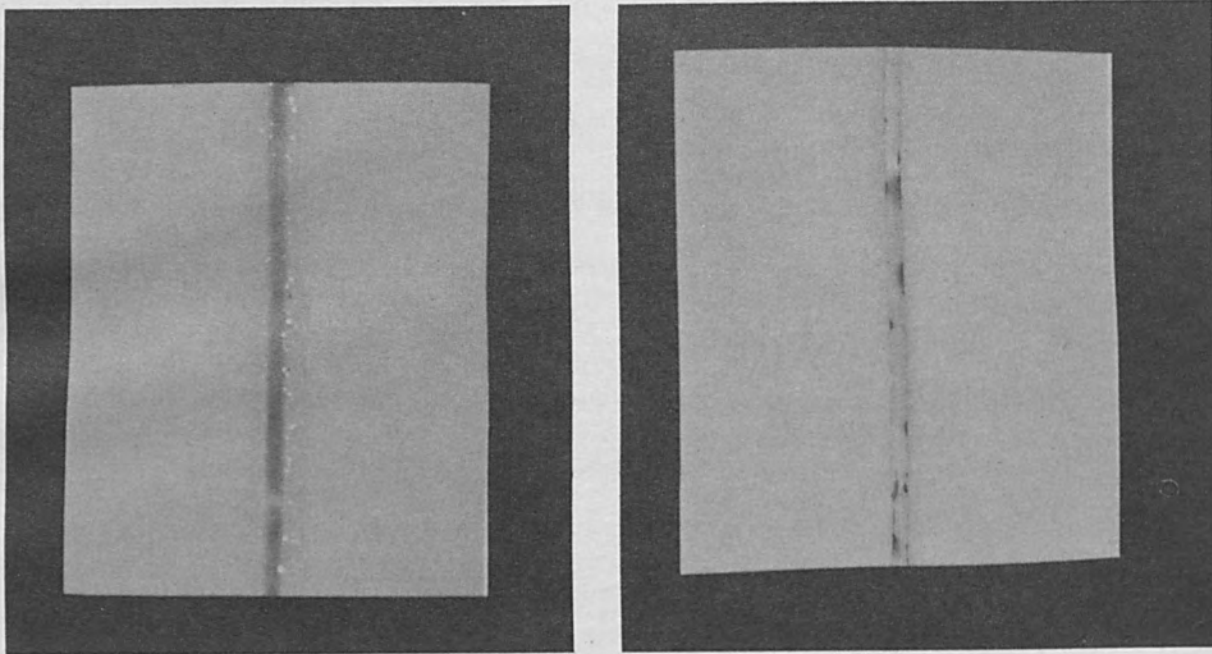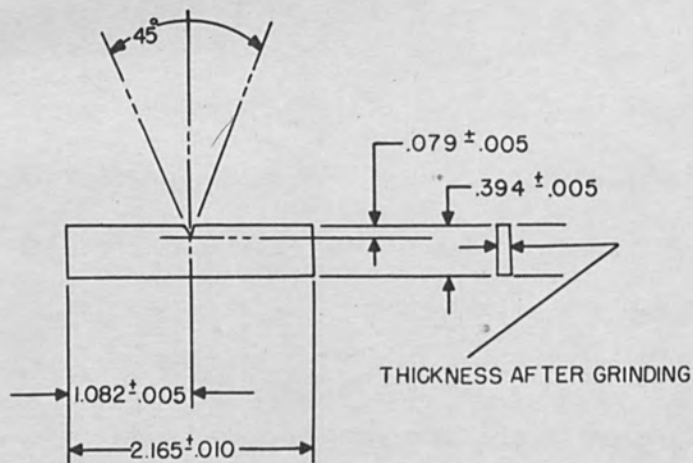
195

FIGURE 3

Radiographs of Two Weld Widths in 5Al-2 1/2 Sn Alloy
Left - 0.187 Inch Weld Width
Right - 0.090 Inch Weld Width

MTL-TITANIUM

FIGURE 4

IMPACT SPECIMEN

The impact strengths of welded joints were also determined for these alloys and compared to values obtained from unwelded base plate. The specimen used in these evaluations is shown in Figure 4. It is a Charpy specimen in all dimensions except for the thickness which is that of the sheet used. In the case of weldments, specimen thickness was reduced to completely eliminate the effect of crown, fillet, or other deviations from flatness. This specimen type, developed by the Watertown Arsenal Laboratories[3,5,6], incorporates the technique of introducing a natural fatigue crack at the base of the notch. This crack depth could be accurately controlled to 0.050 inch ± 0.015 inches. The specimens were impacted, and the area through which the crack propagated was measured on each specimen.

This technique made it possible to measure crack propagation energy only, since the crack proceeded from a pre-existing natural crack. This represents the mode of fracture usually occurring in actual weldments where failures most often begin at existing stress raisers since it eliminates measuring the energy associated with crack initiation. Since crack initiation energy is a function of specimen geometry and elastic strain energy, any true changes in propagation values could be entirely masked when utilizing specimens not having such a natural crack and, thereby, requiring significant imparted initiation energy. The crack propagation energies of fusion zones were determined by centering the notch on the fused centerline. Base plate impact values were determined utilizing unwelded material.

DISCUSSION OF RESULTS

The results of the three series of strain readings representing

197
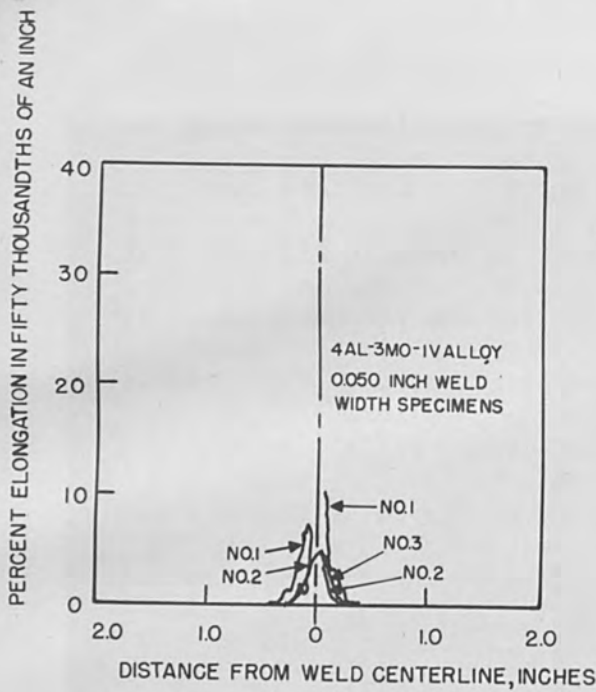
FIGURE 5

INCREMENTAL STRAIN PERCENTAGES FOR THREE SPECIMENS
REPRESENTING ONE WELDING CONDITION
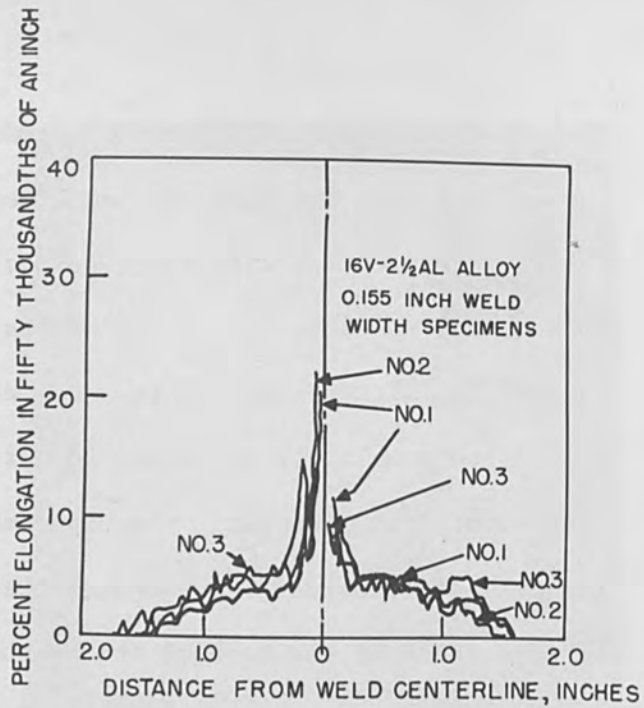
FIGURE 6

INCREMENTAL STRAIN PERCENTAGES FOR THREE SPECIMENS
REPRESENTING ONE WELDING CONDITION
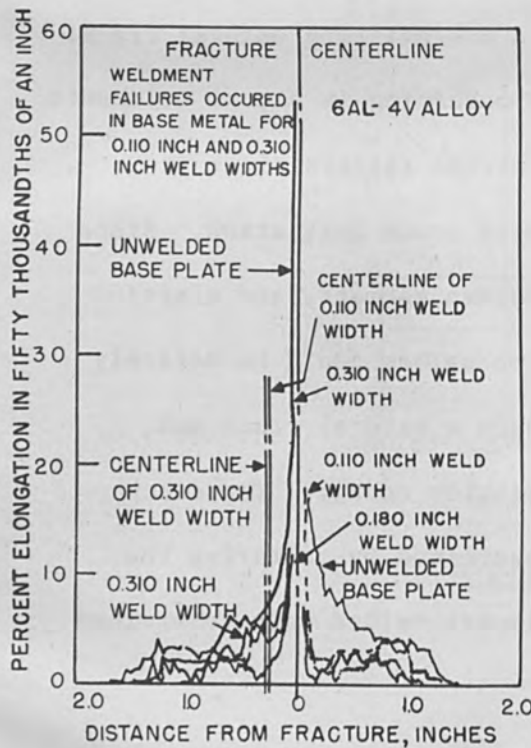
FIGURE 7

INCREMENTAL STRAIN PERCENTAGES IN VARIOUS
WIDTH WELDMENTS IN ONE ALLOY
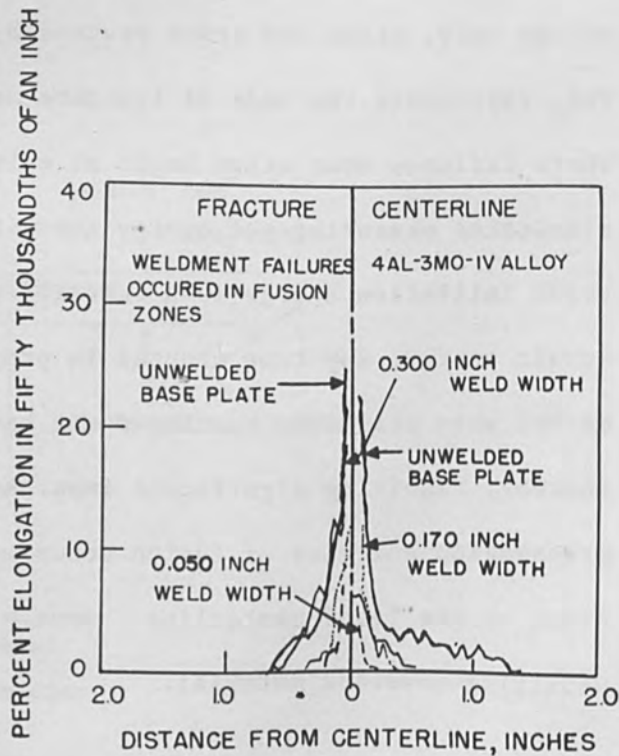
FIGURE 8

INCREMENTAL STRAIN PERCENTAGES IN VARIOUS
WIDTH WELDMENTS IN ONE ALLOY

198
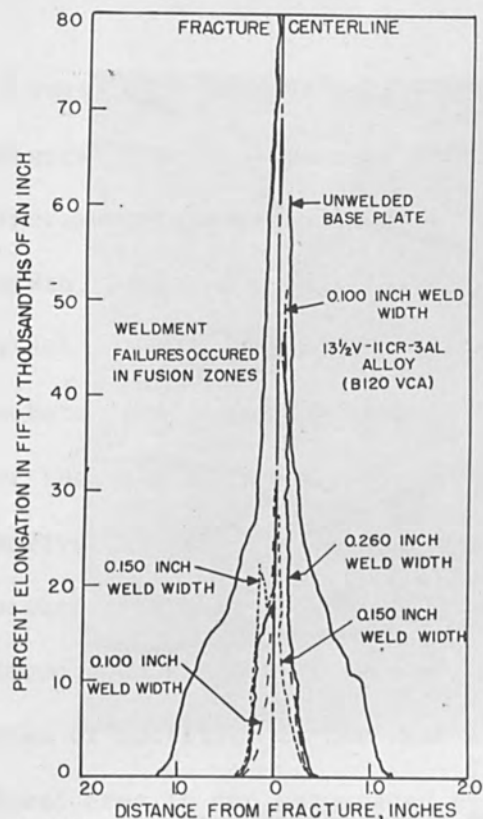
FIGURE 9. INCREMENTAL STRAIN PERCENTAGES IN VARIOUS WIDTH WELDMENTS IN ONE ALLOY

FIGURE 10. INCREMENTAL STRAIN PERCENTAGES IN VARIOUS WIDTH WELDMENTS IN ONE ALLOY

FIGURE 11. INCREMENTAL STRAIN PERCENTAGES IN VARIOUS WIDTH WELDMENTS IN ONE ALLOY

FIGURE 12

Cross - Sectional Area 1 1/2 inches
From Centerline of 4Al-3Mo-1V
Weldment Specimen No. 4
500 x Magnification
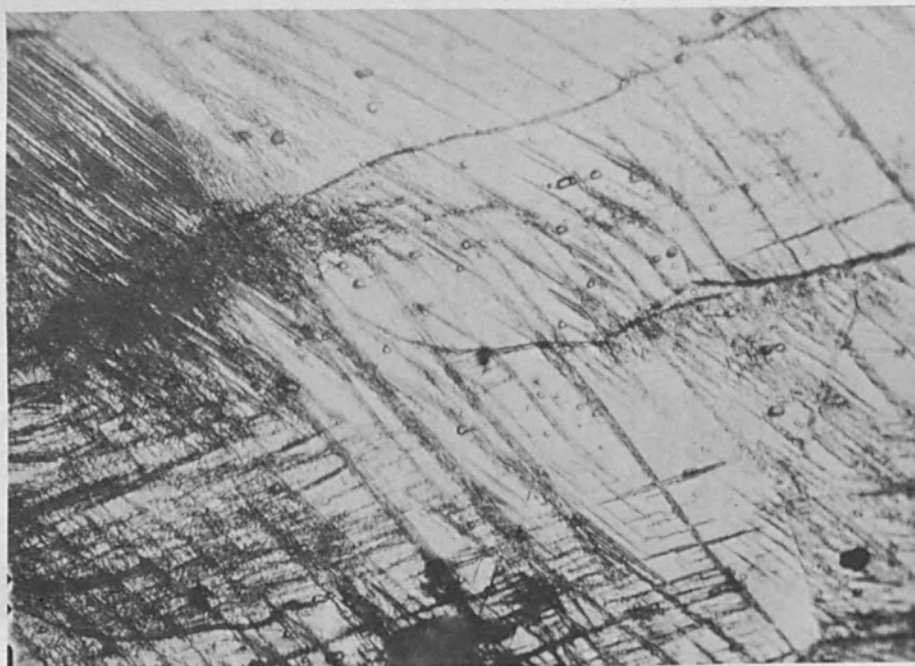
FIGURE 13

Cross - Sectional Area 3/4 Inch
From Centerline of 4Al-3Mo-1V
Weldment Specimen No. 4
500 x Magnification

a particular weld were highly consistent as evidenced in Figures 5 and 6. Figures 7 through 11 show, for the five alloys heats used, that the increment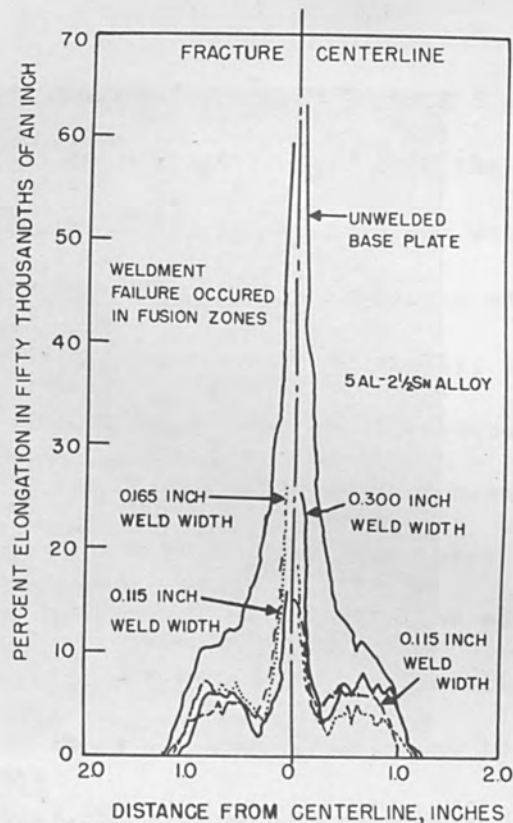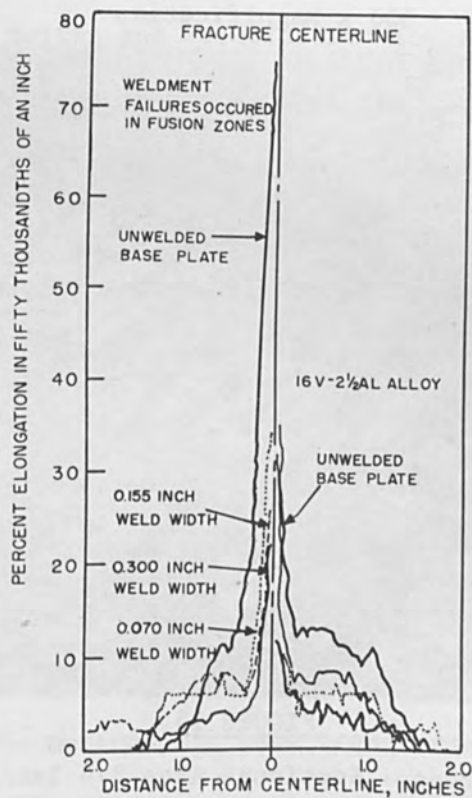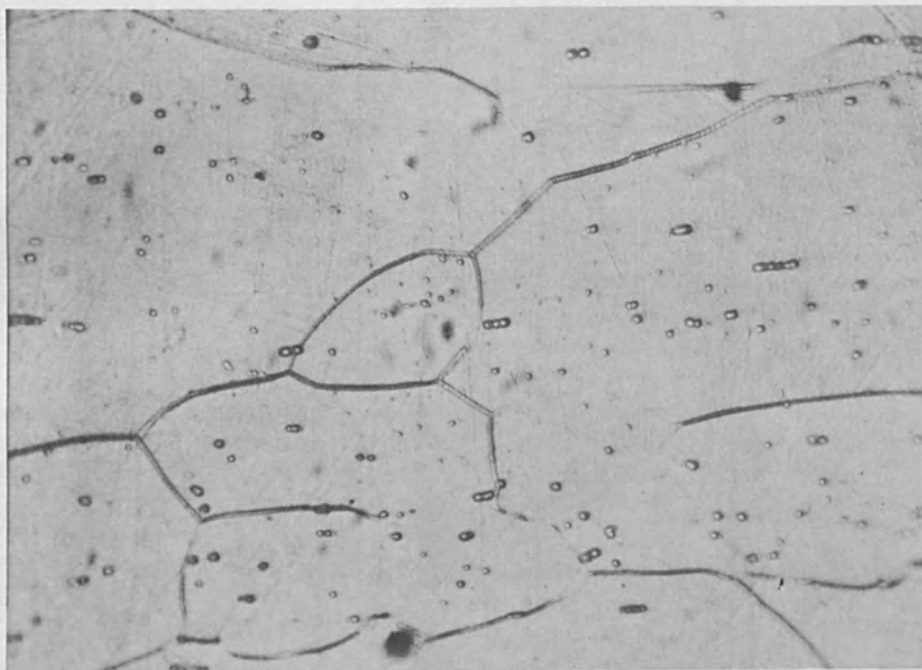al strain measurements are substantially independent of weld width, although a suggestion of greater ductility with increasing weld width is evidenced by the 4Al-3Mo-1V alloy (Figure 7). Generally, a substantial amount of plastic strain potential is lost as a consequence of the welding process when the fusion zone becomes the weakest area. However, it is significant that fusion zone strains, when fractures occurred therein, occasionally showed evidence of approaching the strains found when fracture took place in the unwelded base plates. The slight loss of ductility in the heat-affected-zones immediately adjacent to the fused area is not unexpected since these portions of the weldments under-went substantial grain-growth without the benefit of the purification which occurred in molten and resolidified zones. The ductility loss occurring throughout the remaining base plate and low temperature heat-affected regions cannot be explained on the basis of the particular welding technique used. However, the physical upsetting which resulted from the fixturing was found to yield regions of strain transformations extending as far as one inch away from the weld centerline. Figure 12 shows the unaffected base plate of the 4Al-3Mo-1V alloy, and Figure 13 shows a region 3/4 inch away from the weld centerline on the same material. Temperature sensitive lacquer measurements show that this region was never heated above 300°F. This fact, combined with no change in grain size between the unaffected base plate and the transformed base plate demonstrate that the Martensitic beta transformations are the result of upsetting. This is probably common to all weld fixturing in which the

FIGURE 14

Cross - Sectional Area of Heat-Affected-Zone in 4Al-3Mo-1V
Weldment Specimen No. 4
500 x Magnification
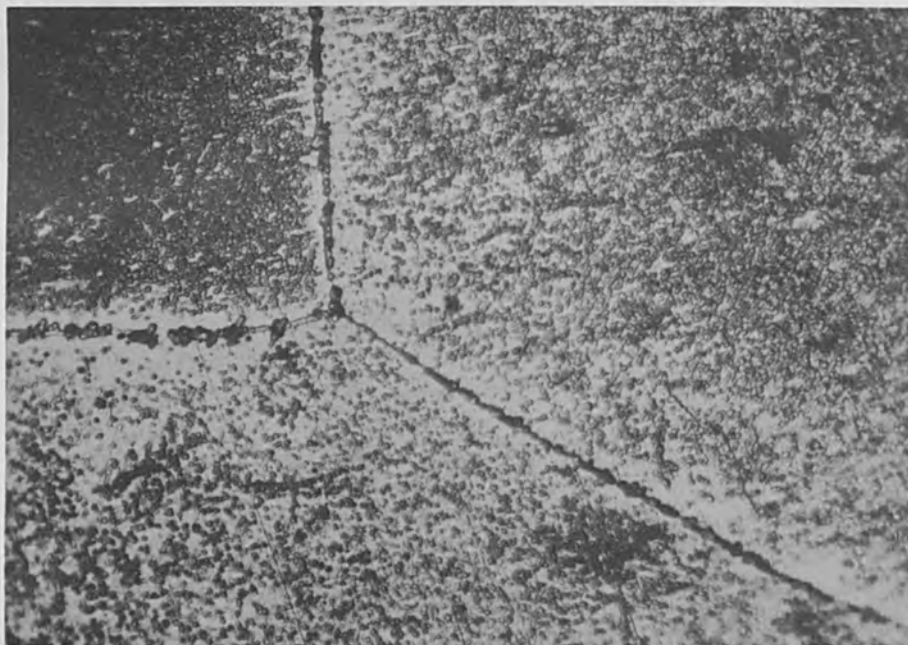
FIGURE 15

Cross - Sectional Area of
Fusion Zone in 4Al-3Mo-1V Weldment
Specimen No. 4
500 x Magnification

titanium plates are rigidly clamped in place, and attended by all of the strain loss common to such partial transformations.

The heat-affected zones and fusion zones are typically represented for this same material in Figure 14 and 15 from which it may be seen that ductility is not directly related to grain size.

The tensile testing results are presented in Figure 16, where ultimate strength is plotted as a function of weld width. It may be seen, for the heats used in the as-received conditions, that the 4Al-3Mo-1V alloy and the 16V-2 1/2Al alloy decreased in tensile strength as a function of weld width. The ability of vacuum melting to help produce materials of lower institial content will be expected to produce such results, regardless of grain size increase or precipitation or work hardening loss. However, it may be seen that the 6Al-4V alloy yielded fusion zones substantially stronger than the base material. Almost all specimens pulled of this alloy broke in the base metal. Similar results were obtained with 5Al-2 1/2Sn alloy and the all beta 13 1/2V-11Cr-3Al alloy, in which almost all failures occurred in the fusion zones but at strengths significantly higher than evidenced in the unwelded base plate, or at levels compatible with the base plate strength.

The strengthening of the 5Al-2 1/2Sn alloy throughout all of the metallurgical portions of the weldment, and the strengthening of the fusion zone of the all beta alloy, may be at least partially attributed to upsetting. Any increase in contamination may have been a factor in fusion zone strengthening, or could even have resulted in fractures consistently outside of the fused portion (6Al-4V alloy).

Since the operating pressure was 10^{-4} microns, the only contamination source which could cause such strength increases was the
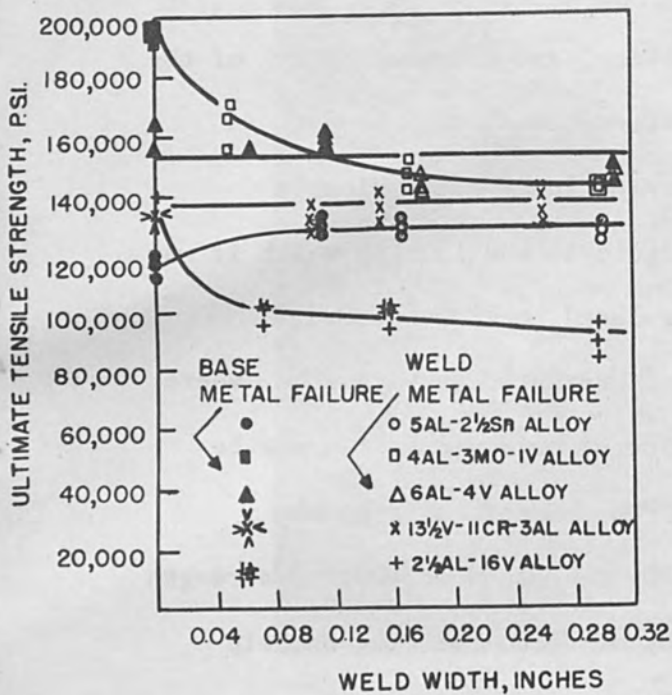
FIGURE 16

TENSILE STRENGTH VS. WELD WIDTH
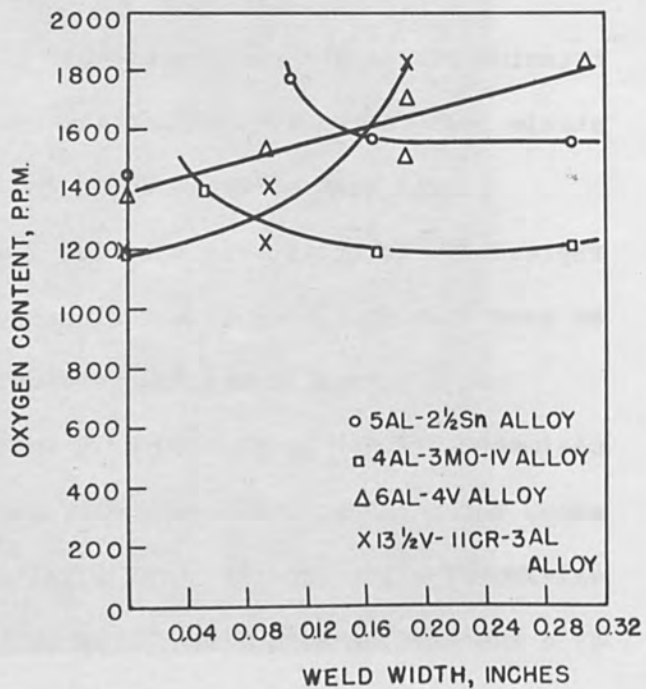
FIGURE 17

OXYGEN ANALYSES
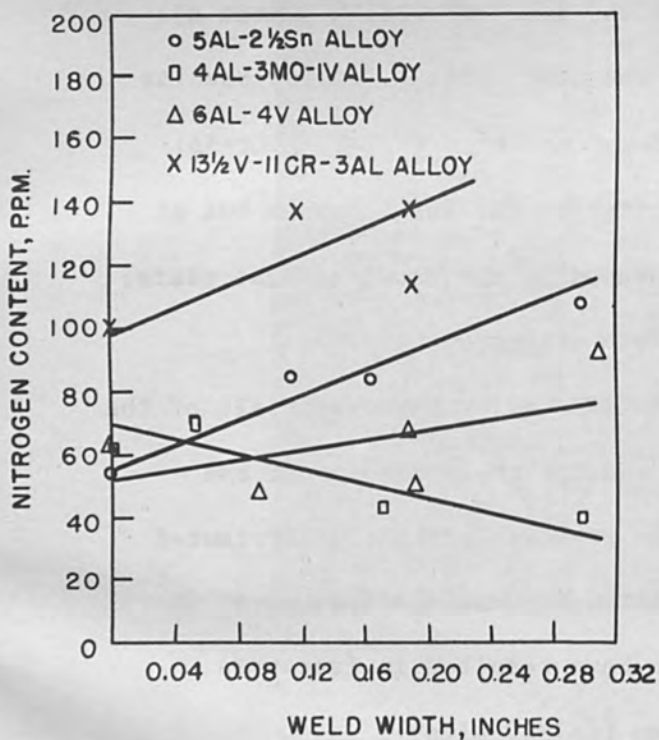
FIGURE 18

NITROGEN ANALYSES
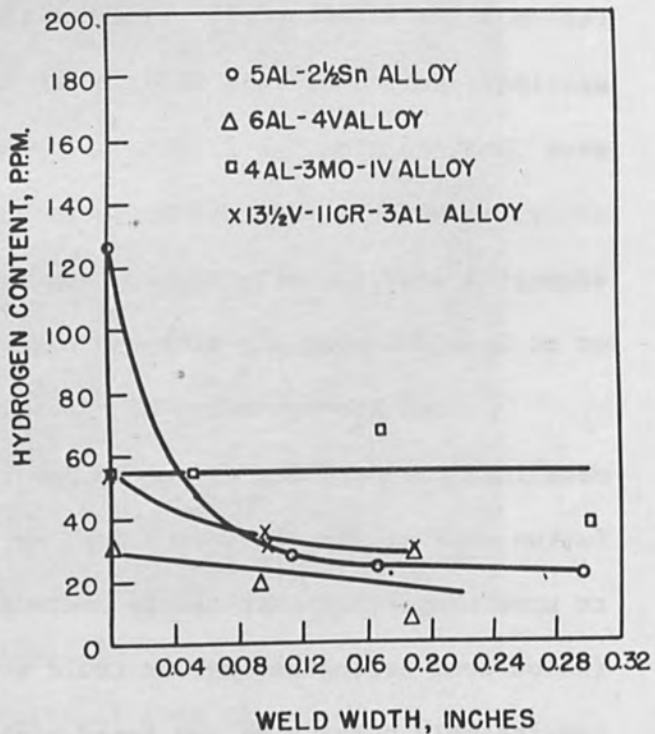
FIGURE 19

HYDROGEN ANALYSES

pre-existing oxide or nitride surface film. Corroborating evidence for this is furnished in Figures 17, 18, and 19 in which the oxygen, nitrogen and hydrogen contents for four of the heats used are plotted as a function of weld width. A 1/16 inch cube was machined for vacuum fusion analysis from plate or weldment center. Thus, all surface gas content was not included in these specimens. In all cases, hydrogen content was either unchanged or decreased, depending on the alloy. Particular attention is drawn to Figure 17 on which for both the 5Al-2 1/2Sn alloy and 4Al-3Mo-1V alloy, oxygen content increases from the base metal value and decreases to substantially the same base metal value as weld width increases. Such action is to be expected from the initial dissolution of an oxide film, and the subsequent decrease of this oxygen content as weld width, and thereby exposed molten surface area, are increased for a given carriage dwell time.

The oxygen contents of the all beta and 6Al-4V alloys had apparently not yet reached such an equilibrium limit, as was true for the nitrogen content of these two alloys and the 5Al-2 1/2Sn alloy.

While the degree of strengthening which may be attributed to the separate gaseous contents of several materials is not clear, the 4Al-3Mo-1V alloy does seem particularly sensitive to oxygen content. It may be seen that, for this alloy, both nitrogen and hydrogen contents changed relatively little with an increase in molten surface area. However, the oxygen concentration was found to vary linearly with ultimate tensile strength (see Figure 20). Replotting Figure 20 on the basis of ultimate strength change vs. oxygen content change, yields the linear relationship shown in Figure 21, demonstrating that for every one hundred parts per million increase in oxygen content, tensile strength increased
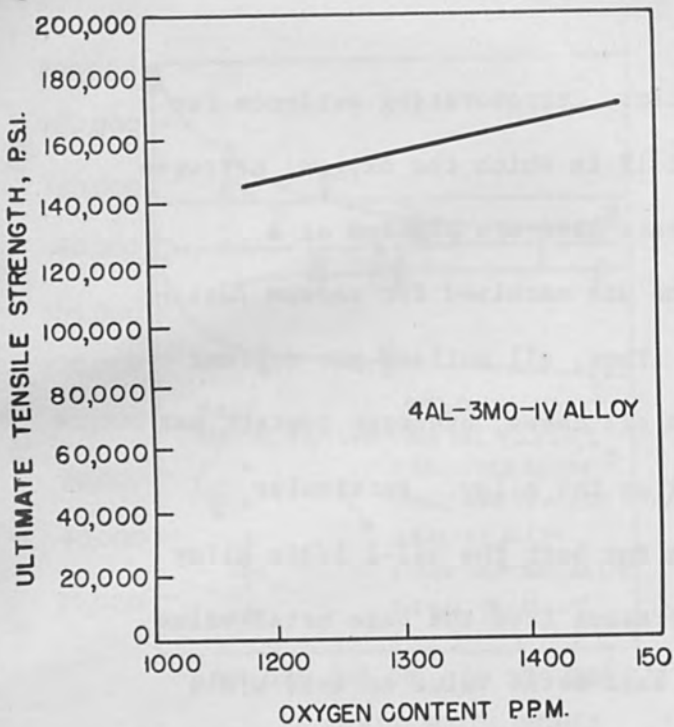
FIGURE 20

DEPENDANCE OF STRENGTH ON OXYGEN CONTENT
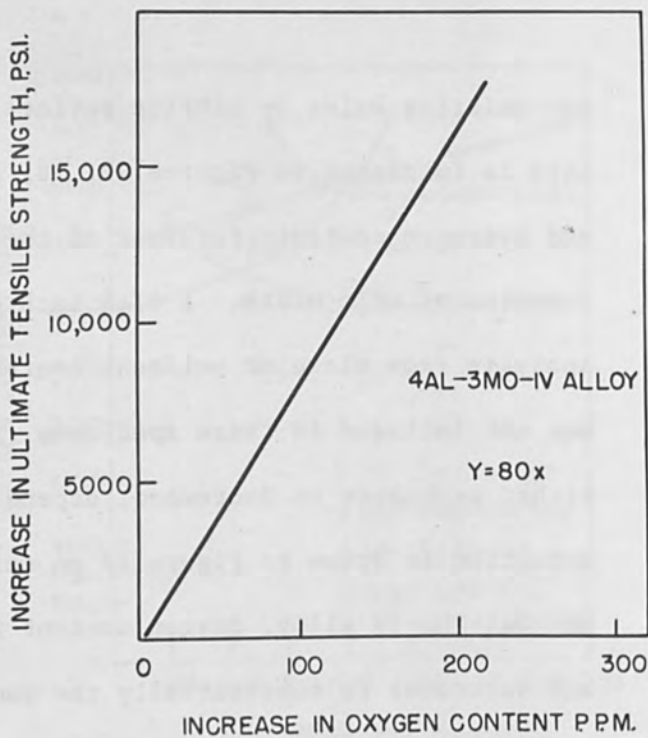
FIGURE 21

DEPENDANCE OF STRENGTH ON OXYGEN CONTENT
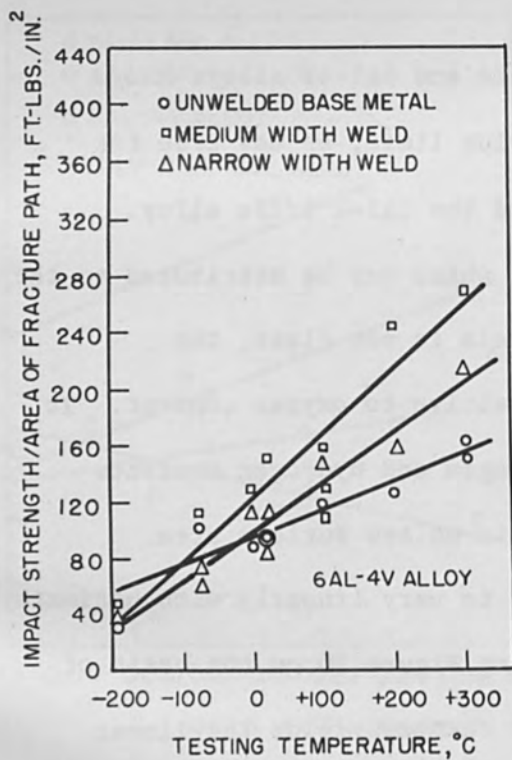
FIGURE 22

IMPACT RESISTANCE
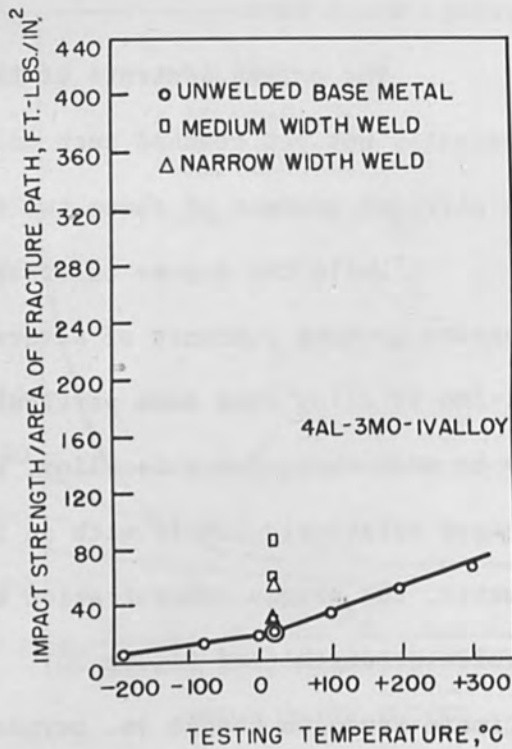
FIGURE 23

IMPACT RESISTANCE

8,000 lb. per square inch under welding conditions. This figure is not necessarily to be taken as a general parameter for strength increases with gaseous content increases for this alloy, since, under welding conditions, both grain growth and mechanical upsetting were introduced.

A complete analysis of all substitutional alloying elements was undertaken. It was found that despite wide variations in alloying elemental partial pressure and melting point, no significant change in substitutional anslyses from base plate values was discovered. Presumably, this was a consequence of the relatively short dwell time occurring in the welding process, such time being insufficient to allow for significant percentage decrease in lower melting point materials in the fusion zone. Thus, any strength increases which are to be attributed to changes in composition are entirely due to interstitial composition variations.

The results of impact testing these several alloys are shown in Figure 22 through 26, in which impact strength per area of fracture path is plotted against testing temperature in °C. Two different weld widths, a medium width (0.188 inches) and a narrow width (0.094 inches), are compared in impact resistance to unwelded base plate, with full curves presented for all base plates and the 6Al-4V alloy, and room temperature results reported for the weldments of the other four alloys. It may be seen that there is, generally, little loss in impact strength from the base material, with a general increase in impact resistance caused by welding. This impact resistance increase is also a function of weld width with Charpy values increasing as weld width increases.

The 6Al-4V alloy is particularly interesting since impact values are significantly higher in the fusion zone than in unwelded material.
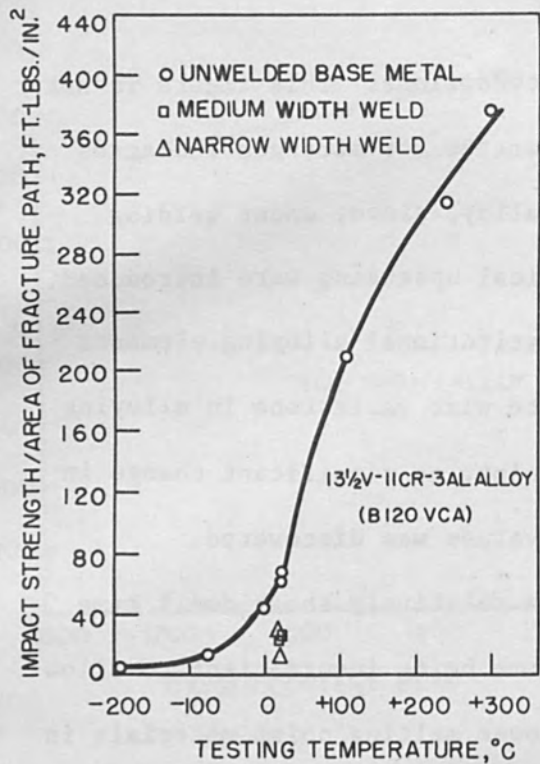
FIGURE 24

IMPACT RESISTANCE
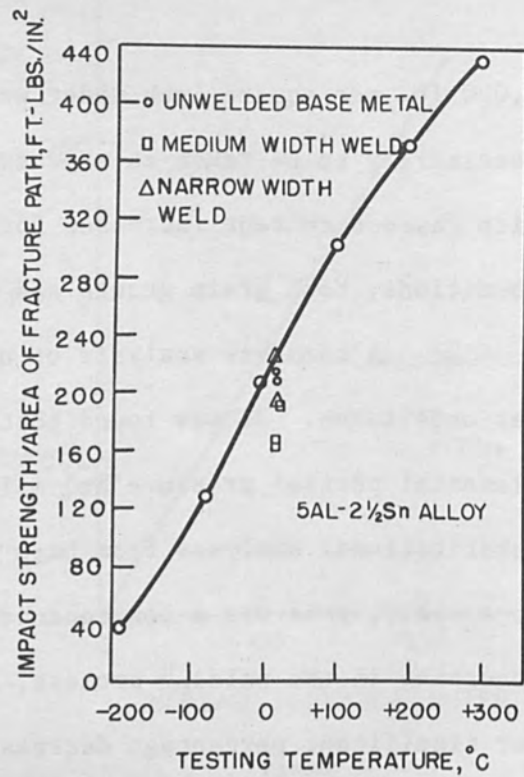
FIGURE 25

IMPACT RESISTANCE
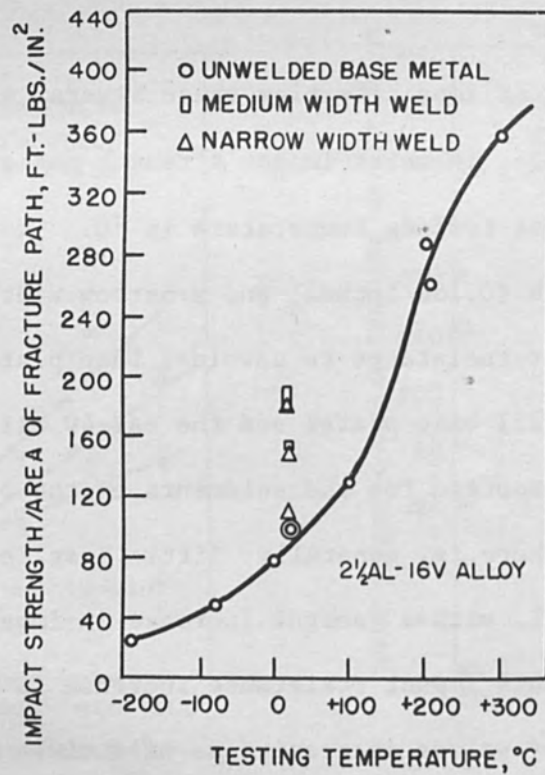
FIGURE 26

IMPACT RESISTANCE

This, despite the fact that fusion zone strength was increased above the base plate strength as shown in Figure 16, suggests that impact strength may be much more dependent upon slight decreases in hydrogen and/or nitrogen content than upon increase in oxygen content which, according to the gas analyses presented in Figures 17, 18, and 19 is obviously a prime reason for strength increase.

These results are felt to be particularly significant since arc welding of this and similar titanium alloys has consistently shown a drastic lowering of impact strength, presumably due to contamination.[5]

CONCLUSIONS

1. Titanium alloys in thicknesses up to 1/8 inch can be electron beam welded by a low voltage gun in a single pass without excessive joint preparation.

2. Weld widths varying from 0.050 inches to 0.300 inches are attainable with proper tooling and power density.

3. Fusion zone strengths may match or exceed base plate values.

4. Weldment strengths have been shown to be related to elemental gases in solution and physical upsetting of the weld; no significant loss of substitutional elements was found.

5. For three of the five alloys investigated, weld width bore no relationship to ultimate strength. For the remaining two alloys, strength decreased as weld width, and thereby degree of purification, increased.

6. Impact resistance values were found to be either similar to or higher than those of the base plates.

7. Impact resistance was found to increase as weld with increased.

8. Incremental strains in welds were substantially lower than base plate values; however, fusion zone ductility occasionally approached that of base plate fracture locations.

9. Some evidence was found that hydrogen content overshadows, in importance, that of oxygen and nitrogen insofar as impact resistance is concerned.

ACKNOWLEDGEMENT

REFERENCES

1. Hartbower, C.E., Orner, G.M., Daley, D.M., "Feasibility of Titanium for Welded Missiles", The Welding Journal, 39 (9), P. 345-S, 1961.

2. DMIC Report 46H, 1 June, 1960.

3. Hartbower, C.E., "Fusion Welding High-Strength Titanium Sheet", Proc. Sagamore Conference, 1960.

4. Hartbower, C.E., D'Andrea, M.M., Jr., White, S.S., Orner, G.M., "Low Energy Fusion Welding of Titanium Alloys," scheduled for publication in The Welding Journal, 1961.

5. Orner, G.M., Hartbower, C.E., "An Engineering Evaluation of Notch Sensitivity in High Strength Sheet Materials", The Welding Journal, 39, (4), P. 147-S, 1960.

6. Orner, G.M., Hartbower, C.E., Metals Joining Branch, Watertown Arsenal Laboratories, 12th, 13th, and 14th Progress Reports on Notch Sensitivity in High Strength Sheet, 16 May, 30 Sept., 10 Nov., 1960.

IRRADIATION "FACTOR-DEPENDENCY":
SOME PARAMETERS FOR VINYL MONOMERS

By
Ed. F. Degering, Head
Radiation Chemistry Laboratory

Charles Merritt, Jr.

M. L. Bazinet
Pioneering Research Division
Quartermaster Research and Engineering Command
Natick, Massachusetts

E. F. Grey
Headquarters
Middletown Air Material Area
Olmstead Air Force Base
Middletown, Pennsylvania

ABSTRACT

Studies by the Radiation Chemistry Laboratory
during the past seven years on the effect of parameters
for the irradiation-induced polymerization of monomer systems
have shown that: (1) the effect of parameters is dependent
on the monomer system, (2) molecular weight of the polymer
may be a function of both does rate and temperature, (3)
benzene as a diluent in the systems studies served as a
moderator, and (4) reaction rate , $kI^{\frac{1}{2}}$ is not applicable
for the parameters used in these studies.

Irradiation "Factor-Dependency":
Some Parameters for Vinyl Monomers

In exploratory studies in 1954 on the applications of ionizing radiation to various polymeric materials, it was observed that the most obvious effect of electron bombardment of cotton, fabrics, leather, rubber, and similar materials, is the deterioration of their mechanical and physical properties.

The results obtained for the irradiation-induced deterioration of fabrics are shown by Figures 1, 2, and 3. In each case the rate is relatively rapid initially and then gradually decreases with dose. Kuralon, acrylan, and nylon fabrics were the most resistant of those studied. When nylon was irradiated in a vacuum, however, the rate of deterioration with increase in dose was significantly decreased (cf. Figure 3).

Data from the studies on leather are shown graphically in Figures 4 and 5. Chrome tan leather evidenced a decrease in burst strength with an increase in dose at about the same rate that grey cotton duck undergoes loss in its tensile strength (cf. Figure 4). The vegetable tan leather was the most resistant. The burst strength and the stitch-tear test showed significantly less loss when the leather was irradiated wet than was the case for dry leather.

The rubbers studied were more resistant to irradiation than were the fabrics and the leathers (Figure 6).

IRRADIATION of GREY COTTON DUCK in AIR (D-130 & D-131).

FIGURE 1

IRRADIATION OF FABRICS

D-46 KURALON
D-43 ACRYLAN
D-41 NYLON, OXFORD
D-44 NYLON, SATEEN
D-42 SATEEN, X-51
D-49 BA109, SRRL
D-48 BA110, SRRL
D-1 COTTON DUCK, GREY
D-50 AMINIZED COTTON
D-45 SATEEN, CORDED

FIGURE 2

HIGH TENACITY NYLON (1) IRRADIATED IN NUCLEAR REACTOR

CONTROL
15X10^{18} NVT IN VACUUM
3.8X10^{18} NVT IN VACUUM
1.8X10^{18} NVT IN AIR
8.9X10^{17} NVT IN AIR

FIGURE 3

IRRADIATION OF TANNED LEATHER AND COTTON DUCK.

X CHROME TAN, D-123
O CHROME RETAN, D-124
● VEGATABLE TAN, D-125
-- COTTON DUCK, D-130 & 131, GREY, 8½ OZ.

FIGURE 4

214

At the time these studies were undertaken, it was generally believed that irradiation is irradiation; dose alone being a significant parameter. This postulate now seemed questionable inasmuch as an atmosphere and a moisture effect had been observed in these exploratory studies. An investigation of parameters seemed to be indicated. Vinyl monomer systems were selected for this evaluation of the effect of parameters because of the relative ease with which polymer formation could be determined. An indication of the reproducibility of results by the procedure developed in this laboratory is indicated by Table I.

Table I.

Monomer Polymerization by Irradiation:

Reproducibility of Results

Code No.	Monomer	Dose	% Polymer
D588A3-a	Styrene/vacuum	3 passes at 0.1 Mr	7.3
-b	"	"	7.3
D588F2-a	Styrene/helium	3 passes at 0.1 Mr	3.0
-b	"	"	2.8
D588A3-c	Styrene/benzene	3 passes at 0.1 Mr	3.9
-d	"	"	3.6
D-604E1-a	Isoprene	130 passes at 2 Mr*	19.3
-b	"	"	18.3
-c	"	"	19.3
-d	"	"	18.3

Note:* Considering both the high dose rate and the high dose, these checks are reasonably good.

215

The combined effect of dose rate and atmosphere on the irradiation-induced polymerization of methyl acrylate and vinyl acetate is tabulated in Tables II and III.

From the data of Tables II and III, one may conclude that: (1) the atmosphere may be significant, (2) the significance of the atmosphere is a function of both dose rate and the monomer system, (3) a given atmosphere may produce an optimal yield per unit of energy at a given dose rate, and (4) there is no indication that the

Table II.

Methyl Acrylate: Reaction Rate = $kI^{\frac{1}{2}}$?

Rads: Dose Rate	$(Dose Rate)^{\frac{1}{2}}$	Calculated F D-608	Per cent Polymerization in				
			Air	Argon	CO_2	Helium	Nitrogen
25×10^3	158	1.58	2.3	6.9	5.2	6.3	8.6
50×10^3	223	1.41	1.7	1.9	2.9	2.4	2.5
100×10^3	316	1.41	1.8	2.6	3.0	2.6	2.4
200×10^4	1414	4.5	47.5	50.4	63.1	47.8	23.6

reaction rate for either of these systems follows the $kI^{\frac{1}{2}}$ formulation under the conditions used in this study. All the tubes at a given dose rate were irradiated at the same time, and all the tubes were made up by use of a routine procedure. A meticulous procedure which has been developed in this laboratory has been considered in

216

detail in Section D of Research Reports Nos. 3 and 4 (1960) of the Radiation Chemistry Laboratory Series. It has been shown by other investigators that: A (argon or other noble gas) + e → A* (activated) + e, and A* + M → M$^+$ + A + e. The inert gas in these studies may act, therefore, as an energy transfer agent. Additional evaluation of the composite effect of atmosphere and dose rate is contemplated. The F factor in these tables indicates the multiple that should be applied to the data on the preceding line if the $kI^{\frac{1}{2}}$ formulation is valid for these experimental conditions. It is obvious from an examination of the data of these tables that the $kI^{\frac{1}{2}}$ formulation is not applicable under the experimental conditions of these studies.

Comparable studies on styrene in benzene (1/1, v/v) are shown graphically as Figure 7. Under these conditions, the highest yields of polymer were obtained in an air atmosphere. The curves for the atmospheres of argon and carbon dioxide are approximately the same as the curve for helium. The effect of atmosphere and dose rate on molecular weight is indicated by Figure 8.

The effect of dose rate on allyl acrylate, butyl acrylate and styrene, with the results plotted per unit of energy, are given by Figure 9. A comparable log-log plot is shown by Figure 10. The dose rate implications for styrene, in which dose is plotted against the per cent polymerization, are indicated by Figure 11. Other data from studies on dose rate, in which irradiation was continued on a twenty-minute cycle until solidification was effected, are reported in Table IV.

TENSILE STRENGTH OF IRRADIATED RUBBERS

Natural Rubber
Nitrile Rubber
GRS Rubber
Polysulfide Rubber

TENSILE STRENGTH

3000
2000
1000
0

0   100   200

MEGAREPS

FIGURE 6

IRRADIATED STYRENE: with BENZENE, 1/1 MIXTURE (75°C)

$[\eta]$

D-630 He
$1x10^3$ $1x10^4$ $1x10^5$ $1x10^6$

D-631 N$_2$
$1x10^3$ $1x10^4$ $1x10^5$ $1x10^6$

D-627 AIR
$1x10^3$ $1x10^4$ $1x10^5$ $1x10^6$

D-628 ARGON
$1x10^3$ $1x10^4$ $1x10^5$ $1x10^6$

D-629 CO$_2$
$1x10^3$ $1x10^4$ $1x10^5$ $1x10^6$

Points-Left to Right   Rads,(15) P
1,000
10,000
100,000
1,000,000

DOSE RATE

FIGURE 8

EFFECT OF IRRADIATION ON BURST STRENGTH
AND STITCH-TEAR STRENGTH

PERCENT RETENTION OF INITIAL VALUE

133.6
100
80
60
40

D. Stitch-tear, irradiated moist in air — x
B. Burst strength, irradiated moist in air — ⊗
C. Stitch-tear, irradiated dry in air — ⊙
A. Burst strength, irradiated dry in air — ⊙

10   20

DOSE IN MEGAREPS
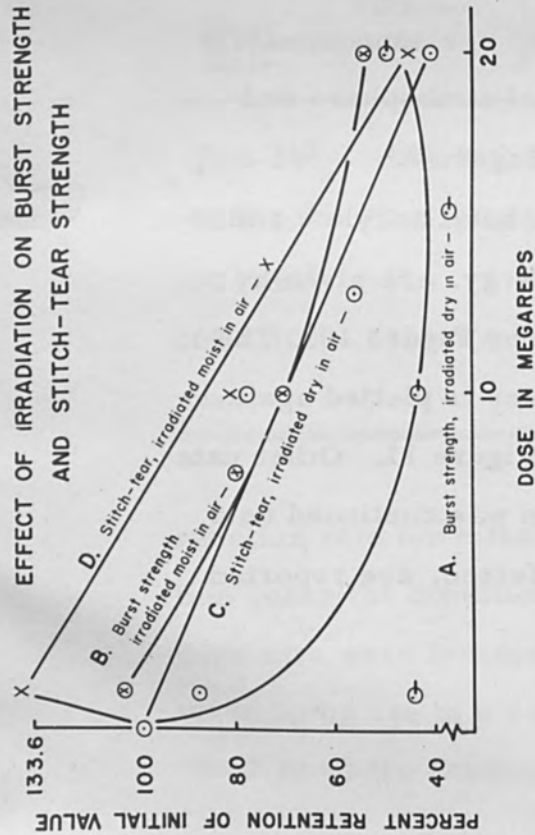
FIGURE 5

IRRADIATION of STYRENE-BENZENE MIXTURE:
DIFFERENT DOSE RATES and ATMOSPHERES

% Polymerization

28
24
20
16
12
8
4
0

Helium
Nitrogen
Air

$1x10^4$ $1x10^5$ $1x10^6$ $1x10^7$

Total Dose (rads)

FIGURE 7

Inasmuch as the solidification point is at best a close approximation, the values of Table IV are only relative. The trend toward a low dose rate for the conservation of radiation energy in irradiation-induced polymerization, however, is well defined by this group of vinyl monomers.

The effect of temperature on the molecular weight of samples of styrene in benzene (1/1, v/v), in which each sample was given an exposure at the indicated dose rate and at the designated temperature, is illustrated by Figure 12, on which molecular weight is plotted against the per cent of polymerization per 0.1 megarep. The temperature effect appears to be more pronounced as the dose rate is decreased.

A post-irradiation-heating effect at 75°C. is indicated by Figure 13. Both samples were given a single exposure at 0.1 megarep and then heated for the time indicated on the graph. The optimal polymerization for vinyl acrylate was obtained after about six hours. Subsequently, deterioration of the polymer appears to be dominant. Butyl methacrylate, methyl methacrylate, and styrene, subjected to a similar treatment, evidenced an increase in polymer formation for the duration of a twenty-four-hour post-irradiation heating period at 75°C.

Styrene was irradiated in the presence of four atmospheres, at four dose rates, and at four temperatures, and the results subjected to statistical analysis. The effect of temperature on molecular weight, as a function of dose rate, is illustrated by Figure 14. The highest molecular weight was obtained at the lowest dose rate used (0.025

IRRADIATION OF STYRENE

AT 0.1 and 2.0 Mr./Pass

FIGURE 10 COMPARABLE LOG-LOG DATA PLOT OF INFORMATION GIVEN IN FIGURE 9.
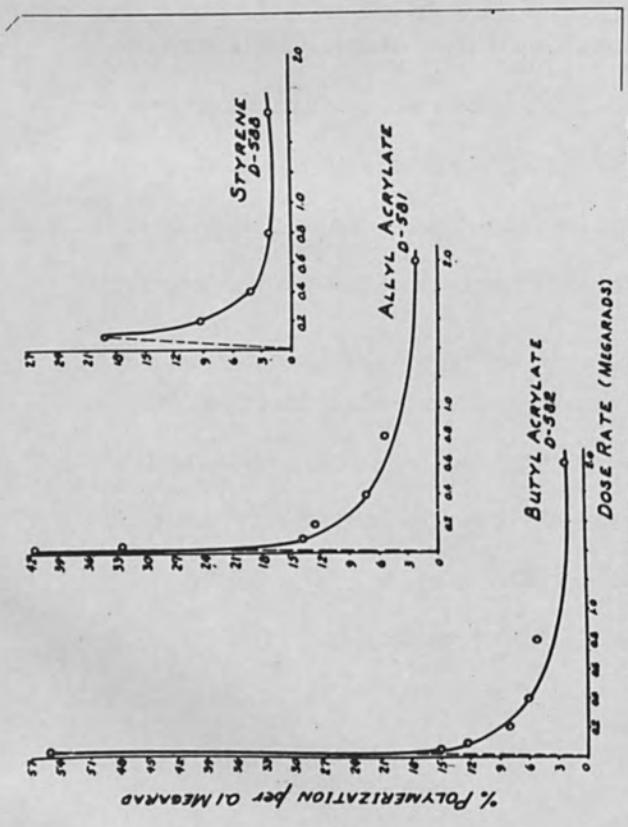
FIGURE 9 EFFECT OF DOSE RATE ON ALLYL ACRYLATE, BUTYL ACRYLATE AND STYRENE.

FIGURE 11

FIGURE 12

IRRADIATION OF STYRENE AT 0.1 and 2.0 Mr./Pass
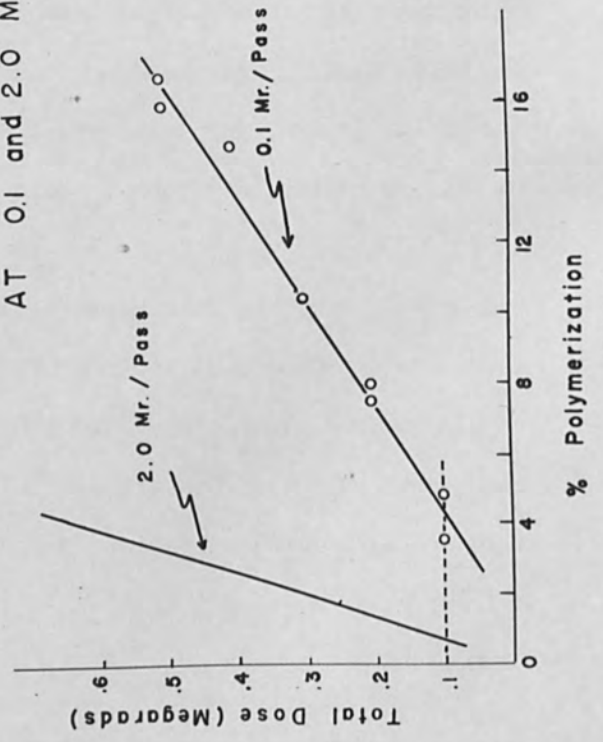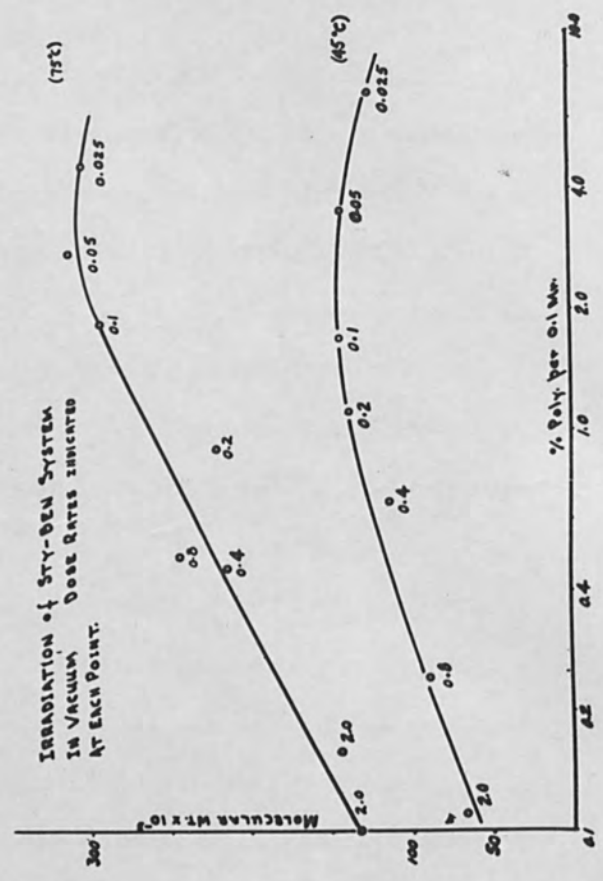
Table III.

Vinyl Acetate: Reaction Rate = $kI^{\frac{1}{2}}$?

Rads: Dose Rate	$(\text{Dose Rate})^{\frac{1}{2}}$	Calculated F	Per cent Polymerization in				
			Air	Argon	CO_2	Helium	Nitrogen
5×10^3	71	---	.0	.2	.2	.2	.3
10×10^3	100	1.4	1.0	3.3	3.0	2.7	2.2
25×10^3	158	1.6	1.5	2.6	2.8	2.8	2.9
50×10^3	223	1.4	24.7	1.3	1.3	1.2	1.1
100×10^3	316	1.4	12.7	1.5	1.6	1.6	1.7
200×10^4	1414	4.5	5.4	1.4	1.5	1.5	1.5

Table IV.

Comparison of 0.1 and 2 megareps per Exposure to a 2 Mev Accelerator

Monomer (no heat)	Megareps for Solidification	
	at 0.1 Mr/pass	at 2 Mr/pass
Ethyl acrylate	1.6	4
Methyl acrylate	1.5	16
Methyl methacrylate	3.8	40
Isoprene	2.0	12
Stearyl methacrylate	0.8	32
Styrene (10% Acrylic acid)	5.7	118
Triallyl cyanurate	2.7	14
Vinyl acetate	6.3	20
Vinyl butyrate	6.3	24
Vinyl triethoxysilane	8.6	160

221

megarep per exposure) and the lowest molecular weight resulted
from the use of 2 megareps per exposure. A decrease in dose rate
with an increase in temperature appear to be compatible for an in-
crease in molecular weight within the limits of the studies in this
experiment. The highest molecular weight (386,000) was obtained
at a dose rate of 25,000 reps per exposure in a helium atmosphere
at 75°C., whereas the lowest molecular weights resulted from the
use of air, nitrogen, helium, and vacuum at a dose rate of 2 mega-
reps at 25, 40, 60, and 75°C. At 25,000 rads per exposure the
molecular weights by atmosphere were: 386,000 in helium at 75°C.,
203,000 in nitrogen at 60°C., 121,000 in vacuum at 25°C., and
62,000 in air at 40°C. A plot of per cent polymerization per 0.1
megarep is given in Figure 15, in which the dose rate, temperature,
and atmosphere effects are indicated.

The results from the analysis of variance for this study are
given in Table V.

Table V.

Analysis of Variance

Source of Variance	S. S.	D. F.	Mean Square	"F"
Atmosphere	4.1176	3	1.3725	11.33
Dose Rate	9.3674	3	3.1225	25.78
Temperature	4.7841	3	1.5947	13.17
Residual (chance)	0.7266	6	0.1211	

For significance at the 1% level, "F" should exceed 9.78.

75°C (D567A)

45°C (D567B)

4 Passes
18 Hrs. Heating

75°C (D567A)

45°C (D567B)

10
8
6
4
2
0

3
2
1

0.025 0.05 0.1 0.2 0.4 0.8 2.0

DOSE RATE IN RADS — (Semi-log, 2 Cycle)

STYRENE IN BENZENE (1/1) IN VACUUM

FIGURE 14

• MOLECULAR WEIGHT x 10⁻⁵

× % POLYMERIZATION PER 0.1 MEGARAD

Normal

0.1 Mr.

85°C
3.6:1

65°C
N6 Mr.1

85°C
0.1 Mr.

0.3 Mr.

Heat,
Irradiation,
Germination,
Emergence, and
Post-Germination
of Spores.

HOURS

FIGURE 16

5
4
3
2
1
0

μLO₂/MIN.

Vinyl Acrylate, D-590-N

Vinyl-2-Pyrrolidone, D-590-F

HEATING TIME (Hrs.)

3 6 9 12 15 18 21 24 27 30 33 36 39 42 45 48

% POLYMERIZATION

8.0
7.2
6.4
5.6
4.8
4.0
3.2
2.4
1.6
0.8
0.0

FIGURE 13 POST IRRADIATION-HEATING EFFECT AT 75°C.

AIR

NITROGEN

HELIUM

HIGH VACUUM

σ = 0.16

TEMPERATURE °C

100
90
80
70
60
50
40
30
20
10

% YIELD

2.4
2.2
2.0
1.8
1.6
1.4
1.2
1.0
0.8
0.6
0.4
0.2

DOSE RATE MEGARADS/PASS

0.2 0.4 0.6 0.8 1.0 1.2 1.4 1.6 1.8 2.0

FIGURE 15 POLYMERIZATION DEPENDENCE ON RADIATION DOSE.

It is evident from Table V that (1) atmosphere, (2) dose rate, and (3) temperature are significant parameters in this study, and that dose rate is about twice as important as either atmosphere or temperature.

The question arises as to the significance of these parameters to the irradiation of systems other than monomers. In some studies by Elwin T. Reese and one of the authors, strips of cotton duck were inoculated with both Chaetomium globsum and Trichoderma viride and irradiated at a dose rate of 0.1 megarad per exposure, with and without a heating period of about forty-five minutes at 60°C. Samples in which the combined effect of heat and irradiation were used required only 0.1 megarad to effect sterilization. Samples which were irradiated at 25°C., however, required about 0.7 megareps for sterilization.

The effect of irradiation on spores has been investigated by Hillel S. Levinson[1] and one of the authors. The results are shown as Figure 16. It is apparent that a dose of 0.1 megarad in conjunction with a heating period at 85°C. is more effective in disrupting the normal germination, emergence, and post-germination of spores than is 0.3 megarads at 25°C.

In their studies on roaches, Dennis and Martha Wharton have found that the effect of irradiation is age dependent.

---

(1) Levinson, Hillel S., and Mildred T. Hyatt, J. Bacteriol., 80, 441-451 (1960).

Summary. The data derived from these studies of the effects of ionizing irradiation, clearly indicate factor dependency with respect to: (1) atmosphere, (2) dose rate, (3) temperature, and (4) the monomer system. There is an indication also of the probable application of the irradiation-parameter concept to the irradiation of other systems.

METHODS AND TECHNIQUES FOR EVALUATION OF CHEMICAL CHANGES IN MATERIALS UPON ELECTRON BEAM RADIATION

By

Charles Merritt, Jr., Head
Analytical Chemistry Laboratory
Pioneering Research Division
Quartermaster Research and Engineering Center
Natick, Massachusetts

ABSTRACT

An important use of electron beam radiation is for the preservation of food. The destruction of bacteria is, unfortunately, accompanied by chemical changes in the food which sometimes alter its flavor. Some aspects of radiation preservation of food and the chemical changes which occur will be discussed along with the methods and techniques which are used to evaluate them.

Methods and Techniques for Evaluation of
Chemical Changes in Materials upon
Electron Beam Radiation

An important use of electron beam radiation is for the preservation of foods. The purpose of irradiation, of course, is to destroy the bacteria present in foodstuffs which are responsible for its spoilage. The destruction of bacteria is, unfortunately, accompanied by chemical changes in the food which sometimes alter its flavor or otherwise affect its acceptability.

The chemical compounds which are responsible for odor in foods are present for the most part in extremely minute quantities. Furthermore, a large number of volatile compounds are present in foods, some of which are odorous and some of which are not. It has therefore been necessary to develop rather elaborate methods of analysis to detect, identify and determine these volatile compounds.

The volatile components of the sample are first collected, usually by a vacuum distillation procedure. The total condensate is fractionated, either by low-temperature vacuum distillation, gas chromatography, or both, and the compounds are finally identified by mass spectrometry.

One of the most important aspects of the whole problem of odor determination is the method of collecting samples. There are two factors which greatly affect the final results obtained. The first is to insure the collection of sufficient amounts of the odorous

compounds to permit their detection. The second, of equal importance, is the ability to collect the volatile odor components without introducing extraneous compounds.

Figure 1 shows a schematic diagram of the basic high vacuum-low temperature distillation apparatus which is used for collecting the samples and which is also used for some of the subsequent separations. The apparatus consists of two gas bottles fitted with stopcocks attached to a vacuum manifold. The sample is placed in one of the gas bottles and cooled to $-196°C$. with liquid nitrogen while air is pumped from the system. The vacuum pump is then closed off and the sample is allowed to warm up to room temperature. A final pressure of about one micron can usually be obtained. The volatile components are now condensed in the receiver flask by cooling it with liquid nitrogen.

A photograph of a typical laboratory setup is shown in Figure 2. When collected exhaustively, that is, by allowing the distillation to proceed until the pressure in the system is very low, the total condensate contains all of the volatile compounds present in the original substance. The total condensate from many substances, however, consists mainly of water and carbon dioxide, and frequently contains less than a hundredth or perhaps even a thousandth percent of an odorous compound, and it is, therefore, necessary to separate efficiently the trace amounts of the odorous materials from the bulk of the carbon dioxide and water before an accurate mass spectrometric analysis can be made. This separation can be accomplished by further high-vacuum distillation at dry-ice temperatures or below.

BULB TO BULB DISTILLATION APPARATUS
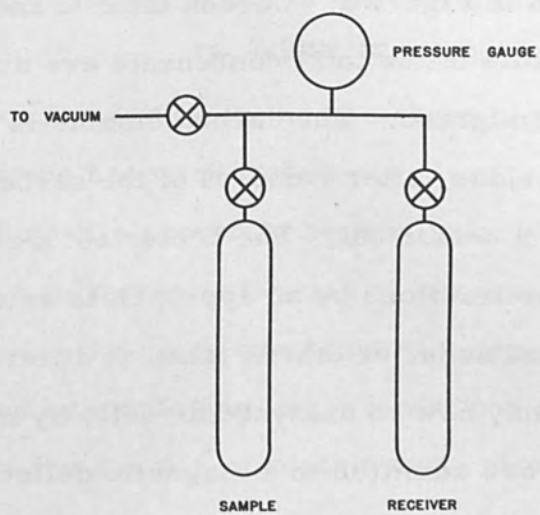
FIGURE 1
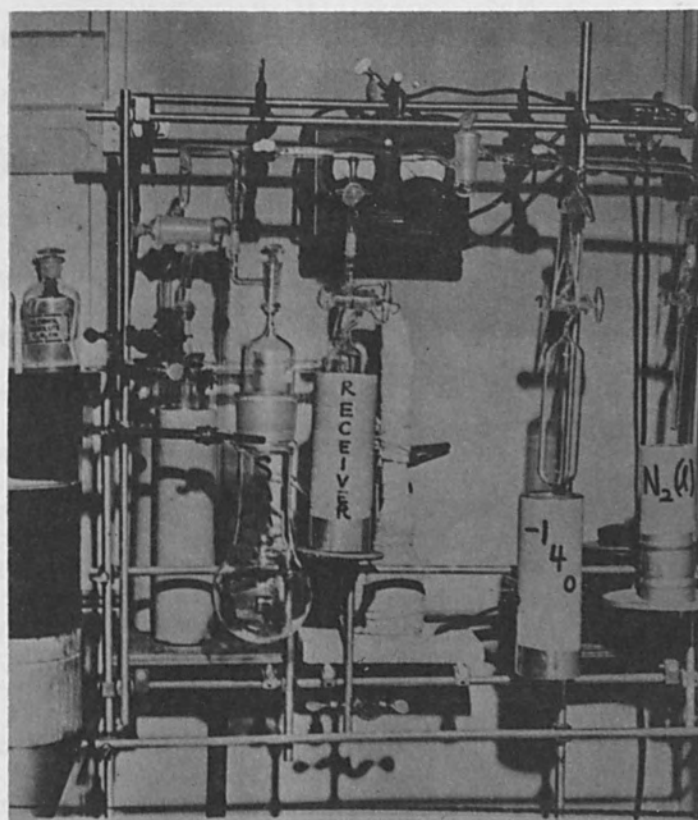
FIGURE 2   LABORATORY SET-UP CORRESPONDING TO
BLOCK DIAGRAM IN FIGURE 1.

A typical low temperature-high vacuum fractionation scheme is shown in Figure 3. Carbon dioxide and the other more volatile components of the total condensate are distilled from the water at -80° Centigrade. The carbon dioxide is then separated at -140°C. The residue, after removal of the carbon dioxide and water, is called a center cut. The center cut may be further subdivided into other fractions by an appropriate selection of temperatures. These fractions, or others taken at differently selected temperatures, may now be analyzed directly by mass spectrometry.

Samples are admitted to a magnetic deflection type mass spectrometer through the inlet system as gases. They are allowed to diffuse through a small pinhole leak into the evacuated analyzer section of the instrument where the molecules first enter an ionization chamber called the isatron. The molecules are bombarded by a stream of electrons having an energy of about 70 volts, and ions are produced. The positive ions are accelerated in a high potential electrostatic field. The ions then enter a perpendicular magnetic field, are deflected in a circular path as they pass through the analyzer tube, and finally strike the collector plate where they are discharged and give rise to an ion current which is subsequently amplified and recorded. The separation of the ions is accomplished by varying the potential of the electrostatic field so that only those ions having an appropriate mass to charge ratio will strike the collector plate. Various ion fragments produced from a molecule can be scanned by continuously varying the voltage of the accelerating field, and the relative amount of a given ion is indicated by the magnitude of the ion current appearing at the collector plate.

The identification of a single unknown component is accomplished by comparison of the spectrum of the unknown with the reference spectrum of a known. However, since the spectra of individual components are additive in the spectrum of a mixture, the spectrum of a mixture becomes rather complex.

A technique which has proven to be particularly useful in the analysis of complex mixtures is the use of low ionization voltage spectra. This is because the mass spectrum of a compound can be considerably simplified by employing lower ionization voltages.

Figure 4 shows the spectra of acetaldehyde obtained at various ionizing voltages. As seen at the bottom of the graph, 10 volts is below the ionization potential for the compound, and no spectrum is seen, since the energy of the bombarding electrons is not enough to cause ionization. At 11 volts the threshold of the ionization potential has been passed and the least energetic process which can occur, the loss of a single electron, produces the molecular ion seen at mass 44. At $11\frac{1}{2}$ volts, the energy level is greater than the appearance potential for dissociation of the hydrogen atom from the molecular ion and a peak at mass 43 is observed. At 14 volts the appearance potential for the dissociation of the CHO group from the molecule is exceeded and a peak at mass 29 is also observed in the spectrum. Finally at the top of the graph the normal spectrum obtained at 70 volts is shown.

The ionization potentials of organic compounds are generally found to vary with functional group type. For example, amines have ionization potentials in a range from about 9 to $9\frac{1}{2}$ volts; ketones between 9.6 and 9.9 volts; aldehydes, alcohols, esters, ethers and acids in the range between 10 to 11 volts. If an ionizing voltage

slightly higher than 12 volts is selected, the parent masses of most organic compounds in a complex mixture will be observed in the spectrum. On the other hand, if one wishes to distinguish between different types of compounds, voltage settings can be made in the appropriate range. An example of how low ionizing voltage can be employed to simplify the mass spectrum of a complex mixture is shown in Figure 5. The spectrum at the top of the graph is taken at the normal ionizing voltage of 70 volts, whereas the spectrum at the bottom of the graph was taken at 12 volts. In the low-voltage spectrum only the parent masses for the nine components of the mixture can be seen.

The many volatile components in irradiated products are poorly separated by vacuum distillation procedures. Gas chromatographic methods, on the other hand, have been found to be extremely effective.

The apparatus consists principally of a tubular column which is filled with some inert material such as ground firebrick or diatomaceous earth carrying a thin coating of a high-boiling liquid. Volatile compounds are carried through the column by means of a stream of helium gas. As the compounds in the carrier gas stream pass through the column, they tend to be more or less selectively absorbed on the liquid phase of the column so that they emerge successively. As they leave the column they pass through a device which measures the relative amount of each component on the basis of its thermal conductivity. A graph is usually obtained on a recording potentiometer which plots the relative amount of each component as a function of its

millivolt output from the thermal conductivity cell and its retention time on the column. If it is desired to collect an eluted component, cold traps may be placed at the end of the apparatus and the components are condensed in the trap from the gas phase.

The efficiency of a chromatographic separation depends upon a number of parameters, such as the flow rate of the carrier gas, the type of liquid coating on the support, the length of the column, and particularly the temperature. When dealing with extremely complicated mixtures, temperature can be employed quite effectively to accomplish difficult separations.

Figure 6 shows the chromatogram for a sample of irradiated meat volatiles obtained from a column operated at room temperature. From this graph it would appear that the sample contained about seven or eight components.

Figure 7 shows a chromatogram of the same sample run on the same column but where the temperature was allowed to rise from -65°C. at the start to room temperature at the rate of about 2°C. per minute. The efficiency of this separation compared with that shown in Figure 6 is remarkable. The peaks on this scan show there are more than forty components present. It is another interesting consequence of this mode of operation that with the type of detector employed, which in this case was not a thermal conductivity detector but a beta-ray ionization detector, the sensitivity of detection is also greatly enhanced. This accounts for the much larger size of the peaks since the same size of sample was employed in each case.

SPECTRA OF CH₃CHO

FIGURE 6   CHROMATOGRAM FOR A SAMPLE OF IRRADIATED MEAT VOLATILES
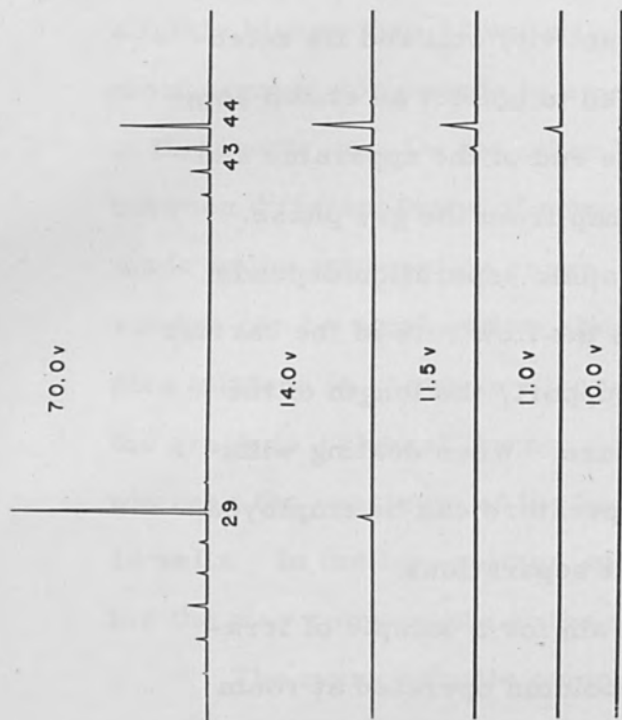   OBTAINED FROM A COLUMN OPERATED AT 25°C.
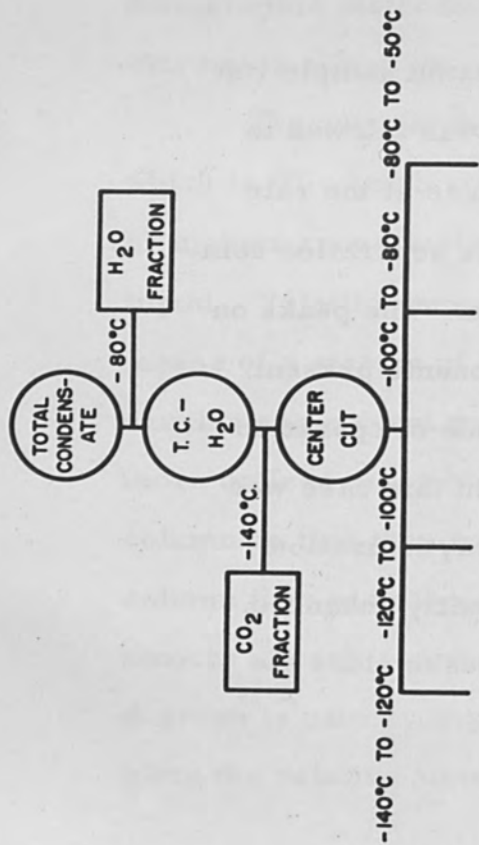
FIGURE 3   LOW-TEMPERATURE HIGH VACUUM FRACTIONATION SCHEME
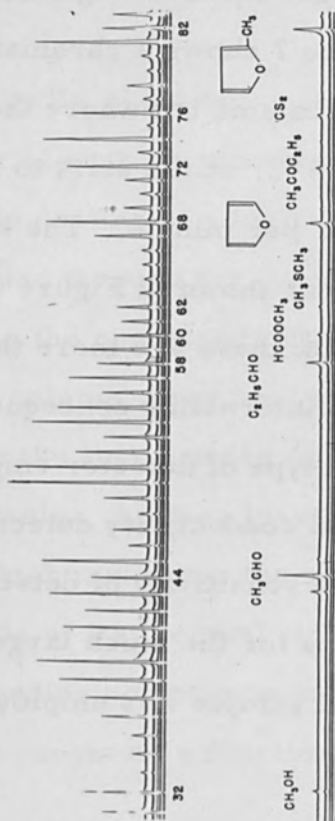
FIGURE 5   AN EXAMPLE INDICATING HOW LOW IONIZING VOLTAGE
            IS EMPLOYED TO SIMPLIFY THE MASS SPECTRA OF A
            COMPLEX MIXTURE.

Of course, it is an extremely difficult proposition to collect the components as they are eluted from a complex chromatogram for subsequent mass spectrometric analysis on a magnetic deflection type instrument. Fortunately, another type of mass spectrometer is available. This instrument is called the time-of-flight mass spectrometer.

As in the magnetic deflection type spectrometer, the time-of-flight instrument contains a source of electrons which bombard the gas molecules and produce ions. The ions are then accelerated by means of an electrostatic field, and after passing through the exit slits, travel down the field-free flight tube until they strike the collector plate of the electron multiplier. Obviously, the lighter ions will reach the collector before the heavier ions. The presentation of spectra from this type of instrument can be made very rapidly by pulsing the electron beam. The accelerating field is also pulsed synchronously with the filament source, so that the separated ions reach the electron multiplier as bunches of ions that are separated slightly in time during each pulse. By rapidly scanning the output of the electron multiplier, the spectrum can be displayed almost instantaneously on the face of an oscilloscope. By coupling, then, the effluent gas stream of the gas chromatographic unit to the inlet of the time-of-flight mass spectrometer, the mass spectrum of each chromatographic peak can be displayed on the oscilloscope as it is eluted.

By utilizing some of the techniques which have been described above, studies have been made of the changes that may occur in the composition of the volatile compounds when meat is

CH₃CHO

CH₃COCH₃

CH₃COOC₂H₅

PARTIAL PRESSURE — MICRONS

250 200 150 100 50

RADIATION DOSE — MEGARADS

FIGURE 8   RADIATION INDUCED CHANGES OF ACETALDEHYDE, ACETONE AND METHYL ETHYL KETONE.

RETENTION VOLUME

a - irradiated Feb 1960

b - irradiated Nov 1960

RESPONSE
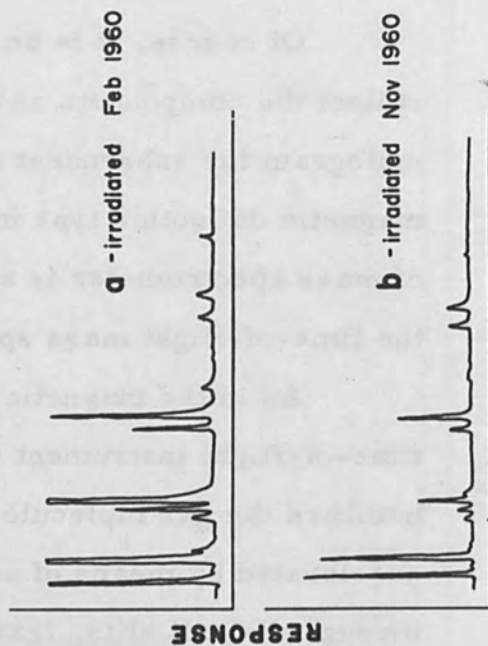
FIGURE 10   PROGRAMMED TEMPERATURE CHROMATOGRAMS FROM REFRIGERATED COLUMNS OF DIFFERENT SAMPLES OF BEEF.

RETENTION TIME

RECORDER RESPONSE

FIGURE 7   CHROMATOGRAM OF SAMPLE SHOWN IN FIGURE 6, RUN, HOWEVER, WAS CONDUCTED IN THE TEMPERATURE RANGE FROM -65°C TO ROOM TEMPERATURE, INCREASING TEMPERATURE AT RATE OF ABOUT 2° PER MINUTE.

C₂H₅SH

CH₃SCH₃

(CH₃)₂CHCH₂SH

CH₃SH

CH₃SSCH₃

PARTIAL PRESSURE — MICRONS

RADIATION DOSE — MEGARADS

FIGURE 9   RELATIVE CHANGE IN COMPOSITION AS FUNCTION OF RADIATION.

irradiated at various doses. It has been found that in samples
of irradiated beef the same compounds are present in nearly all
samples, but the relative amounts of the compounds tend to vary
widely with dose.

Figure 8 shows the behavior of certain carbonyl compounds
such as acetaldehyde, acetone and methyl ethyl ketone. Large
increases in the amount of acetaldehyde are found with increasing
radiation dose. Moderate increases are found for acetone, but
only a slight increase is found for methyl ethyl ketone.

Figure 9 shows the relative change in composition of
certain sulfur-containing compounds upon irradiation at various
doses. Here again compounds such as ethyl mercaptan and
dimethyl sulfide are seen to increase rather markedly with in-
creasing dose whereas compounds such as isobutyl mercaptan,
methyl mercaptan, and dimethyl disulfide were not so greatly
affected.

Figure 10 compares two programmed temperature chro-
matograms from refrigerated columns of different samples of
beef irradiated at the same dose but at different times. These
chromatograms indicate fairly well that the production of the
volatile compounds on irradiation of beef is quite reproducible.

The successful development of a satisfactory food preser-
vation process employing electron beam radiation depends greatly
on the acquisition of a fundamental understanding of the nature of
the interaction of electron energy with matter. This objective has
been considerably enhanced by the methods of analysis which have
been described.

ELECTRON BEAMS IN ANALYTICAL WORK

By

Robert E. Ogilvie
Professor
Department of Metallurgy
Massachusetts Institute of Technology

ABSTRACT

The electron microbeam probe is discussed.

A survey of underlying principles with factual information

on the different components of the system and its applica-

tions are covered in detail.

ELECTRON BEAMS IN ANALYTICAL WORK

Introduction

Tremendous strides have been made in electron beam technology
during the past few years. Applications in every field of science
is quite obvious from the large collection of papers presented at
this symposium. The use of electron beams in analytical work dates
back to the early studies of Moseley[1] and in particular von Hevesy[2].
In fact, many of these early experiments produced the first electron
beam melted materials, which of course, was due to improperly cooled
anticathodes.

The Electron Microbeam Probe is one of the most unique tools
to be applied to metallurgical problems. It has also found many
applications in other fields where only a minute quantity of material
is available for analysis. It was not until 1949 when Castaing and
Guinier[3] presented the results of their experiments that the potential
of electron beams in analytical work could really be appreciated. In
1953 Castaing and Descamps[4] presented the detailed analytical
procedure, initially presented in Castaing's thesis, that is now used
extensively by investigators in this field today. With this technique
the Electron Microbeam Probe is competitive with conventional chemical
techniques which of course, must use a sample many times larger.

The principle of the electron microbeam probe is based on the fact that when a specimen is irradiated with a finely focussed electron beam, approximately one-micron in diameter, an x-ray spectrum is produced which consists principally of the characteristic radiations of the elements present. The subsequent analysis of this spectrum with an x-ray spectrometer permits one to determine what elements are present and by measuring the intensity of the individual spectrum lines, determine the concentration of each element. At present the range of elements that can be measured is from sodium through uranium of the periodic table.

Components of the Electron Microbeam Probe

In order to measure precisely the chemical composition of an area one-micron in diameter it is necessary to integrate four very complicated systems. These consist of essentially the following components:

1. Electron Optical System

2. Specimen Chamber

3. X-ray Spectrograph

4. Specimen Observation System

1. Electron Optical System

The electron optical system is by far the most complex of the four components mentioned. This consists of an electron gun followed by one or more reducing lenses. It is necessary that these components produce a stable beam on the specimen of approximately 0.1 to 2.0 microns in diameter.

The optimum design of the electron gun for such a system is one that will produce a high intensity of electrons at a low angular aperture. The telefocus[5] gun comes closest to giving the desired results. Here the electrons that are emitted from the hairpin filament enter a diverging-converging field, with such a field and the proper bias potential on the grid cap the crossover of the electron beam may be adjusted over a wide range.

Several gun designs that are used in the electron microbeam probes are illustrated in Figure 1. The French model

(a)   (b)   (c)
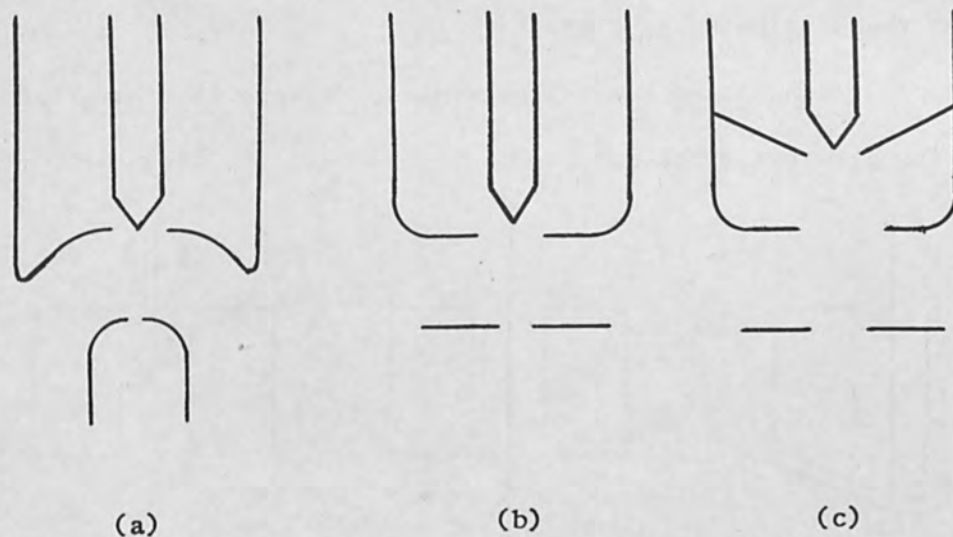
Figure 1

of the electron microbeam probe uses the re-entrant grid cap as shown in Figure 1 (a). This gun has a crossover below the anode where it is advantageous to place an aperature. Figure 1 (b) is the RCA type and has been used on many of the probes built in the United States. The Steigerwald gun in Figure 1 (c) used in the Elion probe has many advantages, as previously mentioned.

There are in general, two magnetic reducing lenses in which the first acts as a condenser lens with a variable focal length from one or two millimeters to infinity. The first lens may be of the conventional condenser lens type, however, the second lens is far more complicated. In this case the pole pieces must protrude beyond the lens coil so that the x-rays produced at the surface of the specimen can enter the spectrometer with a reasonable take-off angle (15-20°). The working distance should be 2-3 bore diameters so that magnetic specimens will not interfere with the field. Thus a focal length of one-centimeter is desirable.

Figure 2 illustrates several pole piece designs that have been used in the electron microbeam probe.

(a)   (b)   (c)
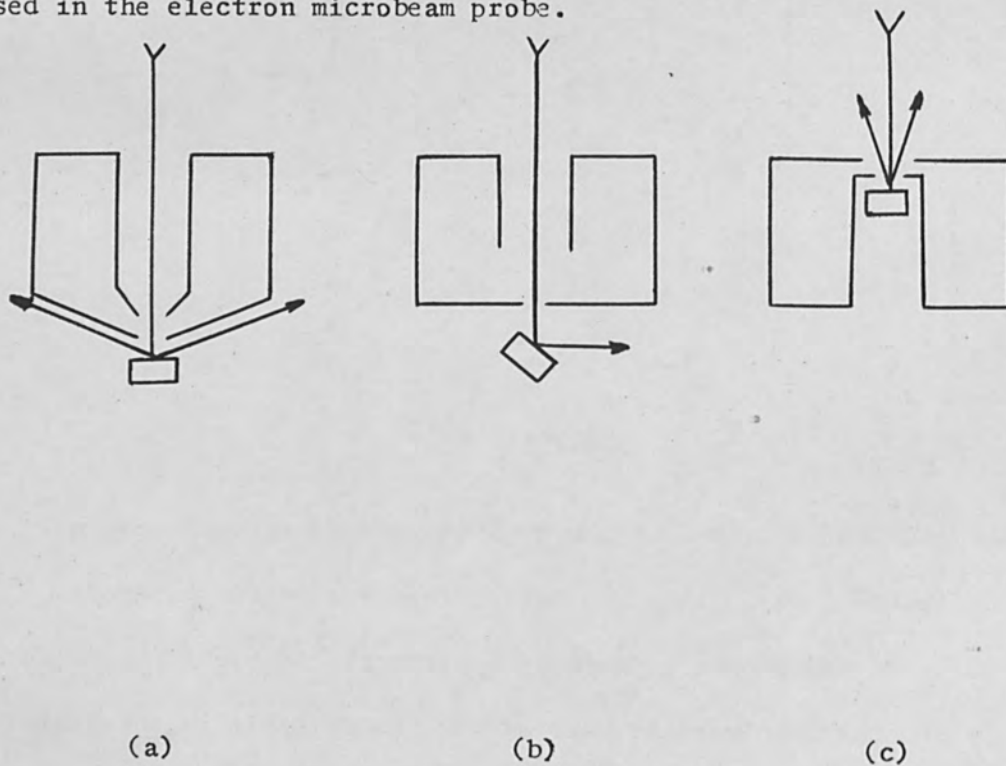
Figure 2

Figure 2 (a) is the French design and used at M.I.T. and Advanced Metals Research. Figure 2 (b) is Mulvey's design and Figure 2 (c) is used by A.R.L.

The probe current determines the magnitude of the x-ray intensity and it has been shown that the brightness of the probe is given by Langmuirs[6] equation but correcting for spherical aberation of the lens using Zworykin's[7] treatment we can arrive at the following equation for the optimum aperature angle:

$$i = \frac{9\pi^2}{64} \ i_o \ \left(\frac{eV}{kT}\right) \ \frac{dp^{8/3}}{C_S^{2/3}} \tag{1}$$

where i_o is the electron emission of the source (amps/cm^2/steradian), V the voltage on the gun, dp the diameter of the probe and C_S the spherical aberration coefficient of the lens.

With a probe diameter of one-micron the incident current usually corresponds to approximately 0.1 microamps. With suitable x-ray optics this will give over 20,000 counts per sec off of pure copper, therefore we see from equation (1) that for conventional electron optics the intensity would be approximately 20 counts per second for a 0.1 micron probe.

2. Specimen Chamber

The specimen chamber must not only provide a precise stage so that the specimen may be properly located under the electron beam but should be so designed as to make use of the small source of x-rays. This may be for projection micro-radiography or special x-ray diffraction techniques.

3. X-ray Spectrograph

The design and in particular the alignment of the spectrometers will determine the overall efficiency of the electron microbeam probe. The monochromating crystal must be of the focussing type and whose structure should be as perfect as possible. With these conditions the maximum signal to noise ratio will be achieved, this of course determines the detectibility limit of the system which is approximately 100 parts per million for elements like Cu, Ni and Co in steel.

The spectrometers must have a vacuum or helium path for wavelengths shorter than about three angstroms. This means that elements from sodium to titanium (K series) and zirconium to cesium (L series) must have the vacuum or helium path.

4. Specimen Observation

It is imperative that the operator is able to locate a predetermined area of the specimen in the electron microbeam probe with a precision better than one micron. This has been accomplished by one of two methods; (1) normal light optics and (2) scanning techniques.

It has been found by the author that the reflecting objective, as used by Castaing, has many advantages over refractive optics. The prime advantage of such a system is the long working distance. The scanning technique developed by Cosslett and Duncumb[8] is a very unique method of locating areas of interest. This is done by synchronizing a cathode ray tube with the scanning probe. The z-axis modulation of the cathode ray tube may receive its signal

244
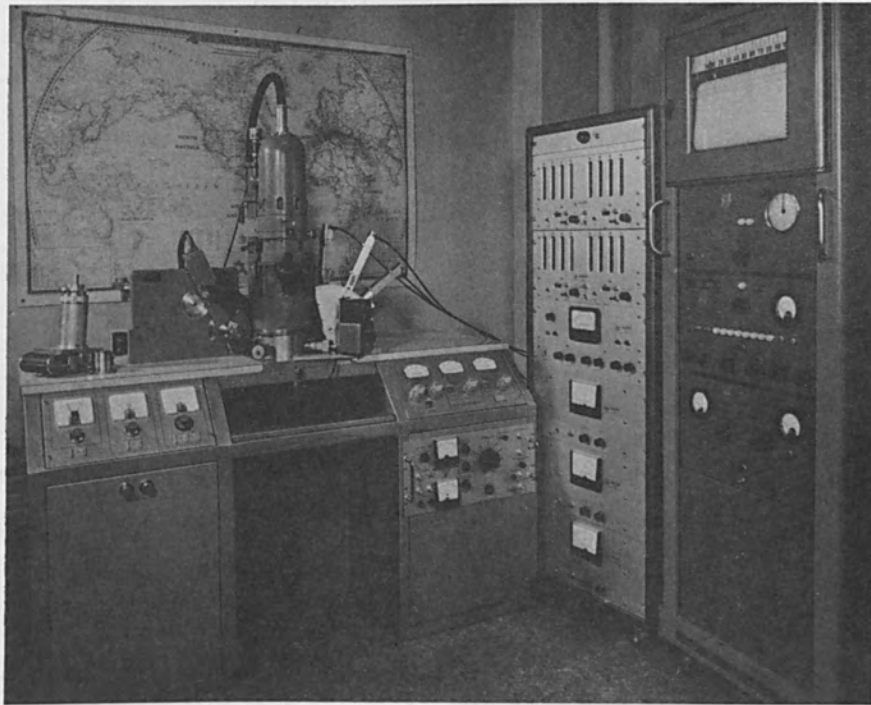
FIGURE 3   M.I.T. ELECTRON MICROBEAM PROBE
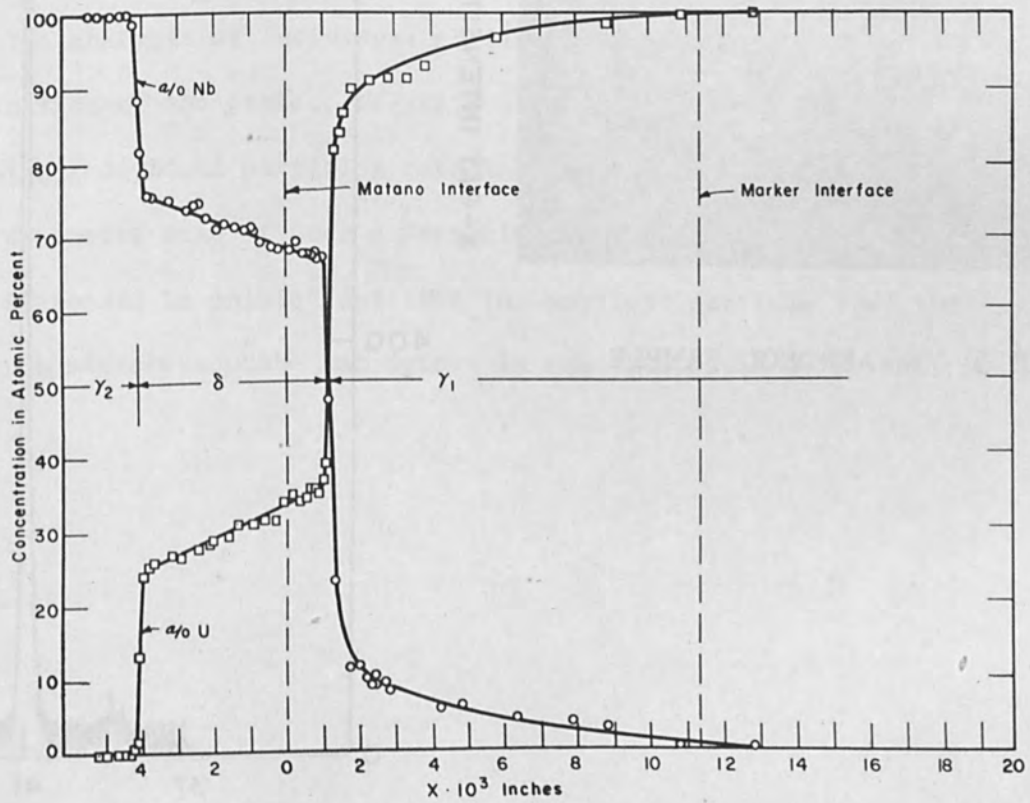
FIGURE 4   URANIUM-NIOBIUM DIFFUSION COUPLE
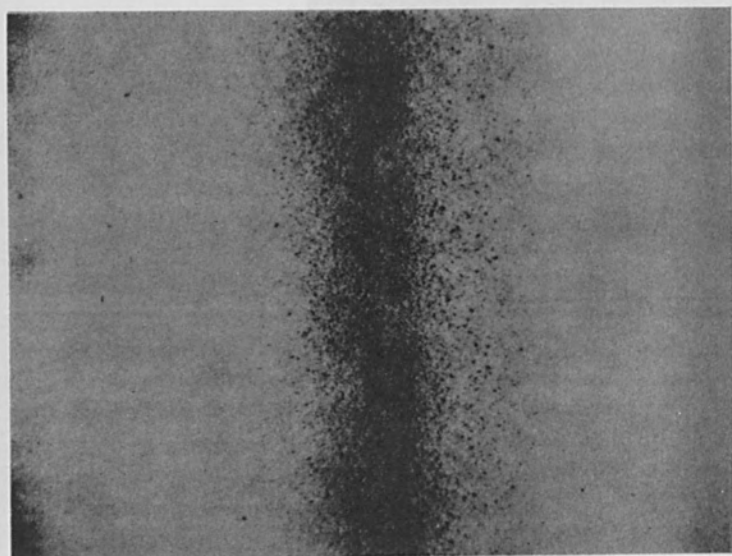
FIGURE 5   AEROSOL SAMPLE
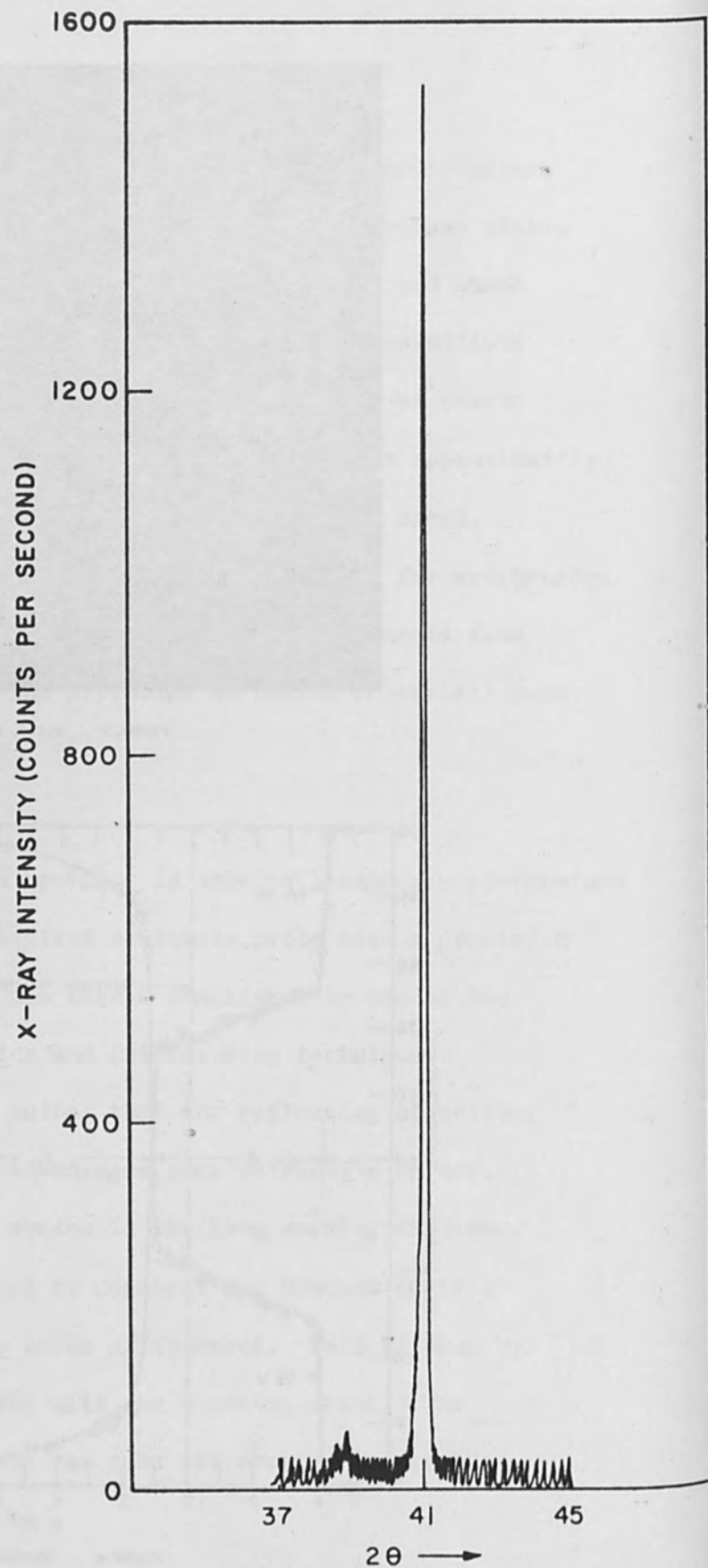
FIGURE 6

SPECTROMETER SCAN OF SILICON
RICH PARTICLE

from the backscattered electrons, specimen current or an x-ray detector set for a particular element. This will give information on the cathode ray tube that is related to the topography of the specimen or the distribution of a particular element within the specimen.

The electron microbeam probe at M.I.T. is shown in Figure 3. This unit has one scanning x-ray spectrometer and three hand spectrometers. This enables the operator to analyse four elements simultaneously.

Applications

The principal advantage of the electron microbeam probe is that it is capable of analysing an extremely small quantity of material. Therefore, its principal application has been in the field of diffusion. An example of such an analysis is illustrated in Figure 4[9].

The analysis of individual particles in aerosols is a unique application of the probe. Figure 5 is an example of an aerosol[10] in which individual particles have been examined. Figure 6 illustrates a spectrometer scan of such a particle that is silicon rich.

It should be pointed out that the smallest particle that the electron microbeam probe can detect is one that would weigh only 10^{-14} grams.

List of References

1. Moseley, H. G. Phil Mag. 26 10 24 (1913)

2. von Hevesy, G., Chemical Analysis by X-rays and its Applications,
    McGraw Hill, New York (1932)

3. Castaing, R., and Guinier, A., Proc. Int. Conf. Electron Microscopy
    Delft (1949)

4. Castaing, R. and Descamps, J. Compt Rend. Acad. Sci 237 1220 (1953)

5. Steigewald, K. H., Optik 5, 469 (1949)

6. Langmuir, D. B., Proc. I.R.E. 25 977 (1937)

7. Zworykin, V.K. et al, Electron Optics and the Electron Microscope,
    John Wiley & Sons, Inc. New York 555 (1945)

8. Cosslett, V.E. and Duncumb, P., Nature 177 1172 (1956)

9. Peterson, N. L. and Ogilvie, R. E., Trans. AIME 218 439 (1960)

10. Ogilvie, R. E. et al, Research Report AMR 1005, Contract No.
    AF 19(604)-4146 (1960)

ELECTRON BEAM TAPE RECORDING

by

H. G. Wehe
Member Technical Staff
Bell Telephone Laboratories
Murray Hill, New Jersey

ABSTRACT

This paper briefly reviews some published methods
for high speed permanent electron beam recording on tapes
both in vacuum and in air with image permanence established
(a) directly by the beam, or (b) by subsequent development by
means of chemical change, or (c) by electrostatic charge
patterns revealed and fixed by Xerographic techniques, or (d)
by erasable plastic deformation followed by image projection
in black and white or in color, or (e) by metal vapor
deposition in vacuum both with and without subsequent image
projection.

This paper briefly reviews some published methods for using electron beams for recording on tapes in vacuum or in air. The recordings may be either permanent or erasable. Thus storage tubes[1,2] with their electronic or visual read-out are beyond the scope of this discussion as no tapes are used. Also, magnetic tape[3] recording of T.V. programs are omitted as the electron beams involved are in the T.V. cameras and not in the recorder. Ferromagnetography[4] or General Electric's high speed printing with shaped magnetic fields is omitted due to the absence of an electron beam. Movies of kinescope displays with either Xerography (dry development)[5,6] or with ordinary film (wet development)[7,8] are likewise excluded. It is not proposed to discuss the comparatively slow electrographic[9] recording. Since tapes are not used, electron beam recording on carbon supported collodion[10], on metals[11] and on magnetic films of $BiMn$[12,13] or permalloy[14] are mentioned only. Since tapes and sparks instead of electron beams are used for a very interesting Burroughs computer printer, it is mentioned only[15]. The following recording methods remain to be herein discussed:

1. Recording directly with an electron beam on photo-graphic film in vacuum with subsequent wet development[16].

2. Use of a thin (slot) window[17] cathode ray tube to let light from a phosphor directly affect (without

250

lens imaging) a light sensitive Electrofax tape with subsequent dry image development.

3. Use of fine wires[9,18] in end of cathode ray tube to apply beam charges to Videographic tape for subsequent dry development.

4. Thermoplastic recording[19].

5. Electron beam recording on untreated plastics[20,21] with image development by vacuum deposition of evaporated metals.

Recording directly with an electron beam on photographic film in vacuum is usually confined to the electron microscope[16] where plates rather than tape or film are ordinarily used. Use of film in movie cameras is generally preferred for T.V. recording rather than recording directly on the photographic film with the scanning beam in vacuum. Possible reasons are the difficulty of handling a hydroscopic film in a hard vacuum, the necessity for shielding from light, and having to use subsequent wet development as though a camera were used. The extra detail potentially feasible is not really needed sufficiently to warrant the extra trouble.

More promising is the use of a thin window cathode ray tube for high speed printing with "Electrofax"[17] reported by Dr. R. E. Olden of RCA. Traces have been recorded with spot speeds in excess of 44,000 inches per second. Tape

speeds exceed 90 ft/min. Ten thousand characters per second
have been recorded. Dr. Olden in a recent private communica-
tion says that he has made satisfactory exposure under condi-
tions equivalent to 150,000 characters per second with no
loss of definition of 200 photographic lines per inch. Also,
that the limit to the printing speed lies in the ability to
handle and process the Electrofax paper rather than in the
thin window tube.

Essentially Dr. Olden's process is as follows: A
metal cathode ray tube has a narrow slot in its output end.
The slot is covered with a 2.5 mil mica window with a P-11
phosphor on the vacuum side. The outside of the window is
protected with Mylar* from abrasive action of the contacting
Electrofax paper which is sensitized with .10 parts of fluo-
rescein sodium per 120 parts of zinc oxide. The paper is
corona charged as usual just before exposure to light from
the phosphor (activated by the electron beam) and the image
is developed either temporarily or permanently with Electro-
fax powders. Beam currents are measured in microamperes.
Figure 1 shows a thin window metal cathode ray tube with
8-inch long mica window. Figure 2 shows an experimental
printing arrangement with Mylar* (from roll) in contact with
the thin window. Figure 3 shows an "Electrofax" print by

- -
*Du Pont trade-mark.

252

direct development with the cathode ray beam "off" in letter
areas. Reverse development can also be used with the cathode
ray beam "on" in letter areas. The image in both instances is
revealed by means of an iron powder with a resin toner.

Fine wires have been used in the end of a cathode
ray tube to convey the charges from the electron beam to
Xerographic film for subsequent dry development[9], or develop-
ment with an electrically charged atomized ink[22]. One such
tube using dry development is the Printopix of Litton Industries.
Another is Videograph printing[18] with a matrix type cathode ray
tube recently described at the AIEE Convention in New York City
by Messrs. H. A. Dahl and G. H. Jenkinson of A. B. Dick Company.

Figure 4 shows the appearance of the Videograph tube,
while Figure 5 shows the basic principle of its operation. The
wires may be arranged in a single row or in multiple rows as
shown. The wire ends receive a charge in response to the modu-
lated electron beam. The charge is transferred to a dielectric
coating in contact with the outer ends of the wire array leav-
ing a latent (electrostatic) image on the thin dielectric which
has high electrical resistivity and a low dielectric constant.
The dielectric film is supported on a comparatively low resis-
tance paper which appears to be in contact with a metal plate
during recording. The latent image is developed by using a
mixture of iron powder and resinous toner, the toner being
attracted to the charged areas to make the image visible.
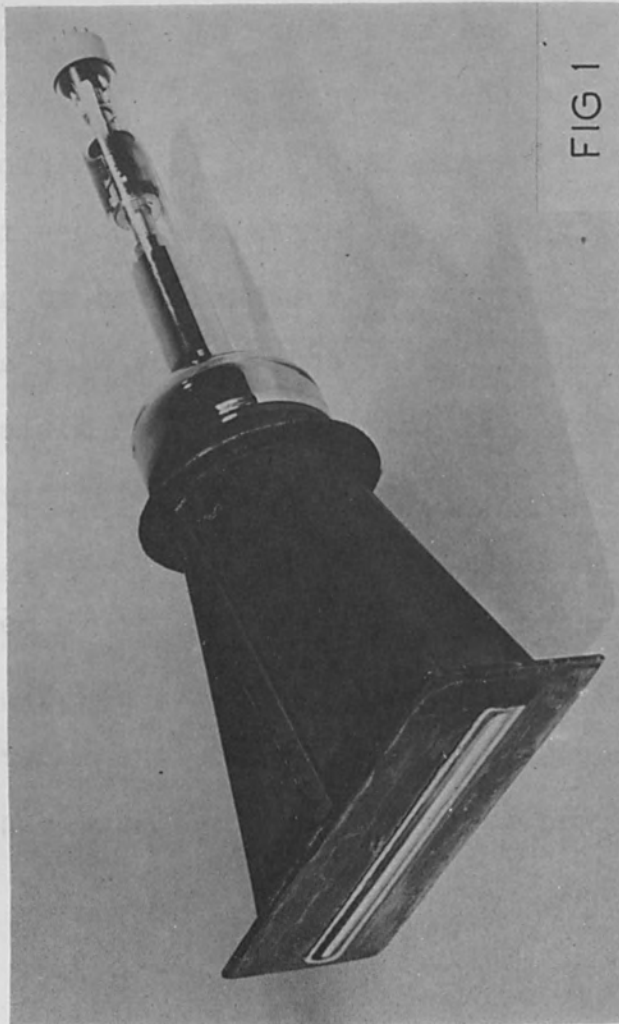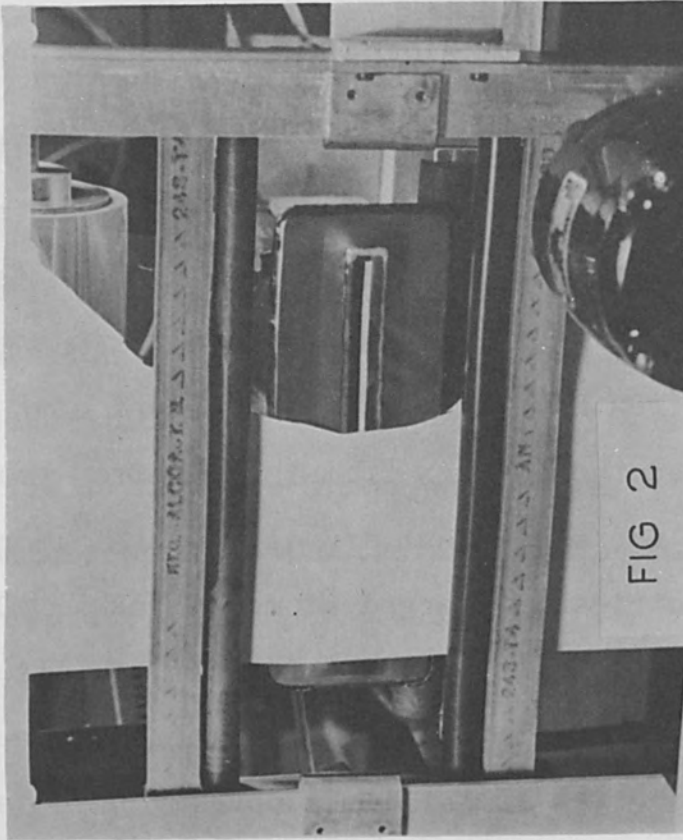
EXPERIMENTAL PRINTING ARRANGEMENT SHOWING "ELECTROFAX"
PAPER IN CONTACT WITH THIN WINDOW

FIG 2

FIG 1

THIN WINDOW METAL CATHODE RAY TUBE WITH 8-INCH LONG MICA WINDOW

ELECTRON GUN

GLASS ENVELOPE

WIRE MATRIX ARRAY
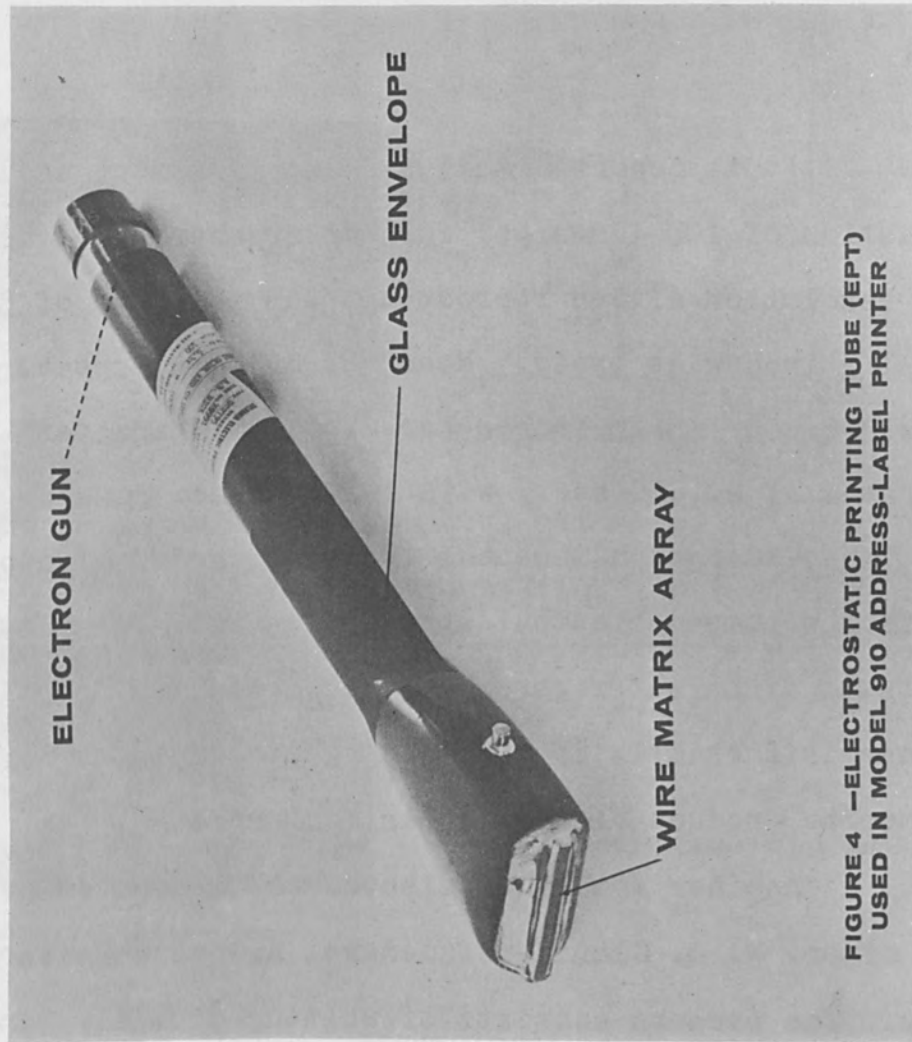
FIGURE 4 —ELECTROSTATIC PRINTING TUBE (EPT) USED IN MODEL 910 ADDRESS-LABEL PRINTER

This print was produced on "Electrofax" paper by contact printing from the face of a thin-window cathode ray tube. The thin window is a mica strip, .0025 inch thick, sealed by a special technique to a metal face plate. The height of the window is .150 inch which is sufficient to reproduce a typewritten capital letter. The window is 8 inches in length and was designed to accommodate the writing space on standard 8.5 x 11 paper. For this copy, the image is formed facsimile-wise by line-by-line scanning. The printing speed is 10,000 characters per second with the paper moving at 19 inches per second. At this speed the average beam current is 1.5 microamperes. Since the paper is abrasive, a sheet of "mylar", .0005 inch thick, protects the mica window. The "mylar" shield is renewed from time to time as it becomes worn. With the present geometry of the tube face plate, the diameter of the printed spot is .005 inch. This corresponds to a definition of 200 photographic lines per inch.

FIG 3

"ELECTROFAX" PRINT BY DIRECT DEVELOPMENT; CATHODE-RAY BEAM "OFF" IN LETTER AREAS

It is reported that present equipment provides resolution of 100 lines per inch at a paper speed of 180 ft/min. This resolution allows reproduction at the rate of 3 ft/sec. on 8-1/2 inch wide paper. Measured printing speeds have been up to 250,000 linear inches per second. Characters have been generated at 20,000/sec., with 100,000/sec. considered feasible. The Videograph tube has two basic areas of application. One is the computer output applications which employ digital inputs to a character generator for character printing. Another is facsimile applications which employ a hard copy scanner to produce video signals for printing.

Another method of electron beam tape recording is that of Dr. W. E. Glenn[19] of General Electric Research Laboratory. The process consists of writing directly (in a vacuum chamber) on a plastic consisting of a high melting base film coated with a transparent conductor which has a thin film of thermoplastic on its surface. When the film is heated, the charge pattern laid down by the electron beam causes ripples to form in the thermoplastic and these ripples are frozen in place when the plastic is cooled. (See Figure 6) The recorded information may be projected on a screen by means of a modified schlieren optical system shown in Figure 7. A photograph of the video thermoplastic recorder being operated by Dr. Glen is shown in Figure 8, with a schematic shown in Figure 9.
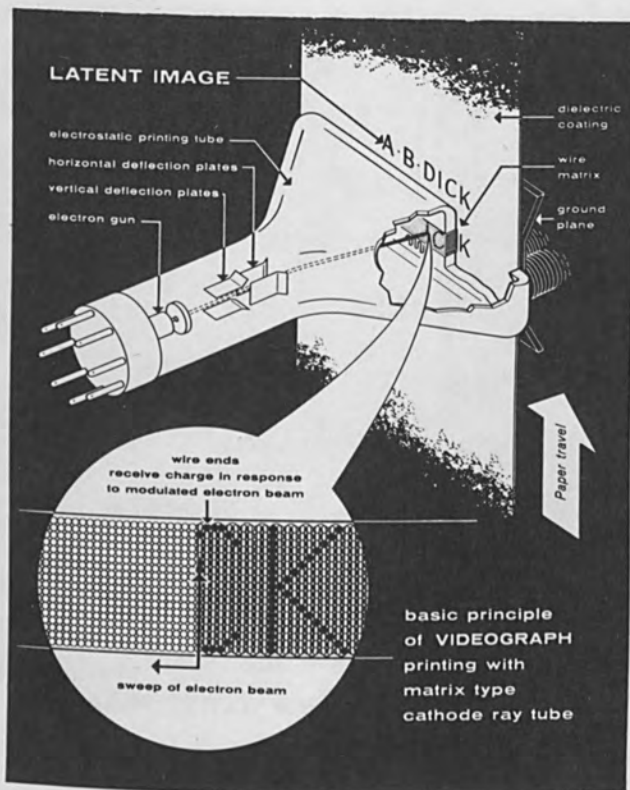
FIG 5   BASIC PRINCIPLE OF VIDEOGRAPH PRINTING
WITH MATRIX TYPE CATHODE RAY TUBE

LATENT IMAGE

electrostatic printing tube
horizontal deflection plates
vertical deflection plates
electron gun

dielectric coating
wire matrix
ground plane

A·B·DICK

wire ends receive charge in response to modulated electron beam

sweep of electron beam

Paper travel

basic principle of VIDEOGRAPH printing with matrix type cathode ray tube

ELECTRON BEAM

R.F. HEATER

FILM MOTION

THERMOPLASTIC SOLID   LIQUID   SOLID

BASE

FIG 6

RECORDING MECHANISM AND CROSS SECTION OF THERMOPLASTIC TAPE

PICTURE ELEMENT GRATING

SCREEN

LIGHT SOURCE

CONDENSING LENS

PROJECTION LENS
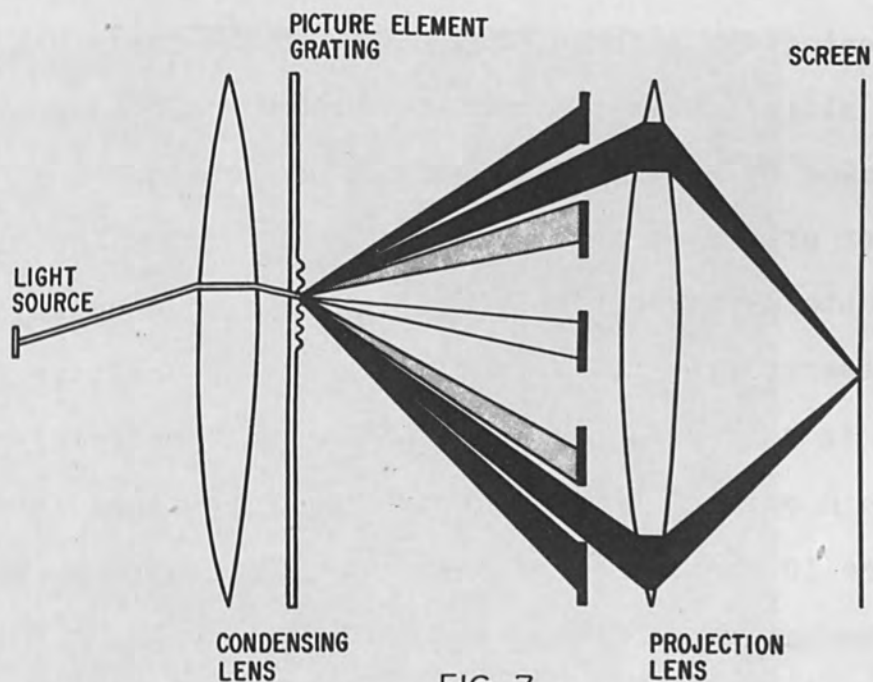
FIG 7

COLOR OPTICAL SYSTEM

257

Both black and white and color can be recorded in the ripples and projected to a screen. It is reported that 200 lines per mm resolution has been achieved with about one microampere beam current, and with a five micron spot size recording at tape speed of 5"/sec. on 1/10" wide track. Replicas can be made by pressing as for phonograph records, the ripples being about 2×10^{-5} inches deep. I understand that Dr. Glenn's process is an outgrowth of the Eidophor[23] process for using an electron beam to produce the ripples on an oil film on a slowly revolving disc, the schlieren pattern being arc projected to a theater screen before the ripples disappear.

Another method of electron beam tape recording is one briefly examined a number of years ago at Bell Telephone Laboratories [20,21]. It consists of writing in vacuum on an untreated plastic and then exposing the invisible beam trace to a slight invisible nucleation deposit of evaporated silver followed by a heavier deposit of evaporated zinc. The metals either prefer or abhor the area acted on by the beam, so that one obtains a record of the beam path. Generally a preference is observed, so that a photographically positive trace of the path is recorded, but with some organic materials or under certain critical conditions, a negative trace is observed. Figure 10 shows the apparatus used for these experiments. The mechanism for re-reeling and continuously plating paper and plastic is a 36-inch vacuum bell which is raised in the

FIG 8

VIDEO THERMOPLASTIC RECORDER
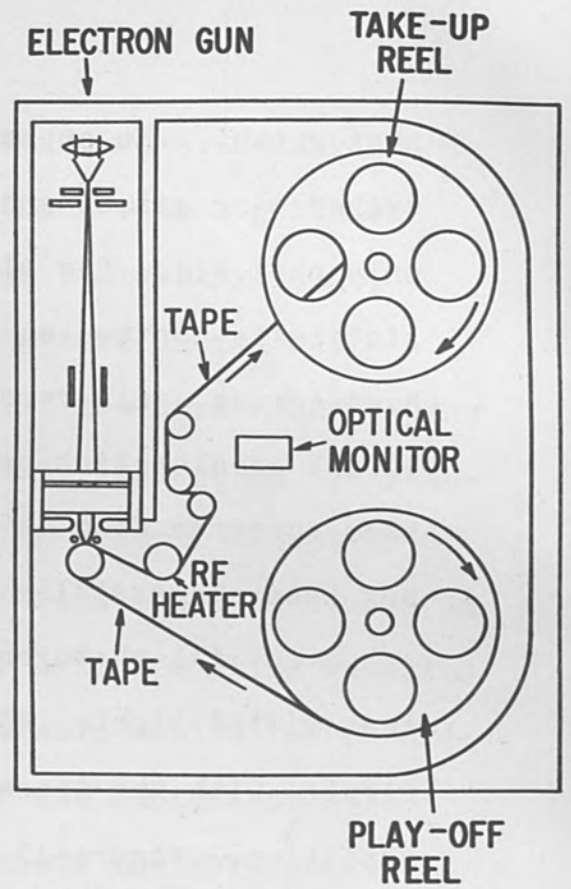
FIGURE 9. SCHEMATIC VIEW OF VIDEO THERMOPLASTIC RECORDER

ELECTRON GUN   TAKE-UP REEL

TAPE

OPTICAL MONITOR

RF HEATER

TAPE

PLAY-OFF REEL

FIG 10
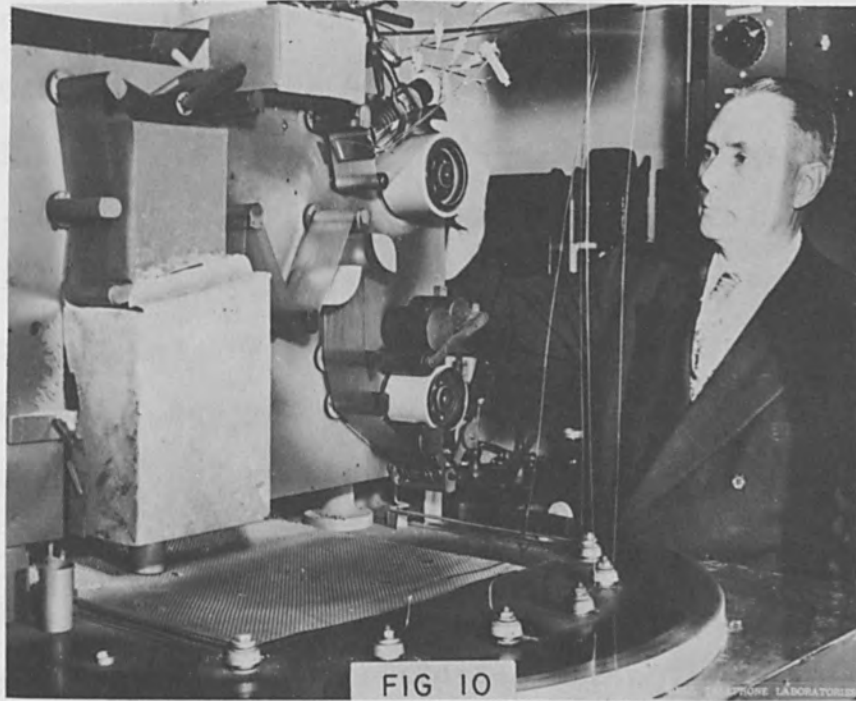
AUTHOR WITH APPARATUS FOR RECORDING ON A MOVING PLASTIC STRIP

photograph. The apparatus contains a tungsten filament for evaporating silver and a crucible for evaporating zinc. The only part added for electron beam recording was an electrostatically controlled electron gun shown in the upper right-hand corner. All recordings shown were made with less than 1000 V accelerating potential. A wide variety of electron beam currents from about a microampere to about a milliampere has been successfully used.

All photographs of recordings shown were taken with transmitted light. Figure 11 is a recording of a 60 cycle ripple, with the trace at the top having a slow superimposed variation. Figure 12 shows an enlarged recording of a 2000 cycle tone with a 60 cycle ripple superimposed. This record was made at 70 lines/inch with a trace velocity of 500 ft/sec. There has been some loss of definition in the enlarged reproduction, but the original recording had about the contrast of a good quality newspaper photograph. The limits of recording speed and of image quality have not been determined. Figure 13 is a photograph of a television test pattern made with this equipment except that the electron gun was replaced by an open-ended television picture tube. Whereas in the other photographs shown, the sub-strate was moving, in this case it was momentarily held stationary during the recording and then developed with silver-zinc. The pattern was sent over two telephone lines from another building. This experiment was

performed with the co-operation of Messrs. F. W. Reynolds and G. R. Stilwell. When recordings were made with a grounded metal plate placed under the moving (or stationary) film, intensity and contrast of the recording were increased.

Exploratory tests were made of the permanence of the latent image. If the beam was allowed to impinge on the plastic and this was immediately coated with a small amount of silver (approximately a monolayer) the film could be stored in air for several months, and thereafter a zinc coating revealed the trace with no visible loss of contrast. While the recordings have in general been positives in the sense that more metal adheres where the beam has impinged, the reverse result was obtained on a cellulose nitrate sub-strate. This result is illustrated in Figure 14.

On the basis of the limited work done, chemical modification of the surface appears the most likely of the possibilities for explaining all of the effects described. The fact mentioned above that recordings on cellulose acetate and on cellulose nitrate are strikingly different favors this view. It has been found furthermore that if a portion of cellulose acetate is exposed in air to ultraviolet light for some minutes, the pattern of exposure can be developed with silver-zinc, the metallic coating preferring the areas exposed. It is known that ultraviolet light promotes oxidation and other chemical changes.

FIGURE 12. ELECTRON BEAM RECORDING OF 2000 CYCLE TONE WITH
60 CYCLE RIPPLE (ENLARGED FROM 70 LINES/INCH)

FIGURE 14. RECORDING ON CELLULOSE NITRATE LACQUER ON KRAFT CAPACITOR PAPER
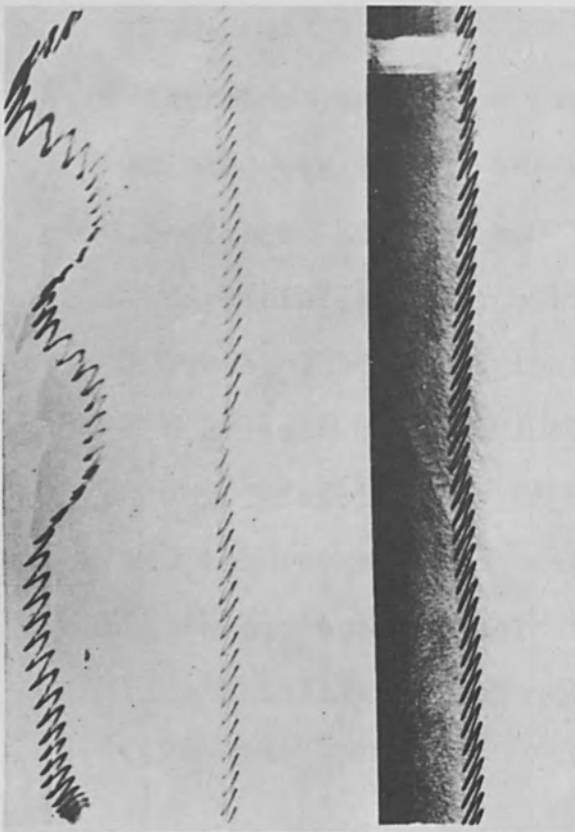
FIGURE 11. RECORDINGS OF 60 CYCLE RIPPLE

FIGURE 13. ELECTRON BEAM RECORDED TELEVISION TEST SIGNAL (X4)

If one employs a gas leak in the metallizing system in which electron beam recordings are made, one can influence the plating with the nature of the gas. If the leak is hydrogen, the record comes out clear and intense. If, on the other hand, the leak is oxygen, the recording is poor in the sense that the background comes up strongly, indicating a lowering of the threshold of sensitivity with a probable resultant need for decreasing the metals evaporation rates. This result, along with that obtained with ultraviolet light, suggests that free radical induced reactions such as oxidation and reduction may be factors in electron beam recording on cellulose acetate.

Considering the recording environment of 1 to 5×10^{-4} mm Hg pressure of residual air and hydrocarbon oil vapor through which is passed an electron beam contacting various organic plastics, it is to be expected that electrostatic charge may be laid down or produced by secondary electron emission. Especially is it to be expected that free radical induced reactions such as oxidation, reduction, depolymerization, ploymerization, and/or cross linking may occur at high velocity, perhaps in 1×10^{-6} to 10^{-9} seconds. While many questions regarding mechanism remain unanswered, it is the conclusion of the author that the evidence favors promotion of chemical change by the electron beam, and that

this in turn modifies the reception of metal. More work would be required to establish this and to identify the particular chemical reactions.

For a comparative evaluation of the various processes of electron beam tape recording, one needs to go much beyond these brief descriptions and report of published claims regarding speed and quality. As a basis for judgment, some first hand experience with each system could be helpful. Also, an agreed upon figure of merit is needed regarding the ability of the systems to record fine detail[24,25,26]. In the light of trying to meet some specific need or application, other considerations might be (a) the stage reached by research and development, (b) equipment costs both initial and operational, (c) simplicity and practicability of the process, (d) speed not only of recording, but of development and of read-out, (e) storage capacity per unit area and per unit volume, (f) ease of access to the information, (g) erasability or correctability of the record, (h) usable life of the record, (i) environmental conditions for storage, and (j) possible need for special equipment to read or make available the recorded information. Such comparisons await the future. Last but not least, one must never forget that there are other methods (some very successful) for high speed recording without the use of electron beams.

In conclusion, this paper has attempted to give a brief resumé of some published methods of tape recording via electron beams. No attempt has been made to exhaustively cover the field. Yet it is hoped that no significant development has escaped mention. Included in the references are reports of some interesting effects of electron beams which could well warrant further exploration.

Acknowledgment

REFERENCES

(1)   Knoll, M. and Kazen, B: "Storage Tubes and Their Basic
       Principles," J. Wiley and Sons, N. Y., 1952.

(2)   Stranix, Richard G.: "Electron Gun Finds New Role in
       Recording and Storing Data," - Electronic Industries,
       19, pp. 164-178, March 1960.

(3)   Olson, H. F., Houghton, W. D., Morgan, A. R.,
       Zenel, J., Artzt, M., Woodward, J. G. and Fischer, J. T.:
       "A System for Recording and Reproducing Television Sig-
       nals," - RCA Review, 15, #1, pp. 3-17, March 1954.

(4)   Berry, T. M. and Hanna, J. P.: "Ferromagnetography -
       High Speed Printing with Shaped Magnetic Fields,"
       General Electric Review, pp. 20-21, July 1952.

(5)   McNaney, J. T.: "Electron Gun Operates High Speed
       Printer," - Electronics, 31, #39; 74-7, September 26, 1958.

(6)   Hutter, E. C., Inslee, J. A., and Moore, T. H.:
       "Electrostatic Imaging and Recording," - Jnl. of the
       SMPTE, 69, 1, pp. 32-35, January 1960.

(7)   Ross, R. J.: "Exposure Control in Television Film
       Recording," - Jnl. of the SMPTE, 69, #9, pp. 580-586,
       September 1960.

(8)   Gillette, F. N. and Plakun, B. D.: "Shutter Cycles for
       Television Film Recording," - Jnl. of the SMPTE, 69, #9,
       pp. 587-592, September 1960.

(9) Heynick, L. N., Wohl, R. J., and Andrews, D. H. :   "A
     Direct Writing Cathode-Ray Tube Recorder," - Proc. of
     Nat. Electronics Conference 1955, Vol. 11, pp. 172-182.

(10) Möllenstedt, G.:   "Electron Optical Microwriter with
     Electron Microscope Monitoring of the Work" (In German) -
     Physikalische Blätter 16, No. 4: 192-8, 1960.

(11) Hirsh, E. J.:   "Image Formation by Electron Bombardment
     of Metal Targets," - British Jnl. Appl. Phys., 11, #12,
     pp. 547-50, December 1960.

(12) Williams, H. J., Sherwood, R. C., Foster, F. G.,
     Kelly, E. M.:   "Magnetic Writing on Thin Films of BiMn," -
     Jnl. Applied Physics, 28, 1181-4, 1957.

(13) Mayer, L.:   "Magnetic Writing with an Electron Beam," -
     Jnl. Appl. Physics, 29, #10, 1054-6, 1958.

(14) Sanders, Richard M.:   "Further Observations on Reversi-
     ble Rotation in Magnetic Films," - Jnl. Appl. Phys.
     Vol. 29, #6, 1003, June 1958.

(15) Stowell, P. A.:   "Techniques of Digital Electrostatic
     Recording," AIEE Conf. Paper CD-61-441, January 31, 1961.

(16) Norelco Reporter, Vol. 4, #6.

(17) Olden, R. E.:   "Thin Window Cathode Ray Tube for High
     Speed Printing with Electrofax," - RCA Review, 18:343-350,
     September 1957.

(18) Dahl, H. A. and Jenkinson, G. H.: "The Videograph Printing Process," AIEE Conf. Paper #CP-61-288, January 31, 1961.

(19) Glenn, W. E.: "Thermoplastic Recording," - G. E. Research Lab. Reprint #3715 from Jnl. of the SMPTE, Vol. 69, pp. 577-580, September 1960.

(20) Wehe, H. G.: US Patent #2,883,257, of 4/21/59.

(21) Wehe, H. G.: "Electron Beam Recording," - Bell Telephone Systems Monograph #3576 reprinted from 1958 Fifth National Vacuum Symposium on Vacuum Technology Transactions, pp. 242-246.

(22) "Standard Register's Electronics Find," - Bus. Week, Feb. 27, 1954.

(23) Bauman, E.: "The Fischer Large-Screen Projection System," - Jnl. of the SMPTE, Vol. 60, pp. 344-356, April 1953.

(24) Perrin, F. H., "Methods of Appraising Photographic Systems - Part I - Historical Review," Jnl. of SMPTE, Vol. 69, #3, pp. 151-156, March 1960.

(25) Perrin, F. H. "Methods of Appraising Photographic Systems - Part II," Jnl. of SMPTE, Vol. 69, #4, Part II, pp. 235-249, April 1960.

(26) IRE Standards Committee - "IRE Standards on Video Techniques: Measurement of Resolution of Camera Systems, 1961" Proc. of IRE, pp. 599-602, March 1961.

ELECTRON BEAM MILLING

By

K. H. Steigerwald
Head, Electron Beam Department
Carl Zeiss Corporation
Oberkochen, Germany

ABSTRACT

A brief historical background of developments
which lead to electron beam milling are presented. The
physical principles underlying the process, and their
relation to material properties are discussed with an
evaluation of present day achievements and future prospects
of this technology.

Within a few years, it will be a century since Hittorf discovered electron

radiation in Goettingen, in the year 1869. Subsequently Edison discovered

the glow emission of electrons. The year 1900 already witnessed the

emergence of the first electron beam apparatus, namely the Roentgen tube,

projecting so considerable a beam current as to make it feasible to melt

the material of the anticathode, and to vaporize it. Thus it happened some-

times by accident, that the anticathode material, tungsten, was welded by

the electron beam to the copper support.

In 1920, in the city of Aachen, Rogowski built the first cathode beam

oscillograph, by means of which it was possible to achieve a writing speed

of 20000 km/s on a photographic plate. However, once again, one had to

cope with the problem that the stationary beam was in fact capable of boring

through a sheet metal plate. Occasionally this ability was utilized in

electron beam units of that time for practical applications. Thus, for

instance, rather than a diaphragm provided with a ready bore, a solid sheet

metal plate was interposed along the path of the beam, so that the electron

beam was used to produce the bore. The diaphragm was now automatically aligned

with the beam, thereby avoiding the necessity of complex mechanical alignment

devices.

In 1924, de Broglie discovered the wave nature of corpuscular radiation,

and in 1926 Busch discovered the optical properties of electrical and magnetic

fields. This opened an avenue to the advent of electron optics. In 1930 two

groups in Berlin independently undertook basic research concerning electron

microscopy. Zworykin, Hillier and Gabor followed their lead. The fine

diaphragms with a diameter of 50 μ and less, required in electron micros-
copy, provided the first targets for electron beam boring. It was a common
occurence that sometimes the electron beam bored a hole next to the already
existing hole in the diaphragm, if the beam was not properly aligned. In 1939
M. v. Ardenne disclosed a device for the boring of diaphragms with corpuscular
beams. Fig. 1 illustrates this unit which functioned on the principal of
cathodic evaporation.

Within approximately the same period, Ruehle constructed in Stuttgart the
first equipment for the melting of metal and for their evaporation with the
aid of electron beams, which already at so early a date anticipated all of
the properties of modern equipment. Fig. 2, taken from the patent disclosure
published in 1939, already shows the separation between the beam generating
space and the melting space by means of a two-stage device and a diaphragm.

In 1938, Ruska and Ardenne published the idea whereby collodion membranes with
a thickness of 0.01 μ are provided for filtering purposes with extremely fine
bores.

I have cited here only the most important priorities. A more exact research
concerning the historical development of the electron beam, its employment as
a source of thermal energy, as a tool for welding, milling, and other thermic
applications will be published.

I am sure that you will concede the fairness of the following summation:-
The feasibility of using the electron beam as a source of heat was recognized
at an early stage, and was employed for the most varied purposes, such as
melting, welding, boring, etc.. This, of course, took place on a rather
restricted laboratory scale. Only the later development of electron optics,
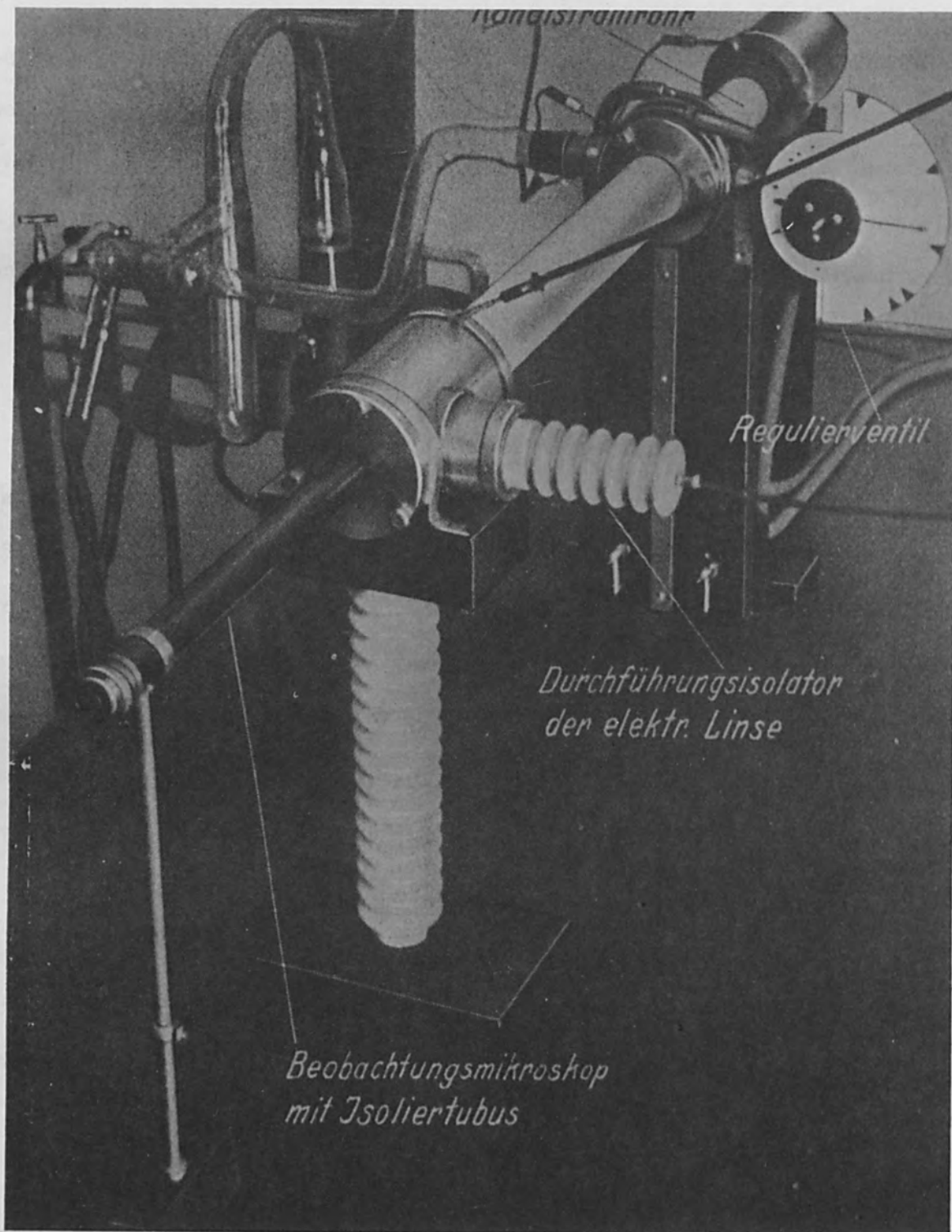
Fig. 1

Manfred V. Ardenne – 1938

Apparatus for the boring of small diaphragm
aperatures by ion bombardment.
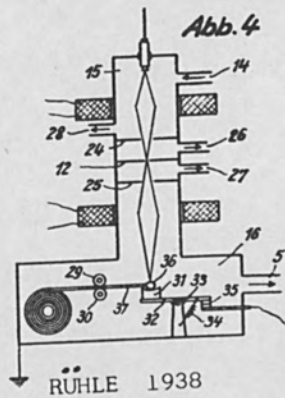
Figure 2.   Rudolph Ruhle - 1938
Apparatus for melting and vaporizing
by electron beam

Lokalisierbarkeit der Wärmewirkung und maximale Energiedich

Wärmequellen	Kleinster Querschnitt cm^2	Höchste Energiedichte W/cm^2
Azetylen-Schweißbrenner-flamme	10^{-2}	10^4
Lichtbogen	10^{-3}	10^5
Elektronenstrahl	10^{-7}	10^9

Table I
Two heat sources compared with electron beam

273

electronics, and vacuum engineering provided the fundamentals for its use on a larger scale.

Hence, when we began in 1948 to investigate the manifold possibilities afforded by the electron beam, it was not our intention just to reiterate the simple applications of the electron beam as a thermal source for melting, welding and evaporation in vacuum under improved technical conditions, but along the same lines as other known heat sources. It was rather our aim to avail ourselves of the special properties of the electron beam for the purpose of achieving entirely unique thermal effects which could not be achieved with the aid of the thermal sources familiar hitherto, both with and without vacuum.

Let us restate here the special properties of the electron beam:—

1) Uncommonly high energy densities are attainable by means of electron beams.

2) At electron velocities lower than 300 keV the absorption takes place on solid bodies in a very small layer. Here approximately 100% of the irradiated energy is converted instantaneously into heat in the material.

3) Beam intensity, shape of the beam, and its position lend themselves to high precision and practically instantaneous control.

Table 1 compares the practically feasible minimum cross-sections and energy densities of 3 thermal sources. These data relate to an electron beam of 150 keV. In each instance, the electron beam surpasses the other two energy sources by a factor of 10^4.

For instantaneous control of the beam, impulse durations of 10^{-8} sec can be achieved by normal electronic means. Just what this signifies is perhaps revealed by the fact that 100 keV electrons cover within that time-span a distance of only 1.5 m.

274

To give an idea as to the possibilities of removing material by vaporization, we should take a closer look at the thermal processes which take place on the material. Fig. 3 gives a schematic of the situation obtained when an electron beam strikes solid material. The electron beam, here designated by S, strikes the solid body, indicated by a hash-line, and is absorbed in the layer having a thickness of R. It is assumed that the beam has already bored to some extent into the material, which means that this has already been subjected to evaporation. At the instance of observation, the irradiated energy is consumed by the following processes:-

a) Heating of the material in the layer R q_2

b) Melting of the material heated above the
   melting point q_3

c) Evaporation of the removed material q_1

d) Heat dissipation through radiation q_4

e) Heat dissipation by conduction q_5

If we plot the characteristics of the various processes as a function of the average temperature of layer R, we get the picture obtained in Fig. 4 which represents the values in the case of steel.

The tabulation begins at $2000^\circ K$ which is above the melting point of steel. The indices of curves $N_1 - N_5$ coincide with the indices of the aforesaid $q_1 - q_5$, and designate the same processes.

These values relate to a steel plate of 1 cm thickness whose lateral expansion is appreciably greater than the thickness. The electron beam S impinges on a surface area of $0.01 \ mm^2$, which is approximately 12 μ in diameter. The beam heats this area to a men temperature T while the underside of the plate is maintained at room temperature. The values of $N_1 - N_3$ were obtained by measure-
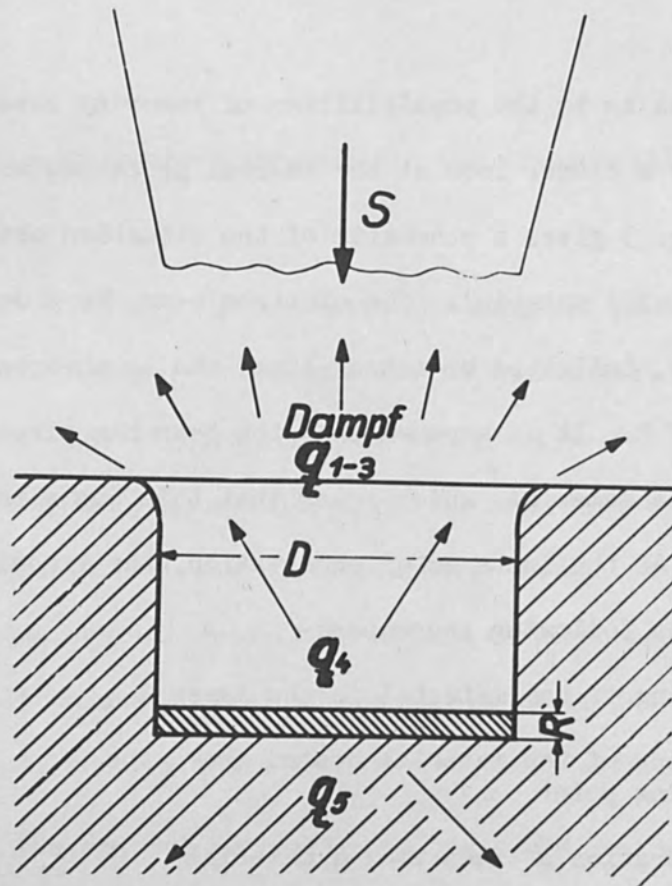
275

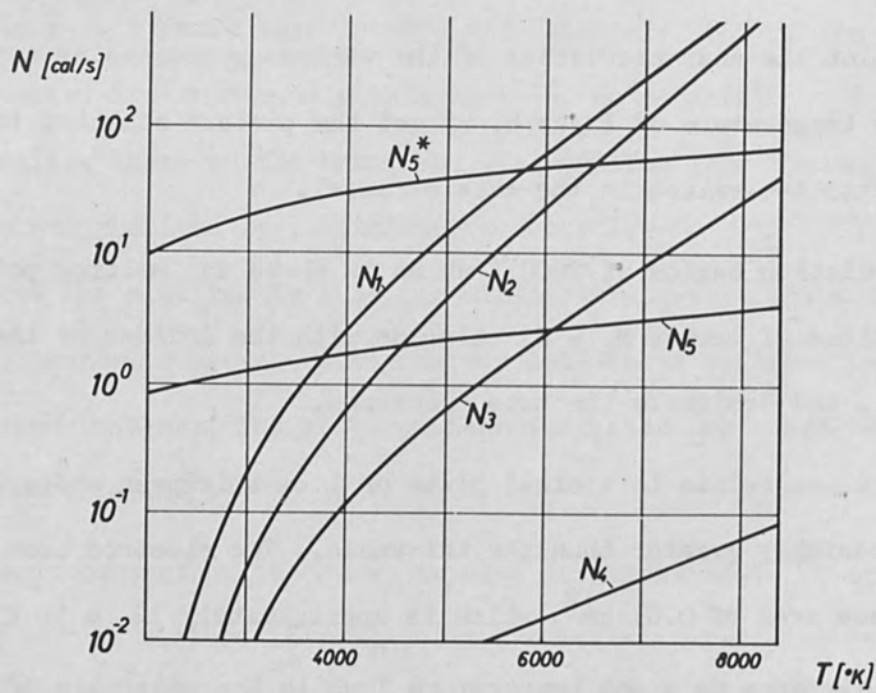Figure 3. Localized heating by electron beam.

Figure 4. Energy balance of different processes as achieved by electron beam heating.

ments and computations provided in part by Langmuir and colleagues (1). N_5 was determined by the Alex Mueller method (2) for the computation of the heat capacity of anticathodes in X-ray tubes. This method has been used to prevent the welding of anticathodes by the electron beam.

It will be noted that at $2000^{\circ}K$ the energy flowing into vaporization is very low as compared to the energy loss dissipated by heat conduction. Here the material evaporates to only a very slight degree while a considerable quantity of material is melted. If we consider, however, the situation at higher temperatures, it will be noted that the useful output rises rapidly exceeding the power loss N_5 at $3500^{\circ}K$. This is due to the rising vapor pressure which mounts exponentially with the temperature, while, as is well known, the power loss dissipated through heat conduction rises practically only in a linear relation to the temperature. It is obvious that a geometrically exact removal of material can be achieved only if the energy utilized for the melting and heating of the remaining material is negligibly small compared to the energy employed for evaporation. The different nature of the above processes with respect to their dependence on temperature was the main reason for our confidence that the electron beam could be used as a good technical means for milling and boring operations.

To make it possible to maintain close tolerances, one is confronted with the problem of generating a high temperature sufficient to evaporate while on the other hand low enough to prevent changes in the material by thermal effects. A view of the conditions prevailing in a practical case is given by the course of the power loss N_5^*. It was calculated for a stationary case and predicated on the condition that the temperature at a distance of 4 μ from

the worked surface should not exceed the value of 900°K. An appreciable increase of power loss N_5^* by about a factor of 10 is produced compared to the case represented under N_5.

It can now readily be demonstrated that the aforementioned conditions regarding temperature distribution in the material are unattainable in nearly all practical cases for stationary operation. On the other hand it is possible not to exceed the critical temperature within the tolerance depth in the material for a short time. The duration of this critical time is governed by the properties of the electron beam and of the material. The critical time-span can be estimated in a simple manner if it is assumed that it is feasible with the aid of an electron beam to heat the surface of the target material to an adequate evaporation temperature within an appreciably shorter time-span. This calls for a beam with an extraordinarily high energy density. It is also essential to know to some extent the energy loss at specific depths of the electrons penetrating the material. Fig. 5 shows by way of an example, the energy loss of an electron beam of 100 keV velocity in tungsten as a function of depth. It will be noted that it does not by any means take place uniformly. This notwithstanding, it can be said that the layer of material penetrated by the electrons does not deviate appreciably from a mean temperature at the beginning of a sudden intensive radiation.

We will now assume that we are in a position to fire electrons with a velocity of 100 keV with an energy density of 10^9 W/cm^2 into the surface of a tungsten plate. This is a value which is in effect attainable in the case of a well focussed beam. It can be easily computed that in such an event the layer in which the electrons are absorbed can be heated in about 10^{-8} sec. to a melting temperature of 3650°K.

To make it possible to judge what tolerances could be maintained in the case of a practical processing of material, it is necessary to know the time required for a given point in the material, lodged at a given distance from the hot layer, to heat to the melting temperature by means of heat conduction. If we regard for simplification the non-stationary case of heating a tungsten plate as an unidimensional problem, we get:-

$$\frac{\partial T}{\partial t} = \frac{\lambda}{c \cdot \varrho} \cdot \frac{\partial^2 T}{\partial x^2}$$

Here, $\frac{\partial T}{\partial t}$ is the change of temperature with time in a flat layer traversed by heat perpendicularly in the X direction. $\frac{\partial^2 T}{\partial x^2}$ is the change of the temperature gradient across the thickness of the layer, λ being the thermal conductivity, c the thermal capacity, and ϱ the density of the material. As a first approximation we get for the time:

$$t = T \left(\frac{\lambda}{c \cdot \varrho} \left[\left(\frac{dT}{dx} \right)_1 - \left(\frac{dT}{dx} \right)_2 \right] \right)^{-1} \cdot \Delta x$$

If we substitute the values derived from the above example for the heating of a tungsten plate, we get for a layer thickness $x_1 = 8\,\mu$, a time of $t_1 = 10^{-5}$ sec. If we assume the thickness of the layer to be $x_2 = 1\,\mu$ we get a time of $t_2 = 7 \cdot 10^{-6}\,\mu$. These time-spans are 100 times longer than the time required for the heating of the layer which absorbs the electrons. We thus find that we have a good opportunity to vaporize in the meantime an appreciable quantity of material. It is possible to quickly interrupt the heating by the electron beam in order to obtain tolerances of the range of μ.

The values indicated here have been obtained on the basis of highly simplified assumptions. All simplifications, however, have been so chosen that under actual working conditions the situation could only be more favorable. Furthermore, the material constant

$$\frac{\lambda}{c \cdot \varrho} \quad [\ cm^2 \ . \ s^{-1}\ ]$$

represents a temperature conductivity value, affording an interesting insight into the possibilities made available by the electron beam with respect to different materials. I am therefore citing here a number of values reported under Table 2 for different materials.

It can be noted that the values indicated here for the temperature conductivity differ from each other by a factor of about 25. On the other hand, materials which are thermally as diverse as iron and aluminum oxide or silicon and tungsten lie clearly within the same limits. The electron beam provides far-reaching possibilities regarding differences in material properties by appropriate selection of the electrical values. If we set up a comparison between the mechanical treatment of materials and electron beam techniques, it will be found that the electron beam is the most adaptable tool for the most diversified characteristics of materials.

It can be seen from the data that, where material is being processed by electron beams, it is most important to perform the work with high energy densities and low time constants. This is the only means of achieving technically useful precision and sufficient speeds of operation while properly preventing changes in the properties of the material.

280
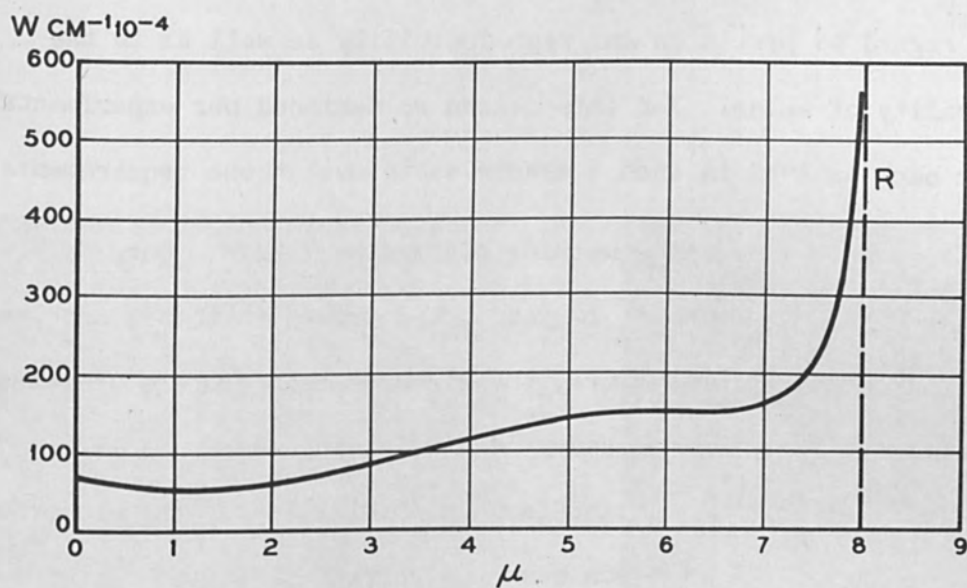
Figure 5.   Energy loss as function of depth
of a 100 keV electron beam in
tungsten.

	λ CAL $\overline{\text{CM S GRAD}}$	C CAL $\overline{\text{G GRAD}}$	ς G $\overline{\text{CM}^3}$	$\frac{\lambda}{c\cdot\varsigma}$ CM^2 $\overline{\text{S}}$
Al_2O_3	0.08	0.18	3.8	0.12
Cu	0.92	0.092	8.93	1.1
Fe	0.21	0.108	7.86	0.26
Fe Cr Ni 18/8	0.035	0.114	8.3	0.04
Si	0.2	0.168	2.4	0.5
W	0.39	0.032	19.3	0.63

Table II
Values of temperature conductivity
for different materials.

It can be readily shown that this principle is equally important in the case of welding with regard to precision and reproducibility as well as to the metallurgical quality of welds. For this reason we designed our experimental equipment as far back as 1948 in such a manner as to meet these requirements.

I should like to say at this point something concerning X-Rays. Our experience, gathered over a period of 12 years, has proved that this problem has been solved completely. Furthermore, the electron beam process operates in a vacuum chamber, so that the necessary lead shielding adds very little extra cost. To fully exploit the advantageous possibilities of the electron beam process, we must give the electron beam the correct properties without effecting a compromise. When electricity was first introduced into industry and into the daily lives of the people, a great outcry was raised about the danger lurking in the high electrical voltages used. However, time taught us differently, and I am sure there is hardly one among you who doesn't shave with an electric razor undisturbed by any perils. This is probably equally true of those who are bothered by the x-rays produced. It is the prime task of advancing technology to cope and solve problems and not to circumvent them if we are to take full advantage of the physical capabilities of this process.

I should like to mention at this point a few additional examples concerning the working of materials with the aid of the electron beam.

On the occasion of the last symposium, Dr. Opitz cited several examples taken from the Zeiss development program. This program got under way in 1948. *(3)* An electron beam welding and boring apparatus operated in the year 1950 is shown in Fig. 6. Another 1 kW electron beam unit of the year 1952 is shown in Fig. 7.
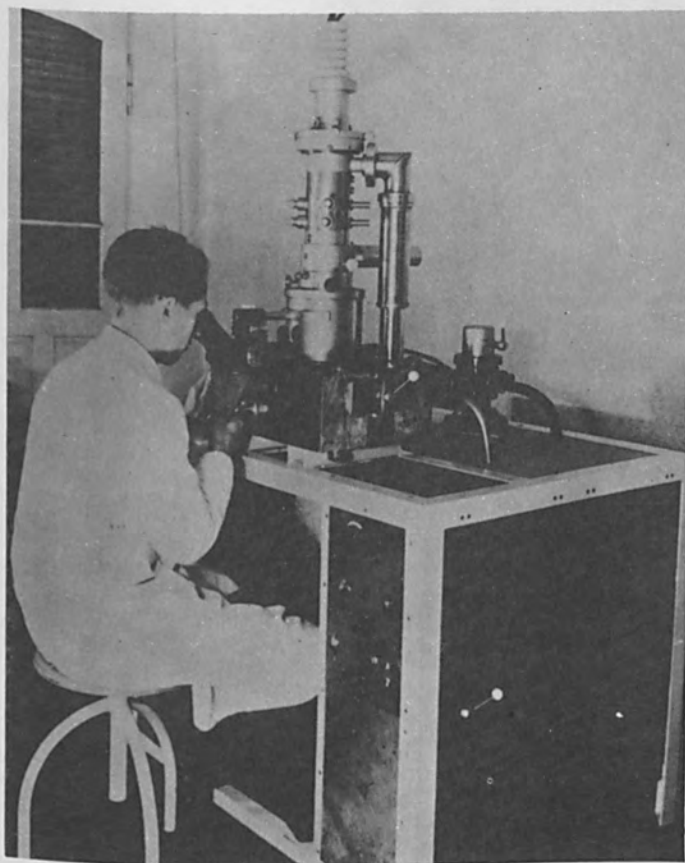
Figure 6. Apparatus for experiments in electron beam welding and milling used in the year 1950.
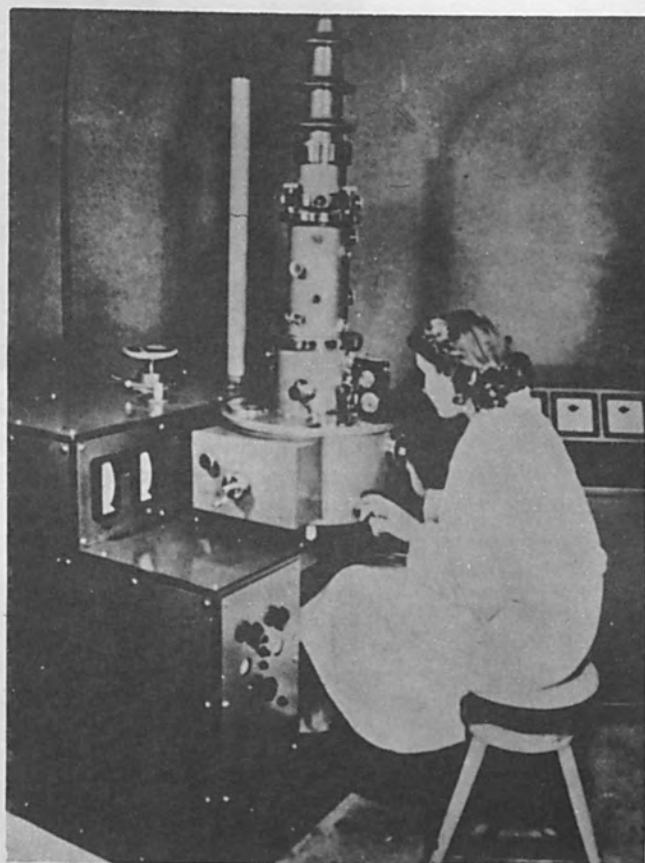

Figure 7. Electron beam welding and milling machine with 1 kw beam power built in the year 1952.

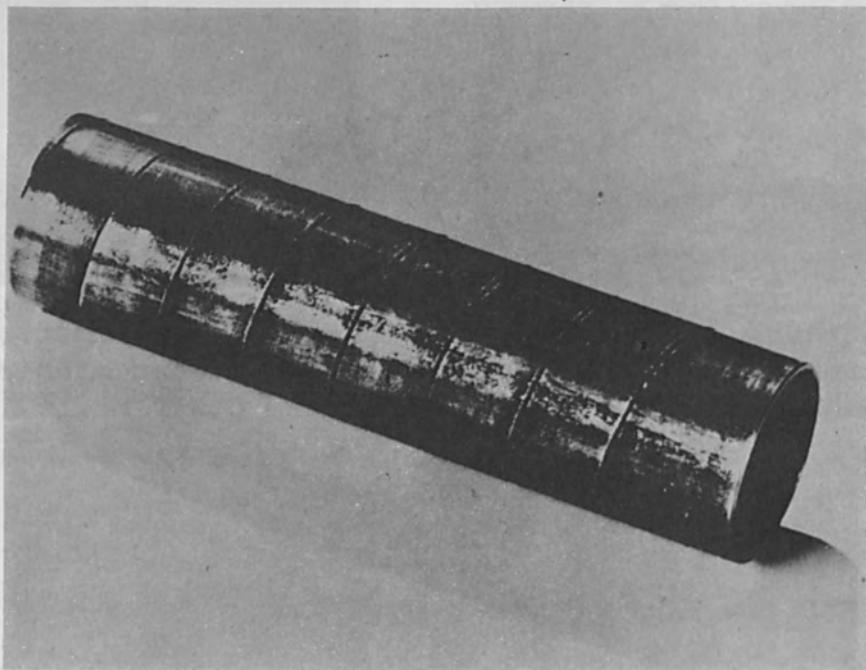Figure 8. Zeiss electron beam milling
machine 1960.

Figure 9. High speed cutting with electron
beam. Wall thickness of steel cylinders
1 mm; cutting speed 48" per minute.

As a matter of fact, this unit was capable of a power output of 2 kW, but the energy density attainable in excess of 1 kW we considered as too meagre. One of these machines was brought to the United States in 1958 and is still operating to this day.

The current milling machine, with an output of 100 W, is shown in Fig. 8. It attains energy densities of about 10^9 W/cm^2 or 6.5×10^9 W/in^2. Fig. 9 shows a tube with a wall thickness of 1 mm which was cut through by means of an electron beam at a rate of 48 inches per minute.

Slot–cutting on thin layers is particularly important from the standpoint of microminiaturization. Figs. 10 and 11 show point and slot cutting in thin layers on glass. Slot–cutting of chromium–nickel layers on ceramics have already been shown here by Opitz. Figs. 12 and 13 show a wafer resistor and a highly magnified photo of this type of milling. Fig. 14 shows an electron microscopic picture of the same type of milling. You can see how the surface of the ceramic material has been smoothed out by the electron beam. You may see the feasibility of polishing such a surface by scanning it with the electron beam.

It was possible to produce milling cuts on the surface of silicon where the material was stripped off only to a depth of 0.5 μ and to a width of 3 μ. The interference microscopic picture of Fig. 15 shows milling work of this type.

Last, Fig. 16 shows fine bores produced in a lens which is to serve as a substitute for the lens of the human eye after grey Star operations. The electron beam bores, which were made parallel to the central plane of the lens, assure from the anatomical standpoint, a particularly good suspension

285
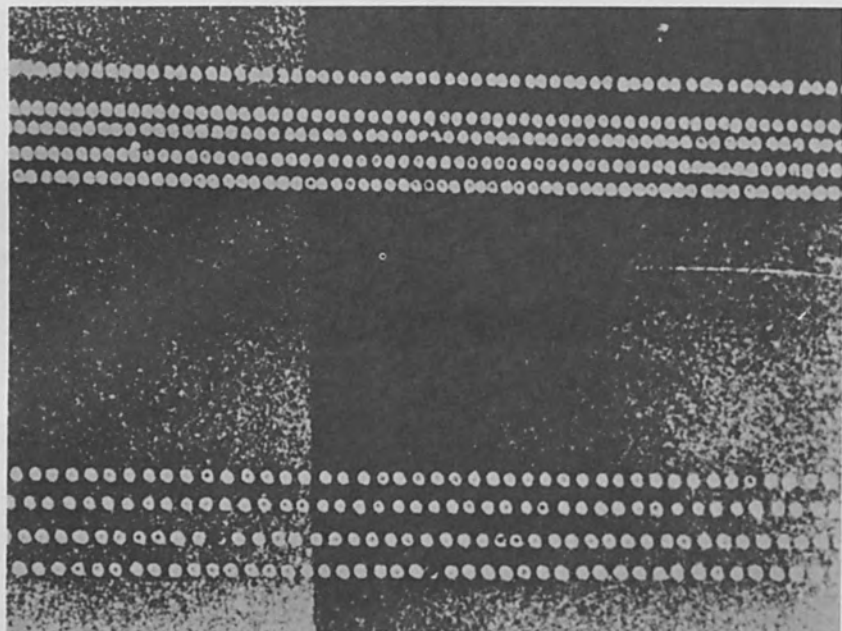
Figure 10.   Point milling in thin layers
on glass.
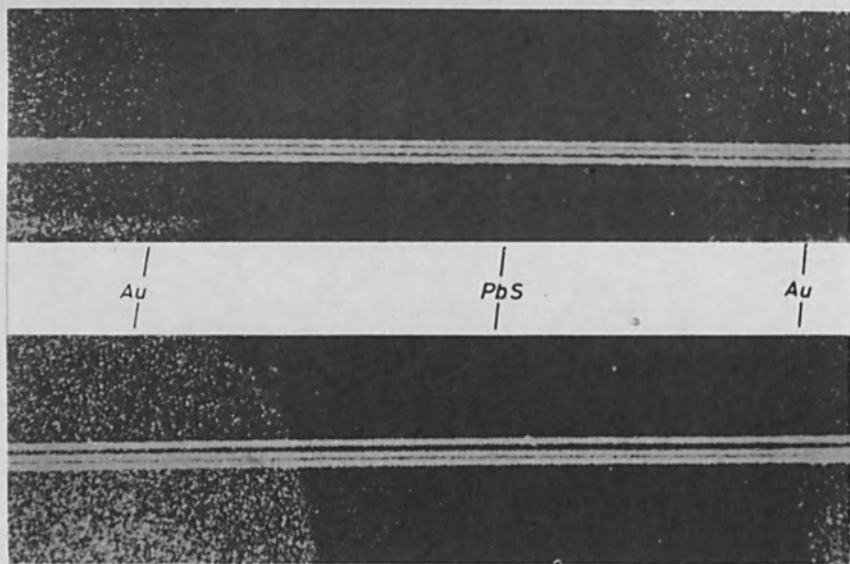
Figure 11.   Slot milling of thin layers on
glass with smallest land approximating
3μ in width.
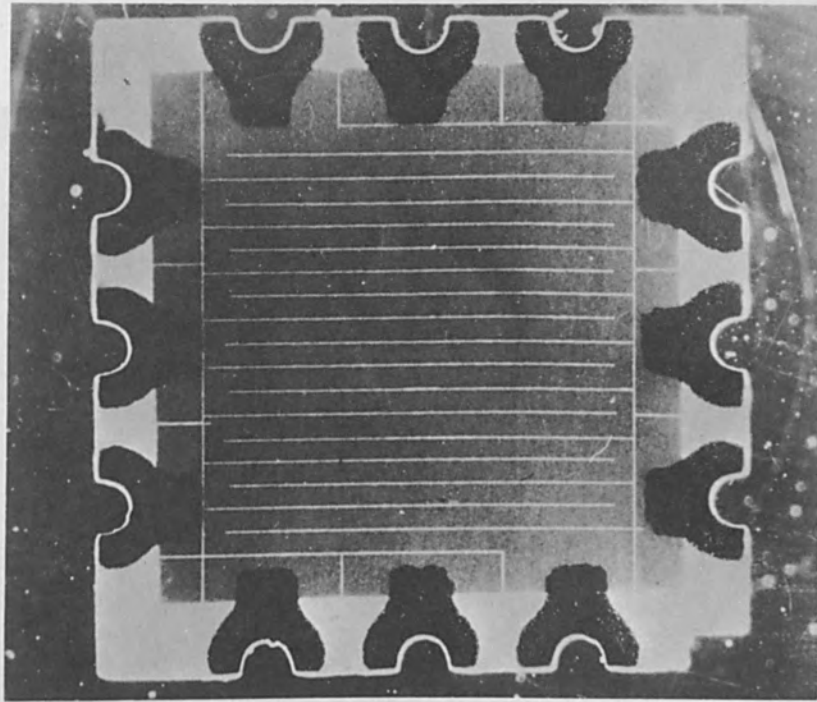
Figure 12.   Wafer Resistor

Figure 13.   Highly magnified slots on wafer
resistor with a slot width of 10μ.

Figure 14. Electron microscopic picture of slot milled by electron beam on the surface of aluminar ceramics. Magnification 4420.
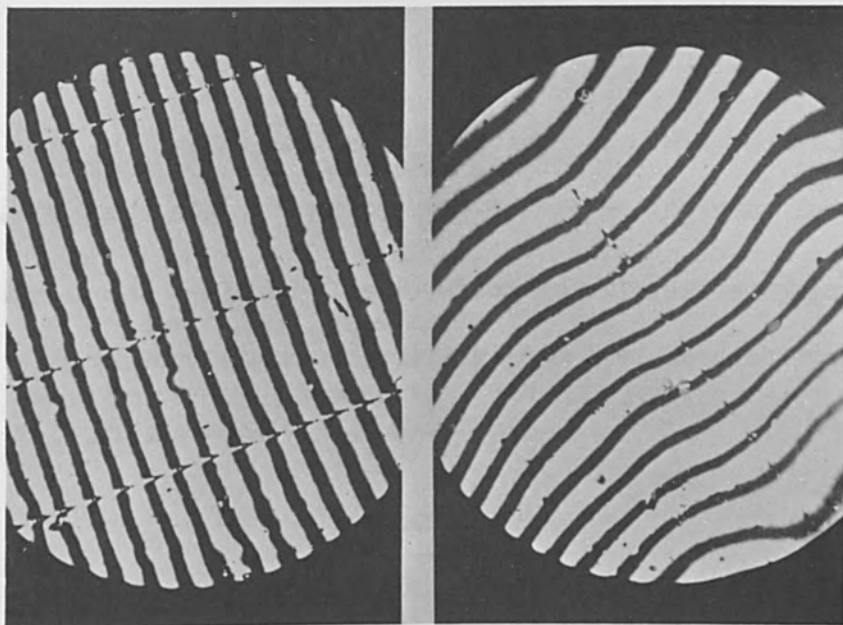
Figure 15. Interference microscopic picture
of 3 and 5μ wide slots milled in the surface
of silicon by electron beam.

1 mm
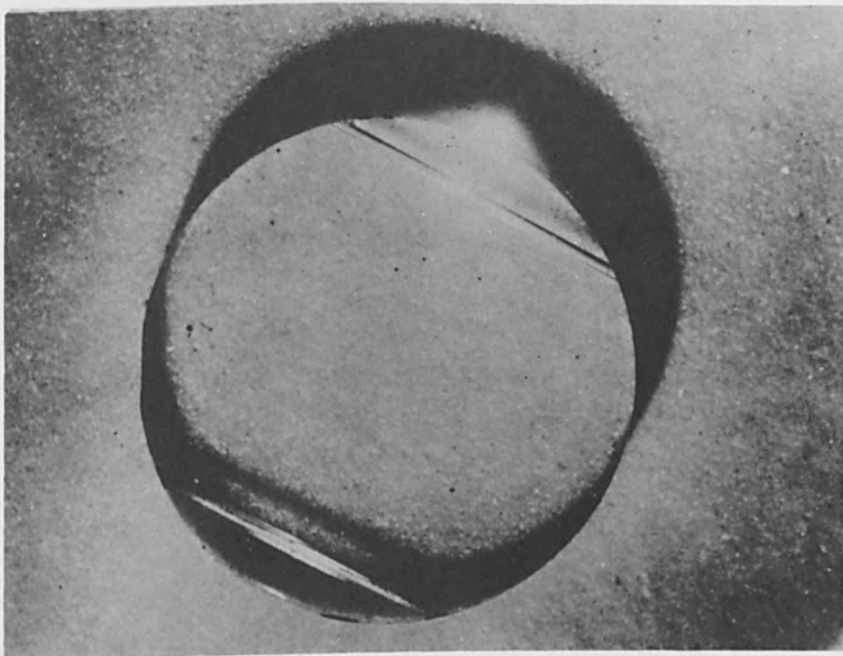
Figure 16. Artificial lens for the human eye
with electron beam drilled holes.

of the lens in the eye. In addition, microscopically fine eyes have been bored in steel surgical needles for operations on the human eye.

I believe that the last two examples clearly manifest the universal importance that the electron beam tool has in all spheres of technology.

REFERENCES

1. Jones, H. A., Langmuir, J. and Mackay, G. M., Physic. Rev., 30, 202 (1927).

2. Mueller, A., Proc. Roy. Soc. A., 117, 30 (1928).

3. Steigerwald, K. H., Phys. Verh. 4, 123 (1953).

ELECTRON BEAMS IN MICRO-ELECTRONICS

By

Oliver C. Wells
Research Physicist
Electronics Department
Westinghouse Research Laboratories
Pittsburgh 35, Pennsylvania

ABSTRACT

Electron beams may be used in microelectronics
either to perform well-known tasks or to carry out fabri-
cation operations which are entirely new. Techniques are
being developed for processing a wide range of materials
at a fine resolution with a low level of stress and
structural damage. The methods of electron probe micro-
scopy may be applied for process control.   These techniques
are being investigated as part of the Westinghouse Molecular
Electronics Program.

I. Introduction

Electron beams may be used in microelectronics either to perform well-known tasks or to carry out fabrication steps which are entirely new. In this paper a review of present methods is made, the requirements are analyzed, and the future possibilities are examined. Emphasis is given to the development of fabrication processes having a significantly better resolution than present techniques will allow; how to coordinate one such high resolution process with another; and generally how to apply them in practice. Methods by which electron beams may be used for the preparation of materials will be mentioned but will not be described in detail.

At the present time there are three basically different approaches to microelectronics:

(i) in which conventional components are used, but in which they are packed together more closely;

(ii) in which the individual components are redesigned to make possible an order of magnitude increase in the components backing density, as is done, for example, in the U. S. Army micromodule program;

(iii) in which the circuit is fabricated from the basic materials directly, in which case a still further reduction in the amount of nonfunctional substance present may be achieved.

In microelectronics the number of active elements that may
be packed into the cubic inch is limited by the heat that is generated
by them. The need for a high resolution fabrication process arises
therefore not so much from the desire to increase the packing density
as from the requirement to fabricate each active element to a close
tolerance. If the tolerances can be made closer, then the heat dissipated
in each individual component can be reduced, and the packing density
can be increased. Even in some present-day solid state devices dimensions
of the order of a few microns are occasionally specified, and to hold
a dimension of this order to within a close tolerance a resolution
of the order of tenths of a micron will be required. (The requirement
for close tolerances will also, of course, refer to the thicknesses
and chemical purities of the layers, as well as to their outlines,
as discussed below.) It is to be expected that the requirement for
close tolerances will become more stringent as operating frequencies
are increased. In this paper processes will be described by which
resolutions in some cases as good as one tenth of a micron may be obtained.

II. A Discussion of the Problem

(a) What is to be Achieved by the use of Electron Beams.

The usefulness of an electron beam in microelectronic fabrication
work is either as a tool, for example, as a method for heating materials
for evaporation work (1,30), or for processing materials with a high
resolution, or as a probe for obtaining information from the workpiece
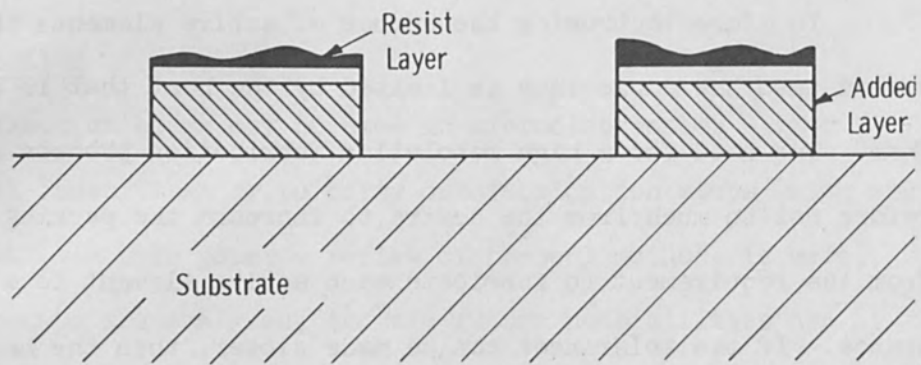to be used for process control.
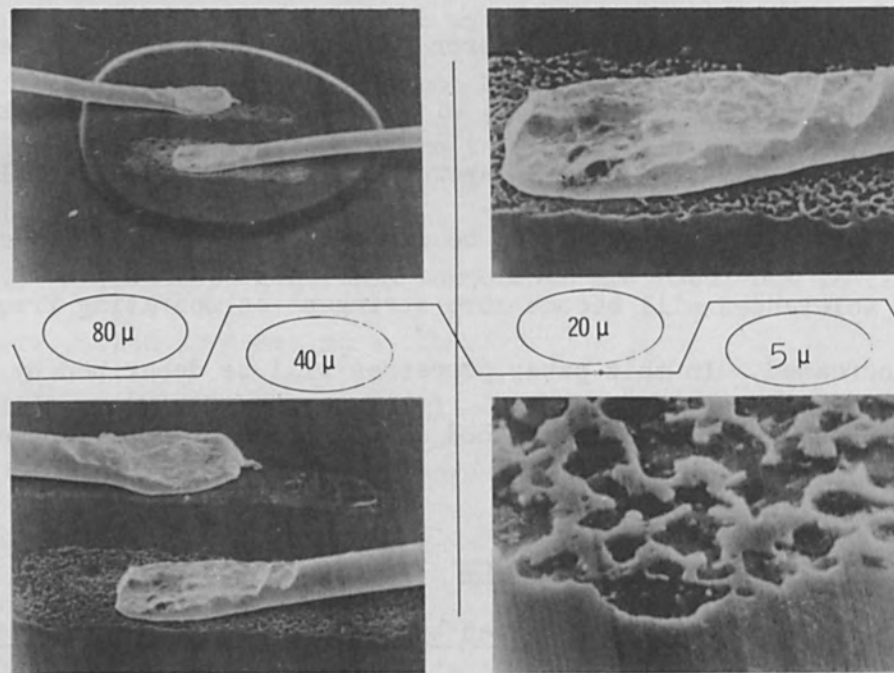
Figure 1. Ideal Etching Process

Figure 2. An Experimental n-p-n Silicon Mesa
Transistor as Viewed in the Scanning Electron
Microscope(12)

(b) Thermo-Compression Bonding (an example).

To begin the discussion with a specific example, it will be relevant to consider the thermo-compression bonding process, which is used for the attachment of lead wires to transistors. There are two ways by which this process might be developed by utilizing electron beams. The electron beam could either be used as a source of heat, for the purpose of carrying out the weld, in which case it would be said that the electron beam was being used as a tool; or else the electron beam could be used in the manner of the scanning electron microscope to obtain information from the workpiece so that the existing technique of using a mechanical tool to press a wire down into the workpiece could be carried out more accurately or even made automatic.

Examples of images obtained in the scanning electron microscope and relevant to this discussion will be given in Figs. 2, 3, and 4 below.

(c) A Discussion of the Ideal Fabrication Process.

Before discussing fabrication techniques it might be as well to pause and consider what the ideal fabrication process would consist of. In Fig. 1 a layer of some material is shown being deposited onto a substrate as a step in the fabrication process. This layer might either be a silicon dioxide mask to be used for controlling the diffusion of an impurity into silicon or else a layer of either conducting or dielectric material as required for the fabrication of the device.

To lay down such a layer in a satisfactory manner there are about seven or eight quantities each of which must be held within tolerance. There is the thickness and chemical purity of the material in the layer.

There is the adhesion and cleanliness of the interface. In addition, it may be necessary that the material in the layer should be strain-free. The outline of the layer must be defined with an adequate resolution and it must be correctly placed both as regards position and angle relative to the remainder of the workpiece. All of these quantities must be held within tolerance.

As an indication of the degree of purity that might be required at the interface, in the case of an oxide layer placed over silicon for purposes of passivation, it is only necessary to have one ten thousandth of a monolayer of ionic impurities present and the polarity of the surface layer of 1 ohm/centimeter silicon may be reversed, and the device may be unstable (16). It is for a similar reason that it is usual to form an oxide diffusion mask by oxidation of the silicon substrate, so that the interface may be kept as clean as possible.

In Fig. 1 a process has been illustrated in which an electron image or possibly an ion image has been used to form a resist layer which is then used to control the etching away of the underlying substance. In the ideal etching process it might be required to obtain a steep sided cut of controllable depth; it would definitely be required that a satisfactory action be obtained from the resist layer regardless of the degree of uniformity in the thickness of the resist layer, and for high resolution work it would be necessary that the method used for the formation of the resist layer should be economical in its use of electrons. In a practical case it may be desirable that parameters such as evaporation rate, deposit thickness, etching rate, etc., should be continuously monitored so that closed loop control may be applied.

In the resist method there is the advantage that practically all of the basic requirements may be quite closely met, but in a practical case it is convenient to have other approaches available as well. The direct composition method, the alloying method, and the evaporation mask method will be described below.

III. Present Techniques - I. Electron Probe Microscopy

(a) Scanning Electron Microscopy.

An example of an image obtained in the scanning electron microscope (2-12) is shown in Fig. 2. The object under examination was an n-p-n silicon mesa transistor and the thermo-compression bonded lead attachments may be clearly seen. In Fig. 3 the effect of applying a reverse bias to the emitter junction is shown, which is to render the p-n junction visible. It is also possible to obtain information from the workpiece by measuring the junction current as the electron beam is scanned or pulsed across.

In Fig. 4 a series of images obtained from a Westinghouse Type 2N615 germanium/indium alloyed junction transistor are shown, and the depth of focus that is obtained by this method in comparison with that obtained in the optical microscope is quite striking. A part of the problem, therefore, of applying electron beams to microelectronics will consist of investigating ways by which the methods of scanning electron microscopy and X-ray microprobe analysis may be applied for quality control and for process control. As stated above, it is considered that by the application of scanning electron microscopy it would be possible to supervise the attachment of lead wires to devices on a very small scale.

Experimental Silicon
N-P-N Mesa Transistor
  (A) Unbiassed
  (B) Emitter Junction
      Back-Biassed 4½ V.

40 µ
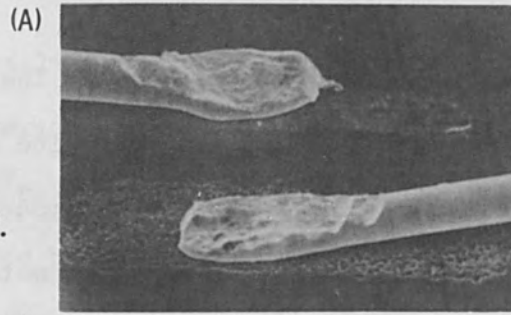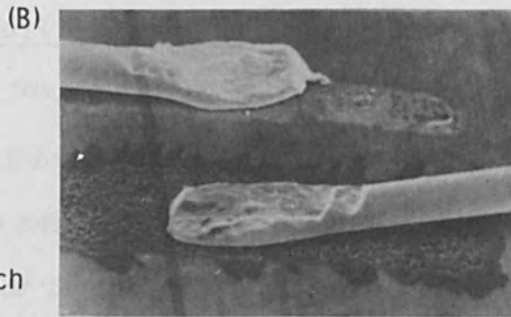
Figure 3. Comparison Photographs with the Emitter
Junction Unbiased and Back Biased, to Show the Posi-
tion of the Junction and to Demonstrate the Irregular
Diffusion, as Obtained in the Scanning Electron Micro-
scope.[12]

SCANNING ELECTRON MICROSCOPY

Westinghouse Type 2N615
Alloyed Ge/In Transistor:

120 µ

200 µ

Figure 4. A Westinghouse 2N615 Germanium-Indium Alloyed
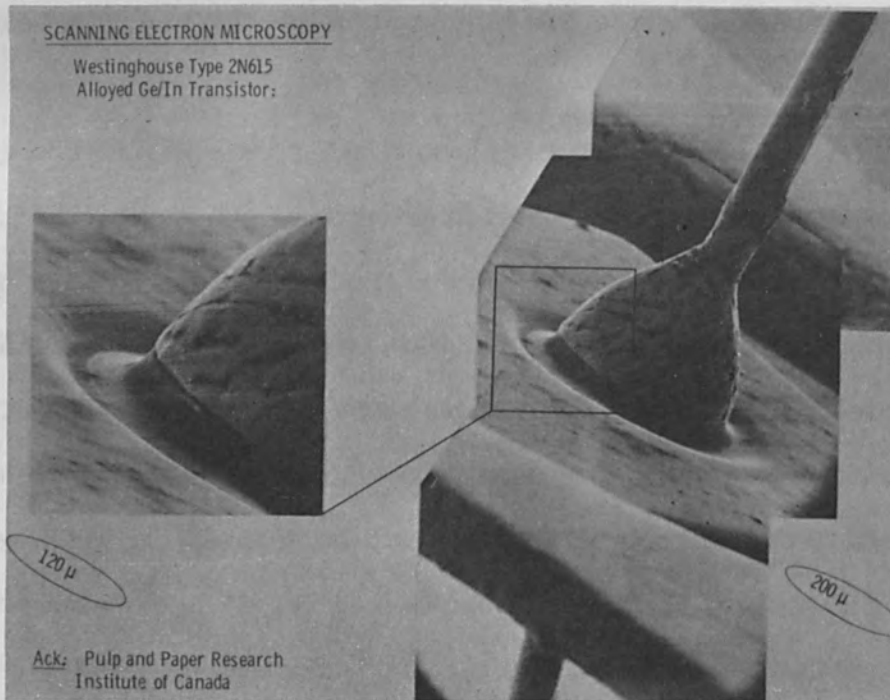Junction Transistor as Viewed in the Scanning Electron
Microscope.[12]

The manner of operation of the scanning electron microscope is shown in Fig. 5. An electron probe is scanned over an area of the workpiece, and a cathode ray tube is scanned in sympathy with it. The brilliance of the cathode ray tube is modulated either by the reflected electrons or else by the secondary electrons liberated from the specimen by the probe. In this way an image of the workpiece is built up point by point.

(b) X-ray Microprobe Analysis.

In the X-ray microanalyzer (13-15) an arrangement similar to the scanning electron microscope is used, except that it is the output of characteristic X-rays from the workpiece that is collected instead of the reflected or secondary electrons. By the X-ray method a positive identification of the workpiece material may be obtained, but the resolution is unfortunately limited in the region of 1 micron. The reasons for this limitation are firstly, that in order to generate the characteristic X-rays an incident electron energy of the order of 10 KV or greater is required, leading to a resolution limitation imposed by electron penetration; and secondly, owing to the very poor quantum conversion efficiency at the specimen when generating X-rays, a micron-sized beam must be used to ensure an adequate current. In the scanning electron microscope neither of these limitations apply and a resolution as good as 300 A.U. has been obtained (8).

The reasons why electron beams are thought to be superior to light beams for some of these applications are firstly that the resolution is sharper; secondly, that the depth of focus is very much greater for a

given beam diameter; thirdly, that the positions of p-n junctions may be indicated; and finally that by the use of an X-ray spectroscope a positive identification of the local workpiece material can be obtained.

(c) Selected Area Electron Diffraction.

By the methods of selected area electron diffraction (34) information concerning the state of cleanliness, crystal orientation and workpiece constitution may be obtained. As compared with the X-ray diffraction method, the atomic-scattering cross sections for electrons are much greater than for X-rays, so that the electron diffraction method is particularly suitable for the examination of very thin films (or surface layers) and small amounts of material (34).

IV. Present Techniques - II. Electron Beam Fabrication Techniques Utilizing the Thermal Effect

(a) The Electron Beam Welding and Drilling Processes.

The electron beam welding and drilling processes are illustrated in a greatly simplified manner in Fig. 6.

In Fig. 6(a) an electron beam is shown striking the workpiece and heating part of it. The volume that is heated will depend on the penetration of the electrons into the material, on the thermal properties of the material, and on the time cycle of the electron beam. Generally, if the electron beam energy is of the order of kilovolts and if the beam is switched on and off with an active period of the order of milliseconds, then the depth of this heated zone might be measured in microns. In Fig. 6 it has been assumed that the diameter of the electron beam is greater than ten microns.
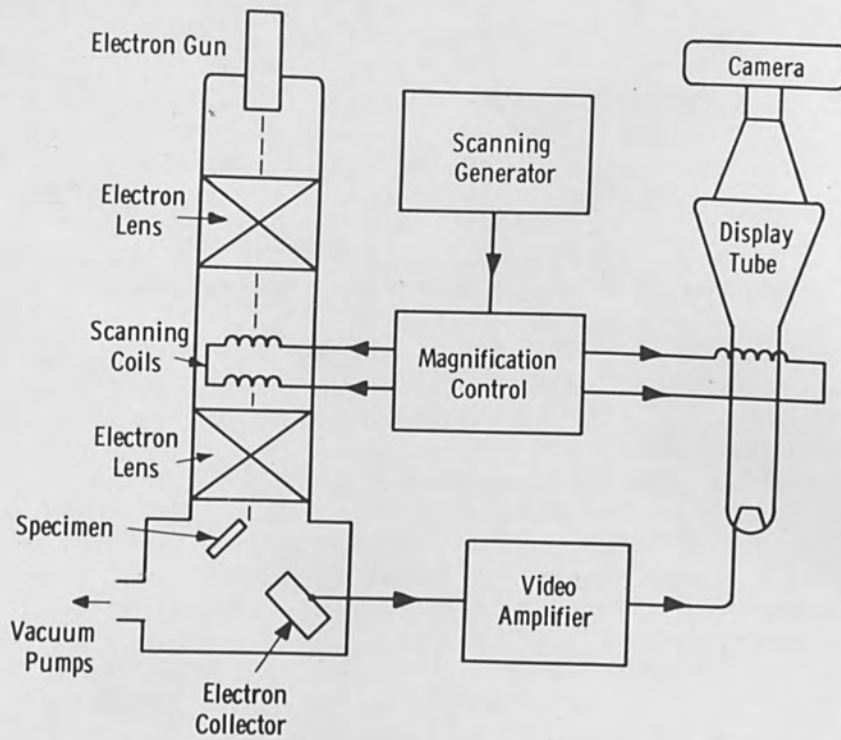
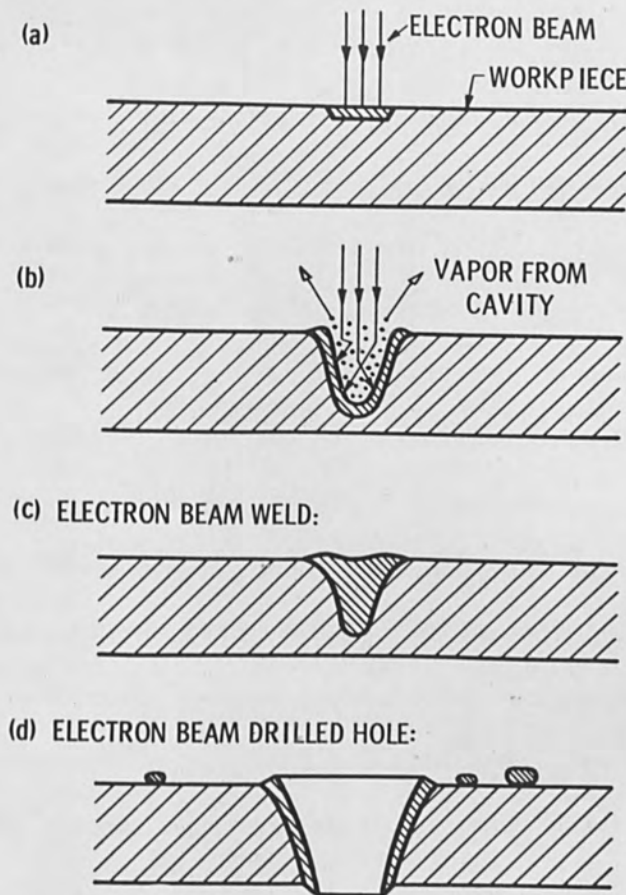Figure 5. Scanning Electron Microscope Schematic Diagram[4,5]

Figure 6. Simplified Diagram to Illustrate the Electron Beam Welding and Drilling Processes.

In Fig. 6(b) it has been assumed that the material of the work-piece has melted so that evaporation is taking place. The molecules of the material as they boil off will travel upwards with a significant momentum; and this momentum, by means of Newtons third law, will exert a downwards force on the liquid. The electron beam, therefore, will dig a cavity in the workpiece, the liquid material being pushed aside. This cavity will then move around the workpiece under the beam, the liquid material flowing from the hotter to the colder side as the electron beam moves across the workpiece. According to references cited by Burton and Frankhouser (22) the pressure exerted on the workpiece as a result of the momentum of the electrons can be neglected.

The material will flow round from the hotter to the colder side of the cavity because the speed of departure and also the number of the molecules will be greater on the hotter side, so exerting a greater force on the liquid surface.

In the case of the welding process this study is allowed to fill up again behind the beam to give a deep, narrow, weld as shown in Fig. 6(c). The quantity of material that is lost from the workpiece by evaporation will, in a practical case, be much smaller than the volume of the metal that was melted.

In the drilling process, the intensity of the bombardment and the degree of locallization is increased so that vaporization will occur beneath the surface of the melted zone, so that quantities of the molten material will be lifted bodily out of the hole and projected upwards. In addition, if the beam is pulsed then the lining of the cavity can be allowed to resolidify each time before the next pulse

arrives, so that the movement of the cavity under the beam does not occur. The sort of hole that may be drilled through a piece of material is as shown in Fig. 6(d). The walls of the hole slope outwards slightly and there is in many cases a crust present of melted and resolidified material.

On the upper surface of the material there is sometimes a raised ridge formed by the molten material pushed upwards by the pressure of the evaporating material, while on the surface of the material adjoining the hole there are sometimes refrozen globules of material from the hole. The shape in which the liquid resolidifies is determined partly by surface tension. These features have been somewhat exaggerated in Fig. 6(d) for the sake of clarity.

A typical set of curves showing the dependance of weld depth and weld depth-to-width ratio are shown in Fig. 7, showing the manner in which both of these quantities increase rapidly as the incident electron energy is raised (22). In a practical case, if it is assumed that the density of the gas in the cavity is 10^{-4} times the density of the solid material then for each centimeter depth of the cavity there will be a scattering power equivalent to approximately 1 micron of the solid material*. The high energy of the electrons necessary to achieve a deep weld is therefore required not only so that an adequate power density may be obtained, but also so that the electron beam may penetrate the vapor without excessive scatter. The cross-section of a single pass

---

*note added in proof - The precise action will be complicated by the ionization of the gas in the cavity and by the non-equilibrium nature of the process.
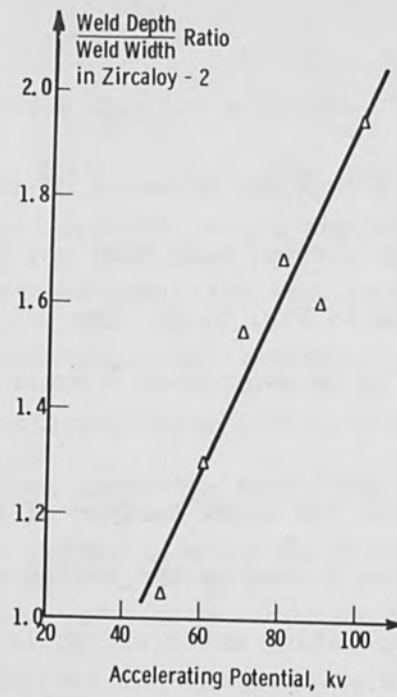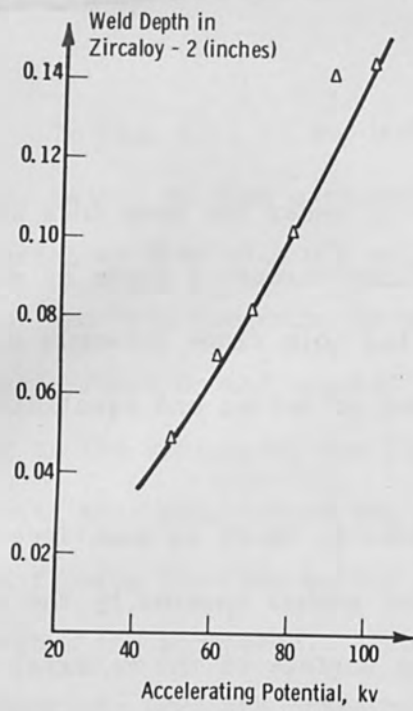
Figure 7. Electron Beam Weld Characteristics
(Experimental Points after Reference 22).
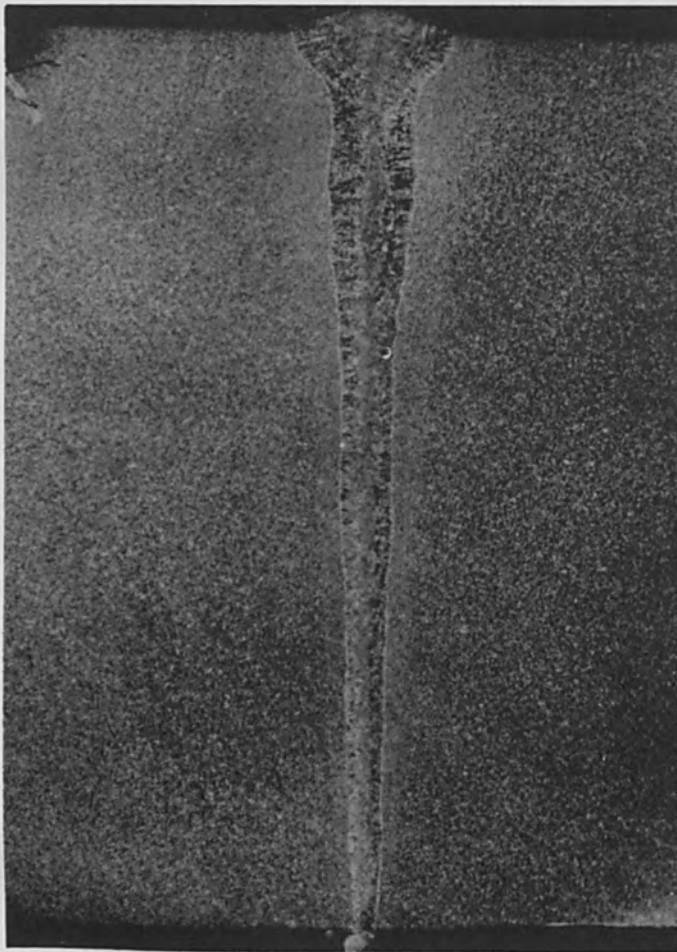
Figure 8. Cross section of One-Pass Weld in 0.4" Thick Stainless Steel Using 2 Kw Electron Beam Welder(24)

electron beam weld in 0.4" thick stainless steel is shown in Fig. 8 (24).
The narrowness of this weld is most striking. The problem, then, is to
find ways by which such techniques may be applied to microelectronics.

(b) The Cutting of Resistors.

In Fig. 9 the use of the electron beam is shown for cutting
grooves in metal films for the production of resistors (24). The
resistive material, which might be a nickel chrome alloy, typically
100 A.U. thick, is deposited on a ceramic substrate and the electron
beam is then used to remove areas of it to form nonconducting paths.
The resolution demonstrated here is of the order of ten microns. In
this application there is the possibility of monitoring the resistance
value as it is being cut.

There would appear to be no reason why a conducting coating
laid down onto a ceramic substrate by the vapor deposition process (18)
could not also be cut by this process to give conducting as well as
resistive paths.

For applications involving semiconductors this method has the
disadvantage that the surface of the material is damaged. As the physical
dimensions of any device are reduced, the ratio of surface area divided
by enclosed volume becomes greater, and for semiconductor work a great
emphasis must therefore be placed on the development of methods for
cutting and shaping materials so as to leave a clean exposed surface
that is free from strains, otherwise the recombination of carriers and
the existence of unwanted energy levels at the surfaces will interfere
with the operation of the device.
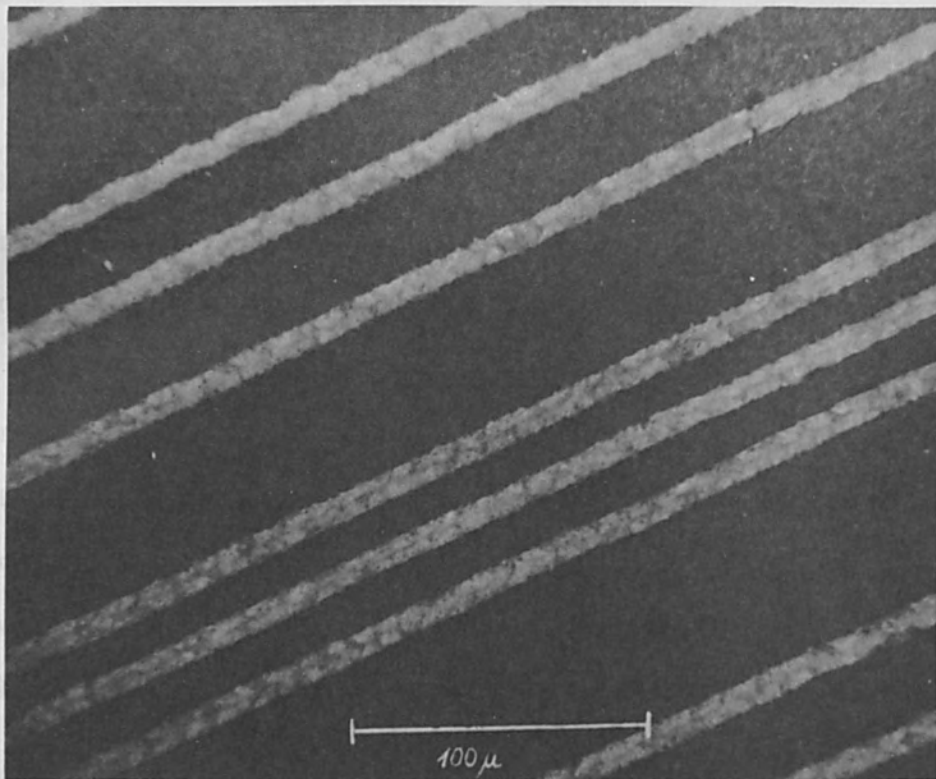
Figure 9.   Cutting of Nickel-Chrome Resistor Film
on Ceramic Substrate[24]
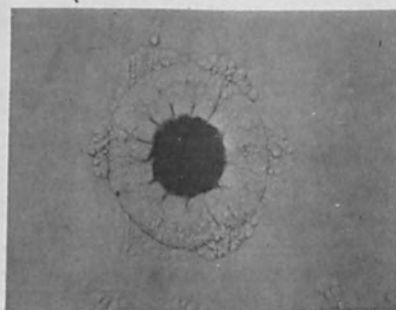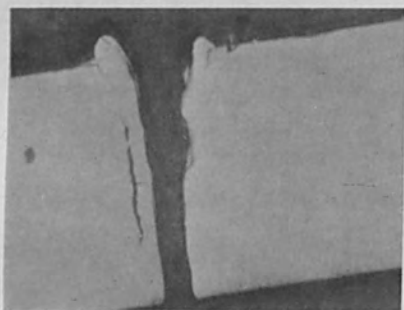
Figure 10.   Electron Beam Cutting of Germanium

In Fig. 10 some typical electron beam work on germanium is shown. In Fig. 10(a), the presence of a melted and resolidified lining on the sides of a cut made through a germanium dendrite can be clearly seen. For the drilling of holes in ferrite and certain other materials a much cleaner cut than is shown in Fig. 10(a) can be obtained. In Fig. 10(b) an area on the surface of a germanium has been melted and then allowed to refreeze, and the sample has then been given a brief etch. The presence of dislocation clusters in positions related to the crystal structure can be seen. The material surrounding the refrozen zone has been found to be under strain. However, in spite of these strains, the material inside the refrozen zone was found to be recrystallized in the same orientation as the original lattice. In Fig. 10(c) the effect of a 20 second CP4 etch on this sample is shown which is to reduce it to a pyramid oriented in line with the crystal lattice.

(c)   The Formation of p-n Junctions.

There has been some interest in the formation of p-n junctions by the electron beam. The possibility of doing this was described by W. Shockley (25). The method is to deposit a layer of impurity onto the semiconductor and then to raise the temperature locally to produce alloying. The unalloyed impurity layer is then selectively etched away. It is expected that a resolution of the order of 5 microns can be obtained by this method*. Work on the formation of p-n functions by the electron beam method has also been initiated by the CBS Laboratories (27,28).

---

*An analysis of the heat flow will not be given here. For the heat flow analysis in a thin film see reference 26.

(d) Chemical-Assisted Methods.

As a clue to a possible approach by which the resolution might be improved and by which the degree of strain in the material might be reduced, the diagram reproduced in Fig. 11 was published by K. H. Steigerwald in his U. S. Patent No. 2,793,281 referring to the drilling of holes with electron beams. With reference to it Steigerwald writes:

"In attempting to drill holes in diamonds, I have found that the temperature to which my electron stream raises the diamond is of the order of 3000°C. But diamonds even at temperatures of the order of 2000°C tend to disintegrate into graphite. I accordingly have found, that I can achieve the required drilling by a chemical reaction. To this end, I admit oxygen into the area where the electron stream impinges upon the diamond. In this case, I control the electron stream as described hereinabove to a lesser intensity and raise the temperature of the diamond only to a temperature of the order of 300°C.

At this temperature, the carbon in the diamond will combine with the oxygen to form CO_2 or CO. In effect, therefore, I burn away the diamond to form the minute hole therein as described."

The advantages of such a method if it could be applied more widely are firstly, that a finer resolution is obtained; secondly, that the strain in the material is reduced; and thirdly, that the presence of the melted and resolidified layer is avoided. It is to be expected that if a thin film of material to be cut by this process is laid on top of a very thin silica layer with a substrate or with other thin
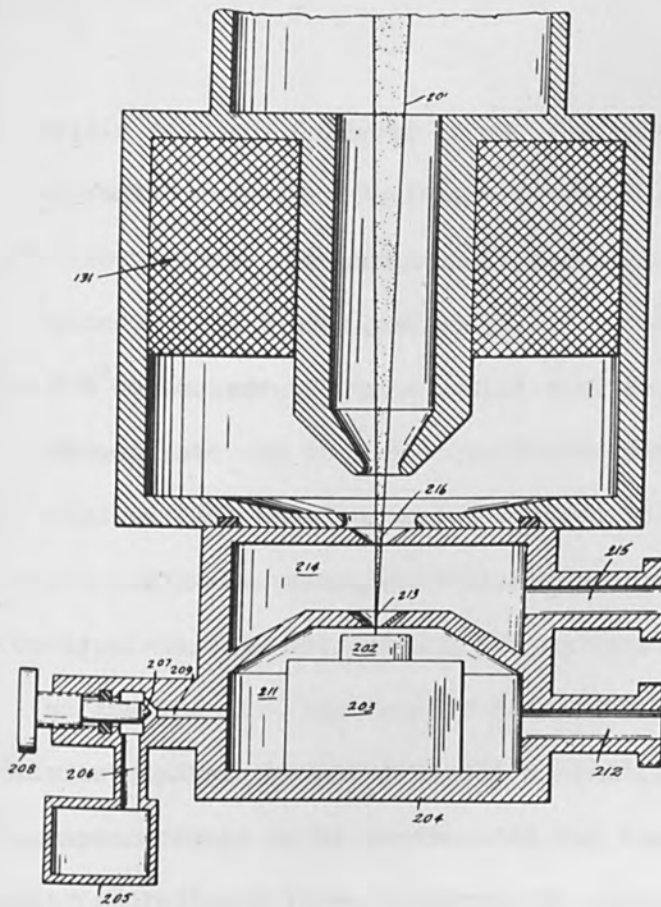
Figure 11. Diagram
from U. S. Patent
2,793,281

Electron
Beam

Etchant Chemical Vapor

Metal
Layer

Silica Resist
Layer

Substrate
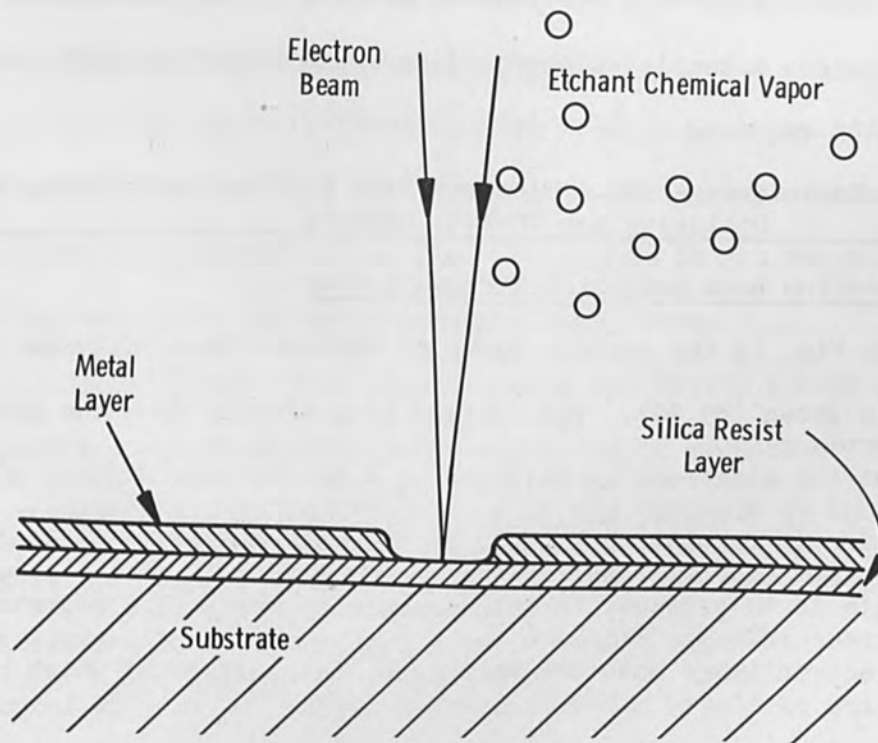
Figure 12.   Chemical-Assisted Electron Beam Drilling

films underneath (as shown in Fig. 12), then, provided that the silica is able to withstand the action of the chemical etchant used, fine lines may be cut in the upper film without damaging the structure underneath, even though the underlying layers might be heated locally to the same temperature as the surface film. Also, by the use of a mass spectrometer to detect the chemical byproduct of the reaction it is expected that an indication of correct focus could be obtained.

For the development of a fabrication process having a resolution of the order of 0.1 microns the penetration of the electrons into the material must be no greater than this amount. In a practical case this will impose an upper limit on electron energy of the order of 5 keV. The amount of energy that can be conveyed in an electron beam of this diameter and at this energy is extremely small, so that for the successful development of a fabrication process to operate with a 0.1 micron resolution a sensitive chemical-assisted (preferably non-thermal) method will be required.

V. Present Techniques - III. Electron Beam Fabrication Techniques
Utilizing Non-Thermal Effects

(a) Electron Beam Activated Micromachining.

In Fig. 13 the process known as electron beam activated micro-machining is shown (29,30). This method is different from the previous ones in that the electrons as utilized in a non-thermal manner, so that the limitation on resolution imposed by thermal conduction is avoided. The principle is to project, in this example by means of a magnetic lens, an electron image onto the workpiece, the surface of which has been

covered with a layer of a chemical such as triphenylsilanol. This chemical has the property that under electron bombardment a latent image is produced, which can be converted into a silica mask by heating the specimen to 200°C. A gaseous etch is then used to remove the unprotected parts of the workpiece. In these micrographs a resolution better than 0.1 microns is demonstrated, and there is the probability that even the degree of resolution demonstrated here can be improved. This work was carried out by K. R. Shoulders at the Stanford Research Institute (30).

The protective silica layer used in this method may either be obtained by the decomposition of a solid layer as described, or by the decomposition of a vapor admitted into the system. There are advantages and disadvantages in each case. The use of such a layer for the control of a subsequent electrodeposit has also been described (31,32).

(b) The Molecular Beam Etching Process.

In Fig. 14 the gaseous etching process is shown being carried out at reduced pressure, so that instead of having the etchant gas incident on the surface of the workpiece from all angles it can be collimated to form a molecular, or in some cases an atomic, beam.

It is evident that if an etchant gas having a high reaction efficiency can be found, and if the migration of etchant across the surface of the workpiece can be eliminated and if the pressure in the etching chamber is low enough then a steep-sided cutting action will be obtained (30). A consideration of the mean free paths involved suggests that an etchant pressure of 10^{-4} or 10^{-5} millimeters of mercury should be suitable and that a cutting speed of 0.1 microns or 0.01 microns per second should be feasible. The ability to obtain a steep-sided cut will be important for

Mask Illuminated
With Electrons

Demagnifying
Electron
Lens

50 AU Layer of
Triphenylsilanol

(a) 200 Å Mo ON 200 Å AL$_2$O$_3$
(b) 200 Å Si ON 100 Å SiO$_2$

(a)

├─────┤ 0.5 μ

(b)

├─────┤ 5 μ

Figure 13. Electron Beam Activated Micromachining[30]

(a)

SiO$_2$ Resist
Layer

Substrate

Angle of Collimation
of Etchant

Profile With
Liquid Etchant

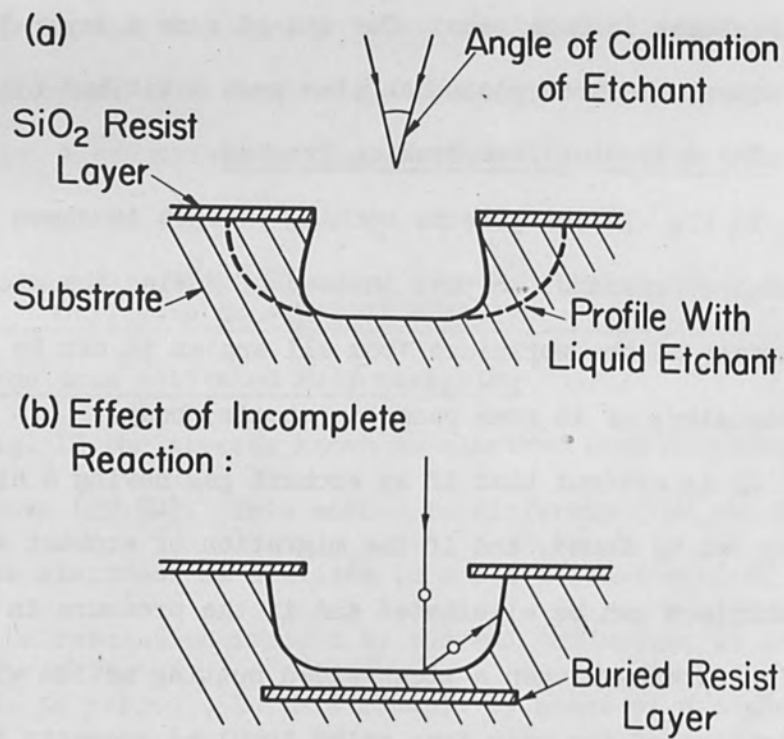(b) Effect of Incomplete
Reaction :

Buried Resist
Layer
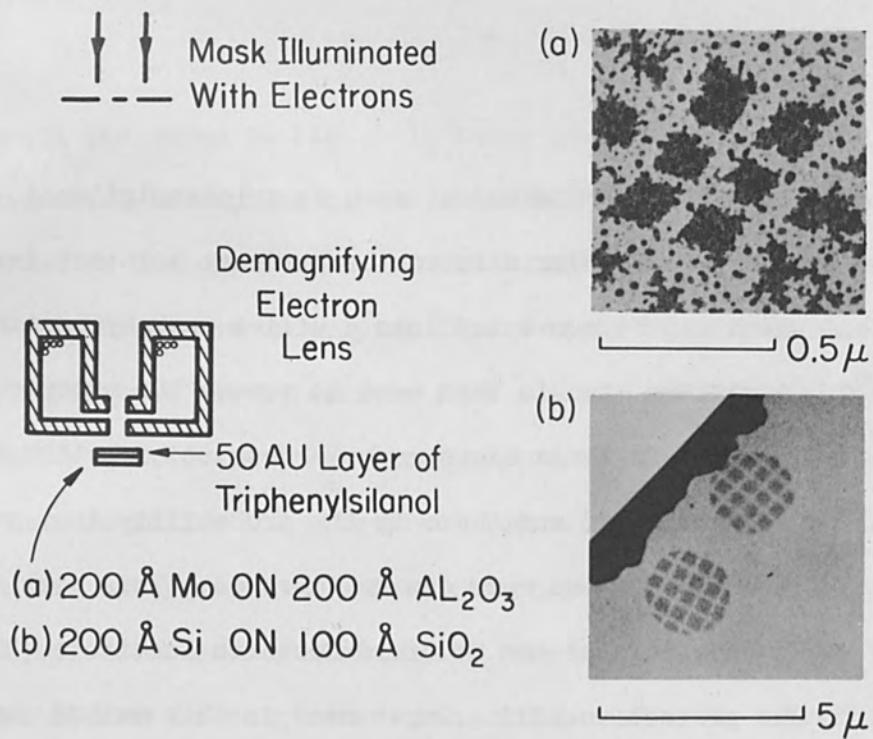
Figure 14. The Molecular Beam Etching Process

312

certain types of microcircuit in which the thickness of the layers is
of the same order of magnitude as the horizontal dimensions involved.
For thin film work this method makes it possible to work on the surface
layer without damaging the layers underneath.

In   Fig. 14(b)   the effect of an incomplete
reaction between the etchant and the workpiece is shown, which is to
undercut the resist. This undercutting can be reduced by raising the
temperature of the workpiece, by the use of an atomic instead of a
molecular etchant beam, by the use of a flood electron beam, or in some
cases by the use of an etchant in solid form (30). A similar effect
occurs if the gas pressure in the vacuum chamber is too high so that
scattering occurs. This may be compared with the outline shown in the
upper section of the slide obtained by the use of a liquid etch. The
use of chlorine to etch either silicon (16,30,33) or molybdenum (29,30),
or the use of carbon tetrachloride vapor to etch metal oxides (29), or
the use of phosgene to etch aluminum oxide, in each case with a silica
resist layer; or the use of hydrogen fluoride to etch silica protected
by aluminum oxide; and a number of other combinations, have been described (30).

(c)   The Direct Decomposition Method.

In the direct decomposition method (17,20,29,30), a vapor is
admitted into the vacuum system at a pressure of 10^{-4} mm Hg and forms a
monolayer on the surface of the workpiece. This monolayer may be decomposed
by the electron beam to give either an insulating or a conducting deposit,
depending on the vapor used. It is believed that a high resolution deposit
may be obtained in this way. This method is similar to the electrical
discharge method for depositing dielectric layers (19).

The advantages of this method are:

(i) The deposit is obtained directly, so that intermediate steps are not required;

(ii) by admitting different vapors into the system in turn a series of deposits may be obtained in sequence;

(iii) by interrupting the supply of vapor into the vacuum system the electron beam may be used to locate and to examine the workpiece without causing a deposit (provided that the vacuum is sufficiently good).

The disadvantages of this method are:

(iv) To deposit N monolayers a number of electrons is required that is N times the minimum number as defined by the shot noise in the electron beam. This may impose a limit on high resolution work.

(v) There is the possibility that the deposit may be contaminated by decomposition byproducts from the diffusion pump oil.

(vi) To prevent the formation of deposits in the electron optical system a metal lining held at a temperature of $250^{\circ}C$ will be required. (this is to prevent the formation of a monolayer.)

(d) Photoresist Techniques.

For the exposure of photoresist coatings electron irradiation can be used in place of visible light. This method offers a potential improvement in resolution and also the possibility that by the investigation of novel chemicals a more tenacious and acid-resistant mask may be obtained. This method also admits the possibility of locating the outlines of the workpiece by means of the electron beam before the exposure of the photoresist is carried out.

(e)   The Evaporation Mask Method.

The final method by which the electron beam may be used to control the high resolution deposit of a substance onto a substrate is by controlling the position of an evaporation mask relative to some feature or features of the workpiece by the methods of scanning electron microscopy so that some material may be evaporated through it in the conventional manner.   This method is complicated but has the advantage that a wide range of materials may be used.

V.   Future Techniques

(a)   Future Developments of the Technique.

For the future development of the technique it is clear that there are three potential areas of development:

(i)   In which the electron beam is to be incorporated into production processes without any further delay.   The cutting of resisting and conducting paths on a ceramic substrate is an example of a process that could be utilized immediately for production work.

(ii)   In which the use of the electron beam as a source of localized heating is further developed to carry out such operations as localized alloying of semiconductors or chemical-assisted cutting of materials with a fine resolution.   If such methods are to be successfully utilized for production work it would appear to be essential to improve the instrumentation of the apparatus so that the methods of closed loop control can be applied.

(iii)   In which electron beams of sub-micron diameters are
to be utilized in a non-thermal manner for high resolution fabrication
work.

(b)   Fabrication Techniques Utilizing Electron Beams of Sub-Micron Diameters

Perhaps it should be emphasized that the reason why it is
desirable to work with sub-micron sized electron beams is not so much
so that extremely small components may be fabricated, or so that
extremely high packing densities may be obtained, but rather so that
components of present day size might be fabricated to closer dimensional
tolerances, which is considered to be essential if a satisfactory degree of uni-
formity, yield and reliability is to be obtained. In the remarks which
follow it will be assumed that the electron beams are of sub-micron size.

Specifically, the work should be directed

- to provide methods for working as wide a range of materials as
possible at high resolution;

- to provide methods for working as wide a range of materials as
possible without introducing strain into them;

- to provide methods for working as wide a range of materials as
possible without introducing unwanted contaminating substances into them;

- to provide methods for coordinating one high resolution process
with another; and more generally

- to develop the methods of electron probe microscopy to give quality
control and process control.

A form of apparatus in which the facilities required for scanning
electron microscopy, materials deposition, vacuum etching, and so on, all

in the same ultra-high vacuum enclosure, has been described in the literature (30) and there are a number of variants of this scheme which could be proposed. Even without the assumption of any advances being made in our knowledge of resist formation and molecular beam etching techniques there are a number of attractive types of micro-circuit that could be fabricated, and with further progress it is expected that the prospects will still further increase.

(c) The Coordination of One High Resolution Process with Another.

For the coordination of one high resolution process with another it would seem that the methods of scanning electron microscopy or of X-ray microprobe analysis would be suitable. Using either of these methods or a combination of them, for example, the position of an evaporation mask could be adjusted over some feature of the workpiece with a greater accuracy than could be obtained by optical means. The decomposition of a chemical on the workpiece in some position accurately located relative to structure already present could also be carried out. Other possibilities suggest themselves as well.

If the field of view to be scanned contains more than about 10^8 picture points (equivalent to 10,000 television lines) then an accurate mechanical traverse mechanism in addition to beam deflection will be required. A careful attention to image distortion and image rotation will also be required.

(d) The Attachment of Leads to the Completed Devices.

For the attachment of leads to the completed devices there are a number of schemes that have been suggested in the literature and

the usefulness of the electron beam might be either as a tool in one of the manners described, or as a method for obtaining information to be used in process control. It would not seem that there will be any simple solution to this part of the problem.

VII. Summary

         To summarize, it has been demonstrated that electron beams can be applied either as a method for working material with high resolution; and as a method for coordinating one high resolution process with another; and as a method for obtaining information to be used in quality or process control. If, as is it believed will be the case, it turns out to be necessary to work with resolutions of the order of one tenth to a micron, then the electron beam will provide a way by which this can be done.

         In addition, other applications of electron beams such as for the vaporizing of materials for evaporations or for the local heating of substrates are likely to be of use.

VII. Acknowledgments

IX: REFERENCES

1. Thun, R.E., Proc. Second Symposium on Electron Beam Processes (Alloyd Corporation), p. 70, (1960). For a description of the evaporation rate monitors, see Reference 30 or Giedd, G.R., and Perkins, M. H., Rev. Sci. Inst. $\underline{31}$, p. 773 (1960).

2. Knoll, M. Z., Tech. Phys. $\underline{16}$, 767 (1935).

3. Zworykin, V. K., Hillier, J., Snyder, R. L., Bull. Amer. Soc. Test. Mater., $\underline{117}$, 15 (1942).

4. McMullan, D., Proc. Inst. Elect. Engrs., $\underline{100}$, (II), 245 (1953).

5. Smith, K.C.A., Oatley, C. W., Brit. J. Appl. Phys. $\underline{6}$, 391 (1955).

6. Oatley, C. W., and Everhart, T. E., J. Electron., $\underline{2}$, 568 (1957).

7. Everhart, T. E., Smith, K.C.A., Wells, O. C., and Oatley, C. W., Proc. Fourth International Conference on Electron Microscopy, Berlin 1958, p. 269 (Springer-Verlag, Berlin, 1960).

8. Everhart, T. E., Wells, O. C., and Oatley, C. W., J. Electron. $\underline{7}$, 97 (1959).

9. Wells, O. C., J. Electron., $\underline{7}$, 373 (1959).

10. Smith, K.C.A., Pulp and Paper Magazine of Canada, Technical Section, p. 3 (December 1959).

11. Thornley, R.F.M., Proc. Delft. Conf. on Electron Microscopy (1960).

12. Lindsay, R. L., Pulp and Paper Research Institute of Canada, private communication. (1961)

13. Hillier, J., U. S. Patent 2,418,029 (1947).

14. Castaing, R., Guinier, A., Proc. Conf. Electron Microscopy, Delft, (1949) (Delft: Martinus Nijhoff).

15. (Survey Papers) Duncumb, P., Brit. J. Appl. Phys. $\underline{11}$, 169 (1960); Birks, L. S., Analytical Chemistry $\underline{32}$, 19A (1960); Castaing, R., Electron Probe Microanalysis, Advances in Electronics and Electron Physics (ed. L. Marton $\underline{13}$, 317 (1961). See also Ogilvie, R., (this symposium).

16. Atalla, M. M., Tannenbaum, E., and Scheibner, E. J., Bell System Tech. J. $\underline{38}$, 749 (1959).

17. Baker, A. G. and Morris, W. C., Rev. Sci. Inst. (in press). See also Quarterly Progress Report No. 12, Lincoln Laboratories (1961).

18. Powell, C. F., Campbell, I. E., and Gonser, B. W., "Vapor-Plating," J. Wiley and Sons, New York, 1955.

19. Grand, S. and Kraus, A., Proc. 1960 Electronic Components Conference (Washington, D. C.), p. 19 (1960).

20. Christy, R. W., J. Appl. Phys., $\underline{31}$, 1680 (1960).

21. According to Burton and Frankhauser[22], the earliest operation of electron beam welding was by K. H. Steigerwald in West Germany in 1950. The earliest publication of results was Stohr, J. S., "Electronic Welding of Metals," Fuel Elements Conference, Paris, pp. 18-23, November 1957. The earliest reference to electron beam melting is M. Von Pirani, U. S. Patent 848,600 (1907). For a bibliography, see p. 143 of the 1960 Alloyd Electron Beam Symposium Proceedings. See also K. H. Steigerwald (this symposium).

22. Burton, G., and Frankhauser, W. L., Welding J., $\underline{38}$, 401S (1959).

References - Continued

23. K. H. Steigerwald, U. S. Patent 2,793,281 (1957).

24. Nyenhuis, H. A., Hamilton Electrona, Inc., private communication, (1961).

25. Shockley, W., U. S. Patent 2,816,847 (1957).

26. Reed, F. K., _Thesis_, MIT (September, 1959).

27. Second Quarterly Progress Report, Contract DA 36-039 SC-85337 (December, 1960).

28. See Also "Electronics," p. 79 (November 25, 1960).

29. Buck, D. A. and Shoulders, K. R., "An Approach to Microminiature Printed Systems," Special Publication T-114, Proc. Eastern Joint Computer Conference (December, 1958).

30. Shoulders, K. R., publication number PB171027, Office of Technical Services (1960). See also Shoulders, K. R., Proc. Western Joint Computer Conference, May 3-5, San Francisco (1960).

31. Hirsch, E. H., Brit. J. Appl. Phys., 11, 547 (1960).

32. Möllenstedt, G. and Speidel, R., 1961 International Solid-State Circuits Conference (Philadelphia), _Abstract_ (1961).

33. Tannenbaum, E., J. Appl. Phys. 31, 940 (1960).

34. Hall, C. E., Introduction to Electron Microscopy (McGraw-Hill, N. Y.) 1953. See also Pinsker, Z. G., Electron Diffraction Structure Analysis and the Investigation of Semiconducting Materials, Advances in Electronics and Electron Physics (ed. L. Marton) 11, 355 (1959).

HIGH ACCURACY THICKNESS MEASUREMENT
OF
ELECTRON TRANSPARENT EVAPORATED SILVER FILMS

By
Helmut R. Poppa
Staff Scientist
Electronics Research Laboratory
Convair Astronautics
San Diego, California

ABSTRACT

High accuracy thickness measurements of evapor-

ated silver films by electron absorption measurements in

an electron microscope are discussed. The method is

particularly applicable to the detection of removal of

surface layers of electron transparent thin film specimens.

Details on the approach, calibration procedure and sensi-

tivity of the measurements are presented.   The removal

of a single mono-layer can be detected.

HIGH ACCURACY THICKNESS MEASUREMENT OF

ELECTRON TRANSPARENT EVAPORATED SILVER FILMS

By Helmut Poppa

Electronics Research Laboratory, Convair-Astronautics

San Diego, California

INTRODUCTION

An appreciable number of methods for thickness measurements of thin films are well known and discussed in great detail in (1). Most of these methods are indirect and refer to the optical properties of thin films. The only direct one which has been developed to a very high degree of reliability and accuracy within the last years is Tolansky's technique of multiple beam interferometry. In any case, however, these techniques are quite elaborate, especially for thickness measurements below 100 $\overset{o}{A}$ and sometimes involve the destruction of the test specimen.

The purpose of this investigation was to test the reliability and accuracy of electron absorption measurements for thickness determinations, mainly in order to develop a method that can easily be used in connection with electron microscope work on thin films. The strict applicability to electron microscope and electron diffraction work imposes some severe restrictions on the technique to be used, e.g. handling of the specimen without removal from the vacuum and determination of the thickness of very small areas preferably in the order of some μ^2. These objectives can hardly be achieved by other than electron optical means. On the other hand, this type of thickness measurement is of course limited to films which are electron transparent.

Thickness measurements by electron absorption is not a new technique and a number of workers have already used it successfully. (2), (3), (4), (5). Reiner (5) probably has conducted the most extensive study on thickness determination of various evaporated metal layers (Ag, Au, Bi, Sb, Cu, Al, Mn, Ni). His results, however, were not too promising for some of the materials which he tested, especially not for gold and silver. Because of a lack of data concerning the accuracy of his calibration process it was impossible to decide whether more satisfactory results could eventually be obtained. It was hoped that another method of calibration and an improved experimental setup would yield the accuracy of thickness determination which was needed.

A number of interesting applications with regard to the growth and structure of thin films are on hand, for instance, in the field of epitaxy quantitative data concerning the removal or growth of additional surface layers is very badly needed as would be data regarding a controlled etching process of thin film substrates in vacuum. Experiments of this type will be conducted using an already existing auxiliary apparatus attached to the specimen chamber of the electron microscope which permits the thin film specimen to be etched by sputtering or coated by evaporation without being removed from the vacuum.

Experimental Procedure

The process of scattering of electrons in thin films is extremely difficult and not enough theoretical knowledge has been accumulated as yet to allow an accurate calculation of the scattering parameters. However, it

is well known that the simple absorption law holds experimentally for the part of the electron beam passing undeviated through a thin film:

$$\frac{I}{I_o} = e^{-\alpha d} \tag{1}$$

(I_o = electron beam intensity before passing through the film; I = intensity after passing through the film; d = film thickness; α = absorption constant).

The absorption constant α had to be calibrated and because of the highly accurate thickness measurements obtainable with multiple beam interferometry the Tolansky method was chosen. Other reasons for selecting the Tolansky method were that the actual geometrical thickness is directly measured and that light microscopic small areas can be selected and measured. In addition to electron absorption experiments light absorption measurements were also employed in order to find out if and to what extent the rather elaborate Tolansky measurements could be replaced by simple light transparency tests for future calibration purposes.

1. Preparation of specimens: Electron microscope specimen grids with a collodion support were placed on partly collodion covered microscope slides and the whole arrangement was masked in such a way that only half of each grid was exposed to a silver evaporation source. Four microscope slides were placed at different distances from the evaporation source. After evaporation the specimen grids were removed from the microscope slides which were used for light absorption and Tolansky measurements at locations as close as possible to the

325

location of the grids. The electron microscope specimens were either
directly measured using the collodion foil as support during exposure
to the electron beam or the collodion was dissolved before examina-
tion, or the silver collodion layer was covered by another carbon
support layer and the collodion dissolved later.

2. Tolansky measurements: The accuracy that can be obtained by Tolansky's
   multiple beam interferometry (6) depends upon the sharpness of the
   interference fringes. Three major prerequisites have to be met for
   the production of extremely sharp fringes:

   (1) Use of fringes of low order.
   (2) Silvering of the test specimen to exact values of reflection and
       absorption.
   (3) Use of exactly parallel monochromatic light.

   All but the last prerequisite can easily be fulfilled if the speci-
   mens are tested using a normal light microscope for observation. To
   overcome this difficulty without alteration of optical parts a method
   of photographic densitometry was employed (7). As an example of what
   can be achieved by this technique, fig. 1a shows a Tolansky pattern
   without and fig. 1b the same pattern with application of this photo-
   graphic technique. Thus very sharp interference fringes could be ob-
   tained at magnifications up to about 200X.

3. Light Absorption Measurements: A metallograph light microscope was
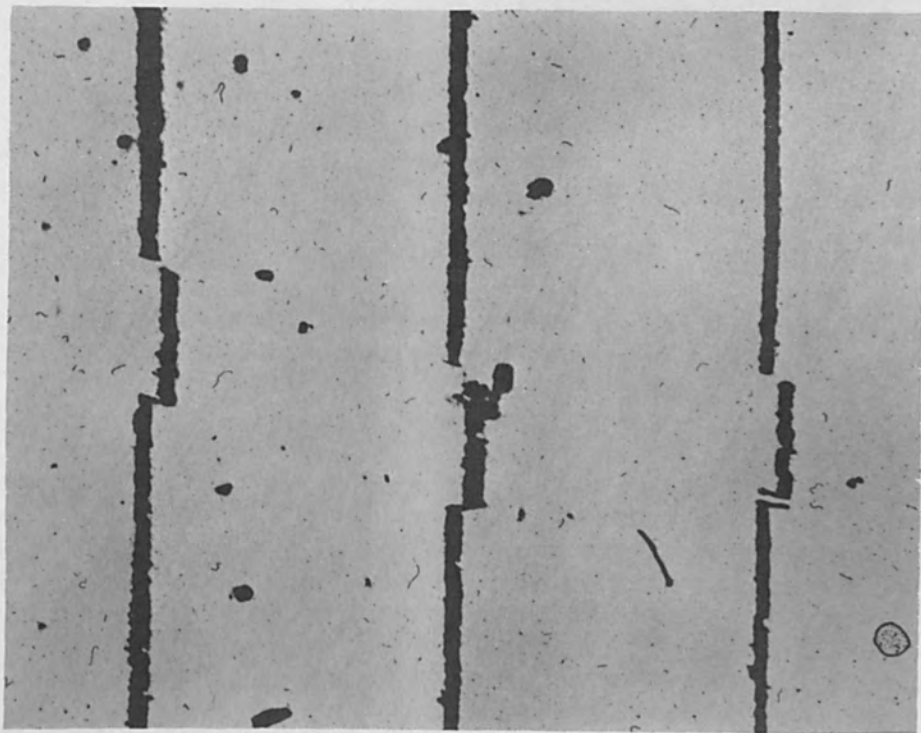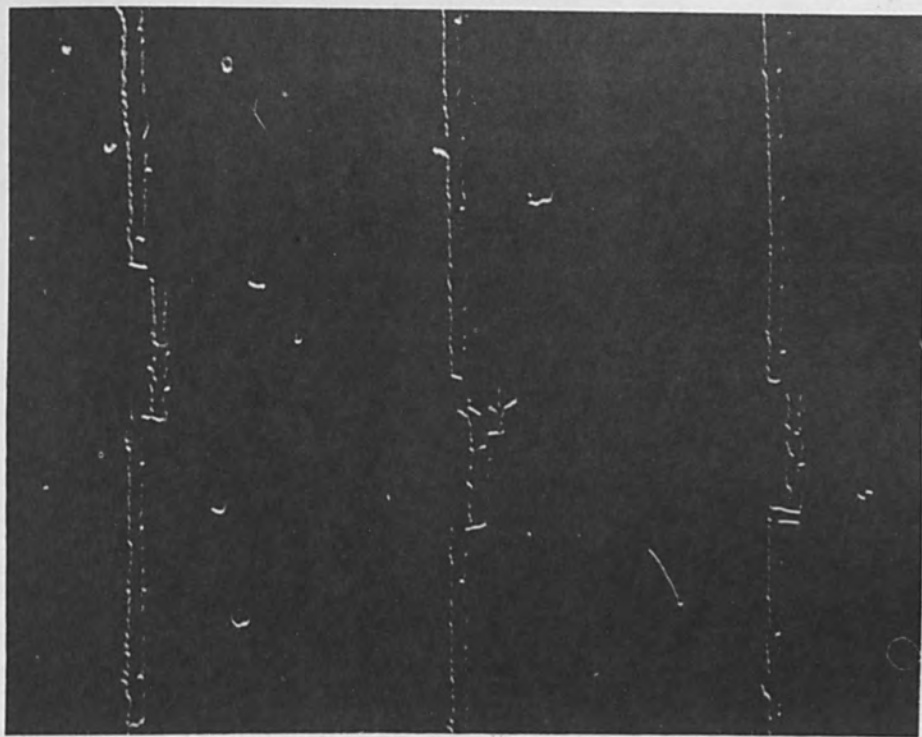   used and a variable aperture introduced into the illuminating system

Figure 1 (a)

Figure 1 (b)

Figure 1. Light micrographs (200X) of multiple beam inter-
ference fringes of an evaporated and scratched silver film
on glass; (a) fringes without and (b) fringes with application
of photographic densitometry technique.

so that a specimen area of about $(100\,\mu)^2$ was tested. The light intensities at $\lambda = 6900\,\overset{\circ}{A}$ were measured by means of a photoresistor attached to the final viewing screen of the scope.

4. Electron Absorption: According to equation (1) two intensity measurements I_o and I of the undeflected electron beam are necessary for thickness measurements by electron absorption. To accomplish this the electron microscope was operated as a selected area diffraction camera using a dopple condenser system to achieve a relatively small area of illumination of the specimen using an adjustable Faraday cage located above the final viewing screen. The electron current was measured by an electrometer connected to a recorder.

As can be seen from fig. 2, which is a ray diagram for selected area diffraction, the diffraction pattern on the screen is caused only by the small area of the specimen that is not masked by the field limiting aperature. The center spot of the diffraction pattern thus corresponds to the undeflected electron beam passing through the unmasked portion of the specimen. The electron beam current density at the center spot is measured with a Faraday cage of an aperture of 1 mm ϕ. This means that at a certain magnification of the projector lens the aperture of the recorded electron beam is about 10^{-3} rad. The fact that the aperture of the recorded beam is very small could be to some extent responsible for the somewhat different results that Reiner (5) reported since the aperture of the recorded electron beam was almost 20 times larger in his experiments.
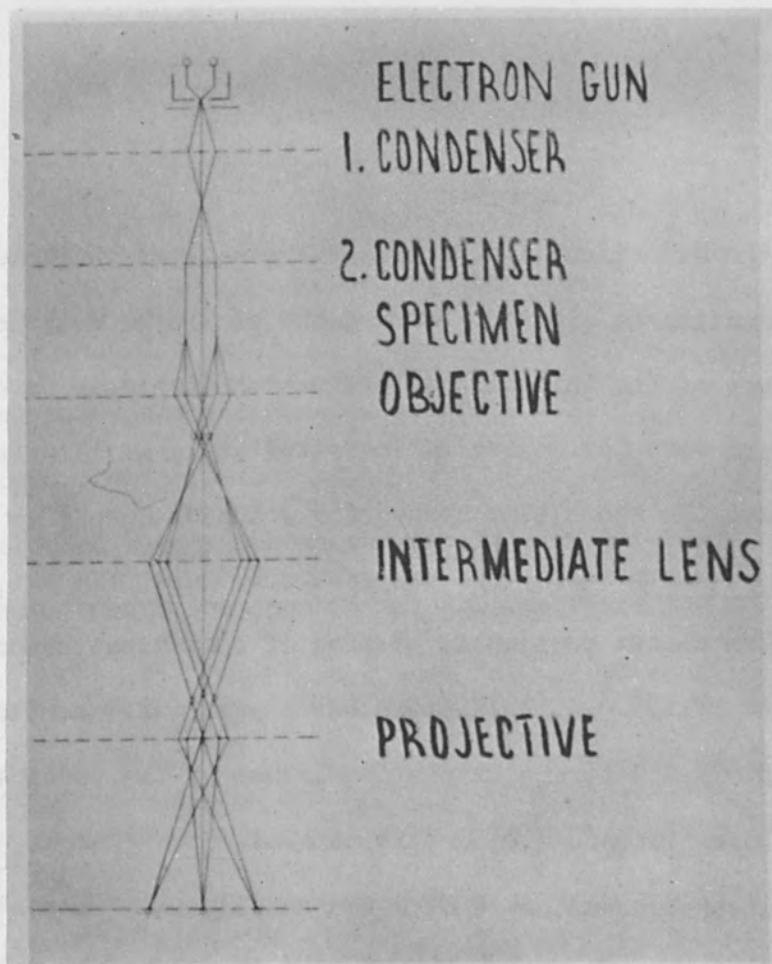
328

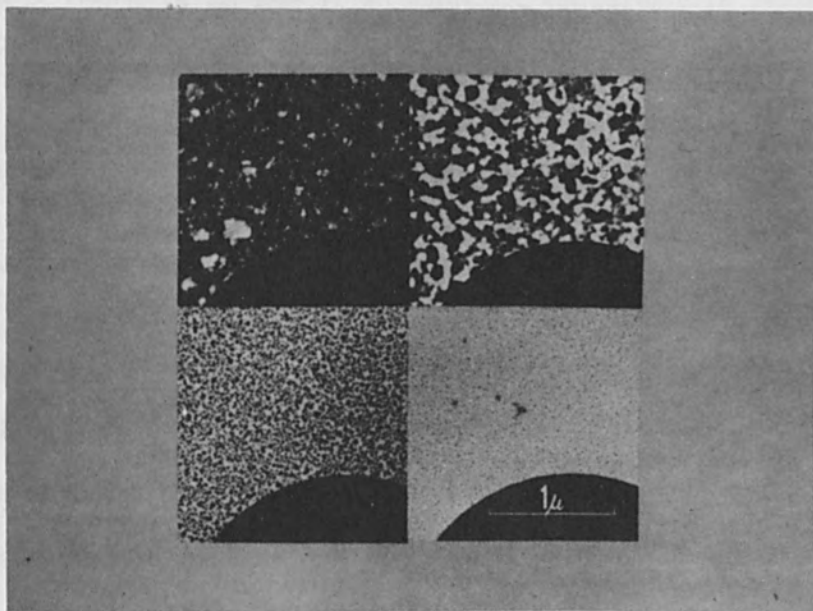Figure 2.   Selected area electron diffraction ray diagram.

Figure 3.   Electron micrographs of four evaporated silver
films of different thicknesses (380Å, 30Å).

Depending upon the experimental objectives, the well known fact of specimen contamination by electron bombardment has to be considered too. The accuracy of the thickness determination itself is hardly limited because of very low contamination rates at large illuminated specimen areas and the short time needed for scanning across an edge of the test film. Furthermore, the use of a substrate film elimi-nates this problem almost completely because of contamination of both substrate and test film. If, however, other experiments are planned with the test specimen after thickness measurements, the specimen con-tamination sometimes imposes serious limitations. For example, if a metal film is already contaminated by a carbonacious layer, the film cannot be sputtered later; also a contaminated thin film substrate is worthless for further epitaxial studies.

In principle there are three methods known to prevent specimen con-tamination by electron bombardment (8): cooling and heating the spec-imen and washing the specimen with oxygen during exposure to elec-trons. All three complicate electron microscopy appreciably but cool-ing and heating stages for electron microscopy are available. Some-times, however, it is not completely necessary to examine exactly the same specimen area again. In this case small area illumination is sufficient and makes it possible to examine a neighboring uncontami-nated area later on. Unfortunately, small area illumination increases the contamination rate immensely and thus a compromise has to be found.

For the experiments reported here the compromise was as follows:

Illuminated area $(30\,\mu)^2$

Test area for thickness measurements $(1.5\,\mu)^2$

Contamination rate 5 Å/min

Recorded electron beam current 5.10^{-12} A (which means an approximate electron current density at the test specimen of 10^{-4} $\frac{A}{cm^2}$).

5. Calibration procedure for films thinner than 100 Å.

In principle there is no question that multiple beam interferometry can be used for measuring step heights much smaller than 100 Å. The accuracy of the Tolansky measurement described earlier in this report also is sufficient for step height determinations down to about 20 Å, but for thickness measurements of evaporated films - especially silver films - there is no use in attempting measurements below 100 Å as can be clearly seen from fig. 3. The electron transmission micrographs of silver films of different thicknesses show that below 100 Å total thickness the layers are no longer continuous at all but consist of an agglomeration of isolated silver particles. Therefore, a different calibration method has to be used for very thin films.

During the first evaporation run four silver films were produced ranging in thickness from about 100 Å to 400 Å by placing the substrates at different distances from the evaporation source. For the second evaporation run four new substrates were placed at exactly the same locations and the evaporation time was cut down to a value so

331

that the thickest of these new specimens turned out to be in the 100 $\overset{o}{A}$ range.

The ratio of thicknesses at the four different locations were calculated from the first run:

$$d_1 : d_2 : d_3 : d_4 = a_1 : a_2 : a_2 : a_4$$

The same relationship holds for the second run.

Thus:

$$d_5 : d_6 : d_7 : d_8 = a_1 : a_2 : a_3 : a_4$$

The thickness of d_5, which is in the same thickness range as d_4, was measured now by electron absorption and d_6, d_7 and d_8 were calculated

$$d_6 = \frac{a_2}{a_1} d_5; \quad d_7 = \frac{a_3}{a_1} d_5; \quad d_8 = \frac{a_4}{a_1} d_5.$$

RESULTS

The Tolansky measurements of the first four specimens fundamental to the entire calibration process were analyzed very carefully from micrographs like fig. 1b using a good object stage of a light microscope and taking into account that the fringes are not strictly parallel. The relative error of these thickness measurements was found to be about 4%.

Thus the first four films were measured to:

$$d_1 = 384 \ \overset{o}{A}, \ d_2 = 194 \ \overset{o}{A}, \ d_3 = 128 \ \overset{o}{A} \ \text{ and } \ d_4 = 97 \ \overset{o}{A}.$$

The accuracy of the electron transparency measurements depends mainly upon two factors: the stability of the electron beam current and the kind of supporting film used.

As an example fig. 4 shows typical recordings of the electron beam current while (slowly) scanning the edge of a test film. In fig. 4a, the well known transformation of the collodion substrate into a more transparent carbon film by electron bombardment is evident. Fig. 4b shows that with a carbon substrate a satisfactory stability can be achieved (contamination is negligible) and an accuracy for electron transmission measurements of

$$\Delta T_{el} \approx 1\% \text{ is obtained.}$$

The final calibration curve T_d versus d is shown in fig. 5. For the 384 $\overset{o}{A}$ film the error of transmission (ΔT_{el}) and thickness measurement (Δd) is indicated.

The light absorption measurements included to supplement the Tolansky method for future calibration processes were not very useful with respect to the range of thicknesses to which they are easily applicable. It was found that light transparency measurements are easily interpreted only above about 150 $\overset{o}{A}$. This result is in agreement with the well established fact (1) that the simple absorption formula $T = e^{\frac{-4\pi K_d}{\lambda}}$ has to be substituted below 150 $\overset{o}{A}$ by the more exact one:

$$d = \frac{\lambda}{4\pi K} \left\{ \ln\left(\frac{1}{T}\right) + \ln \frac{16 n_o n_T (n_s^2 + K^2)}{[(n_s + n_o)^2 + K^2][(n_s + n_T)^2 + K^2]} \right\} .$$
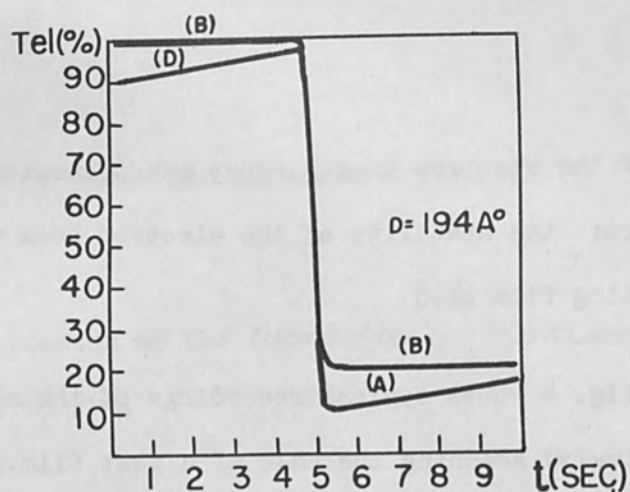
Tel(%)

(B)

(D)

90
80
70
60
50
40
30
20
10

D= 194A°

(B)

(A)

1 2 3 4 5 6 7 8 9   t(SEC)

Figure 4.   Electron transparency measurement of a
colloidion supported silver film (d= 194 Å) while
scanning across the edge of the silver film. Note
increasing transparency of the collodion support
during electron bombardment.
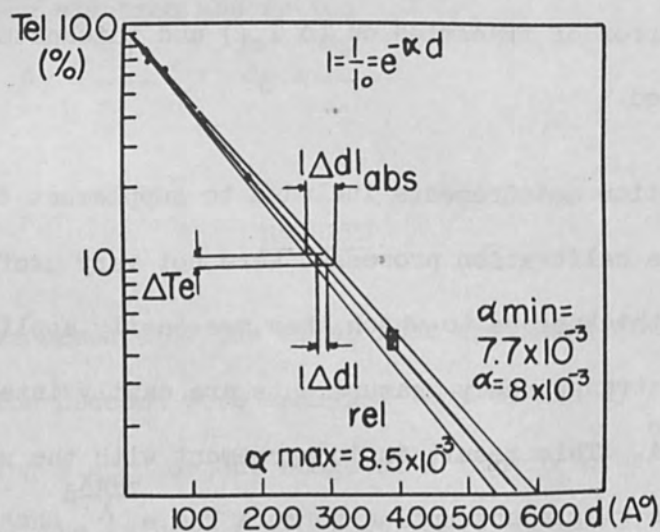
Figure 4b. The same silver film on carbon substrate.

Tel 100
(%)

$I = \dfrac{I}{I_o} = e^{-\alpha d}$

$|\Delta d|_{abs}$

10

ΔTel

$\alpha\,min=$
7.7×10^{-3}
$\alpha = 8 \times 10^{-3}$

$|\Delta d|$
rel

$\alpha\,max = 8.5 \times 10^{3}$

100 200 300 400 500 600 d (A°)

Figure 5.   Transparency of evaporated silver films
to 50 kv electrons.

334

APPLICATION

To what extent thickness measurements by electron absorptions are useful for future experiments can be seen from a short error estimate. In fig. 5 two additional straight lines are drawn representing curves of maximum and minimum absorption constants enveloping the points of measurement. For a given value of T_{el} and ΔT_{el} two different errors of thickness measurement $|\Delta d|_{abs.}$ and $|\Delta d|_{rel.}$ are indicated. $|\Delta d|_{abs.}$ is the absolute error of total thickness determination and $|\Delta d|_{rel.}$ is the relative error if the removal or addition of surface layers is measured and the same average value of $\alpha = 8 \times 10^{-3}$ is used for all measurements.

A numerical calculation for both errors yields

$$|\Delta d|_{abs.} = 12 \ln (T_{el}) + 148 \ln \left(\frac{\Delta T_{el}}{T_{el}}\right)$$

$$|\Delta d|_{rel.} = \frac{1}{d} \left(\frac{\Delta T_{el}}{T_{el}}\right).$$

Both errors as a function of film thickness are plotted in fig. 6a and 6b. For a thickness of 150 $\overset{o}{A}$ for instance $|\Delta d|_{abs.} \approx 20 \overset{o}{A}$ which is not particularly impressive. However, $|\Delta d|_{rel.} \approx 4 \overset{o}{A}$ which corresponds to a monolayer of silver atoms.

Concluding it can be seen that electron absorption measurements are particularly suited to detect the removal of surface layers of thin films.

To demonstrate the feasibility of detecting the removal of surface layers by electron absorption measurements a thin silver film was measured before and after sputtering for 10 seconds by 400 eV argon ions. The sputtering apparatus was attached to the specimen chamber of the electron microscope so that the thickness of the silver film could be determined without removal from the vacuum. Measuring the argon ion current and the decrease in thickness of the silver film the sputtering yield constant H could be calculated:

$$H = \frac{\text{number of sputtered silver atoms}}{\text{number of incident argon ions}}$$

$$= \frac{n_{Ag} \cdot F \cdot \Delta d \cdot e}{I_{ion} \Delta t}$$

n_{Ag} = volume density of silver atoms = $6 \times 10^{22} \; \frac{1}{cm^3}$

F = sputtered surface = $19.6 \times 10^{-2} \; cm^2$

Δd = change in thickness of silver film = 20 Å.

I_{ion} = ion current = $50 \mu A$

t = sputtering time = 10 sec.

e = 1.6×10^{-19} C

These values yield

H = 0.8

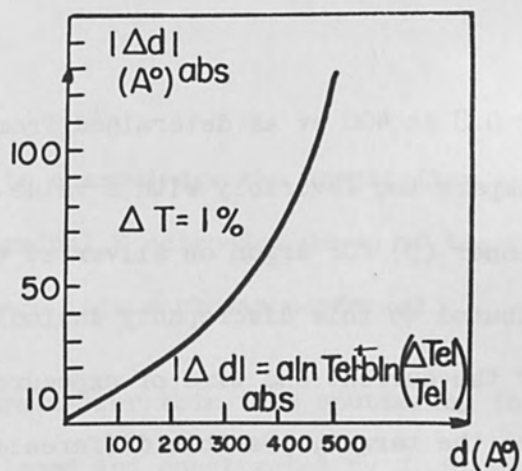Figure 6a
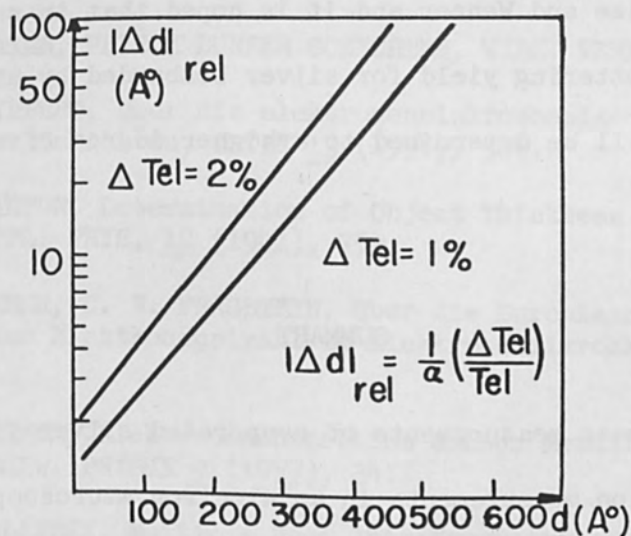

Figure 6b

Figure 6a and 6b.   Error of total thickness measurement
$|\Delta d|_{abs}$ and error of relative thickness measurement
$|\Delta d|_{rel}$.   as a function of film thickness.

The sputtering yield of 0.8 at 400 ev as determined from the preliminary measurement does not compare too favorably with a value of a little less than 2.0 obtained by Wehner (9) for argon on silver at this energy. Many factors may have contributed to this discrepancy including such questions as accurate measurement of the current and time of exposure, the energy distribution of the ions on the target, possible differences in the properties of the films investigated, differences in surface contamination and so on. This measurement is merely to be take as illustrative of the technical properties. It should also be pointed out that there is some discrepancy in the data of Guntherschulze and Wehner and it is hoped that in subsequent work the variation of sputtering yield for silver bombarded by argon in the energy range of interest will be determined to a higher degree of accuracy and reliability.

SUMMARY

High accuracy thickness measurements of evaporated silver films can be obtained by electron absorption measurements in an electron microscope. The method is particularly applicable to the detection of removal of surface layers of electron transparent thin film specimens. The removal of one monolayer can be detected. The calibration process for evaporated silver films is described in detail. The same technique is suitable for any type of thin film manufacturing process that produces thin films of equal thickness over an area of at least $(3mm)^2$. The capability of the method is demonstrated by measuring the sputtering yield constant of silver bombarded by argon ions inside the electron microscope.

The author wishes to acknowledge the hospitality and assistance of the Solid State and Physical Electronics Group of the Convair-San Diego Physics Section where this work was performed.

The auxiliary apparatus for thin film sputtering in situ in the electron microscope was designed and constructed by J. Strozier and M. Seltzer.

LITERATURE

(1) H. MAYER, PHYSIK DUNNER SCHICHTEN, WISS. VERL. GES., STUTTGART 1950.

(2) W. LIPPERT, Uber die elektronenniskroshopische Duchlassigkeit dunner Schichten, OPTIK 13 (1954), 506.

(3) L. MARTON, Determination of Object Thickness in Electron Microscopy, J. APPL. PHYS. 12 (1941), 759.

(4) K. WEBER, C. V. FRAGSTEIN, Uber die Durchlassigkeit von Tragerfolien fur den Elektronenstrahl im Elektronenmikroskop. OPTIK 11 (1954), 511.

(5) L. REIMER, Elektronenabsorbtion dunner Metallaufdampfschichten A. ANGEW. PHYSIK 9 (1957), 34.

(6) S. TOLANSKY, Multiple Beam Interferometry of Surfaces and Films, Oxford Press 1949.

(7) W. KRUG E. LAU. Die Aquidensitometry ein neues MeBoerfahren fur Wissenschaft and Technik, FEINGERATETECHNIK 9 (1952), 1.

(8) G. MOLLENSTEDT, H. NIEHRS, E. RUSKA: Fourth International Conference on Elektron Microscopy, Berlin 1958.

(9) G. K. WEHNER, Annual Report, Department of the Navy, Office of Naval Research, (1959).

NEWER DEVELOPMENTS IN MICROMINIATURIZATION

By

G. Möllenstedt
Professor
Institute for Applied Physics
University of Tübingen
Tübingen, West Germany

R. Speidel
Research Associate
Institute for Applied Physics
University of Tübingen
Tübingen, West Germany

ABSTRACT

Recent developments utilizing a modified

electron microscope and especially designed beam

guidance system for micro recording and other special

applications are discussed. The resolution of this system

as well as products of this system are presented.

NEWER DEVELOPMENTS IN MICROMINIATURIZATION

I. **INTRODUCTION**

Figure 1 shows a product of the already known approach for the production of electrical resistors of any desired resistance value through the utilization of intense electron beams for property modification. By the process of K. H. Steigerwald[1] from Zeiss of Oberkochen, West Germany, a program-controlled electron beam can draw a recognizable trace, as in Figure 1, by vaporizing a metallic coating which has been applied to a ceramic plate (R.C.A. Micro-Module). The resistance is between terminals 1 and 2. While in this example an intensive electron beam of about 10 microns in diameter was used, in the following, the work will involve an electron probe of several orders of magnitude smaller in diameter.

II. **ELECTRON-OPTICAL MICROWRITING UNDER ELECTRON-MICROSCOPICAL WORK CONTROL**

Through reduction of an electron source by means of an electrical or magnetic lens, electron-microprobes of about 200 A in diameter or width can be easily produced.

The difficulties in utilizing such microprobes lies in the difficult task of their guidance and their recording, because neither photographic plates nor light microscopes are suitable for this purpose.

As a consequence of the lack of structure, collodion layers of about 500 to 1000 A are particularly suitable as recording film. H. König [2,3,4] has already shown that a collodion foil will be decomposed to carbon by electron irradiation and will lose both in weight and in thickness.

The effect of the electron microprobe on the collodion foil, which has been stablized with a carbon film of 100 A thickness, is shown in Figure 2. One observes a constricting action at the irradiated point. For observation with electron microscope the trace of the electron beam must be delineated in high contrast by using low angle shadowing with Pt-Ir in high vacuum. (Figure 2, lower left). In order to get high contrast pictures in a light microscope, the upper and lower surfaces of the film have to be covered with an evaporated semi-transparent silver coating, thus obtaining a light optical line interference filter [5].
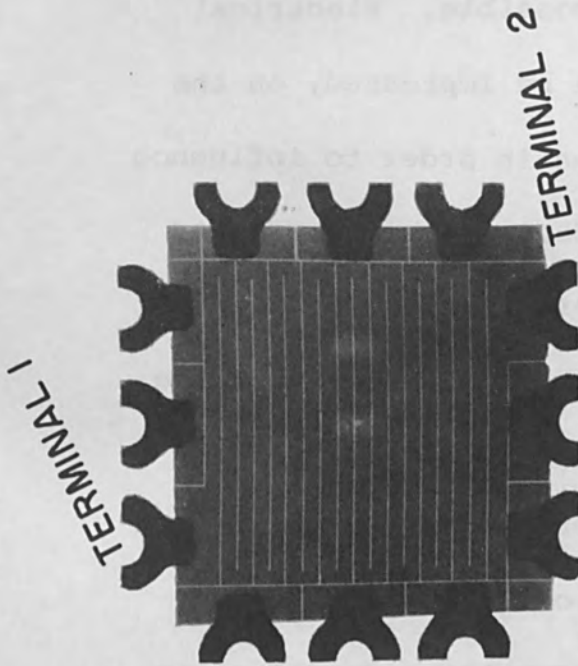
Figure 1

A flat metal coated ceramic resistor.
Lateral length 8 mm. Observe electron
beam cuts on the evaporated resistive
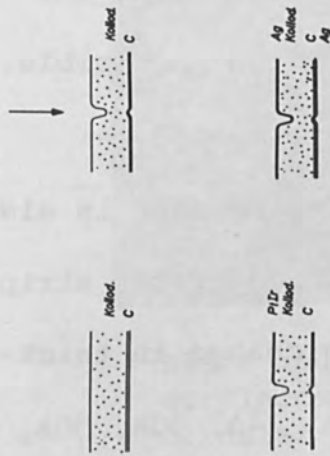material. (R.C.A. Micro Module)

Figure 2

High contrast delineation of the
electron beam trace.
Upper left: Unirradiated collodion
foil reinforced with a carbon layer.
Upper right: Foil after processing
with a 500 A wide electronprobe.
Lower left: Foil after Pt-Ir - low
angle shadowing in vacuum.
Lower right: Foil after silver evapor-
ation on both sides enabling the use
of interference filter.

0 · 5 ·14·30·80·110 A   DIELECTRIC
STEPS

Figure 3

Color changes of a light-optical line-
interference filter made visible on
black and white printing through the
thickness changes of the dielectric.

As a consequence of the change in refractive index and the reduction of thickness of the foil at the irradiated points, a clear color displacement is visible. The excellent sensitivity achieved by this method is demonstrated in Figure 3. This color displacement is also visible in black and white reproduction. The first strip shows the base color of the filter. The change in thickness of the dielectric corresponds to 5A, 14A, 30A, 80A, and 110A respectively. The possibility of the conversion of electrical signals in a color picture or correspondingly in different light intensities is possible. Electrical signals in the form of voltages can be impressed, on the Wehnelt cylinder of the electron gun in order to influence the intensity of the beam. The effect of the irradiated charge quantity on the collodion foil results in different colors when observations are made through an interference filter or in different shades of gray in black and white reproduction (see Figure 4). The original from which this example is obtained had a diameter of 0.2 mm.

A method of guiding a microprobe under electron microscopical control which has been achieved in Tübingen is shown in Figure 5. We have used the Siemens Elmiskop I
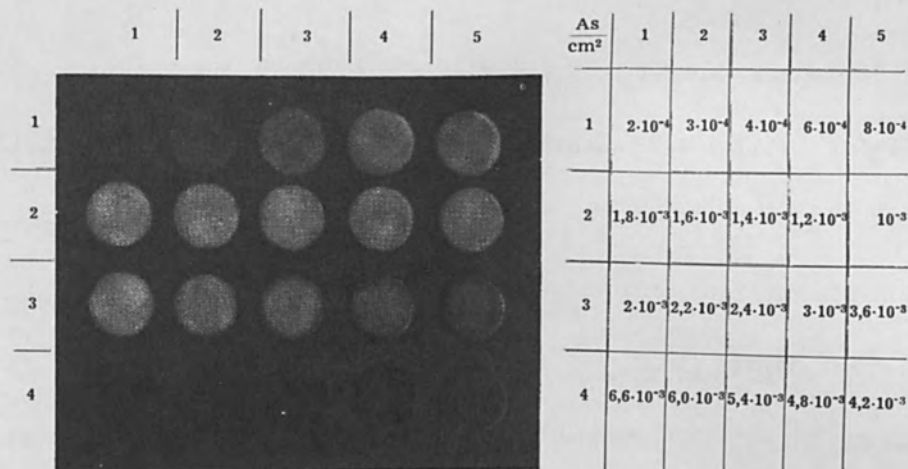
$\frac{As}{cm^2}$	1	2	3	4	5
1	$2\cdot10^{-4}$	$3\cdot10^{-4}$	$4\cdot10^{-4}$	$6\cdot10^{-4}$	$8\cdot10^{-4}$
2	$1{,}8\cdot10^{-3}$	$1{,}6\cdot10^{-3}$	$1{,}4\cdot10^{-3}$	$1{,}2\cdot10^{-3}$	10^{-3}
3	$2\cdot10^{-3}$	$2{,}2\cdot10^{-3}$	$2{,}4\cdot10^{-3}$	$3\cdot10^{-3}$	$3{,}6\cdot10^{-3}$
4	$6{,}6\cdot10^{-3}$	$6{,}0\cdot10^{-3}$	$5{,}4\cdot10^{-3}$	$4{,}8\cdot10^{-3}$	$4{,}2\cdot10^{-3}$

Figure 4

Black and white reproduction of color
displacements in electron bombarded
circular fields of a collodion foil
made visible through interference
filter. The background remains unir-
radiated. The table on the right side
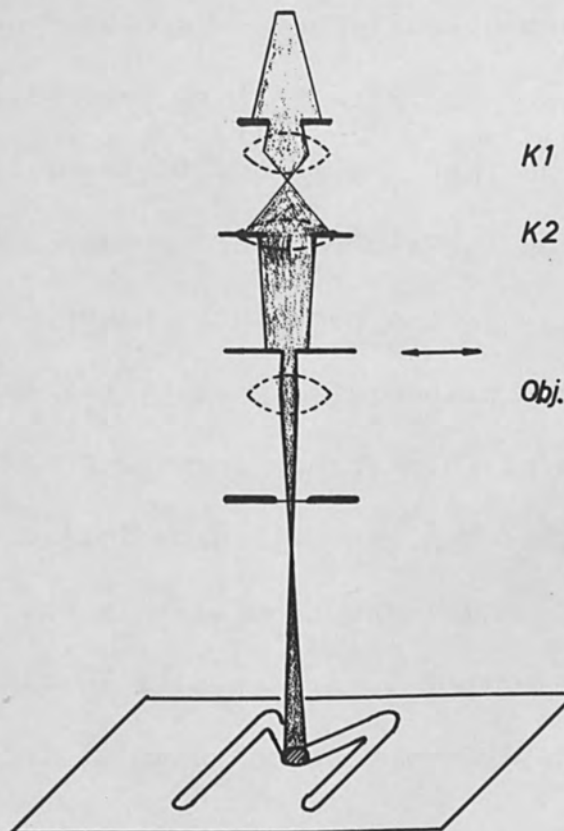indicates the amount of radiation.

K1

K2

Obj.

Figure 5

Electronoptical beam path for the pro-
duction and guidance of the electron-
microprobe under electron-microscopical
observation.

for the production of extremely fine line marks and micro

recordings. With the double condenser lens (K 1 and K 2

in Figure 2) switched on, a fine slit or a 4μ aperture

is inserted in the usual specimen plane. The fine slit

made in the institute is 1μ wide, 100μ long, and 2μ deep.

Because of the very small beam angle with which the slit is

irradiated, the beam width in the back focal plane of the

objective lens, which can be varied by varying the focal

length, can be made as small as 100 A. The collodion target

is extended over the hole of a normal 50μ aperture and

brought in the beam slightly over the back focal plane of

the objective lens. The thin foil is well penetrable for

60 keV electrons so that a distinct image of the slit can

be well observed on the fluorescent screen. If the collodion

foil is not exactly in the back focal plane, an additional

shadow image of the transmitted part of the foil is produced.

The magnification of this shadow image depends on the dis-

tance between back focus and collodion foil and yields,

besides, a criterion for the beam size in the plane of the

foil. A displacement of 1μ of the slit in the specimen

plane causes a displacement of the beam on the foil of 100 A

only, so that the usual precision drives can be used for the slit displacement. The corresponding displacement of the beam on the foil can be observed on the screen. If a round aperture is used instead of the slit, the specimen motion drives can be used to let the beam follow a stencil pattern of several centimeters' size which may be placed on the fluorescent screen or in the intermediate image plane of the viewing light microscope. In this case the corresponding pattern will be recorded on the foil in a reduced scale.

Applications:

a) Scales and Fine Gratings -   In Figure 6 an example for the efficiency of the micro recorder is shown. The specimen slit was made of copper and was 1μ wide. The total width of the ruled area on the foil is 1.5μ. The mutual distance of the short lines in the middle is 1000 A while the width of each line is 140 A. For the calibration of the specimen micrometer we have to measure a distance of 50μ with an accuracy of 1% in the light microscope and divide this distance in 10 equal parts. These micrometers can be measured at medium electron optical magnification. For higher magnification the scale is subdivided into parts of 1000 A distance.
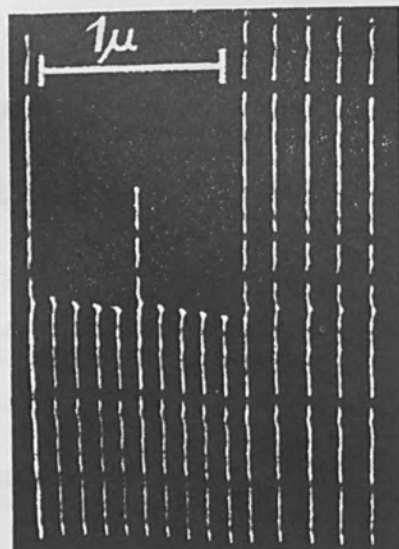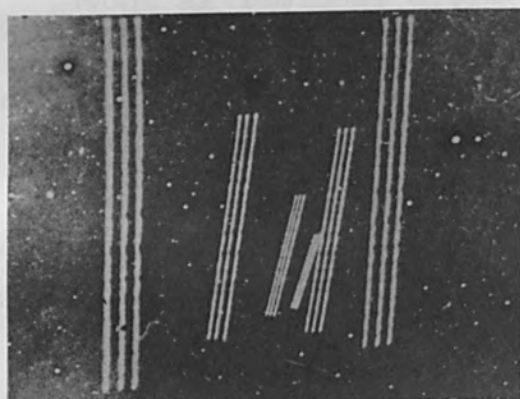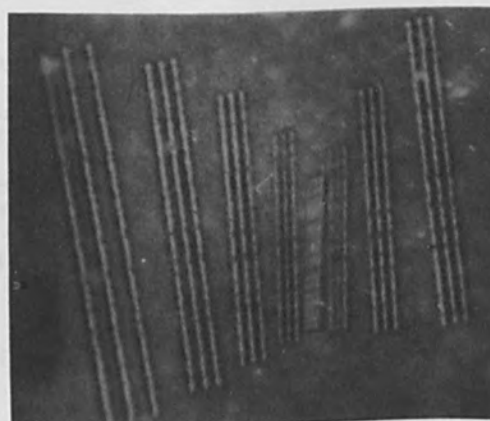
Figure 6
25,000X electron-microscopical magnifica-
tion of an object micrometer for
electronmicroscope. Collodion foil
reinforced with carbon. Contrast is
increased by Pt-Ir - low angle shadowing
in vacuum.

INTER LINEAR DISTANCE

1,1μ 0,5μ 0,3μ 0,2μ 0,4μ 0,8μ

(a)   (b)

Figure 7
a) Test traces for light-microscopy resolved
    in an electron microscope.
b) Light-microscope picture (N.A. 1.32) showing
    limits of resolution.

An example for purposes of exercise in optics courses in the University is given in Figures 7a and 7b. In 7a the lines are written at distances partly above and partly below the resolving power of the light microscope, and made visible through the electron microscope. While the electron microscope certainly resolves all distances the light microscope achieves resolution to examine quantitatively Abbe's limiting formula $\delta = 0.62 \dfrac{\lambda}{n.\sin\theta}$ and to test the light microscope objectives for their efficiency.

b) <u>Micro Recording (Storage of information on very small area)</u>

With a platinum aperture of 4μ diameter in the specimen plane the electron beam was guided along a stencil pattern on the fluorescent screen to write letters on the foil. The focal length of the objective lens was chosen so that the letters were 0.5μ high. The result is shown in Figure 8. With this size of letters it would be possible to write the complete text of the Bible on the 30th part of the area of a postage stamp (1 sq. in.). In the described example the recording was effected by a mechanical lateral displacement of the aperture above the objective lens but in a just completed instrument the
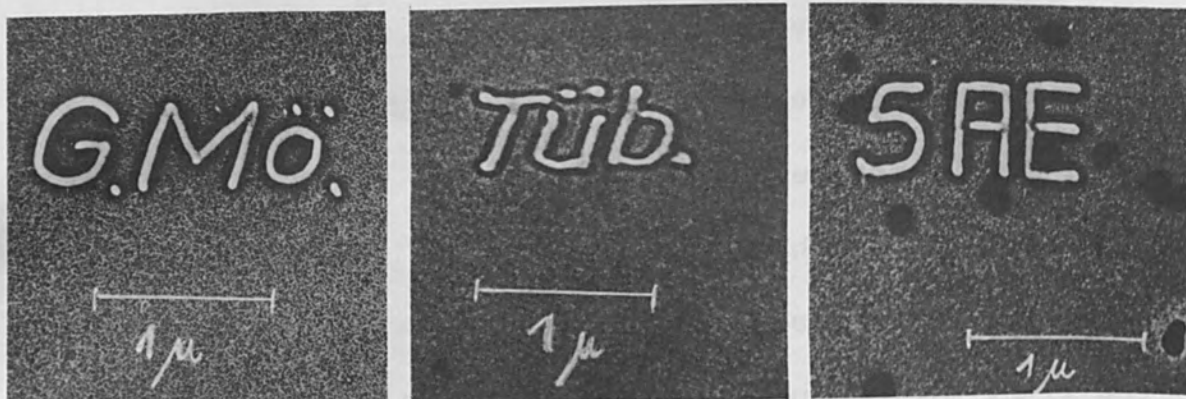
Figure 8

Capital letters 0.5µ size recorded on collodion
foil with the electronprobe micro recorder.

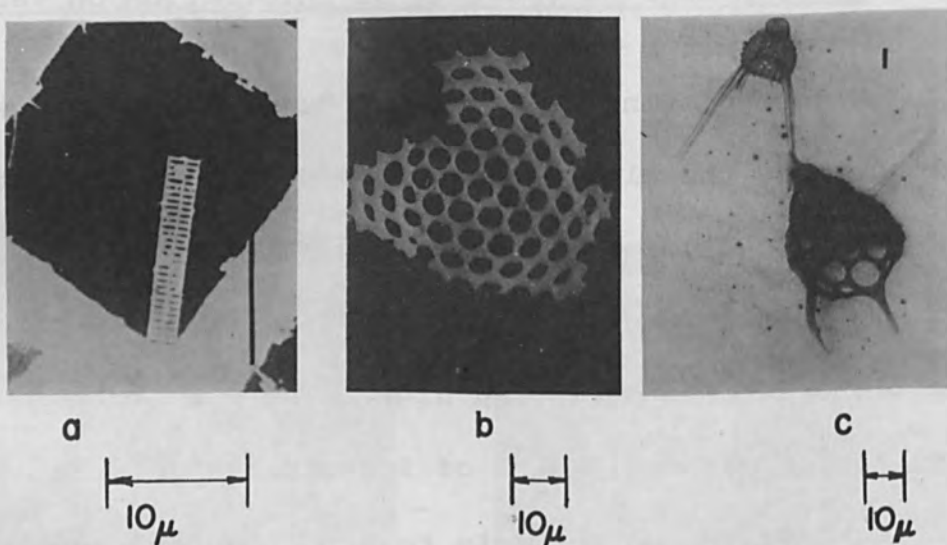a   b   c

10µ   10µ   10µ

Figure 9

Contrast pictures of Diatomeen on grain and
structure free interference filter plate.
Radiography of the object with
a) 25 KV ions
b) 40 KV electrons
c) 20 KV x-ray in vacuum 10^{-4} mm Hg.
Photographed by V. Rao

350

gratings and letters can be produced by magnetic deviation of the beam.

The collodion foil can also be used to make contact reproductions by electron, ion, UV or x-ray beams of specimens which can be viewed neither in the light nor the electron microscope. We have already had good results with such reproductions as can be seen in Figure 9.

III. <u>REDUCTION OF ELECTRICAL CONDUCTIVITY BY USE OF POLYMERIZED</u>
<u>LAYERS AND ITS APPLICATIONS FOR THE PRODUCTION OF FINE</u>
<u>GRATINGS</u>

It is known long since that a polymerized hydrocarbon layer is deposited on surfaces which are irradiated by ion, electron, UV or x-rays in a vacuum of 10^{-4} mm Hg. This effect is used for the production of self supporting microslits[7]. A silver layer on a glass plate as shown in Figure 10 is irradiated by a 1000 A wide linear electron probe with 50 kV and 10μ Amp. By means of deflecting electrodes this probe is projected successively to several equidistant positions until a polymerized deposit of about 100 A thickness has been formed. This deposit is sufficient to prevent the precipitation of copper in the irradiated places in an electrolytic bath. By stripping the copper foil fine slits are obtained as shown in Figure 11. The

200A SILVER

GLASS CARRIER

10-50 A
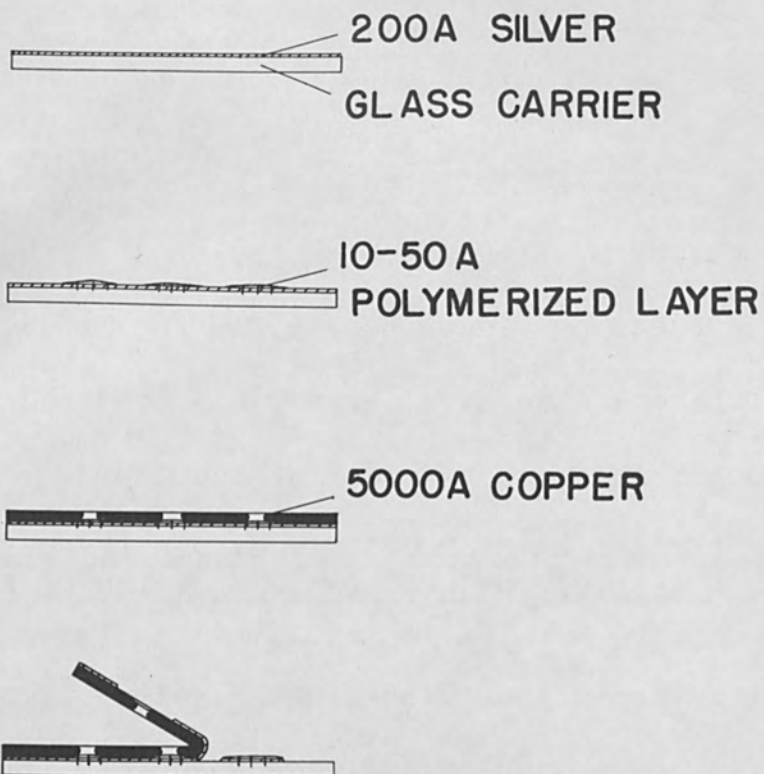POLYMERIZED LAYER

5000A COPPER

Figure 10
Method for the production of fine slits
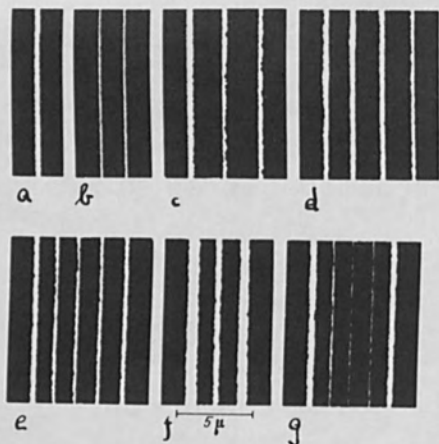with electron-microprobe.

Figure 11
Fine slits made with the electron-
microprobe.
a) 1 slit
b) 2 slits
c,d,e,f and g) multiple slits and
slits of different widths.

352

slits are fine enough to use them as gratings for multiple beam electron-interference experiments (Figure 12).

IV. PRODUCTION AND REPRODUCTION OF VERY FINE MESH GRIDS FOR IMAGE-ORTHICONS ETC.

a) Contact Method - If a fine grid is already available, it is laid on a silvered glass plate (Figure 13) and ir- radiated with ions. Again a polymerized hydrocarbon layer is formed which has an electrical conductivity much below that of silver. Therefore, the precipitation of copper in an electrolytic bath is prevented and a distinct contact copper copy of the original grid is obtained.   Another example of the production of a contact copy of the original can be seen in Figure 15.

b) Production of Grids of Any Desired Mesh Size - A narrow linear ion beam is selected by a fine slit to form a polymerized hydrocarbon strip on a glass plate with an evaporated copper layer. By a precision displacement mechanism with interferometrical control the slit can be displaced and turned into a rectangular position to its former direction (Figure 16). If the copper layer is then treated with gaseous chlorine, the copper is transformed to copper chloride at all places which are not protected by
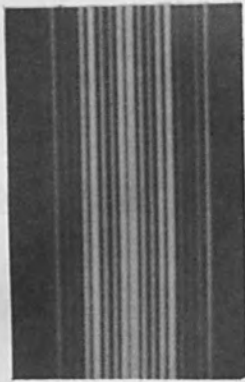
Figure 12
Electron interference pattern on five
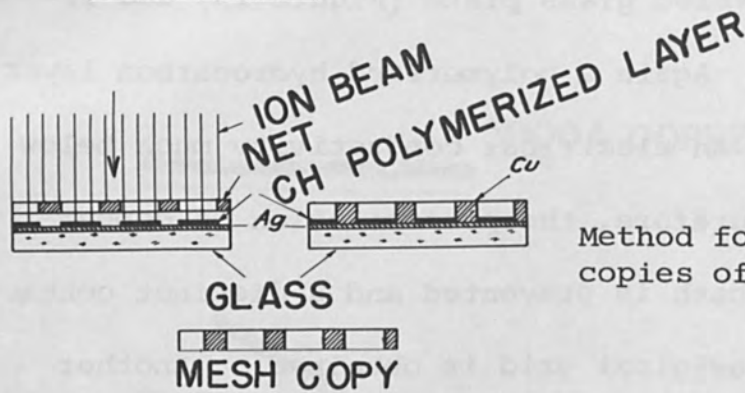fine slits. Photograph by Claus Jönsson.

ION BEAM
NET
CH POLYMERIZED LAYER
Cu
Ag
GLASS
MESH COPY

Figure 13
Method for the production of contact
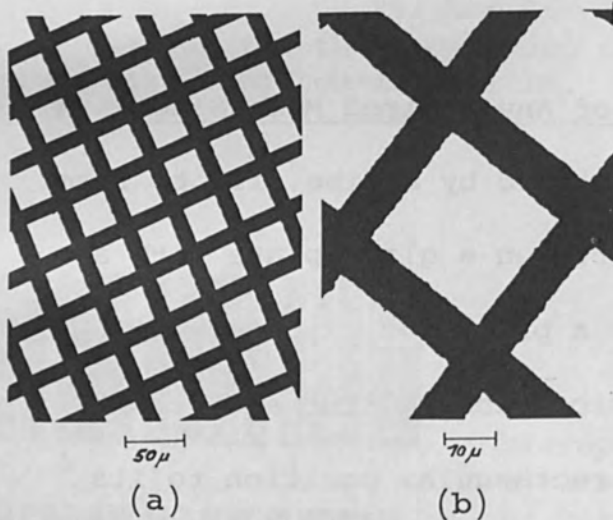copies of originals.

50μ

(a)

70μ

(b)

Figure 14a and 14b
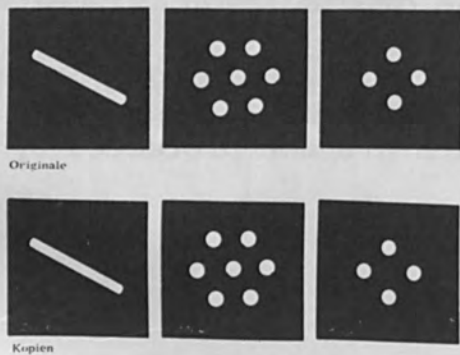Production of very fine nets by
the copy method.

Originale

Kopien

Figure 15
Example of the production of contact
copies (below) from the existing
originals (above).

10⁻⁴ Torr

ION BEAM

SLIT

CH POLYMERIZED
LAYER

Cu
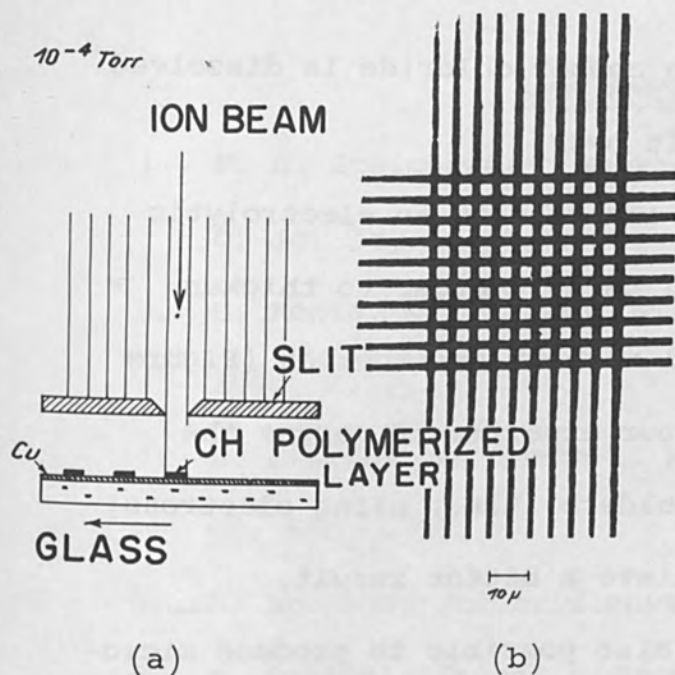
GLASS

(a)   (b)

Figure 16
Production of nets with regulated mesh
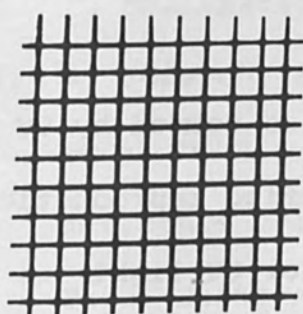width.

Figure 17
Net produced with 15 micron mesh width.
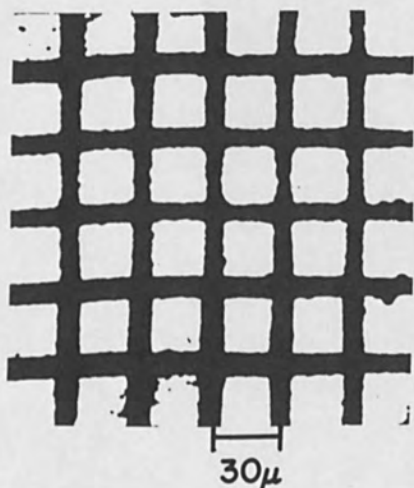Mesh width can be regulated.

30μ

Figure 18
A wire net with 4 mm distance between wires
reduced 133 times by UV optics and electro-
lytically produced. The wire distance of
the reduced net measures 30 microns. The
net above is magnified 310X. (H. H. Gauss)

the polymerized layer. When the copper chloride is dissolved

in water, the copper grid is left over.

The grid will then be immersed in an electrolytic

copper or correspondingly nickel bath in order to thicken

it and make possible its removal without destruction (Figure

17). We used an ion bundle in our experiments versus the

process of Buck, D. A., and Shoulders, K.R., using electrons,

to prevent diffusion and to achieve a better result.

By this method it is also possible to produce micro-

resistors of copper with 1μ width, 1000 A thickness and 1 mm

length with a resistance of 300 kΩ .

Since polymerized deposits are also formed by UV

irradiation, it is possible to make demagnified reproductions

of an original by means of objective lens for UV light

(Figure 18).

REFERENCES

1. K. H. Steigerwald, Werkzeitschr. Carl Zeiss-Oberkochen.
    8. Jg. 38, s. 74.

2. H. König, Nachr. Akad. Wiss. Göttingen, Math. Klasse
    1946, s. 25.

3. A. Brockes, M. Knoch u. H. König, Zs.f.wiss.Mikrosk.
    62, 450, 1955.

4. A. Brockes, Ztschr.f.Phys. 149, 1957, s.364.

5. R. Speidel, Ztschr.f.Phys. 154, 1959, s.154.

6. G. Möllenstedt u. R. Speidel, Phys. Bl. 16, 1960,s.192.

7. A. Jönsson, Zs. Phys. 161, 454 (1961).

8. Buck, D. A., Shoulders, K. R., "An Approach to Micro-
    miniature Printed System", Special Publication T-144
    Proc. Eastern Joint Computer Conference (Dec. 1958).

ELECTRON BOMBARDMENT EVAPORATION OF TANTALUM
FOR
THIN FILM COMPONENTS

By

R. W. Berry
Member of Technical Staff
Bell Telephone Laboratories, Incorporated
Murray Hill, New Jersey

ABSTRACT

Thin film components based on tantalum have been under investigation at the Bell Telephone Laboratories for a number of years. Until recently, all films had been prepared by cathodic sputtering. An investigation was made to determine difference in device properties between films deposited by evaporation instead of sputtering. This paper describes the design of the evaporation apparatus and also the properties of the films produced. It is concluded that there are no significant difference apparent between films produced by evaporation and those produced by sputtering.

ELECTRON BOMBARDMENT EVAPORATION OF
TANTALUM FOR THIN FILM COMPONENTS

The miniaturization of components and circuitry
has become a major development activity of a large
segment of the electronics industry. Among the concepts
which have evolved is the integrated circuit approach of
the Bell Telephone Laboratories. This concept has not
dealt with any of the active components, but mainly with
resistors and capacitors based on thin films of tantalum
and similar metals. Tantalum metal films have a special
advantage for component use due to their refractory nature,
their ability to form either thermal or anodic oxide films,
their inertness to chemical attack and their unusual
electrical properties. The properties have been described
previously [1,2] but will be reviewed briefly here.

CAPACITORS

The dielectric of the capacitors is anodically
grown tantalum oxide and is formed by making the metal films
the anode in an electrochemical cell which is completed
with an electrolyte and a tantalum or platinum cathode. The
thickness of the dielectric tantalum oxide formed is direct-
ly proportional to the voltage reached in formation, the
capacitance then being inversely proportional. After the
oxide film has been formed, the counter electrode is applied.
This is accomplished by vacuum evaporating a thin film of
gold or other suitable metal. Capacitors produced this way
show outstanding properties, including a high capacitance

per unit area (5 microfarads per square centimeter per rated volt), very low leakage currents (about 750 ohm farads at 1.5 times working voltage), dissipation factors of 1% or less, and a dielectric breakdown strength of about 5×10^6 volts per cm.

RESISTORS

For the basic evaluation of the properties of tantalum film resistors, five parallel stripes are deposited through a mask onto a slide with prefired gold terminations. The dimensions of each stripe are 0.750 inch by 0.050 inch (15 squares) with a 0.25 inch square tab overlapping the gold termination. The resistance can be varied by thickness control over the approximate range of 200 to 10 ohms/square with temperature coefficients falling within the range of ±150 ppm/°C. The resistivity of the tantalum films usually falls in the range of 150 to 250 micro-ohm centimeters, which is 10 to 15 times that of the bulk metal. These large differences from bulk properties are not primarily functions of the thin film geometry, since the high resistivity is essentially independent of thickness in the range from 500 to 2000 Å. Vacuum fusion analyses indicate an oxygen content in the films of approximately 0.5%, and low angle electron diffraction studies generally indicate an essentially amorphous film structure.

As with most thin metal films,[3] a considerable instability of resistance is observed for freshly deposited

films, both at room and elevated temperatures. These changes in resistance can be attributed to both an annealing of film structure and the growth of an oxide film. It is possible, however, to improve the stability of resistors by thermally preaging. This preaging probably results in the growth of a dense adherent thin oxide film. This oxide film apparently acts as protection against further degradation from the atmosphere.

The use of tantalum, with its capability of being anodized to form dielectric oxide films, offers the possibility of providing a precision resistor for microcircuitry. By anodizing, approximately 7 $\overset{\circ}{A}$ of tantalum can be converted to insulating oxide for each volt applied to the electrochemical cell. This then gives a very fine control of the effective thickness of the film. The resistance of the metal film can be monitored during the anodizing process, and any predetermined value of resistance can be achieved to within a tolerance of 0.1% or better.
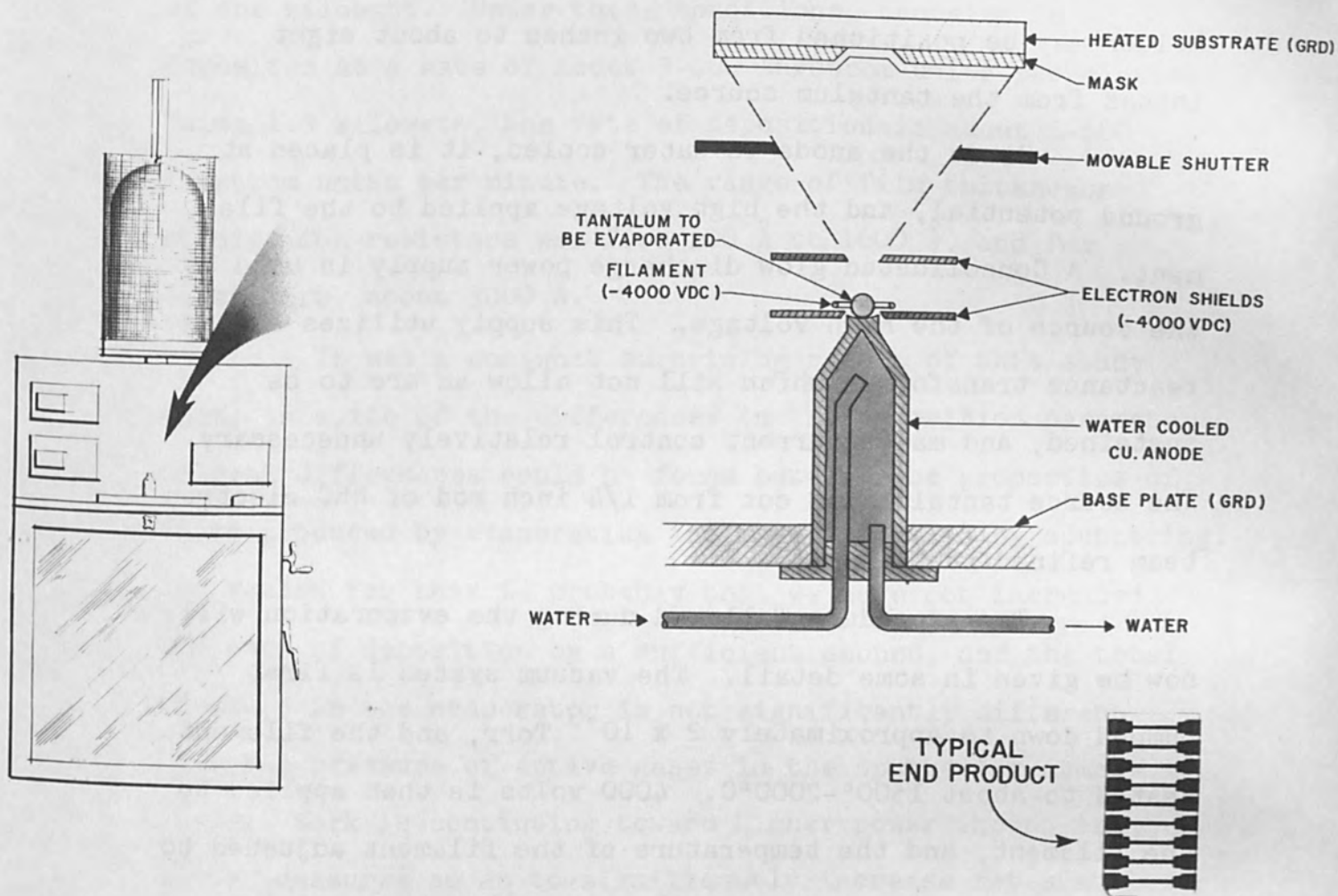
This anodic oxide coating, combined with the previously mentioned thermal stabilization provides resistors whose stability is quite good. After 2000 hours at 150°C, these resistors show a change of the order of 0.2%.

EVAPORATION PROCEDURE

Almost all work done up until recently has been based on tantalum deposited via the technique of cathodic

sputtering. The properties mentioned above all apply to films produced in this fashion. Sputtering, however, has some disadvantages which might outweigh the apparent simplicity of the apparatus. It is a relatively slow process, requiring from 5 to 20 minutes deposition time for resistors to from 45 to 60 minutes for a capacitor film. It is a process which requires a moderate gas pressure, usually 10-50 microns of argon, which is a difficult pressure region to measure accurately. Another difficulty is that the distribution of the deposit is difficult to predict.

It was therefore decided to study films produced by evaporation where the above difficulties do not exist to the same extent. A very simple evaporator was therefore designed and constructed. A standard commercial coater with a 14" glass bell jar was used for the vacuum system, and an annular type "gun" employed. A schematic representation of the electron bombardment apparatus is shown as Figure 1. The tantalum to be evaporated is held on a water cooled copper post, 3/8 inch in diameter, which has a slight depression so the molten metal cannot roll off. The electron-emitting filament is 3/4 inch in diameter, and is made of four 20 mil tantalum wires stranded together. The shields are constructed from 15 mil tantalum sheet and the holes are 5/8 inch diameter. They are spaced 1/2 inch apart with the filament held

HEATED SUBSTRATE (GRD)

MASK

MOVABLE SHUTTER

TANTALUM TO
BE EVAPORATED

FILAMENT
(~4000 VDC)

ELECTRON SHIELDS
(~4000 VDC)

WATER COOLED
CU. ANODE

BASE PLATE (GRD)

WATER →

→ WATER

TYPICAL
END PRODUCT

ELECTRON BOMBARDMENT EVAPORATOR

Figure 1.

centrally between them. A tantalum shutter is positioned about one inch above the top shield, and the heated substrate holder may be positioned from two inches to about eight inches from the tantalum source.

Since the anode is water cooled, it is placed at ground potential, and the high voltage applied to the filament. A Consolidated glow discharge power supply is used as the source of the high voltage. This supply utilizes a high reactance transformer which will not allow an arc to be sustained, and makes current control relatively unnecessary. The source tantalum was cut from 1/4 inch rod of NRC electron beam refined tantalum.

The procedure followed during the evaporation will now be given in some detail. The vacuum system is first pumped down to approximately 2×10^{-6} Torr, and the filament heated to about 1500°-2000°C. 4000 volts is then applied to the filament, and the temperature of the filament adjusted to bring the power input to one kilowatt. When the tantalum first melts, the pressure in the chamber usually rises to about 1×10^{-4} Torr, and the shutter remains in place until the pressure drops to approximately $1\text{-}2 \times 10^{-5}$ Torr. This generally requires about one to two minutes.

The shutter is then opened for whatever time of deposition is desired. After the power is shut off and the system allowed to cool for about 30 minutes, the pressure usually falls to about $3\text{-}4 \times 10^{-7}$ Torr.

364

Almost all samples produced were made with the substrate four inches distant from the source, and with a power of one kilowatt. Under these conditions, tantalum is deposited at a rate of about 3-400 Angstrom units per minute. Using 1.5 kilowatt, the rate of deposition is about 5-600 Angstrom units per minute. The range of film thicknesses studied for resistors was from 100 Å to 1600 Å, and for capacitors, about 3000 Å.

It was a somewhat surprising result of this study that, in spite of the differences in the deposition parameters, no real differences could be found between the properties of films produced by evaporation and those produced by sputtering. The reason for this is probably that we have not increased the rate of deposition by a sufficient amount, and the total pressure in the evaporator is not significantly different from the pressure of active gases in the sputtering atmosphere. Work is continuing toward higher power inputs and lower pressures so as to significantly increase rates at lower background pressures, and thereby produce films of higher purity.

ACKNOWLEDGMENTS

REFERENCES

1. Berry, R. W., and Sloan, D. J., Proc. IRE <u>47</u>, 1070, (1959).

2. Berry, R. W., and Schwartz, N., Proc. 4th Conference on Military Electronics (1960).

3. Belser, R. B., and Hicklin, W. H., Jl. Applied Phys. <u>30</u>, 313 (1959).

RESEARCH ON AN ION BEAM DEPOSITION SYSTEM
FOR
MICROCIRCUIT FABRICATION

By

W. E. Flynt
Research Physicist
Microcircuitry Laboratory
Varo Mfg. Co., Inc.
Garland, Texas

ABSTRACT

Research is being carried out on a technique for fabricating microminiaturized electronic circuits by deposition from a controlled ion beam, thus eliminating many problems associated with present methods using vapor deposition and masks. Research efforts so far have been directed toward the development of a high-current (100 ma) ion source, which will produce a beam of ions (e.g., metal ions), focused and deflected magnetically and/or electrostatically, to be deposited on a substrate in a prescribed configuration.

RESEARCH ON AN ION BEAM DEPOSITION SYSTEM
FOR MICROCIRCUIT FABRICATION

by

W. E. Flynt

PURPOSE OF PROGRAM

The objective of this research program is to develop a technique for
fabricating microminiaturized electronic circuits by deposition from
a controlled ion beam. Such a technique would eliminate many of the
problems of present methods using vapor deposition and masks to control
the geometry.

The present state of the art permits the essentially two-dimensional
deposition of resistive, conductive, dielectric and magnetic materials
on suitable substrates. Metallic or photoresist masks are used to
control the geometry of the deposited material. Figure 1 shows
schematically the proposed apparatus for ion beam deposition.

The ability to deposit a number of materials in prescribed geometrical
patterns and thickness without use of masks would result in several
major advantages:

(1) The resultant three-dimensional deposited network will
eliminate the majority of connections and assembly operations, and
hence substantially improve the inherent reliability.

(2) The three dimensional deposition layers will be orders of
magnitude smaller in volume than the equivalent stack of substrates with
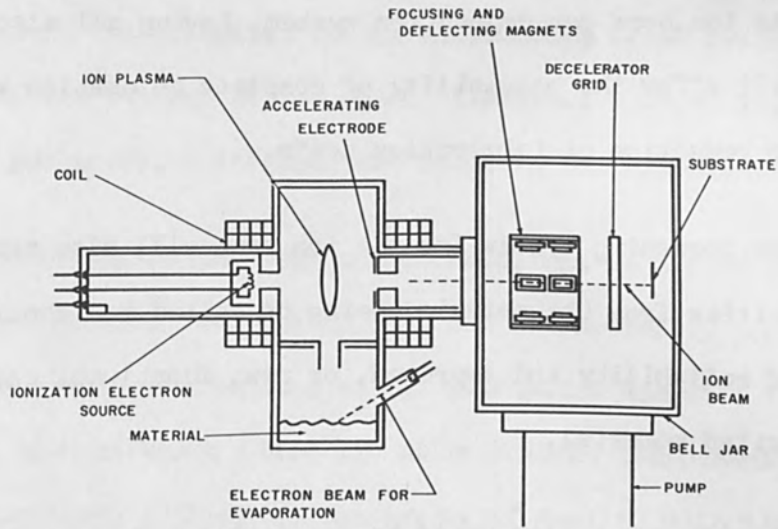two-dimensional deposits.

FIGURE I ION BEAM GUN
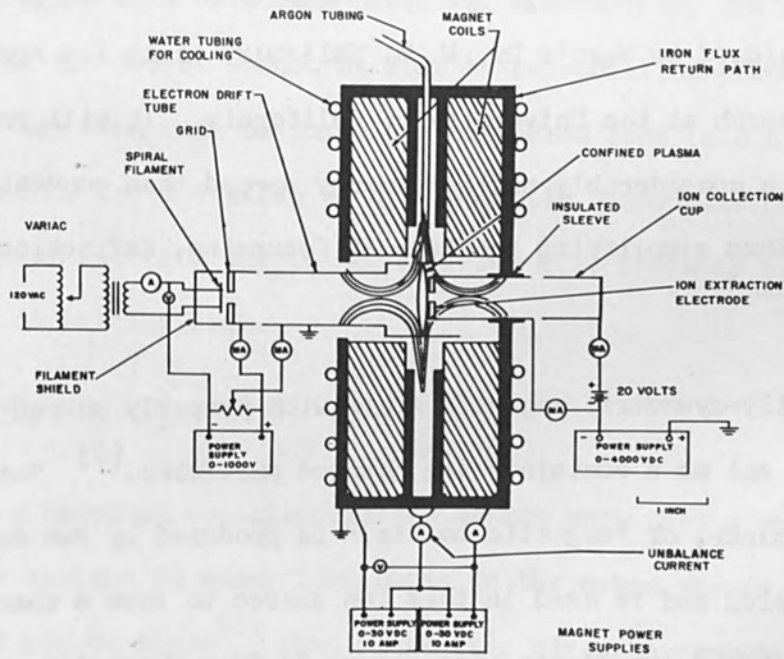
Figure 1. Ion Beam Gun

Figure 2. Schematic diagram of experimental ion
source.

(3) The ion beam gun deposition system, having all electrical controls, will offer the possibility of complete automation with accompanying reduction of fabrication costs.

(4) The focussing system for the ion beam will also serve to remove impurities from the material being deposited and should result in increased reliability and improved, or new, functional characteristics of the deposited material.

(5) The ion gun system would be applicable and valuable for other uses such as fabrication of deposited electrical components, protective coatings, production of special alloys and high purity materials.

DESCRIPTION OF ION SOURCE

The ion gun which is now being developed at Varo is patterned after a larger one designed by Varo's Dr. W. W. Salisbury as an ion source for cyclotron research at the University of California. It will produce an ion beam with a considerably smaller energy spread than conventional ion sources, thus simplifying problems of focussing, deflection, and deceleration.

A strong axially-symmetric magnetic field with properly shaped cusped geometry will act as a container for charged particles.[1] Such a magnetic container, or "magnetic bottle," is produced by two opposing solenoidal fields and is used in this ion source to form a sharply defined lens-shaped ion plasma (See Figure 2) from which ions may be extracted by placing an apertured plate near the surface of the plasma and impressing on this plate a high negative potential with respect to the plasma. The plasma is electrically neutral and is a good conductor;

hence it assumes the potential of the surrounding metal cylinder because of direct contact at its edge. Electrons ejected axially from an electron gun serve to initiate and maintain the plasma.

The apertured plate, or extraction electrode, can be placed very close to the plasma boundary, and the spacing can be accurately positioned by adjusting the relative strengths of the solenoidal magnetic fields. Hence a very high electric field can exist between the plasma and the extraction electrode without the necessity of dealing with high voltage and its attendant problems.

An ion source of the above description has been constructed, using argon gas instead of metal vapor for reasons of availability, inertness, and ease of transport to the plasma region. Up to about three milliamperes of argon ions have been produced, accelerated, and collected, although the ion source cannot be said to be operating properly yet. No attempt has been made to focus the extracted ions into a beam. The proposed method for focussing is by a magnetic quadrupole pair. A combination of electric and magnetic fields will probably be used for deflection of the ion beam.

MAGNET DESIGN

Calculations based on the original ion source show that a magnetic field whose maximum is about 1500 gauss in the cusps should contain the plasma. It can be shown[1] that a magnetic mirror arrangement such as this exerts an inward "magnetic pressure" equal to the energy density of the magnetic field:

$$P = \frac{B^2}{8\pi} \qquad \text{dynes/cm}^2$$

where B is the magnetic field in gauss. It is this magnetic pressure which serves to contain the plasma; charged particles are reluctant to cross magnetic field lines or to enter a region of converging field lines.

The magnet coils are wound "pancake" style, inside the flux return plates. This combination gives a sharp, hyperboloid-like field at the center, as shown in Figure 2. Outside diameter of the magnet assembly is six inches.

Actual field shape was determined using a method suggested in the literature.[2] Here a shallow brass tray was made and then filled with a mixture of iron filings and a very viscous fluid (uncured epoxy resin, in this case). The tray was placed on axis in the magnetic field and, after a few minutes, was removed quickly. The field pattern was preserved in the thick fluid.

Magnet power is about 800 watts, making water cooling necessary (See Figure 2). Power for each magnet is supplied by separate voltage-adjustable sources, so that the magnetic field null ("bottle" position) can be moved over a wide range.

ELECTRON GUN

The filamentary cathode is a flat spiral of .020 inch tungsten wire, which operates at about $2500^{\circ}K$ (See Figure 3). The accelerating grid is a radially vaned structure. Typical operating conditions are 7 volts at 15 amperes. Electron emission is, of course, extremely sensitive to filament temperature variations and to the amount of gas present.

Typical emissions are 100 to 300 ma at an energy of 300 to 1000 volts. Less than about 40 percent of this current arrives at the plasma region as useful ionizing current, the remainder hitting the grid structure or the sides of the drift tube. This yield could be substantially increased by proper geometry and accelerating potentials, as will be discussed later. (Assume for the moment that the potentiometer is at its right-most position.)

Heat generated by the filament is removed by cooling fins mounted on the filament terminals outside the vacuum (See Figure 3).

VACUUM SYSTEM

The vacuum system used in these experiments (See Figure 4) is a six-inch oil diffusion pump, backed by 15 cfm roughing pump, with appropriate gate valves, etc. Two baffles, cooled by liquid nitrogen and Freon, respectively, are provided. High purity tank argon is run through a drying and deoxidizing train before being introduced into the ion source. This system is capable of operating in the region of 10^{-8} mm Hg, but the operating range using the ion source is about 5×10^{-4} mm Hg.

ION EXTRACTION AND COLLECTION

The ion extraction electrode is also a vaned-grid structure in the end of a 1/2 in. diameter metal tube. The plasma can be positioned quite close to this electrode, thus creating a high electric field in such a direction as to extract positive ions from the plasma. Ions pass between the poles of a small electromagnet (60 gauss), not shown, and then to an ion collection cup. Ion current to this cup is measured with
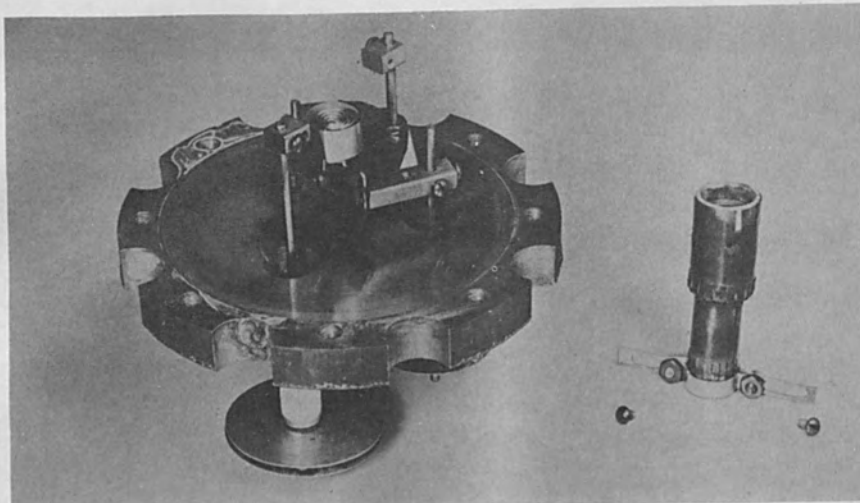
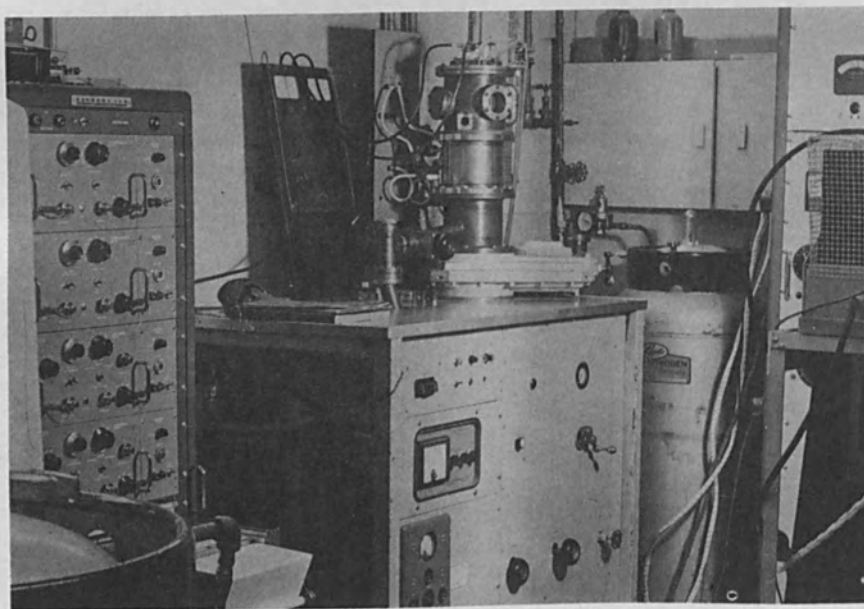Figure 3.   Electron Gun and Drift Tube

Figure 4.   Vacuum System

a conventional milliammeter. The cup is biased about 20 volts positive so that secondary electron emission caused by ion bombardment will not give misleading results. The purpose of the small electromagnet is to deflect any electrons in the beam away from the collection cup, while diverting the ions only slightly from their normal path. The magnitude of the detected current with and without this field quickly establishes the presence of any electrons in the beam. No electrons should be in the beam if the ion extraction voltage is higher than the electron accelerating voltage. The beam may be seen as a faint bluish spray exuding from the source aperture.

Although an argon ion beam current of about 3 ma at 3 kilovolts is readily attained with the present geometry, there is serious doubt that the plasma, even though visible as a blue disc, is being confined to the degree necessary. As the plasma is moved in toward "contact" with the extraction electrode, a radical rise in the extraction electrode current should be observed. No such rise in current has been observed. This probably means that the plasma is not dense enough to exhibit good conductivity; thus only a relatively low electric field is available for drawing ions out of the plasma. Hence the ion current attained is only a small fraction of the current potentially attainable from this type source.

There are several possibilities for improvement of this situation. Since the electron accelerating-focussing arrangement is rather inefficient, an excessive acceleration potential (1000 volts) is necessary to extract sufficient electron current from the filament. Hence they do not spend enough time in the plasma region giving up their energy in

ionizing events. Figure 2 shows a proposed scheme similar to the one used in the original source. The electron drift tube will be split into two segments, as shown, making an elementary electron lens. The electrons will leave the lens (traveling to the right) with less energy than before, and they will be collimated or focussed to some extent. Thus more useful electron current should arrive at the plasma region without hitting the walls.

When a vaporized metal is used instead of argon, the vapor which is not ionized should condense on the cool walls of the apparatus instead of diffusing throughout the system, as argon does. This causes a high background pressure, which gives rise to filament sputtering, high-voltage breakdown, etc., thus imposing limitations on experimental voltages and currents.

FUTURE PROBLEMS TO BE SOLVED

Deflection and Focussing. Magnetic fields of suitable intensity for deflection of an ion beam can be produced and appear preferable over electric fields as a focussing means because of high voltage breakdown. A combination of electric and magnetic fields may, however, prove to be more satisfactory.

Focussing will be done by means of a "strong focussing" quadrupole pair[3](See Figure 1). After the degree of focussing which can be achieved by this means is determined, the deflection possibilities of asymmetric use of these focussing magnets will be investigated as a scanning means. These experiments will indicate the next steps in deposition pattern control.

Deposition of Ions on Substrate. Deposition of the ions is a major problem to be solved. Ions having the energy that probably will be necessary in order to produce ion beams of adequate current value will have energies in excess of the binding energy of the element in question in solid form. This excess energy must be dissipated in some way so as to satisfy conservation of energy and momentum for the particle and leave it at rest at the desired substrate position. Otherwise, sputtering may take place at the substrate and more material will be dissipated in a sputtered cloud than is deposited. In ion isotope separators, this problem is solved by providing condensation traps for the sputtered cloud, but such a solution is not satisfactory for this purpose. The ions must be decelerated to energy and momentum levels suitable for deposition without extensive defocussing of the beam. More detailed approaches to this problem can be made only after the ion source is operating satisfactorily.

Beam Neutralization. Since the substrate surface is an electrical insulator (at the beginning of a deposition, at least) the charge on the beam particles must be neutralized before striking the substrate, or soon thereafter, to prevent surface charge build-up and consequent defocussing. Similar problems occur in ionic rocket research,[4] and several approaches to their solution are being considered here, most of which involve a means of supplying sufficient electrons to neutralize the beam after it leaves the last deflection and/or focussing coil.

Next, the estimated equivalent component density of a microcircuit device produced by the ion beam deposition of all material should be in the order of 10,000 parts per cubic centimeter. Therefore, a device 1 cm. on a side and 2 mm. thick would contain the equivalent of 2,000 parts and appears to be a reasonable maximum module to consider at this time. The above volume of .2 cm^3 represents approximately .03 mole. Approximately 96,000 coulombs are required for the ion deposition of 1 mole or approximately 2900 coulombs for the deposition of .03 mole. It is considered that a complete device should be deposited in one normal work day or approximately 27,000 seconds. This would require a current of slightly more than 100 milliamperes and hence is compatible with the current limit previously stated as an objective.

Resolution of the beam should be as fine as is practical. A beam 10^{-4} cm in diameter would be compatible with the dimensions and tolerances of deposition for the resultant equivalent component density of 10^4 parts 1 cm^3. A current of 100 ma in a beam 10^{-4} cm in diameter would result in a current density in the order of 10^7 amperes/cm^2. Such a current, current density, and focussing diameter appear to be practical insofar as the generation and control of the ion beam is concerned. It further is well within the limits of current densities achieved from point source, and since the beam need not be concentrated at one spot continuously but rather will scan an area and since cooling means can be provided to the substrate, it appears feasible to maintain the substrate temperature within acceptable limits.

CONCLUSION

An experimental ion source has been built as a first step toward the development of a deposited circuitry system using a directed beam of ions. This ion source has shown considerable promise as a source of a relatively intense beam of ions, although a substantial amount of development is still necessary.

ACKNOWLEDGEMENT

REFERENCES

(1) Glasstone, S. and R. H. Lovberg, "Controlled Thermonuclear Reactions," Van Nostrand, New York (1960), p. 421.

(2) Rechen, J. B. and J. C. Jordan, Rev. Sci. Instr. 28, 584 (1957).

(3) Shull, F.B., et al, "Concentration of a Cyclotron Beam by Strong Focusing Lenses," Rev. Sci. Inst. 25, p. 364 (April 1954).

(4) Cloutier, G. and T. Johnson, "Charge Neutralization in an Ionic Rocket," J. Astronautical Sciences, Fall 1960, p. 49.

APPENDIX

Deposition Rate. Analysis of the magnitude of the ion current required necessitates several basic assumptions. First it is assumed that current will be limited by heat dissipation at the substrat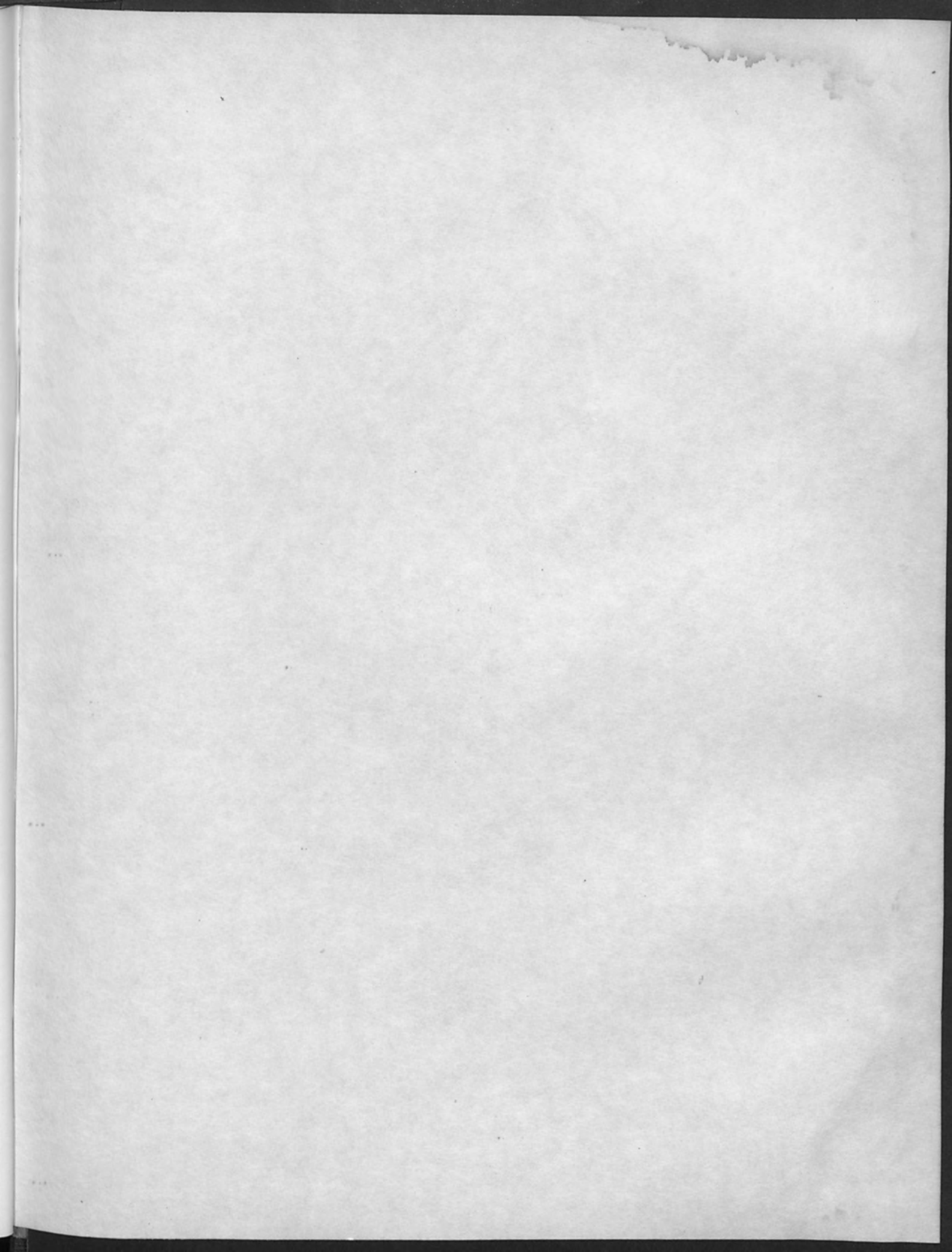e to the order of 100 milliamperes.